AN INTEGRATED COMPUTATIONAL FLUID DYNAMICS AND KINETICS STUDY OF OZONATION IN WATER TREATMENT

Tzu Hua Huang

BScEng (Chemical) (Natal)

Submitted in fulfilment of the academic requirements for the degree of
Doctor of Philosophy in the School of Chemical Engineering,
University of KwaZulu-Natal, Durban.
15 December 2005

ACKNOWLEDGEMENTS

I would like to express my thanks and appreciation to the following people and organisations who have contributed to this investigation:

- The South African Water Research Commission for funding the project.
- My supervisors: Prof Chris Buckley, for his dedication, guidance and philosophy to excel which are invaluable within this work and beyond; Mr Chris Brouckaert, for his advice and technical insight in the study.
- Umgeni Water's Wiggins Waterworks for providing the pre-ozonation facility for the investigation; Mr Martin Pryor and Mr Rachi Rajagopaul of the Process Evaluation Facility (PEF), Wiggins Waterworks, for their technical knowledge in ozonation process and assistance in full-scale plant test planning and equipment arrangement; Ms Sue Freese and Ms Debbie Trollips of the Darvill Wastewaterworks, for their technical knowledge in ozone chemistry and the laboratory utilisation; Mr Mahomed Docrat and Mr Dan Naidoo of the Wiggins Waterworks plant, for their support in on-line parameter tuning; The trainees from PEF for assisting in sample collection during the tracer tests and the ozone residual measurements.
- Prof Mike Mulholland of the School of Chemical Engineering for providing the research exchange opportunity which allows me and the project to set foot abroad. Merci beaucoup!
- My fellow graduate students of the Pollution Research Group and of the School of Chemical Engineering for their friendship and experience shared over the years.

To my family, especially Mom and my brother, Chien-Hao, I am grateful for all your love and care throughout my study. This thesis is dedicated to you all. To Sarushen, I would not have achieved this without your encouragement and support. Thank you God, for giving me the strength to see it through.

ABSTRACT

Computational fluid dynamic (CFD) modelling has been applied to examine the operation of the pre-ozonation system at Wiggins Waterworks, operated by Umgeni Water in Durban, South Africa.

Ozonation is employed in water treatment process primarily to achieve the oxidation of iron and manganese, the destruction of micro-organisms and the removal of taste and odour causing compounds. It also aids in the reduction of the colour of the final water, enhancement of algae removal and possible reduction of coagulant demand.

A hydrodynamic model has been satisfactorily verified by experimental tracer tests. The effect of the gas injection was modelled by increasing the level of turbulence intensity at the ozone contactor inlet. The model prediction of the overall tracer response corresponded closely to the experimental results. The framework of ozone reaction modelling was subsequently established using values of rate constants from the literature. An accurate prediction of the ozone concentration profile requires the application of the correct ozone kinetics involved. In raw waters, the depletion of ozone is influenced by the presence of natural organic matters (NOM). The observed ozone decay was found in good agreement using the pseudo first-order rate law. By measuring the total organic carbon (TOC) as a surrogate for NOM, the experimentally determined rate constants can be calculated to account for the effects of the ozone doses and the water quality. The characterisation study also aimed to provide sufficient information on ozone depletion and to be operated easily, without the lengthy and costly analyses of a detailed kinetics study.

The predicted profile of residual ozone concentration suggests the current operating strategy can be improved to optimise the ozone utilisation. The proposed monitoring point was suggested to be at the end of second compartment where most ozone reactions have been completed. By coupling the transport equations of the target compounds with their chemical reaction rates, the concentration profile of these compounds such as ozone can be predicted in order to assist the understanding of an operation and to attain better interpretation of experimental results.

PREFACE

I, Tzu Hua Huang, declare that unless indicated, this thesis is my own work and that it has not been submitted, in whole or in part, for a degree at another University or Institution.

Tzu Hua Huang

December 2005

TABLE OF CONTENTS

FIGURES

TABLES

$\dot{m}$	$kg.s^{-1}$	mass flow
$\overline{m}$	kg	total mass of tracer
$\overline{u}$	$m.s^{-1}$	mean time-average velocity
$\overline{t}$	s	mean residence time
C	$mg.L^{-1}$	concentration of material
C_μ	-	constant in turbulence equation
C_s	-	roughness constant
G_b		generation of turbulence due to buoyancy,
G_k		production of turbulence kinetic energy
G_k		generation of turbulence kinetic energy due to the mean velocity gradients
I	-	turbulence intensity
k	$m^2.s^{-2}$	turbulent kinetic energy
K_s	m	roughness height
K_s^+	-	dimensionless roughness height
u	$m.s^{-1}$	linear velocity
u^+	-	dimensionless, average axial velocity
u_τ	$m.s^{-1}$	friction velocity
y	m	distance perpendicular to wall
y^+	-	dimensionless distance to wall
α	-	mass-average fraction of tracer
ε		turbulent dissipation rate
θ	-	dimensionless time
κ	-	von Kármán constant
μ		molecular viscosity
μ_t		turbulent (eddy) viscosity
σ^2	-	variance
τ	$kg.s^{-2}$	stress tensor
k_c	s^{-1}	pseudo first-order rate constant
k_d	s^{-1}	rate constant of ozone self-decomposition
k_r	$kL.kmol^{-1}.s^{-1}$ or $M^{-1}.s^{-1}$	rate constant of OCS consumption
k_d	$M^{-1}.s^{-1}$	rate constant of ozone disinfection

subscripts

k	term related to the turbulent kinetic energy

ε	term related to the turbulent dissipation rate
eff	effective

superscripts

'	fluctuating component

AMCEN	African ministerial conference on the environment
BOD	Biological oxygen demand
CFD	Computational fluid dynamics
COD	Chemical oxygen demand
DOC	Dissolved organic carbon
DWAF	Department of water affairs and forestry
HDT	Hydraulic detention time
MDG	Millenium development goal
OCS	Ozone-consuming substances
PDE	Partial differential equation
RANS	Reynolds-average Navier-Stokes
RNG	Renormalised-group
RTD	Residence time distribution
SWTR	Surface water treatment rule
THMFP	Trihalomethane formation potential
TOC	Total organic carbon
US EPA	United State Environmental protection agency
WRC	Water research commission
WSSD	World Summit on sustainable development

Applied ozone	Amount of ozone applied to the sample as determined during calibration of the ozone apparatus
Developed countries	There is no established convention for the designation of *developed* and *developing* countries or areas in the United Nations system. In common practice, Japan in Asia, Canada and the United States in northern America, Australia and New Zealand in Oceania and Europe are considered "developed" regions or areas. In international trade statistics, the Southern African Customs Union is also treated as developed region and Israel as a developed country; countries emerging from the former Yugoslavia are treated as developing countries; and countries of eastern Europe and the former USSR countries in Europe are not included under either developed or developing regions. (UN Statistics Division, 2003)
Half-life (O_3)	Time taken for ozone residual to decrease to half of its initial value at t = 0
Instantaneous ozone consumption/ instantaneous demand	Difference between applied ozone concentration and the sum of the ozone residual and unreacted ozone at a specific time
Ozonation	Addition of ozone-containing gas into the liquid phase
Ozonator	A reactor where ozonation occurs
Ozone dose	Amount of ozone actually transferred to the sample in the kinetic experiment; also refer to the setting of ozone-to-water ratio at Wiggins Waterworks
Ozone residual	Dissolved ozone measured in aqueous phase at time t
Ozone transferred	Ozone transferred into the sample, i.e.: applied ozone subtracts the unreacted ozone exiting
Unreacted ozone	Ozone measured in gas phase exiting the reaction vessel

1

INTRODUCTION

"Water is life, sanitation is dignity"

- Strategic frame work for water services, Ronnie Kasril, Former minister of water affairs and forestry, South Africa

Approximately one-third of the world's population lives in countries with moderate to high water stress (UNEP, 2003). The lack of availability or the inadequate quality of freshwater are the two most restrictive issues for development in Africa; hampering industrial activities, food production and contributing significantly to the spread of disease. However, due to the declining state of the fresh water supply in both quantity and quality, water-stressed countries do not have the freedom to select available sources based only on quality parameters.

In both the Millennium Development Goals (MDG) and the key outcome from the World Summit on Sustainable Development (WSSD), the need to ensure environmental sustainability in eco-social growth and industrial development was reaffirmed. One of the targets is to halve, by 2015, the proportion of people without *sustainable* access to safe drinking water and basic sanitation worldwide (UN, 2003). South Africa, as a member of 191 United Nations Member States who have pledged to meet these targets, has drawn up strategies to provide more South Africans with basic water and sanitation services. This necessitates increasing the supply of potable water. In order to implement the strategy in a *sustainable* manner, efficient and effective operation of water treatment process needs to be sought.

South Africa has limited water resources which largely derive from rivers. Water quality is thus dependent on seasonal changes and river conditions. Furthermore, the accumulated effect of pollutants gathered from many smaller flows into the major rivers leads to treatment problems in waterworks. Ozone, because of its exceptional oxidising ability, has been under research for the past century as an effective oxidant and disinfectant in water and wastewater treatment. Ozonation is one of the advanced treatment processes that have been introduced in local waterworks to treat water to potable water standard.

In this chapter, **Section 1.1** outlines a global and national target on provision of safe drinking water. **Section 1.2** describes Umgeni Water's Wiggins Waterworks and its ozonation system in this study. **Sections 1.3** and **1.4** present the motivation and the objectives of the investigation, and the chapter is concluded by a layout of the thesis in **Section 1.5**.

1.1 Demand on sustainable access to drinking water

AMCEN/UNEP (2003) reports that water stress (less than 1 700 kL.capita^{-1}.year^{-1}) or water scarcity (less than 1 000 kL.capita^{-1}.year^{-1}) is already observed in 14 of the 53 African countries.

Water resources in sub-Saharan Africa, in particular, are subject to climate changes and the consequent effects which include variation in rainfall, reduced precipitation and increased evaporation. With a growing population and demands from the domestic, agricultural and industrial sectors for water, freshwater availability is a priority concern (AMCEN/UNEP, 2003). The high demand for water is driving unsustainable practices and competition for water resources between sectors, communities and nations.

Table 1-1: Population and renewable water resources per capita
([1] World Bank, 2004; [2] World Resources Institute, 2004)

Country/Region		[1] Population	Water resource	
			[2] Internal †	[2] Actual ‡
		(millions)	(kL.person^{-1}.year^{-1})	(kL.person^{-1}.year^{-1})
	Year	2004	2004	2004
South Africa		45.6	990.8	1 105.9
Sub-Saharan Africa		719.0	5 445.0	6 322.5
Developed regions		1 000*	10 434.3	11 513.8
World		6 300	6 879.8	8 549.2

Notes to Table 1-1:

* Data taken as the high-income countries defined by the World Bank.

† Internal renewable water resources (IRWR) per capita are the average annual volume of water generated within a country's borders on a per person basis.

IRWR = surface water resources + groundwater resources - overlap.

‡ Actual renewable water resources per capita provide the maximum amount of water actually available, on a per person basis, for each country. In reality, a portion of this water may be inaccessible to humans. Actual renewable water resources are defined as the sum of internal renewable resources (IRWR) and external renewable resources (ERWR), taking into consideration the quantity of flow reserved to upstream and downstream countries through formal or informal agreements or treaties and possible reduction of external flow due to upstream water abstraction (World Resources Institute, 2004).

Table 1-1 lists the population and the renewable water resources of different regions in the world and compares to those data of South Africa. Both internal and actual renewable water resources in Sub-Saharan Africa (5445.0 kL.person^{-1}.year^{-1} and 6322.5 kL.person^{-1}.year^{-1} respectively) are less than the world average (6879.8 kL.person^{-1}.year^{-1} and 8549.2 kL.person^{-1}.year^{-1}) and are only half of those values in the developed regions (10434.3 kL.person^{-1}.year^{-1} and 11513.8 kL.person^{-1}.year^{-1}). When areas of low rainfall coincide with high evaporation potential, the climate variation can result in severe droughts. This can be seen in the case of South Africa in 2004, which had less than 10% of the internal renewable resources of the developed regions. Regulations such as water restrictions were necessary in major cities and towns in South Africa to cope with water shortages.

Table 1-2 compares the percentage of the population with access to improved drinking water sources in South Africa, with those values of the neighbouring countries. South Africa (total of 87%, 2002) is positioned well above the average value of the Sub-Saharan African region (total of 58%, 2002).

However there was little progress between 1990 and 2002 (total of 87%), when compared to the neighbouring countries such as Namibia (58% in 1990 to 80% in 2002) and Botswana (93% in 1990 to 95% in 2002) which have less water resources than South Africa (AMCEN/UNEP, 2003). In comparison with other regions, South Africa is closer to the level of the Northern Africa or Developed Regions (as defined by UN) in urban areas, but seriously lagging in servicing the rural areas.

Table 1-2: Proportion of urban, rural and total population with access to improved drinking water sources (UN Statistics Division, 2002)

Country/Region	1990			2002		
	urban (%)	rural (%)	total (%)	urban (%))	rural (%)	total (%)
South Africa	**99**	**67**	**83**	**98**	**73**	**87**
Namibia	99	43	58	98	72	80
Botswana	100	88	93	100	90	95
Sub-Saharan Africa	82	36	49	82	45	58
Northern Africa	95	83	88	96	84	90
Developed regions	100	99	100	100	94	98

In the South African context, the Department of Water Affairs and Forestry (DWAF) has set out to meet the target of providing all South Africans with a functional water supply by 2008 and sanitation facilities by 2010, exceeding the targets mentioned in the MDGs and WSSD (DWAF, 2003). The provision of free basic water thus commenced in 2003, supplying each household with 6 kL per month free of charge.

To achieve this target in a sustainable manner, building new water treatment facilities should be avoided if the present waterworks can be operated to meet the demand. Efficient and effective operation and control of the present treatment process is thus important for capital savings and in preventing an additional burden to the environment from waste of chemicalsor energy.

1.2 Project background

Computational fluid dynamics (CFD) research in water and wastewater at the Pollution Research Group, University of KwaZulu-Natal (formerly known as the University of Natal), under Prof. Chris Buckley and Mr Chris Brouckaert, commenced in 1992, funded by the Water Research Commission (WRC). The project at the time was intended to improve the operation and the performance of equipment in water and wastewater by means of CFD modelling. The results from the case studies of a clarifier and an anaerobic compartment indicated the potentials of the CFD technique in better understanding the operations and in designs to avoid undesirable flow behaviour (Brouckaert and Buckley, 2002).

A subsequent WRC-funded project, entitled *Computational fluid dynamics support to water research projects* aimed to extend the above findings by undertaking a modelling exercise on a number of process units in water and wastewater as a service to industries and to promote the use of CFD by water authorities, consultants and water researchers (Brouckaert et al., 2005).

The operation of an ozone contactor in Umgeni Water's Wiggins Waterworks was investigated as one of the main case studies in the abovementioned project, initially undertaken by the author as an MScEng study in 2001 and subsequently upgraded to PhD at the end of 2002.

Attributable to its high chemical activity, ozone is found to be more effective to oxidise certain classes of recalcitrant organic and inorganic species and to inactivate waterborne pathogens resistant to the conventional oxidants or disinfectant. Although the operational cost is high, many water treatment plants have incorporated ozonation in order to provide safer drinking water.

CFD modelling is a numerical procedure to calculate the properties of moving fluid (Brouckaert et al., 2004). It serves as a flexible tool in examining the performance of the ozone contactor. Its application is useful for the purpose of optimisation, design, or retrofitting an existing unit in water treatment processes. The power of CFD is such that a more rigorous approach can be adopted. The reactions involving the target species and the disinfectant can be incorporated in the solution of the flow field so as to explicitly calculate the exit concentration of the target species.

Additional research exchange undertaken by the author in 2001 and 2003 to visit Institut National des Sciences et Appliquées (INSA) de Toulouse, France, were funded by the research grant under the Franco-South African Science and Technology Agreement, entitled *Optimisation of Potable Water Preparation and Distribution in Durban*. This agreement was coordinated by Prof Mike Mulholland, University of Natal, Durban, and Prof Marie-Véronique Le Lann, INSA/LAAS-CNRS, Toulouse. Part of the modelling work was carried out at the Laboratoire d'Ingénierie des Procédés de l'Environnement (LIPE), INSA de Toulouse, under the supervision of Prof Alain Liné.

1.2.1 The water treatment works

Umgeni Water was established in 1974, with the main function of supplying bulk treated water to an area of 24 000 km^2 in the Greater Durban and Pietermaritzburg region, KwaZulu-Natal, South Africa. Most of the water is obtained from the Mgeni River which runs through a number of catchments in the Midlands before reaching the Indian Ocean in Durban.

Inanda Dam, completed in 1987, is the lowest dam situated on Mgeni River and supplies raw water to Wiggins Waterworks. The Wiggins Waterworks (Figure 1-1) is the first large water purification plant in South Africa to employ pre-ozonation.

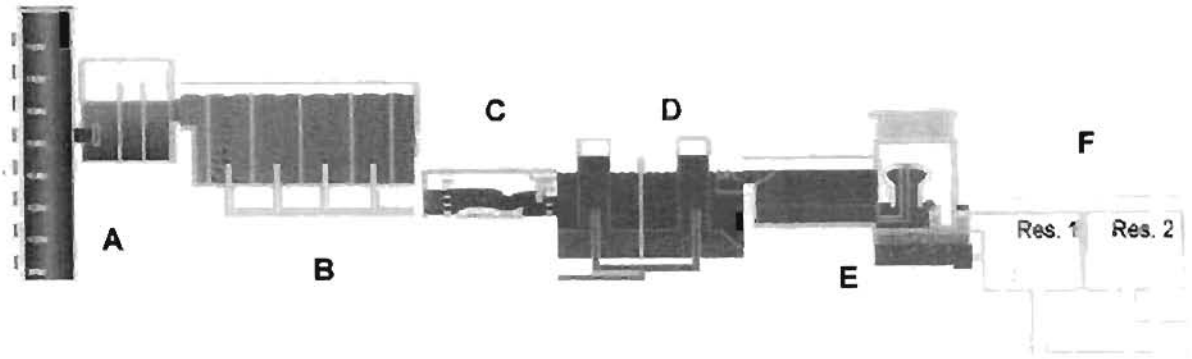

Figure 1-1: Treatment process at Wiggins Waterworks (Umgeni Water, 2002)

Water arrives at the volume-graded tower (A) and is first treated with ozone (B). Coagulant is then added to water in the flocculation step (C) and the agglomerated solids are settled out in clarifiers (D). Thereafter water passes through a series of sand filters (E) to remove any suspended matter which escaped in the previous step. Finally chlorine is added to disinfect water and to protect it from future microbial growth and the water is stored in a large reservoir on-site before being distributed (F).

Table 1-3: Unit chemical treatment costs (cents.kL^{-1}) of waterworks operated by Umgeni Water (Umgeni Water, 2003)

	Umzinto	Aman-zimtoti	Mtwalume	Hazelmere	Wiggins	D V Harris	Umlaas Rd	Craigie-burn	Durban Hts	Midmar	Avg
1998	8.50	4.43	5.45	2.82	1.72	3.26	2.36	2.94	1.93	2.88	3.94
1999	11.72	9.09	7.03	5.56	1.99	4.45	3.23	5.01	3.71	3.68	6.01
1990	10.87	6.64	6.97	6.01	2.19	3.77	3.08	4.81	2.81	1.84	5.54
2001	8.98	6.52	4.92	5.33	1.95	3.45	2.75	2.94	2.65	3.11	4.60
2002	10.66	5.46	5.35	6.94	2.66	4.31	2.62	3.95	3.39	4.09	5.24

The major economic concern of the process is in ozone generation which has a high consumption of electricity. In spite of the cost of operating the ozone generators, the Wiggins Waterworks has the lowest operating cost per volume of water treated in any of the works operated by Umgeni Water (Table 1-3), which is partly due to the low turbidities in the raw water, and partly attributable to the beneficial effect of the pre-ozonation on the downstream purification processes.

1.2.2 Pre-ozonation contacting system

Ozonation of water is carried out by dispersing ozone-containing gas into the liquid phase using techniques of relatively low energy demand, such as diffusers or static mixers (Bin and Roustan, 2000). The ozone reactions occurred in a liquid-gas contacting tank, known as the ozone reactor or the ozone contactor, as referred to in this thesis.

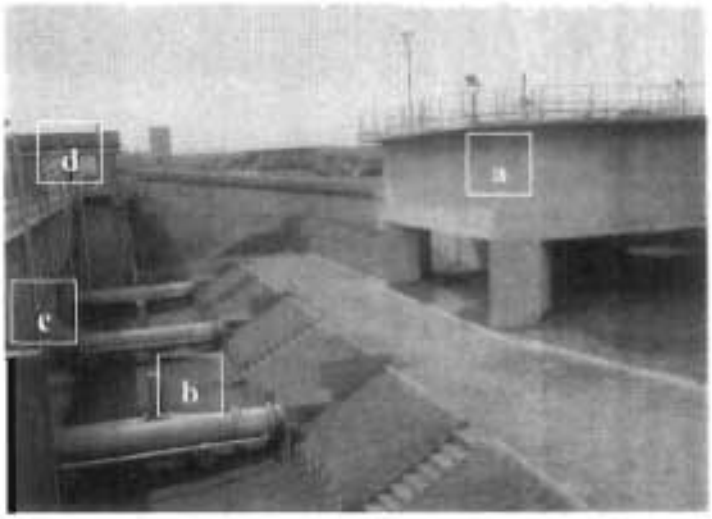

Figure 1-2: Appearance of the pre-ozonation contacting system

Raw water enters the contacting system through a distribution reservoir (Figure 1-2 (a)). The contacting system consists of four contactors. Each of the contactors (c) is preceded by a static mixer (b) such that the contacting chambers can operate individually or in parallel. An ozone-oxygen gas mixture is injected as a side-stream through the static mixer that is employed to achieve high mass transfer of ozone to water. Excess ozone in the gas phase is transferred to the Thermal Destruction Unit (d) before it is released into the atmosphere. Ozone is produced at 10% (m/m) concentration by 3 × 30 $kg.h^{-1}$ Trailigaz ozonators which are fed with evaporated liquid oxygen.

1.2.2.1 Contactors

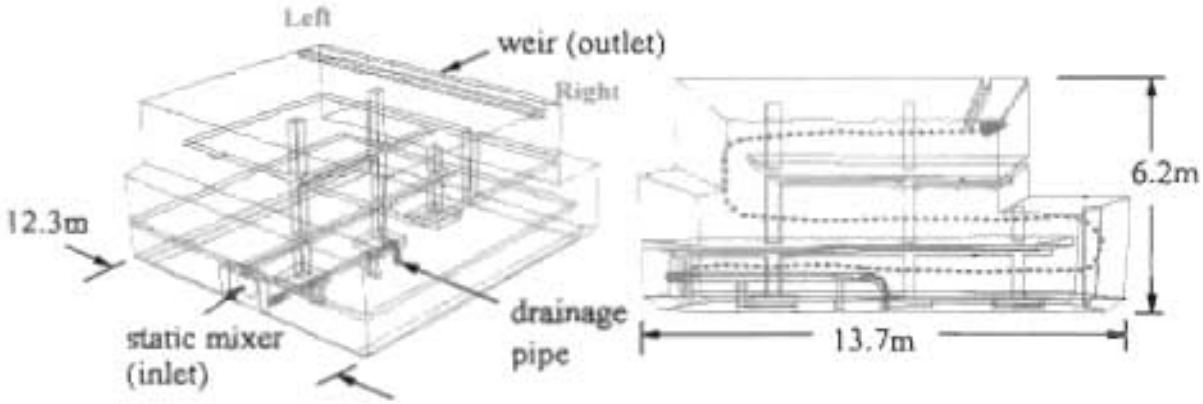

Figure 1-3: Dimensions and flow direction in the ozone contactor (drawings adapted from model)

The configuration of the contactor is unusual as it was converted from an existing structure. Water enters from the bottom at the front end, passes through three horizontal compartments, and exits over the weir at the rear (see the dashed line in Figure 1-3 (b)). A pipe is located to the right of the inlet at the bottom compartment (Figure 1-3 (a)) to discharge sludge periodically. This half of the contactor will be referred as the *right* portion and conversely the other half will be referred as the *left* throughout this thesis.

Conventionally a contactor is designed with vertical flow baffles and accompanied by multiple points in the tank to distribute ozone by diffusers. In comparison, the present contacting system at the Wiggins Waterworks poses complexity in geometry and operation.

1.2.2.2 Static mixer

Wiggins Waterworks uses the Sulzer static mixer model SMX. A section of the internal structure is shown in Figure 1-4. A section of vertical mixing plates is located immediately below the gas inlet. A headspace of 500 mm is left with no mixing plates. Thereafter three alternating orientation of mixing plates which are offset at 90° to each to each other are installed before the water exits the static mixer.

The mixing is caused by the flow passing through a series of mixing elements arranged in such a way that bulk fluid can be broken up into small pockets for improved mixing. One of the operational benefits for a static mixer is its low requirement for energy.

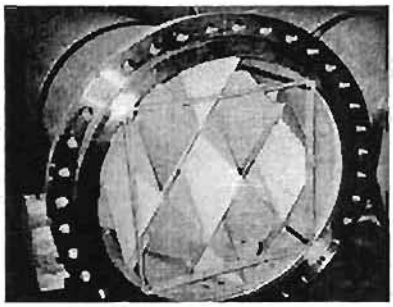

Figure 1-4: View of the static mixer

The high mass transfer efficiency of ozone to water using static mixers has been reported in literature (Zhu et al., 1989; Bin and Roustan, 2000; Heyouni et al. 2002) as a result of enhanced mixing.

1.2.3 Ozone residual concentration

One of the operational objectives of the ozone contactors is to achieve the desired residual ozone concentration in water within the contactor. In relative terms, ozone is supplied in surplus to the ozone-consuming substance (OCS) present in raw water. After the ozone is dissolved, it undergoes various types of aquatic reactions until the OCS are consumed. Ozone is also depleted through self-decomposition, but at a much slower rate and therefore it is possible to monitor ozone at a specific concentration at a suitably chosen point of the contactor.

In this context the term *residual* is the dissolved ozone which remains available. This parameter is important in the control and operation of the contactor as it ensures that sufficient ozone is added to the water. However, overdosing with ozone should be avoided as it could increase the disinfection by-products to an unacceptable level (Rakness et al., 2000). Even when over-dosage with ozone does not adversely affect the quality of water, it will always increase the operational cost.

1.3 Motivation of the study

Presently the control of the pre-ozonation system at Wiggins Waterworks relies on the measurement of the residual ozone concentration to be near zero at the flow outlet. Water leaves the ozone contactors over a broad-crested weir. Turbulence and the de-gassing effect can cause the release of residual ozone. Even when this does not exceed the safety exposure limit, it is a health concern as well as an operating inefficiency. While this measurement provides for operational safety, it gives very little indication of the performance of the ozone contactor.

Due to the intense energy demand in producing ozone, ozonation has one of the largest contributions to the environmental burden of the water treatment processes (Friedrich, 2001). Thus, it is important to optimise the pre-ozonation system by achieving the most effective utilisation of ozone produced.

As described in **Section 1.2.1** , a water treatment works consists of a series of processes. The flow dynamics and the associated physico-chemical phenomena of each process are important aspects for the optimal performance of the entire works. In chemical engineering, the design or the optimisation of a unit operation can be done using various approaches. Do-Quang et al. (2000) have categorised these approaches as follows:

- Empirical relationships
- Bench-scale and pilot-scale testing
- Full-scale plant testing
- Modelling

Empirical correlations, pilot/bench-scale tests, or full-scale tests are the conventional means of resolving such types of chemical engineering problems. However, this classical approach is mainly based on the global balances. Although this usually leads to simplification of describing the overall system and its usefulness is recognised, relations as such are difficult to extrapolate. Modelling thus appears to be a favourable option to represent the physical reality and capture the macro-and micro-phenomena of the process under investigation. The limitations of the computing power and time have been overcome by the continual advances in computer technology.

Among the modelling tools, computational fluid dynamics (CFD) is based on the conservation laws of mass, momentum and energy to model the flow hydrodynamics. The user input requires only the process geometry, fluid properties and boundary conditions, without prior knowledge of the flow regime. In contrast to a mixed-compartment modelling approach, CFD modelling offers the advantage of a fundamental physical basis for representing the complex interaction between flow and chemical reaction phenomena.

Because CFD modelling is a fundamental approach, its application is not limited by the range of the operating conditions as most empirical relationships and small-scale testing are. The model represents the physical process as a *virtual unit operation*. The effects of the upstream processes or the operating

conditions can be reflected by specifying the appropriate boundary conditions. This is an advantage above the physical testing, as the latter often poses disturbances to the rest of the treatment works. However, it should be noted that CFD modelling does not replace experimental tests. As Anderson (1995) and Roache (1985) pointed out, CFD modelling and physical experimentation supplement each other in the understanding of physical phenomena.

1.4 Overall objectives

This work seeks to develop a combined hydrodynamic/kinetic model of the pre-ozonation contactor at the Wiggins Waterworks to examine its operating efficiency. This will be achieved by the following sub-objectives:

i. Determine the actual residence time distribution as a function of flow conditions through the contactor

ii. Establish a qualitative understanding of the dissolved ozone concentration profile throughout the ozone contactor

iii. Determine the ozone reaction kinetic constants for the actual raw water

iv. Select the best possible position for single-point monitoring of residual ozone concentration in order to achieve the most efficient use of the ozone

The first objective required an appropriate *hydrodynamic model* of the ozone contactor. The hydrodynamic model was then verified by performing experimental tracer tests to examine the effects of the flow conditions.

The second objective led to developing a *kinetic model* which builds onto the hydrodynamic model by incorporating the ozone reaction kinetics to the calculated velocity field. Residual ozone concentrations were measured on-site as a partial validation of the model.

The outcome of the kinetic model and the wide range of rate constants found in literature necessitated the *ozone kinetics experiments* to be carried out in order to determine the rate constants applicable for the local water source.

The fourth objective was achieved by the incorporation of all efforts which contributed to the formation of the combined model and the results were interpreted in view of the last objective.

The study was focussed on the modelling of the ozone contactor only. The simplest CFD model considers only the hydraulic aspects of a system (Brouckaert et al., 2005). This type of model is often used to predict the residence time distribution and, in turn, provides the connection to the performance indicators which lead the model to a higher level of complexity. However complex the models may be, they must be supported by experimental studies which identify the physical and the chemical element of the models.

Therefore if the static mixer was to be modelled, the combined contactor and mixer would be inevitably complex. The required experimental data for validating the static mixer model would also pose inherent

difficulty and may not contribute greatly to the understanding of the contactor performance. For the purpose of the investigation, it was considered essential to concentrate on the ozone contactor instead of the static mixer. .

CFD modelling is expected to contribute to the study in several ways, such as improved planning of experiments, better interpretation of results and the prediction of the effects of modifications to the equipment configuration or operating strategy. By incorporating the appropriate reaction kinetics, it is possible to assess the effectiveness of the current operating strategy and to propose a new scheme for achieving the most efficient use of the ozone dosed to the system.

1.5 Thesis outline

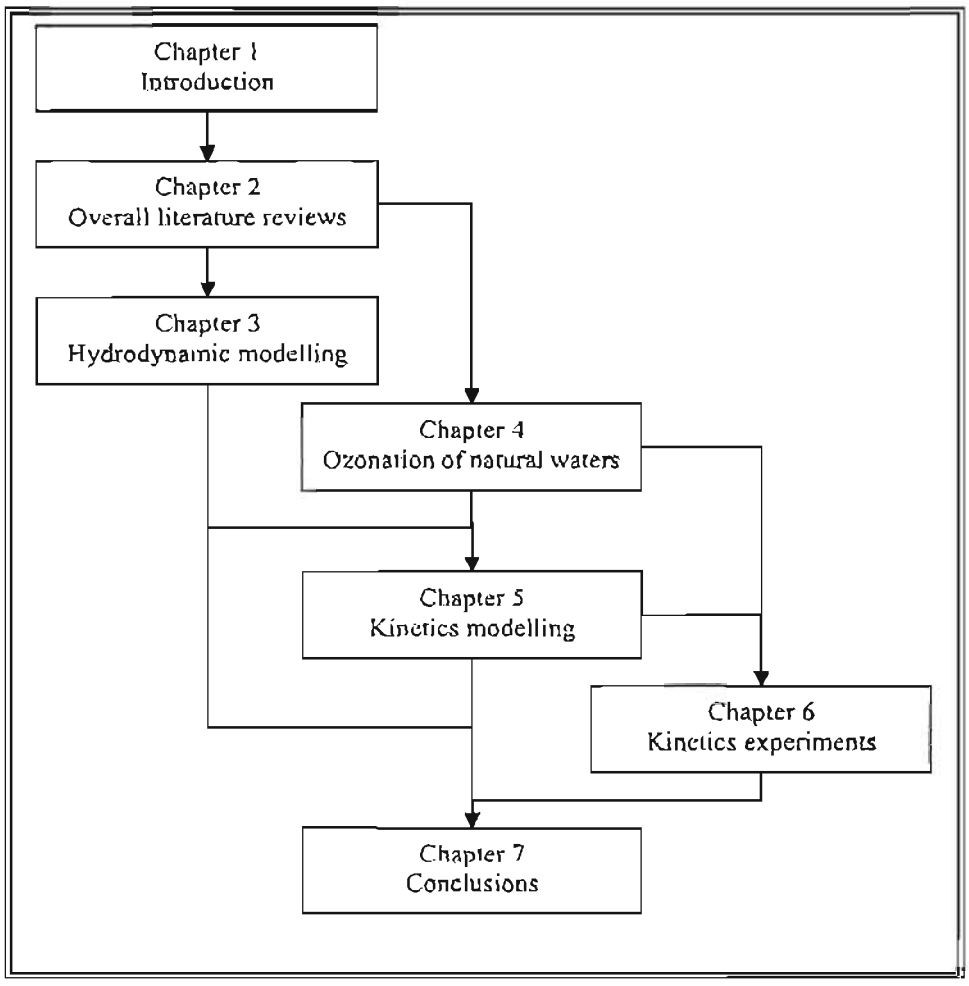

Figure 1-5: Flow diagram of thesis

Figure 1-5 indicates the course of the remaining chapters in the thesis. The inter-dependence of chapters is indicated by arrows.

In Chapter 1 the need for producing potable water in a more sustainable manner is highlighted. One of the means to achieve this is by effectively utilising the present water treatment works. Amongst the many tools available for process optimisation, CFD modelling is a technique which provides comprehensive

details on the flow dynamics in a vessel and, in conjunction with appropriate reaction kinetics, on the chemical species under scrutiny. This investigation is a case study of the pre-ozonation contacting system at Wiggins Waterworks, Umgeni Water. When the more empirical approach is not suitable for the complicated geometry and flow dynamics of the contactor under investigation, CFD modelling is a more robust means to deal with a complex system based on the fundamental laws of fluid dynamics.

In Chapter 2, general reviews are given on the ozone chemistry and ozonation process to provide the background for the subsequent chapters. Important reaction mechanisms and process unit operations are discussed. This converges to the crucial aspects in ozone reactor engineering where the current mode of operation is critically examined and the need for modelling as an engineering tool is discussed. This is then followed by the introduction to the mathematical modelling, a prelude to the fundamental principles of the CFD modelling.

In Chapter 3, the details of the hydrodynamics modelling of the ozone contactor are explained. The application of residence time distribution and the comparison between the simulated flow results and the experimental tracer test are discussed. In Chapter 4, the reaction kinetics of natural waters are discussed in view of the kinetics-related investigation. Chapter 5 describes the development of the kinetic modelling and its full-scale experimental verification. Chapter 6 explains the kinetics experiments involved in obtaining the relevant reaction rate constants. Each of the three chapters is distinctly defined by its own goals more specific to the particular investigation.

Lastly an overall conclusion and remarks on the final model and recommendations are given in Chapter 7.

1.6 References

AMCEN/UNEP (2003) *Africa Environmental Outlook* – past, present and future perspectives. Accessed on 21 August 2004 at URL http://www.unep.org/aeo/index.htm.

Anderson J.D. Jr. (1995) *Computational fluid dynamics – the basics with applications*. International edition. McGraw-Hill Inc., New York, ISBN 0-07-113210-4.

Bin A.K. and Roustan M. (2000) *Mass Transfer in Ozone Reactors*. Proceedings of the International Specialised Symposium IOA 2000, Toulouse, France, 1-3 March: 99-131.

Brouckaert C.J. and Buckley C.A. (2002) *The application of computational fluid dynamics to water and wastewater treatment plant*. WRC report no: 648/1/02, ISBN: 1-86845-857-1. Pretoria.

Brouckaert C.J., Huang T. and Buckley C.A. (2005) *Applications of computational fluid dynamics modelling in water treatment*. WRC report no: 1075/1/05, ISBN: 1-77005-271-2. Pretoria.

Do-Quang Z., Cockx A. and Liné A. (2000) *Recent advances in modelling tool development and application for ozone reactors design: The CFD approach*. Proceedings of the International Specialised Symposium IOA 2000, Toulouse, France. 1-3 March: 275-300.

Driedger A.M., Rennecker J.L., and Mariñas B.J. (2000) *Sequential inactivation of Cryptosporidium parvum oocysts with ozone and free chlorine*. Water Research 34 (14): 3591-3597.

DWAF (2003) *Strategic framework for water services*. Accessed on 2 October 2004 at URL http://www.dwaf.gov.za/Documents/Policies/Strategic Framework approved.pdf.

Friedrich E. (2001) *Environmental life cycle assessment of potable water production*. MScEng Thesis, Pollution Research Group, School of Chemical Engineering, University of Natal, Durban, South Africa.

Gyürék L.L., Finch G.R., and Belosevic M. (1997) *Modeling chlorine inactivation requirements of Cryptosporidium parvum oocysts*. Journal of Environmental Engineering **123** (9): 865-875.

Heyouni A., Roustan M. and Do-Quang Z. (2002) *Hydrodynamics and mass transfer in gas-liquid flow through static mixers*. Chemical Engineering Science **57** (16): 3325-3333.

Hoigné J. and Bader H. (1994) *Characterization of water quality criteria for ozonation processes. Part II: Lifetime of added ozone*. Ozone: Science & Engineering **16**: 121-134.

Lawler D.F. and Singer P.C. (1993) *Analyzing disinfection kinetics and reactor design: a conceptual approach versus the SWTR*. Journal of American Water Works Association **85** (11): 67-76.

Pryor M.J. and Freese S.D. (2000) *The treatment of eutrophic water using pre- and intermediate ozonation, peroxone and pica carbon*. WRC report No 694/1/00, ISBN: 1-86845-588-2. Pretoria.

Roache P.J. (1985) *Computational fluid dynamics*. Revised English edition, Hermosa publishers, Albuquerque, ISBN: 0-913478-05-9.

Umgeni Water (2002) Accessed on 6 June 2002 at URL http://www.umgeni.co.za

Umgeni Water (2003) *Annual Report: Technical and scientific statistics* 2001-2002.

UN (2003) *Millennium Declaration*. Accessed on 9 March 2003 at URL http://www.un.org/millennium/declaration/ares552e.pdf.

UN Statistics Division (2002) Accessed on 16 September 2004 at URL http://millenniumindicators.un.org/unsd/mi/mi_indicator_xrxx.asp?ind_code=30 and http://millenniumindicators.un.org/unsd/mi/mi_worldregn.asp.

UNEP (2000) *Global Environmental Outlook GEO-2000. Chapter 2: The state of the environment – regional synthesis*. Accessed on 8 August 2004 at URL http://www.unep.org/geo2000/english/0046.htm.

US EPA (1999) *Disinfection Profiling and Benchmarking Guidance Manual*. United States Environmental Protection Agency, Office of Water, EPA 815-R-99-013.

World Bank (2004) *Data and statistics: data profile tables*. Accessed on 3 December 2005 at URL http://web.worldbank.org/WBSITE/EXTERNAL/DATASTATISTICS/0,,contentMDK:20535285~menuPK:1192694~pagePK:64133150~piPK:64133175~theSitePK:239419,00.html.

World Resources Institute (2004) *Earth Trends: The environmental information portal*. Accessed on 4 February 2005 at URL http://earthtrends.wri.org/searchable_db/index.cfm?theme=2.

Zhu Q., Liu C. and Xu Z. (1989) *A study of contacting systems in water and wastewater disinfection by ozone. 1. Mechanism of ozone transfer and inactivation related to the contacting method selection*. Ozone-Science & Engineering **11** (2): 169-188.

2

LITERATURE

"Nothing in life is to be feared. It is only to be understood. Now is the time to understand more, so that we may fear less."

- Marie Curie (1867-1934), French (Polish born) chemist

Because of its high chemical activity, ozone has been widely applied in many types of the oxidative water treatment processes. Once ozone is dissolved, complex reactions take place that involve sequences of highly selective, *direct* reactions of the molecular ozone and those reactions of the more reactive but less selective hydroxyl radicals which are produced from ozone decomposition.

Practical experience and fundamental kinetic data have accumulated in recent years, enabling researchers and industry to predict the chemical transformation during ozonation. The parameters affecting the reactions are strongly dependent on the water composition and the ozone dosage. With the aims of achieving the disinfection or the oxidation goals of ozonation, knowledge of the contactor hydrodynamics is critical as it is associated with the ozone dosage and the contact time for the purpose of design and operational control.

In order to characterise the hydrodynamics of a contactor, the option of modelling has become more affordable due to the advances in computer technology. From **Section 1.3** , the use of CFD modelling is of particular interest as it combines the fundamental fluid dynamics laws and the reaction kinetics concepts developed to reveal the performance of a reactor. A unit operation such as an ozone contactor can be described by solving the partial differential equations (PDEs) of continuity, momentum, transport of species and the chemical reactions of ozone. Thus CFD models have also been known as the *deterministic* or *glass box* models, as opposed to the conventional *black box* approach.

Section 2.1 provides an introductory note on ozonation. **Section 2.2** gives the engineering aspects for the ozonation process; whereas **Section 2.3** discusses the fundamental aspects of the ozone chemistry. This is then followed by a series of discussion on flow dynamics and the related mathematical modelling: **Section 2.4** discusses the current principles of the ozone reactor engineering; **Section 2.5** provides the mathematical fundamentals of the modelling and some fundamental discussion of the use of CFD. Finally some concluding comments on the chapter are presented in **Section 2.6** .

2.1 Introduction

A significant amount of research has been given to the application of ozone in water and wastewater treatment. **Section 2.1.1** presents a brief historical note on the usage of ozone in water treatment.

Section 2.1.2 outlines the primary functions of ozonation. Section 2.1.3 discusses the roles of ozonation and the related process benefits. The effects of applying ozone in different stages of a water treatment works are discussed in Section 2.1.4 .

2.1.1 History of use

The use of ozone in the water treatment has been documented for over a century. The first tests of water disinfection by ozone were attained by De Meritens in 1886, 21 years after Marignac and Delarive achieved the transformation of pure oxygen into ozone (Le Paulouë and Langlais, 1999). The French chemist Marius Paul Otto obtained his Doctorate on ozonation from the Sciences Faculty of Paris in 1897, the first of its kind (Brink et al., 1991).

Initially the application of ozone in potable water treatment was in rapid growth predominantly in Western Europe. The first full-scale application of ozone in drinking water treatment was at Oudshoorn, Netherlands, in 1893 (Brink et al., 1991). The trend of ozone application could be observed from the locations of the full-scale ozonation facilities across various countries: Paris, France (1898); Wiesbaden, Germany (1901); Niagara Falls, New York (1903); Saint-Petersbourg, USSR (1905) and Madrid, Spain (1910). The application of ozone treatment became greatly inhibited due to the development of the less expensive chlorine during World War I (Brink et al., 1991). Chlorine, much like ozone, is an oxidant as well as a disinfectant which exhibits a longer half-life than ozone. However, chlorine also produces by-products, such as trihalomethanes (THMs) which cause health risks (Glaze, 1987). The need for reducing the free chlorine level in water has resulted in favour of ozone. Thus ozone became the focus again after World War II as the uses and the benefits of ozonation were gradually discovered.

France, in particular, was reported to have over 500 ozonation plants in operation, mostly for drinking water, by 1961 (Le Paulouë and Langlais, 1999). In Northern America, the spread of ozone application in water treatment only started in the 1980s. From 1977 to 1984, the number of ozonation plants grew from 5 to 20 in the United States, and from 23 to almost 50 in Canada (Glaze, 1987). By 1999, more than 200 water treatment works were using ozonation in the USA (Rice, 1999). Three medium-sized ozonation facilities have been reported to be in operation in South Africa by 1991 (Brink et al., 1991).

Ozone was initially utilised for disinfection and control of taste and odour. In recent years more diverse applications of ozone are being implemented since the traditional treatment processes (chemical coagulation, flocculation, filtration and slow sand filtration) are faced with difficulty to meet the stringent water legislation and standards.

2.1.2 Primary functions

Ozonation is employed in water treatment processes to achieve various functions. Brink et al. (1991) and US Environmental Protection Agency (US EPA, 1999) summarised the functions of ozonation as below:

- Inactivation of micro-organisms
    - Disinfection

- Algae control

- Oxidation of inorganic pollutants
  - Iron and manganese in particular
- Oxidation of organic micro-pollutants
  - Taste- and odour-causing compounds
  - Phenolic pollutants
  - Pesticides
- Oxidation of organic macro-pollutants
  - Bleaching of colour
  - Increasing biodegradability of organics
  - Reduction of trihalomethane formation potential (THMFP) and chlorine demand

Research in ozone chemistry has uncovered important mechanisms and in combination with the effort in the engineering aspect has led to achievement of the above goals.

2.1.3 Roles of ozone and its operational benefits

In potable water treatment, ozone is commonly applied as a primary disinfectant, an oxidant or as a precursor prior to other treatment steps.

Ozone is an effective biocide and achieves the same level of micro-organism inactivation at a lower dosage than other commonly used chemicals such as chlorine, chlorine dioxide and monochloramine (Korich et al., 1990; Finch and Lee, 1999). The inactivation of micro-organisms by ozone ranges from the least resistant bacteria, then viruses to the most resilient cysts (Camel and Bermond, 1998). For example, *Cryptosporidium parvum oocyst*, a coccidian intestinal parasite, has been known for their high resistance to free chlorine (Driedger et al., 2000) and thus pose difficulty to water treatment plants for their removal. Its presence in potable water has led to the outbreaks of diarrhoeal illness documented in Canada, the US and the UK (Hayes et al., 1989; Richardson et al., 1991; Mackenzie et al., 1994). Korich et al. (1990) found greater than 90% inactivation of *C. parvum* by treating oocysts with 1 $mg.L^{-1}$ for 5 min. To reach 90% inactivation, exposure to chlorine dioxide required 1.3 $mg.L^{-1}$ in concentration for 60 min. Using 80 $mg.L^{-1}$ of chlorine and 80 $mg.L^{-1}$ of monochloramine, the same degree of inactivation could only be achieved after 90 min. However, the disinfection use of ozone is limited by the lack of residual disinfectant capacity to prevent biological re-growth in the distribution network. In practice, ozone is coupled with a secondary disinfectant such as chlorine which can maintain a longer residual concentration in water (Rennecker et al., 2000; Driedger et al., 2000; Li et al., 2001). Algae blooms may develop in a warm, stable environment with high nutrient loads such as lakes and reservoirs. Certain types of algae are particularly sensitive to ozone. The most effective algae elimination is to first inactivate the

micro-organisms by oxidants such as ozone before physical removal by flocculation and filtration (Bablon et al., 1991b).

As a powerful oxidant, ozone has been found to be an effective means of oxidising inorganic pollutants such as iron and manganese. Iron and manganese ions are commonly found in raw water. When the concentrations in water exceed 0.3 and 0.05 $mg.L^{-1}$ respectively, the problems associated include staining of plumbing fixtures and laundered clothes, foul tastes and odour due to growth of iron bacteria in distribution network (Lin, 1993). The physicochemical treatments that are most commonly used involve an initial oxidation step to oxidise both ions into the respective insoluble forms, followed by filtration to remove the precipitates (Nieminski and Evans, 1993; McKnight et al., 1993). Conventionally aeration is employed for the oxidation step. Other oxidation methods using chlorine and potassium permanganate are also found.

Initially, as mentioned in **Section 2.1.1** , ozonation was applied to control the taste and odour of water. The taste- and odour-causing compounds are associated with many types of inorganic compounds such as iron; or organic compounds such as polysulfides, aldehydes and alicyclic alcohols. In most cases, odours and tastes are caused by organic compounds as a result of micro-organism metabolic products, industrial pollution, by-products formed in treatment and distribution networks. For instance, geosmin (1,10-trans-dimethyl-trans-9-decalol) and 2-methylisoborneol (2-MIB) are responsible for the earthy or musty taste and odours. The compounds can be detected at very low concentrations and are not easily removed by conventional water treatment processes (Glaze et al., 1990; Ho et al., 2002). Since the taste and odour problems are often transient and from multiple sources, it is not definitive in literature of which common oxidants are the most effective. However, ozone is capable of oxidising geosmin and 2-MIB without the addition of other oxidants such as $\cdot OH$ (Glaze et al., 1990). Ho et al. (2002) and Kim et al. (1997) also found ozone a more effective oxidant for taste- and odour-control. Kim et al. (1997) found geosmin removal of 70 % to 80 % can be achieved when treated with ozone, whereas only 30 % to 40 % was achieved in the conventional treatment.

Ozone is also used to treat synthetic organic compounds (biocides, hydrocarbons, dyes, phenols and solvents) and naturally occurring organic compounds (humic acids, fulvic acids and proteins). Often the synthetic compounds are toxic and not readily degraded in the conventional water treatment processes. For example, pesticides are often detected in raw water of the potable water treatment plant. Degradation of pesticides is hindered when other compounds present in the water source have higher oxidation rates or exist in larger quantity. Wilson et al. (1993) and Kang et al. (1997) both demonstrated the effectiveness of ozonation in improving the pesticide degradation. In practice, the oxidation or mineralisation of resistant compounds are enhanced when ozone is used in conjunction with hydrogen peroxide or ultraviolet light (Glaze et al., 1987; Trapido et al., 1997).

Process benefits have been reported that the addition of ozone enhances the operation of the subsequent treatment, although the actual mechanisms responsible may not be well-understood for all the benefits. Improvements in granular activated carbon (GAC) and sand filtration are partly attributed to the increase in biodegradability of organics due to oxidations (Mastronardi et al., 1993; Graham, 1999; Evans et al., 2003).

In ozonation of natural waters, organic compounds are reduced to lower molecular weight, which may enhance their adsorbability onto activated carbon (Camel and Bermond, 1998). Ozonation also increases the polarity of the organic compounds, which subsequently causes a decline in adsorption. Many studies have found that the ozone/GAC system outperformed the GAC system as the increase in biodegradability compensated for the lost of adsorbability. Vahala et al. (1998) found the removal of organic carbon was greater in ozonated waters. Boere (1992) also found the partial oxidation of dissolved organics by ozone led to changes in the adsorption behaviour and the enhanced biodegradation in the GAC columns.

Ozonation prior to coagulation-flocculation was also found to be beneficial (Bablon et al., 1991b; Jekel, 1994; Paralkar and Edzwald, 1996). There have been a number of postulates concerning the mechanism responsible for this phenomenon. Reckhow et al. (1986a) suggested that oxidation products become more polar (organic compounds) or insoluble complexes (metal ions). Other studies proposed that the enhancement was due to the polymerisation of the organic matter (Farvardin and Collins, 1989) which led to an increased association with aluminium. Furthermore it seemed that ozone could induce the destabilisation of particles coated with natural organic matter only in the presence of a complexing agent (e.g.: calcium) (Chandrakanth and Amy, 1996). An improvement in calcium complexation can lead to direct precipitation of the natural organic matter (Bablon et al., 1991). Amirsardari et al. (1997) investigated the turbidity and the removal of total organic carbon (TOC) by coagulation with and without ozone pre-treatment. Reduction in turbidity and TOC were significantly improved by ozonation (10 to 30%) depending on pH. However, Rencken (1994) found that ozonation was detrimental in the flocculation of algae even at low ozone doses. Such contradictory findings indicate that the mechanisms can be more complex and site-dependent.

Trihalomethanes (THMs) constitute the major disinfection by-products formed during final chlorination (Camel and Bermond, 1998). In raw waters, the predominant haloform precursors such as fulvic and humic acids are known for their oxidation by-products which initiate the formation of THMs upon chlorination (Bablon et al., 1991b). As it is well known that THMs can not be removed by chemical oxidation, their precursors must be destroyed or reduced before the final disinfection step. Numerous studies have shown the possible reduction in trihalomethane formation potential (THMFP) by ozonation as the reactivity of the humic substances towards chlorine decreases (Amy et al., 1986; Graham et al, 1994). In practice, ozone is often applied in conjunction with H_2O_2 and UV radiation, known as advanced oxidation processes (AOPs) to produce hydroxyl radicals. However, the results with AOPs can be uncertain as they are affected by the decomposition of ozone to $\cdot OH$, the balance between the creation and destruction of THM precursors, and the operating condition of the chlorination process (Bablon et al., 1991a; Reckhow et al., 1986b).

2.1.4 Points of application

Depending on the objective of the particular waterworks and the raw water quality, ozone can be applied in a single- or multiple-point manner during the treatment processes. In the United States, it is most common to apply ozone at the head of the waterworks, known as *pre-ozonation*, as a primary disinfection step. In Europe, ozone is commonly applied as the last stage of treatment process, known as *post-ozonation* (Bablon

et al., 1991b). Ozone can also be applied during any point in the waterworks in order to control algae growth within the plant, known as *intermediate-ozonation*.

Camel and Bermond (1998) summarised that pre-oxidation typically leads to the elimination of inorganic compounds, colour, turbidity and suspended solids, bad tastes and odours, and partly degrades natural organic matters and inactivate micro-organisms. Intermediate oxidation is intended to degrade toxic micropollutants, increase biodegradability and remove trihalomethanes precursors; whereas the post-oxidation aims to eliminate all remaining micro-organisms and minimise the disinfection by-product formation. Bablon et al. (1991b) provided a similar summary with slight difference in details. Table 2-1 outlines some of the ozone applications; however, the optimal point of ozone application will require a much more sophisticated investigation.

Table 2-1: Points of ozone application (Bablon et al., 1991b)

Control objective	Points of application	Required dose
Algae	Pre, Inter	Low-Med
Biodegradables	Inter	Med
Cl_2 by-products	Inter, Pre	Low-High
Colour	Inter	Med-High
Fe/Mn	Pre, Inter	Med
Particles	Pre	Low
Pathogens	Pre, post	Med-High
Taste and odour	Inter	High

Pre- or intermediate-ozonation reduces the demand of the subsequent secondary disinfectant in the final water (Jadashecart et al., 1991; Pryor et al., 1999).

2.2 Ozonation process

Ozone is usually produced on-line in an ozone generator fed with dried air or oxygen. Typical ozone concentrations achieved are in the range of 15 $g.kL^{-1}$ if air is the feed gas and may be increased up to 150 $g.kL^{-1}$ if oxygen is used (Hoigné, 1998). The transfer of ozone is accomplished by diffusing the ozone-containing gas into water. As a safety measure, the depleted gas is passed through a thermal or thermal/catalytic process to destroy the residual ozone which remains in the gaseous phase. An ozonation process in drinking water treatment must be effective using reasonably low ozone dose, at ambient temperature and the reaction times within a few minutes (Hoigné, 1998).

The major components of an ozonation system can be globally divided into the generation of ozone and the diffusion of ozone to water in treatment.

2.2.1 Ozone generation

The generation of ozone involves the dissociation of molecular oxygen into oxygen radicals which then reacts with the molecular oxygen to produce ozone (Glaze, 1987), as shown in Scheme 2-1.

$$O_2 \longrightarrow O\cdot + \cdot O \qquad [1]$$

$$\cdot O + O_2 \longrightarrow O_3 \quad [2]$$

Scheme 2-1: Ozone generation

Corona discharge is the most common method to produce ozone in water treatment. The ozone generating *unit* consists of a tubular grounded electrode and a dielectric double-tube lined with high potential electrodes. The cross-section view is presented in Figure 2-1.

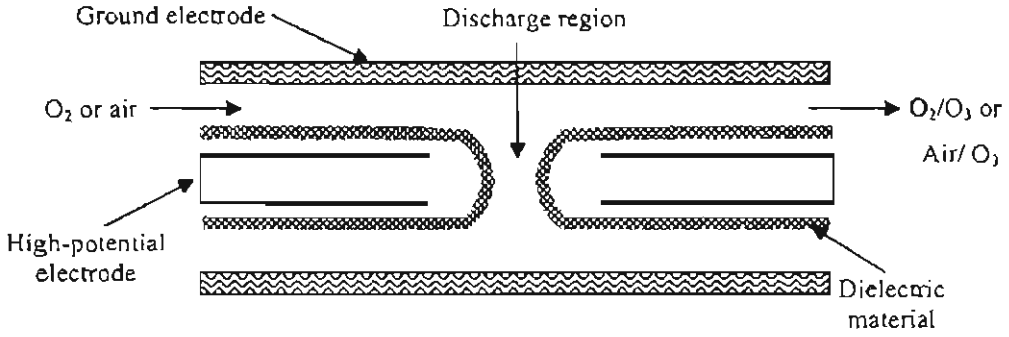

Figure 2-1: Ozone-generating unit (Bablon et al., 1991a; Glaze, 1987)

The electrode is usually a conductor coated on the inner surface of the dielectric material which can be either glass or ceramic. The feed gas (dry oxygen or air) passes through the discharge region while a silent electrical discharge (corona discharge) is supplied in an air gap between the charged electrodes (Hoigné, 1998). Electrons are accelerated to acquire sufficient kinetic energy such that they dissociate molecular oxygen into oxygen radicals for the reactions in Scheme 2-1 to take place (Bablon, 1991a). A cooling water jacket is fitted around the unit to prevent heat build-up and the thermal destruction of ozone.

Ozone production is inherently an inefficient process, with low yield and high energy consumption. Using the corona discharge process, Glaze (1987) reported that ozone is generated at concentrations of 1 to 3% for air as the feed gas, and 3 to 7% for oxygen. Undesirable reactions may occur as follows:

- Dissociated oxygen radicals may recombine to form molecular oxygen.
- High concentrations of oxygen radicals or electrons promote the destruction of ozone.
- Presence of moisture or organic impurities leads to the formation of nitrous and nitric acids which shorten the life of the dielectric or electrode material.

Ozonek and co-workers formulated an exergy model to analyse the energy utilisation efficiency on an industrial scale of ozone generation (Ozonek et al., 1997). The model indicated that most exergy losses are due to the energy losses in the compressor, the reduction valve, the reaction and heat exchange zones and in the cooling water pumps. The applied electrical energy used in the generation of ozone does not exceed 10% or 20 % when the feed gas is air or oxygen respectively (Ozonek et al., 1997).

2.2.2 Diffusion systems and ozone contactors

Ozone transfer is achieved by direct contact of water and the ozonated gas. A number of techniques are available to maximise the dissolution process by increasing the contact area. These techniques and their advantages and disadvantages are tabulated in Table 2-2.

Table 2-2: Comparison of various contacting systems (Bin and Roustan, 2000; Bablon et al., 1991b)

Types	Advantages	Disadvantages
Conventional fine bubble diffusion	• Good transfer efficiency	• Deep contactor basin required
	• Low maintenance	• Possible clogging of diffusers
	• Low hydraulic loss	• Large head loss
Turbine mixers	• High transfer efficiency without deep basin	• Energy is required
	• No clogging	• Possible maintenance problems of submerged parts
Injector		
Packed columns	• Resembles plug flow	• Limited application
	• Reduced gas pressure	• Possible scale build-up
Other systems:		
Deep U-tube	• High transfer efficiency	• Limited experience
	• Smaller area required on-site	• Construction cost

The fine bubble diffuser contactor is the most widely used system for ozone transfer because it is operated without addition of energy input (Bablon et al., 1991b). The gas phase is usually dispersed as bubbles (2 or 3 mm diameter) by porous ceramic diffusers placed at the bottom of the contactor (Bin and Roustan, 2000).

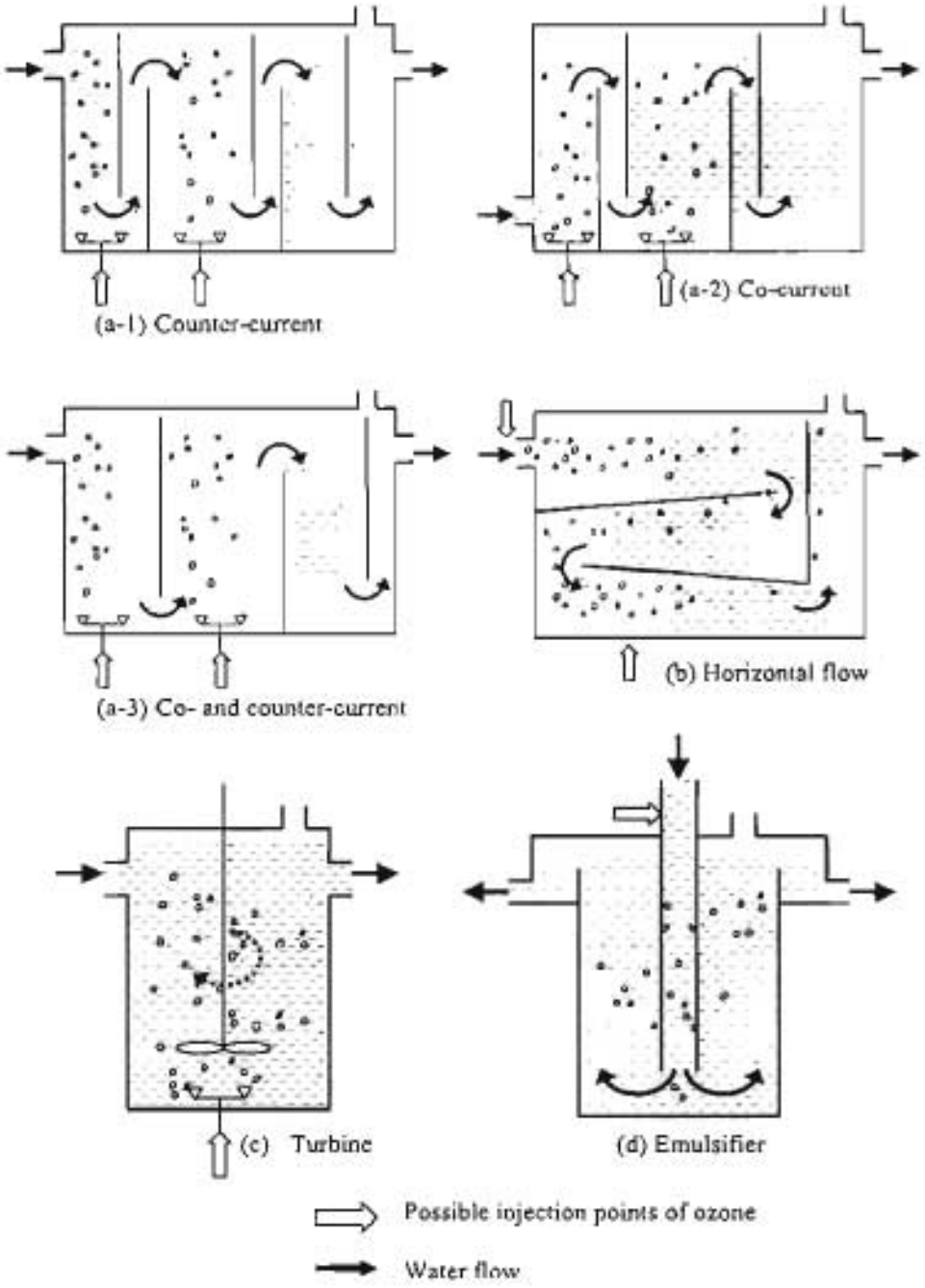

Figure 2-2: Some designs of ozone contactors: (a-1) to (a-3) US EPA (1999); (b) to (d) adapted from Legeron (1982)

There are several contactor configurations, baffle arrangements and flow patterns available as illustrated in Figure 2-2 (a-1) to (a-4). From (a-1) to (a-3) the gas flow is identified to be counter-current against the water flow, co-current with the water flow, or both co- and counter-current to the water flow; whereas (a-4) shows a horizontal arrangement of water flow.

Turbine contacting systems (Figure 2-2 (b)) is more appropriate when a high ozone dose is necessary (Bin and Roustan, 2000). The rotating elements are generally located above and close to the gas sparger so that the gas is dispersed evenly and the water is well-circulated. The main design requirement is to maintain a

constant gas flow rate, irrespective of the water flow rate (Bablon et al., 1991). The ramification includes the cost issue as the energy consumption is constant regardless of the water flow rates, and the transfer efficiency problems as the efficiency decreases with decreasing gas-to-liquid ratio (Bablon et al., 1991).

Ozonated gas can be injected into the liquid stream under pressure. Because of the short contact time, the use of injectors or static mixers is typically followed by a reaction vessel to attain the desired detention time. An example using this device is the Choisy-le-Roi water treatment where the contact column is equipped with an emulsifier, i.e., the injector is situated at the top of vertical dissolution tubes (shown in Figure 2-2 (d)).

Martin and Galey (1994) found high ozone transfer efficiency using a static mixer followed by a plug flow reactor at laboratory-scale, similarly to the arrangement made in the pre-ozonation system at the Wiggins Waterworks. They found the dissolution of ozone is achievable in a very short contact time (15 s) and the ozone transfer rate was obtained at a high-water-flow with low-gas-flow. It is thus possible to carry out the operation in a short contact time and still account for the oxidation and disinfection. The efficiency of the static mixer was also found to be higher than other gas-liquid mixing mechanisms, which was supported by various literature references (Heyouni et al., 2002). This was also found earlier by Zhu et al. (1989) who demonstrated a greatly enhanced ozone mass transfer rate using a static mixer compared to a bubble column.

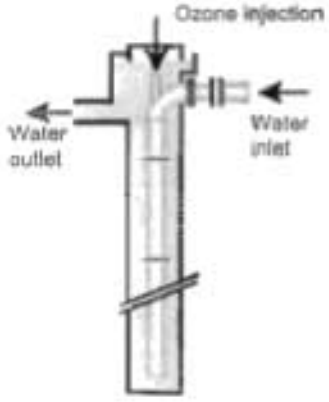

Figure 2-3: An industrial Deep U-tube (Bin and Roustan, 2000)

Another design of ozone contactor is the Deep U-Tube which is a patented design by Lyonnaise des Eaux, a French water treatment company now known as Viola. The design consists of two vertical concentric tubes of approximately 20 m in depth. Water flows downward through the inner tube and ozone is injected through an orifice into the water stream near the top of the inner tube and travels downward with the flow of water (Figure 2-3).

In general, ozone contactors are gas-liquid reactors employed in water treatment, primarily due to the large interfacial area for the mass transfer to occur (Cockx et al., 1999) and also due to the ease of adjusting the residence time for the subsequent ozone reactions to occur (Ekambara and Joshi, 2003). The design of ozone reactors is based on the knowledge of kinetic data, parameters of the gas-liquid transfer and the

hydrodynamic behaviour which has strong dependence on the contactor configuration and operating conditions of systems (Do-Quang et al. 2000).

2.2.3 Ozone destruction

The management of ozone off-gas destruction is generally considered as an additional but important subcomponent to the main ozonation system. Ozone which still remains in the off-gas is at the risk of being emitted to the atmosphere. The process structure and personnel must be protected from possible exposure to high levels of ozone. In a conventional ozone contactor (discussed in **Section 2.2.2**) the off-gas from upstream chamber may contain as much as 0.2 to 0.5 $g.kL^{-1}$ (Bellamy et al., 1991). The maximum allowable concentration of ozone in air varies amongst different countries. The limit is typically < 200 $\mu g.kL^{-1}$ (about 0.1 ppm (v/v)) for an 8-hour working day (Hoigné, 1998). Hence ozone concentration in the off-gas can greatly exceed the maximum allowable limit.

Currently the most common methods are thermal destruction, catalytic and combined thermal/catalytic systems. The thermal destruction systems depend on ozone decomposition at elevated temperatures. The half-life of ozone in dry air may vary from 20 to 100 h at room temperature, which is drastically reduced to 11 to 112 min at 120 °C. The half-life is further decreased to a mere 0.04 to 0.4 s at 250 °C (Bellamy et al., 1991). Ozone is heated in a thermal destruction unit to about 300 to 350 °C. The catalytic or the combined systems make use of a catalyst to achieve a lower operating temperature. Catalytic destruction systems rely on the metal, metal oxides, hydroxide and peroxides for their ability to decompose ozone. Since moisture condensation on the catalyst can greatly reduce the catalyst performance, a heating chamber is usually required to raise the water-saturated off-gas temperature above its dew point (Bellamy et al., 1991).

2.2.4 Instrumentation and control systems

There are a number of functions of ozonation in water treatment, as discussed in **Section 2.1.2** . Control methods depend on the particular ozone application and the measurement techniques and devices. Continuous control systems may focus on one or more of the following criteria:

- Ozone production
- Ozone residual concentration
- Off-gas ozone concentration
- Water flow rate
- Specific water quality parameter(s)

The power of the ozone generator can be varied to produce the ozone required without changing the gas throughput (Bablon et al., 1991b). However, adjusting the ozone generator to match the required ozone dose is not favoured. It is more common to change the gas flow rate, which is at a fixed ozone concentration, to be proportional to the water flow in order to attain the desired ozone dose.

The concept of ozone dose control through the measurements of the off-gas ozone concentration was originally developed for wastewater disinfection where maintaining ozone residual is difficult and fouling of the residual ozone sensors frequently occurs (Bablon et al., 1991b).

If specific water quality parameters are monitored to achieve the objective of ozonation, the basic sensor in the control system is an analyser which measures one or more target compounds (Bablon et al., 1991b). This type of control is not widely applied due to the lack of availability of such a sensor designed for continuous measurements.

A more common control system is to maintain the ozone residual to a pre-determined value. This can be achieved by a dissolved ozone analyser and the residual recorded is compared to a set value (Liechti, 2000; Bablon et al., 1991). Alternatively, the control system can be designed as a cascade system which initially adjusts the ozone dose to the water flow rate and the secondary control trims to the correct treatment rate according to the ozone residual level.

This raises the issue of choosing an appropriate position to measure the ozone residual, since the dissolved ozone concentration can vary greatly from the dosing point to the sampling point (Kilham, 2002). In an optimised system, ozone is often measured in one of the three points: at the injection point; at the contactor vessel; or at the exit of the system (before the thermal destruction unit). The measurement of an ozone residual concentration is critical as the value provides information on (Kilham, 2002):

- The upstream units – whether the units are all working, including the ozone generator
- An indication on the level of the ozone transfer efficiency
- The likelihood of whether the targeted contaminants have been destroyed.

It is clear that an effective control system relies greatly on the measurement techniques of the dissolved ozone. The next section will discuss general consideration of ozone residual sampling.

2.2.4.1 Residual sampling

It should be noted that most methods for dissolved ozone measurement are modifications of chlorine residual methods that determine the total oxidants in the solution (Bablon et al., 1991b). Since ozone and the secondary oxidants produced as a result of oxidation by-products are powerful oxidising agents, specific analytical technique must be selected with care. Reagents used for dissolved ozone concentration are often oxidised by ozone or its oxidation/decomposition products. This can cause interferences affecting the dissolved ozone measurements (Bablon et al., 1991b).

Rakness et al. (2000) and Bablon et al. (1991b) have discussed the residual sampling to a great extent. Both stressed that the sample handling time must be minimised, as ozone found at the pH in most water is subjected to continuous rapid decomposition.

For an on-line sensor, the ozone *loss* due to decay in the sampling line must be reduced in order to obtain near real-time response (Rakness et al., 2000). The sampling detention time should be short enough to ensure that the measured residual is at least 90% of the actual residual inside the contactor (Figure 2-4).

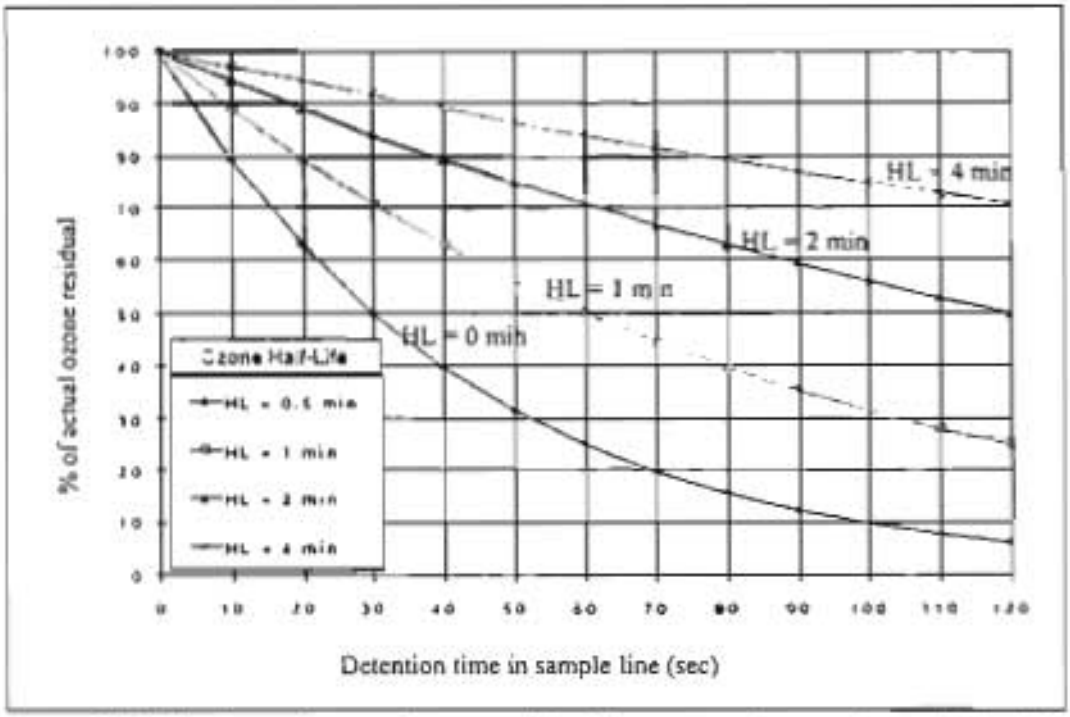

Figure 2-4: Reductions of measured ozone residual due to ozone decay and sample line HDT (Rakness et al., 2000, p242)

On a full-scale ozonation plant, commercial sensors are currently available to measure the ozone residual. Additional equipment may be necessary if a point within the contactor is required.

2.3 Ozone chemistry

Ozone (O_3) was initially detected by its characteristic pungent odour and the name was derived from the Greek word $o\zeta\varepsilon\iota\nu$ (*ozein*), meaning *to smell*, by Schönbein in 1840 (Greenwood and Earnshaw, 1984b; Brady and Holum, 1993). The O_3 molecule has a bent geometry and is described as a resonance hybrid of four canonical forms of dipolar character shown in Figure 2-5.

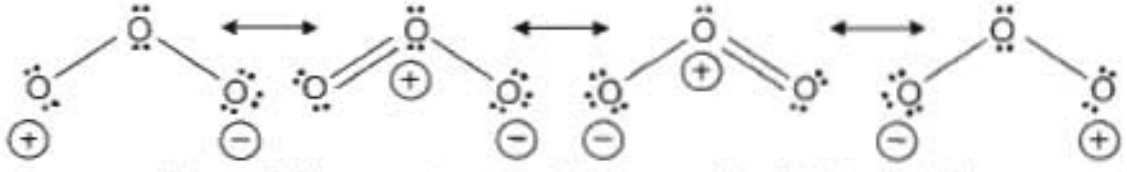

Figure 2-5: Resonance structures of the ozone molecule (Hoigné, 1998)

In Figure 2-5, all structures consist of two σ bonds and one delocalised π bond in which the orbital is stretched over the three oxygen atoms (Greenwood and Earnshaw, 1984b). These structures also indicate the strong electrophilic or electron-deficient nature of ozone where one end of the ozone structure has six electrons (Nebel, 1981). The selectiveness of molecular ozone reactions is attributed to this end-standing electrophilic O-atom.

2.3.1 Chemical and physical properties

At room temperature ozone is a blue gas, diamagnetic and unstable. It is readily detectable at concentrations as low as 0.02 to 0.05 ppm (v/v) and appears colourless in dilute form (US EPA, 1999). When the concentration reaches 240 $\mu g.kL^{-1}$ in air, it is considered a nasal toxicant at the lowest observable level (Hoigné, 1998).

Ozone has a high standard reduction potential in both acidic and basic media (Brady and Holum, 1993). Scheme 2-2 shows the tendency of ozone to transfer an oxygen atom during reaction, producing oxygen gas.

$$O_{3(g)} + 2H^{+}_{(aq)} + 2e^{-} \rightleftharpoons O_{2(g)} + H_2O \qquad E^{\circ} = +2.08V$$

$$O_{3(g)} + H_2O + 2e^{-} \rightleftharpoons O_{2(g)} + 2OH^{-}_{(aq)} \qquad E^{\circ} = +1.24\ V$$

Scheme 2-2: Redox potential of ozone (Brady and Holum, 1993)

This high reactivity makes ozone a health hazard, for example, as a pollutant in smog. Exposure to ozone at a level of 1.0 $\mu g.kL^{-1}$ for over 10 min is dangerous for all people (Brady and Holum, 1993). When applying this high reactivity appropriately, ozone is a powerful oxidising agent. Amongst the commonly used chemicals in water treatment, ozone is only second to the hydroxyl free radical, OH•, in terms of the oxidation ability (US EPA, 1999). Therefore any unutilised ozone in the gas stream requires further treatment (such as a destruction facility) before releasing the spent gas to atmosphere.

Ozone is generated in gaseous form. The mechanism and equipment of ozone generation was discussed in **Section 2.2.1** (page 2-6). Therefore ozone must be dissolved before aqueous reactions can take place. The solubility characteristics of ozone have been studied extensively (Roth and Sullivan, 1981; Bablon et al., 1991a; Rischbieter et al., 2000). In literature, the solubility data are commonly reported either in terms of the solubility, S, or as an absorption coefficient, β. Both are related to the dissolved concentration of ozone in water at saturation, C_{sat}.

S is often expressed as the so-called solubility ratio as milligrams per litre of ozone in water to milligrams per litre of ozone in gas (Bablon et al., 1991a). β, also known as Bunsen absorption coefficient, is the volume of gas expressed at NTP, dissolved at equilibrium by a unit volume of liquid at a given temperature when the partial pressure of the gas is the unit atmosphere (Bablon et al., 1991a). In general, ozone dissolution is accepted to follow Henry's law, shown in Eqn. (2-1):

$$P_j = Hx_j \qquad \textbf{(2-1)}$$

where P_j is the partial pressure of the solute, j, in the gas phase, expressed in atmosphere (atm); H is called the Henry's law constant, in units of atm.mole fraction^{-1}; and x_j is the mole fraction of the solute in the liquid phase.

The dissolved ozone concentration is related to the ozone partial pressure at thermodynamic equilibrium (Lee et al., 1999). Thus C_{sat} can be related to the partial pressure of ozone P_j at a given temperature. Under thermodynamic ideality, the expression for the C_{sat} in $kg.kL^{-1}$ can be written as:

$$C_{sat} = \beta M P_i \quad (2\text{-}2)$$

where M is the density of gas at standard temperature and pressure (2.14 $g.L^{-1}$ for ozone).

Hence the solubility data of gases are also found to be reported in the Henry's law constant. Data of the common water treatment oxidants using air, oxygen (in aeration) or chlorine (Cl_2), chlorine dioxide (ClO_2) (in chlorination) are compared to the values of ozone in Table 2-3.

Table 2-3: Solubility data of various gaseous oxidants (Liley et al., 1997; Bablon et al., 1991a)

Gaseous oxidants	β	C_{sat}	H at 20°C
	v/v	$mg.L^{-1}$ for $P_i = 1$	(atm.mol fraction^{-1})
Air	-	-	66400
Chlorine	4.54	14400	1.773 g $Cl_2.L^{-1}$ at 100 mmHg
Chlorine dioxide	± 60	180000	4.3g $ClO_2.L^{-1}$ at 5% by vol.
Oxygen	0.049	70	4001
Ozone	**0.64**	**1400**	**3760**

Ozone is sparingly soluble in water ($\beta = 0.64$) but more soluble than oxygen ($\beta = 0.049$). At 100% ozone, only 1400 $mg.L^{-1}$ is achieved at saturation; whereas chlorine, under the same condition, is about 10 times more soluble.

Roth and Sullivan (1981) and Rischbieter et al. (2000) have critically reviewed the experimental data on ozone's solubility in water and both found the data considerably scattered. This can be attributed to the decomposition of ozone, pH or temperature of the water. Table 2-4 listed values of the Henry's constant of ozone reported in literature at various temperatures. Although some incongruence of the data may have been contributed by the earlier, less accurate analytical methods (Roth and Sullivan et al., 1981), the dependence of solubility on the temperature can still be marked.

Table 2-4: Effect of temperature on ozone solubility (Bablon et al., 1991a; Roth and Sullivan, 1981)

	H (atm.mole fraction^{-1})					
Temperature (°C)	0	10	20	25	30	40
Kawamura (1932)	-	3400	4610		6910	9520
Strumm (1958)	-	3150	-	3930	4530	-
Kirk-Othmer (1967)	2590	3330	4370	-	6210	8500
Bablon et al. (1991a)	1940	3190	4610	6555	8302	-

The scattering of data can also be attributed to experimental difficulties related to the decomposition of ozone which also depends on a number of variables such as pH (Rischbieter et al., 2000). However the effect of pH is often suppressed by using a buffered aqueous system in order to measure the effect of temperature. In literature, the combination of temperature and pH or the temperature alone constitute the input variables to the prediction of Henry's constant of ozone.

2.3.2 Reactions

Ozone reactions in water are generally known to be complex. Figure 2-6 depicts that dissolved ozone undergoes reactions with various dissolved compounds (M) in two ways:

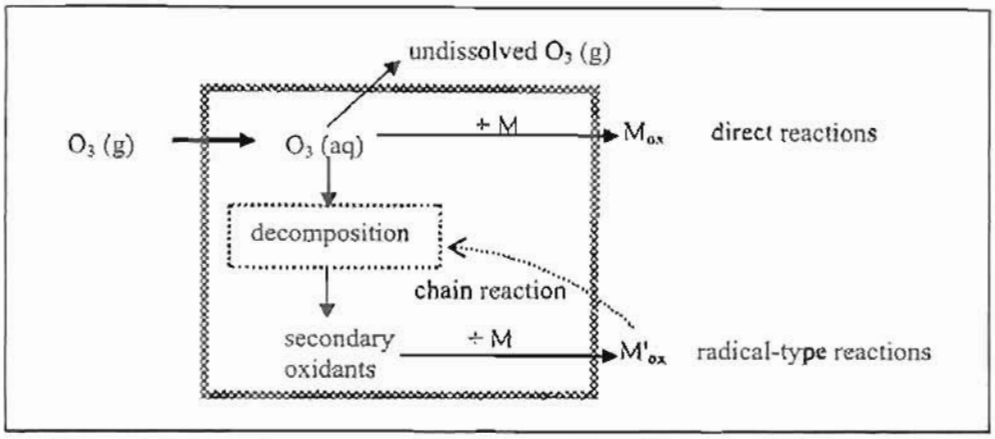

Figure 2-6: Aquatic ozone reactions (adapted from Hoigné and Bader, 1983a)

- Direct reactions: with molecular ozone; *selective* reactions to give Mox as the oxidation product.
- Radical-type reactions: with secondary oxidants; extremely fast (in μs scale) but less selective reactions to generate M'ox as the oxidation product.

The dashed arrow signifies the chain reaction induced by some oxidation products which catalyse the ozone decomposition.

The kinetics of the ozone reactions are typically first-order with respect to ozone and first-order with respect to the dissolved compound. Therefore the rate equation can be written as (Hoigné and Bader, 1983a; Bablon et al., 1991a):

$$O_3 + M \longrightarrow \text{Products} \qquad (2\text{-}3)$$

$$-\frac{d[O_3]}{dt} = k_{O_3}[O_3][M] \qquad (2\text{-}4)$$

Ozone decomposes during the ozonation process and transforms into secondary oxidants such as •OH , the hydroxyl radical. These are highly reactive oxidants but are generally consumed in a fast and non-selective manner. For examples, almost all dissolved organic compounds present act as an OH sink. This renders the radicaly-type reactions to be relatively inefficient for oxidising target compounds which may be present at very low concentration.

In natural waters, these aquatic reactions are affected by various parameters such as pH, temperature and dissolved compounds in the water matrix. In the treatment process, ozone is generated in the gaseous form which requires dissolution methods prior to its aquatic reactions (as depicted in Figure 2-6). Therefore the complexity of reactions is compounded due to the influence of mass transfer of ozone to water. The classification of ozone reactions in literature often incorporates parameters to account for the effect of mass transfer (Beltrán, 1995). The rate of ozone transfer may become a limiting factor when ozone is consumed quickly. However, in the present investigation, the transfer of ozone is assumed to occur mainly in the static mixer before the combined flow of water and the ozone-containing gas reaches the contactor (see **Section 1.2.2**). The present section will thus focus only on the intrinsic kinetics relating ozone to other constituents in the water matrix. The effects of mass transfer will be briefly discussed in Section 2.4.2 .

The kinetics of ozone decomposition is outlined in **Section 2.3.2.1** . An extensive list of ozone reactions with prescribed compounds can be found in literature. For the purpose of this thesis, only the pertinent categories of compounds in the respective ozonation functions (discussed in **Section 2.1.2**) will be discussed.

2.3.2.1 Decomposition

Ozone decomposition occurs through a series of reactions, resulting in the formation of short-lived radical species (Bablon et al., 1991). While ozone reacts more selectively with certain constituents in water, other radicals are responsible for the less restricted reactions. Various reaction mechanisms have been postulated for the decomposition of ozone.

The Hoigné, Staehelin and Bader Mechanism (Bablon et al., 1991a) presents a consistent set of chain reactions, which accounts for initiation, propagation and break-in chain reactions for ozone decomposition at *near neutral* pH values.

Initiation step	$O_3 + OH^- \xrightarrow{k_1} \cdot HO_2 + \cdot O_2^-$	$k_1 = 7.0\times10^1 \ \left(M^{-1}.s^{-1}\right)$	[1]
Propagation steps	$\cdot HO_2 \rightleftharpoons \cdot O_2^- + H^+$	$pK_a = 4.8$	[1']
	$O_3 + \cdot O_2^- \xrightarrow{k_2} \cdot O_3^- + O_2$	$k_2 = 1.6\times10^9 \ \left(M^{-1}.s^{-1}\right)$	[2]
	$\cdot O_3^- + H^+ \underset{k_{-3}}{\overset{k_3}{\rightleftharpoons}} \cdot HO_3$	$k_3 = 5.2\times10^{10} \ \left(M^{-1}.s^{-1}\right)$	[3]
		$k_{-3} = 2.3\times10^2 \left(s^{-1}\right)$	
	$\cdot HO_3 \xrightarrow{k_4} \cdot OH + O_2$	$k_4 = 1.1\times10^5 \ \left(s^{-1}\right)$	[4]
	$O_3^- + \cdot OH \xrightarrow{k_5} \cdot HO_4$	$k_5 = 2.0\times10^9 \ \left(M^{-1}.s^{-1}\right)$	[5]
	$\cdot HO_4 \xrightarrow{k_6} \cdot HO_2 + O_2$	$k_6 = 2.8\times10^4 \ \left(s^{-1}\right)$	[6]
Termination steps	$\cdot HO_4 + \cdot HO_4 \xrightarrow{k_7} H_2O_2 + 2O_3$	$k_7 = 5.0\times10^9 \ \left(M^{-1}.s^{-1}\right)$	[7]
	$\cdot HO_4 + \cdot HO_3 \xrightarrow{k_8} H_2O_2 + O_3 + O_2$	$k_8 = 5.0\times10^9 \ \left(M^{-1}.s^{-1}\right)$	[8]

where M is the molar concentration ($mol.L^{-1}$)

Scheme 2-3: HSB mechanism of ozone decomposition (Bablon et al., 1991a).

In *pure water*, these radical reactions are initiated by the reaction of ozone with the hydroxide ions, OH^- (Staehelin et al., 1984). From the rate constant values, it can be seen that the free-radical initiating step is the rate-determining step in the mechanism. Moreover the generation of hydroperoxide radical $\cdot HO_2$ and superoxide radical $\cdot O_2^-$ in Scheme 2-3[1] from the hydroxyl ion OH^- indicates the stoichiometry is unity and other species capable of consuming the hydroxyl ion without generating the two radicals bring stability on the ozone molecule in water (Bablon et al., 1991a).

However, the HSB mechanism shown in Scheme 2-3 introduces some transient compounds, $\cdot HO_3$ and $\cdot HO_4$ as chain intermediates. Although Staehelin and co-workers demonstrated the existence of $\cdot HO_4$ with the aid of computer simulation (Staehelin et al., 1984), this postulated species has not been

measured directly (Bablon et al., 1991a; Westerhoff et al., 1997). The validity of the model also depends on a controversial equilibrium value for the ozonide radical, $\cdot O_3^-$ (Westerhoff et al., 1997).

$$O_3 + OH^- \xrightarrow{k_1} \cdot HO_2^- + O_2 \qquad k_1 = 4.0\times10^1 \left(M^{-1}.s^{-1}\right)$$

Scheme 2-4: Initiation step of the TGF mechanism

Tomiyasu, Gordon and Fukutomi, have proposed another reaction scheme (the TGF mechanism) that involves a two-election transfer process or an oxygen atom transfer from ozone to OH^- (Bablon et al., 1991a) (shown in Scheme 2-4), as opposed to the one-electron transfer in the HSB model.

The TGF model does not include the postulated intermediates as in the HSB model. However, the mechanism proposed in the TGF model was only verified experimentally in *basic* medium (Tomiyasu et al., 1985; Westerhoff et al., 1997) and further experimental work may be necessary to demonstrate its validity.

Both mechanisms indicate the decomposition increases with alkalinity as ozone is initiated only by OH^- (Staehelin et al., 1984; Tomiyasu et al., 1985). Staehelin and Hoigné (1982) found that O_3 decomposition was slow due to the accumulation of H_2O_2 at pH below 8 and the rates were measurable if pH was below 10. At pH above 10, decomposition was extremely fast.

The decomposition is also dependent on temperature. At pH 7, the rate increases with increasing temperature from 10 to 40 °C and becomes exceedingly fast when the temperature is above 30°C and at a pH above 8 (Sotelo et al., 1987).

In non-pure water, ozone decomposition may also be affected by the type of solute present in water (Staehelin and Hoigné, 1985; Bablon et al., 1991a). Inorganic compounds (such as OH^-, $\cdot HO_2$ and some cations) and organic compounds (such as glyoxylic acid, formic acid and humic substances) and ultraviolet radiation at 253.7 nm are all capable of inducing the formation of $\cdot O_2^-$ (Bablon et al., 1991a), which assist in the initiation step in Scheme 2-3, reaction [1].

Some inorganic (e.g.: phosphate species) and organic (e.g.: primary alcohols, humic acids) act as the promoters of the free-radical reaction. They regenerate the superoxide anion, $\cdot O_2^-$, from OH^-. On the other hand, those compounds which scavenge OH^- without generating the chain carrier $\cdot O_2^-$ are called the inhibitors to the chain reactions. Some common inhibitors include bicarbonate and carbonate ions, tertiary alcohols (e.g.: *tert*-butyl alcohol), alkyl groups and humic substances (denoted as HS in Figure 2-7) (Staehelin and Hoigné, 1985) which consume OH^- but do not produce the chain intermediates. Such solutes quench the radical-type chain reaction and in some way stabilise the aqueous ozone (Hoigné, 1998). The overall mechanism in non-pure water is shown in Figure 2-7.

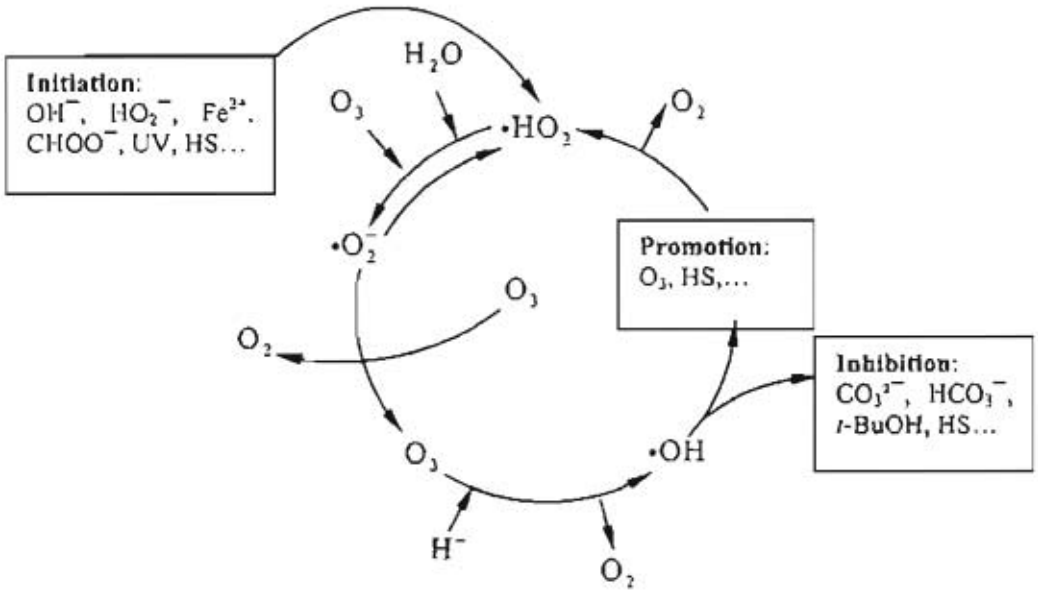

Figure 2-7: Mechanism diagram of ozone decomposition induced by radical-type reaction (Bablon et al., 1991a)

Various rate equations have been suggested for the decomposition of ozone. Since the strong influence of OH^- was observed in the mechanisms discussed, the reaction order is often related to OH^- as well as O_3. Values of the reaction order with respect to ozone typically ranges from 1.5 ~ 2 in acidic environment to 1.5 ~ 1 in basic medium; with respect to hydroxide ion from 0 to 1 (Sotelo, 1987).

Most natural waters that undergo ozonation contain other solutes which may compete with ozone to react with OH^- (Hoigné, 1998). The reaction products also oxidise further by oxygen to form peroxy and oxy radicals, and eventually release $\cdot O_2^-$ or $\cdot HO_2$ or H_2O_2.

In summary, the decomposition of aqueous ozone occurs more rapidly at higher pH or in presence of elevated concentrations of compounds which behave as the initiators or the promoters in the radical-type reaction scheme. The rate is impeded when pH is decreased or compounds which scavenge OH^- but do not produce chain-carrier radicals, such as bicarbonates.

2.3.2.2 Inorganic compounds

In general, the reaction of ozone with inorganic compounds present in water follows a first-order kinetic law with respect to ozone and the compound itself as described by Eqn. (2-4). The rate constants are affected by pH as many inorganic solutes are only reactive when not protonated (Hoigné et al., 1985). A selected range of inorganic compounds that pose problems in the water treatment effort will now be discussed in more detail.

Reactions with iron and manganese. Iron and manganese are two of the most abundant elements present in nature. Both iron and manganese exist in water in the reduced forms (Fe^{2+} and Mn^{2+}) which are soluble and cause unpleasant effects of staining and colouring (Lin, 1993).

The removal of iron and manganese are usually achieved by oxidising the ions into the respective insoluble forms as indicated in Scheme 2-5.

$$2Fe^{2+} \xrightarrow{O_3 \rightarrow O_2} 2Fe^{3+} \xrightarrow{H_2O} Fe(OH)_3 \downarrow \quad 0.43 \text{ mg } O_3/\text{mg Fe}$$

$$Mn^{2+} \xrightarrow{O_3 \rightarrow O_2} Mn^{4+} \xrightarrow{H_2O} MnO_2 \downarrow \quad 0.88 \text{ mg } O_3/\text{mg Mn}$$

Scheme 2-5: The oxidation reaction of iron and manganese with ozone (Bablon et al., 1991a; Bablon et al., 1991b)

Iron can be easily oxidised by ozone directly as shown in Scheme 2-6 [1]; by the hydroxyl radical from the ozone decomposition product [2]; or possibly react with the ozonide, $\cdot O_3^-$ [3].

$$Fe^{2+} + O_3 \longrightarrow Fe^{3+} + \cdot O_3^- \quad [1]$$

$$Fe^{2+} + \cdot OH \longrightarrow OH^- + Fe^{3+} \quad [2]$$

$$Fe^{2+} + \cdot O_3^- + H_2O \longrightarrow Fe^{3+} + O_2 + 2OH^- \quad [3]$$

Scheme 2-6: Mechanism responsible for the oxidation of iron by ozone and its related products

The removal of manganese is more difficult than iron as indicated from the stoichiometry in Scheme 2-5. Per unit manganese requires approximately double the amount of ozone (0.88 mg) as iron (0.43 mg) (refer to Scheme 2-5). The oxidation of manganese can be severely impeded when other substances in water exhibit faster rates of ozone consumption.

Reactions with reduced non-metal species. Although it is thermodynamically possible for the halides to be oxidised by ozone, the reaction rate varies greatly from very fast for iodides to negligible in the case of chlorides (Hoigné, 1998; Bablon et al., 1991). The rapid reaction of ozone with iodide shown in Eqn. (2-5) is often applied for the analysis of ozonated solution when the concentration is high.

$$O_3 + 2I^- + H_2O \longrightarrow O_2 + I_2 + 2OH^- \quad (2\text{-}5)$$

Free bromine (Br_2), hypobromite (BrO^-), free iodine (I_2), hypoiodite ion (IO^-) and iodate ion (IO_3^-) are some of the halogen-containing oxidants that can be produced when bromide or iodide ions are present in ozonated waters (Bablon et al., 1991a). Apart from these oxidants, the presence of bromide ion in the raw water or the use of chlorine as a secondary disinfectant can lead to the formation of halogenated disinfection by-products (DBPs). The halogenated DBPs such as trihalomethanes and haloacetic acids are suspected to be carcinogens and are therefore a health concern (Pryor and Freese, 2000). In particular, the brominated DBPs appear to pose a greater health risk than non-brominated DBPs (US EPA, 1991). Ozone has been found to be effective in reducing the DBPs precursors (Richardson et al., 1999; US EPA, 1991).

Ozone reacts with the inorganic forms of sulphur fairly fast. The reaction rates decrease with the degree of anion protonation (Bablon et al., 1991). Sulphide is oxidized to sulfate by the general reaction shown in Eqn. (2-6). This reaction is of importance when treating sulphide-containing groundwater.

$$S^{2-} + 4O_3 \longrightarrow SO_4^{2-} + 4O_2 \quad (2\text{-}6)$$

Ammonia can be oxidised by the following reaction in Eqn. (2-7)):

$$NH_3 + 4O_3 \longrightarrow NO_3^- + 4O_2 + H_3O^+ \quad (2\text{-}7)$$

The rate of reaction is very slow and it decreases with pH due to the protonation of ammonia as ammonium ion (Hoigné, 1998). The ozonation of surface waters may enhance the nitrification of ammonia as the organic compounds are converted into more biologically degradable types.

2.3.2.3 Organic compounds

Ozone reacts with dissolved organic pollutants, natural or synthetic. In general, ozone reactions with the substrate M_{org} are first-order with respect to M_{org} and ozone:

$$-\frac{d[O_3]}{dt} = k_{O_3,org}[O_3][M_{org}] \quad (2\text{-}8)$$

The reactivity of a target pollutant must be high in order for degradation to occur. For organic pollutants, the functional groups in their molecular structures influence their reactivity towards ozone. The reaction sites are either multiple bonds or atoms carrying a negative charge, attracting electrophilic oxidants such as ozone. Radical reactions are therefore not selective.

Natural water may be polluted by natural substances (e.g.: amino acids and carbohydrates), products or wastes related to human activity (e.g.: solvents, hydrocarbons and pesticides) or compounds produced due to high concentration of organic matter. The presence of organic solutes can influence the ozone consumption and reactions pathways in several ways: the direct consumption of ozone (e.g.: phenol); the initiation of ozone decomposition by producing ozonide and •OH; the inhibition of ozone decomposition by ozone-scavenging species; and the promotion of O_3 decomposition by ozone-scavenging species with production of superoxide radical ions (e.g.: formate).

Many specific pollutants have been studied and data may be found in literature. Bablon et al. (1991) and Hoigné and Bader (1983a & 1983b) have compiled extensive lists of the organic water pollutants and their reaction with ozone. In natural waters, analysis of organic pollutants is usually limited by their diversity and the analytical methods required for quantification of the pollutants, especially at low concentrations. Therefore raw water is generally analysed for the priority pollutants. Some of the more commonly encountered problems with organic pollutants are described in details.

Reactions with odour and taste causing compounds. Amongst the micro-pollutants, control of tastes and odours is a common problem for water treatment works (Ho et al., 2002; Morioka et al., 1993; Glaze et al., 1990). The occurrences of the odour- and taste-causing compounds are as a result of the microbial activities in rivers, reservoirs or the treatment plant. Compounds like geosmin and 2-MIB are detectable at concentrations of nanograms per litre. The removal of the taste and odour is accomplished by altering or breaking the organic structure of the source compounds through oxidation. Because of the bulky chemical structure of geosmin and 2-MIB (shown in Figure 2-8), only strong oxidants such as ozone can oxidise these compounds at reasonably low dosages.

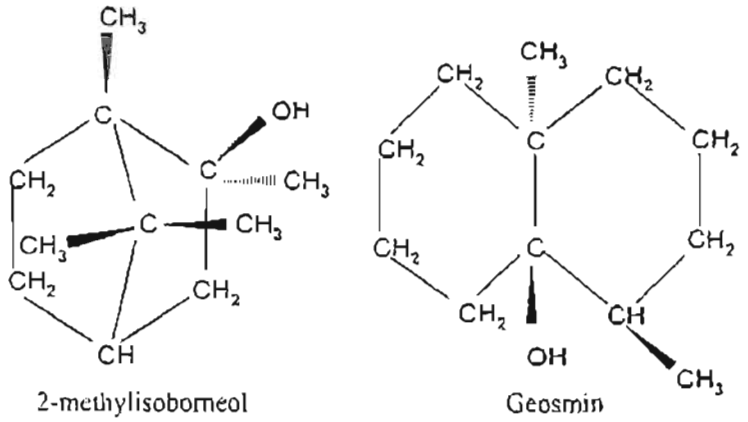

Figure 2-8: Structures of MIB and geosmin (Ho et al., 2004)

Reactions with cell constituents. The cell constituents are the macromolecules which are often of a high molecular weight. A special feature of these macromolecules is that their specific structural conformations are determined by low-energy bonds (Bablon et al., 1991). Hence the reactivity of the cell constituents towards ozone is dictated by the functional group of the chemical structure. While the carbohydrates are less reactive with ozone due to the lack of strongly electrophilic sites, the reaction rates of the amino acids is significant, especially at neutral and basic pH.

Inactivation of micro-organisms by ozone is better understood with the knowledge of the chemical components constituting biological cells. For bacteria, the first site of attack appears to be the cytoplasmic membrane due to the various proteins amongst its constituents (Giese and Christensen, 1954). Furthermore ozone disrupts enzymatic activity by acting on the sulfhydryl groups of certain enzymes. For viruses, the first site of attack is the virion capsid, also due to its proteins (Cronholm et al., 1976; Riesser et al., 1976). Ozone inactivates the bacteriophage f2 ribonucleic acid (RNA) by breaking the phage coat and releasing the enclosed RNA (US EPA, 1999).

Reactions with dissolved natural organic materials. Natural waters contain a spectrum of organic and inorganic compounds. The total organic load or characterised as the total organic carbon (TOC) are present in dissolved and suspended forms. The dissolved organic materials or dissolved organic carbon (DOC) is a fraction that can be analysed after the water has been filtered (0.45 μm) and consists of almost 90% of TOC (Bablon et al., 1991). The main constituents of the organic materials are polymerised organic acids, collectively called humic substances. Although the humic substances are often used as an indicator of the DOC in water due to their relatively high concentration, very few kinetic studies have been conducted. Hoigné (1998) summarised that there seems to be only a small fraction of the functional groups which exhibits a significant rate constant for reacting with molecular ozone.

2.3.3 Competitiveness amongst ozone reactions

The *dissolved* ozone has been known to react with dissolved compounds in water in two ways: the direct and selective oxidation by molecular ozone; the indirect and non-selective oxidation through the generation of hydroxyl radicals. For the latter reason, ozonation is also considered as an advanced oxidation process

(AOP) (Glaze et al., 1987). The question emerged is whether the decomposition of dissolved ozone to the hydroxyl radicals will compete with the more desired molecular reactions of ozone.

Beltrán (1995) examined the extent of direct and decomposition reactions of ozone using the film and the surface renewal models of the gas-absorption theory. The test water was made up from a known solute M with pure water.

The film model was based on a stagnant liquid layer at the surface of the liquid next to the gas. Dissolved gas moves through the film layer by molecular diffusion only (Charpentier, 1981; Danckwert, 1970). The application of the film layer concept allows the concentration profiles of ozone and the solute to be determined in the film layer. Consequently this profile indicates where the ozone is depleted (Figure 2-9): the presence of dissolved ozone in the bulk water (black solid lines) shows that the main oxidation route of solute M would proceed with the dissolved molecular ozone; whereas the absence of ozone in the bulk solution (grey dotted line) indicates that fast depletion of ozone was enhanced by its decomposition into hydroxyl radicals.

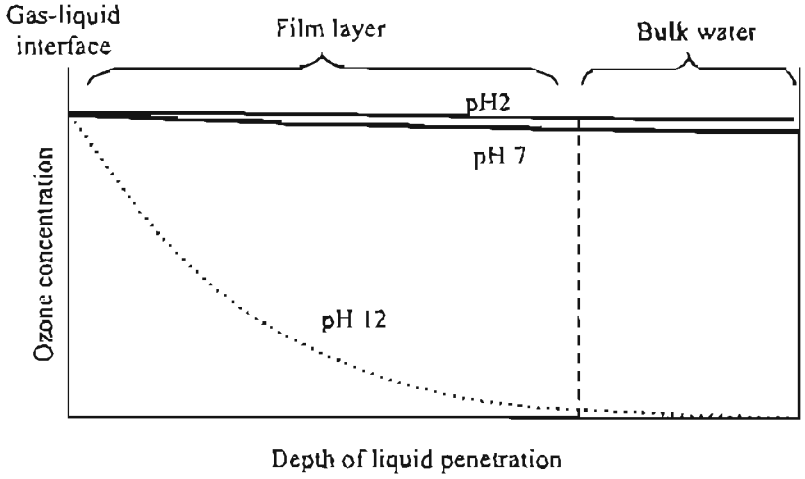

Figure 2-9: Identification of ozone decomposition in organic-free water using film theory (adapted from Beltrán, 1995).

Figure 2-9 also indicates the influence of pH on the ozone decomposition. In his investigation, Beltrán found that at pH values of 2 and 7 ozone decomposition exhibited first-order kinetic behaviour in organic-free water. Since there was ozone residual concentration in the bulk water, it indicated that the decomposition was slow and occurred mostly in the bulk water. However, at pH 12 the decomposition was too fast to allow accurate determination of the reaction constant. Most of the ozone was depleted whilst moving through the film layer.

In the film model, the kinetic regime of a gas absorbing into a liquid and then undergoing chemical reaction is characterised by the dimensionless Hatta number (*Ha*). *Ha* is defined in equation Eqn. (2-9) for an irreversible first-order reaction and in equation Eqn. (2-10) for an irreversible second-order reaction (Charpentier, 1981; Danckwerts, 1970).

$$Ha = \frac{\left(k D_{O_3}\right)^{0.5}}{k_L} \qquad (2\text{-}9)$$

$$Ha = \frac{\left(k_D D_{O_3} C_M\right)^{0.5}}{k_L} \tag{2-10}$$

where k is the first-order rate constant; k_L is the liquid phase mass transfer coefficient; D_{O_3} is the ozone diffusivity in water; C_M is the concentration of the solute M; and k_D is the second-order rate constant of the direct reaction between ozone and M. The classification of the kinetic regimes using Ha numbers is tabulated in Table 2-5.

Table 2-5: Classification of the kinetic regimes according to Hatta numbers (Schwikkard, 2001; Charpentier, 1981)

Ha	Kinetic regimes	Description
< 0.02	Very slow reaction in bulk solution	Reaction does not occur in the film; mass transfer keeps the concentration of absorbed gas in the bulk solution
0.02 to 0.3	Slow reaction in bulk solution	A two-stage process where the absorption of a gas is followed by reaction in the bulk solution; a negligible portion of absorbed gas reacts in the diffusion film
0.3 to 3	Moderately fast reaction	Absorbed gas reacts mainly in the film, only small portion remains in the bulk solution
> 3	Fast reaction in film layer	Reaction is fast and occurs completely in the film layer; concentration of absorbed gas in the bulk solution is negligible.

Hence *Ha* indicates whether the overall reaction rate is controlled by reaction kinetics or the gas-to-liquid mass transfer. The reaction occurs mostly in the bulk solution when *Ha* is below 0.3 and the reaction rate is controlled by the bulk volume. When Ha is higher than 3, the reaction occurs completely within the boundary layer and the reaction rate is controlled by the interfacial surface area, which requires a contacting device to create a large interfacial area. A large liquid volume and interfacial area are required for a reaction that occurs within both the film layer and the bulk solution (Schwikkard, 2001; Charpentier, 1981).

The surface renewal model was based on the concept of continual replacement of liquid elements at the interface from the bulk solution. Thus the rate of gas absorption is a function of the exposure time of the liquid element, which is initially fast and decreasing with time (Charpentier, 1981; Danckwerts, 1970). The diffusion time, t_D, is defined in Eqn. (2-11) as the time between two consecutive renovations of the liquid elements. Therefore it is the time used for ozone to diffuse through the liquid element (Beltrán, 1995).

$$t_D = \frac{D_{O_3}^{0.5}}{k_L^2} \tag{2-11}$$

The reaction time, t_R, is defined by Eqns. (2-12) and (2-13) respectively for a first-order and a second-order reaction.

$$t_R = \frac{1}{k} \tag{2-12}$$

$$t_R = \frac{1}{k_D C_M} \tag{2-13}$$

If the effects of mass transfer and chemical reaction are to be accounted for separately, then t_D corresponds to the boundary dividing the film layer and the bulk water and the exact reaction zone can be established by t_R (Beltrán, 1995). The effects of this are illustrated in Figure 2-10.

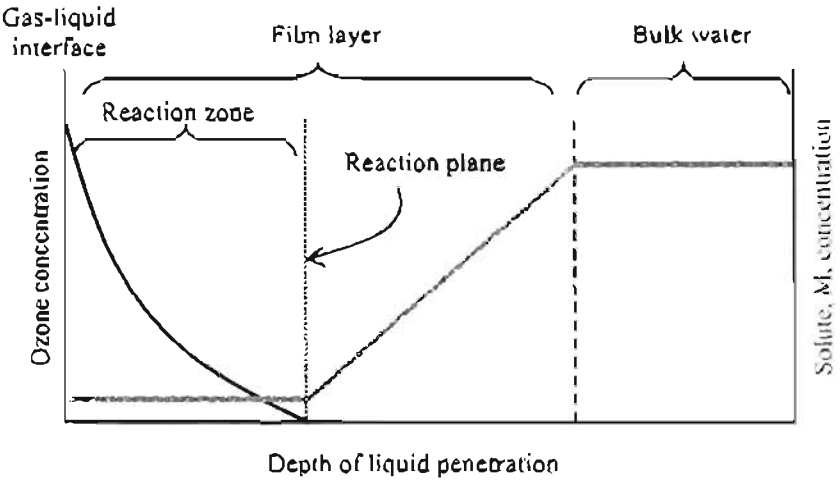

Figure 2-10: Illustration of gas-absorption theory (adapted from Beltrán, 1995). The reaction zone is assumed with a *fast* second-order reaction rate.

If t_D is much less than t_R, it can be deduced that the reactions are slow because the liquid elements are replaced before a substantial reaction can develop. However, if t_R is much less than t_D, fast chemical reactions are expected as the dissolved gas is depleted before the liquid elements are renewed (as shown in Figure 2-10).

Therefore the decomposition and hence the radical reactions will compete with the direct molecular, if both reactions occur in the same zone. Beltrán (1995) found this to be the case if $k_D < 10^6$ $M^{-1}.s^{-1}$) and $C_B < 10^{-4}$ M or when pH ≥ 10 and $k_D \geq 10^6$ $M^{-1}.s^{-1}$) with $C_B < 10^{-6}$ M. In reality, the concentration of pollutants in surface waters is typically low (< 10^{-6} M). Therefore the rate constant of the direct reaction with ozone must be greater than 10^6 $M^{-1}.s^{-1}$ to disregard the decomposition in a kinetic study.

2.4 Ozone reactor engineering

Gas-liquid reactors such as the ozone contactors are often applied industrially to achieve the desired reaction rates.

2.4.1 The $C \cdot t$ concept

The Surface Water Treatment Rule (SWTR) prescribes the $C \cdot t$ approach to establish conditions for achieving various degrees of the chemical removal of contaminants or the inactivation of waterborne pathogens during disinfection of drinking water (USEPA, 1999). The $C \cdot t$ concept is based on the Chick-Watson law which assumes the rate of inactivation of micro-organisms, r_d, obeys a first-order reaction with respect to the number of micro-organisms, N.

$$\frac{dN}{dt} = r_d = -k_d C^n N \qquad (2\text{-}14)$$

where k_d is the disinfection rate constant and n is the reaction order with respect to disinfectant concentration C. It was originally assumed by Chick that $n = 1$.

Assuming that the disinfectant concentration is constant with time and with the initial condition that $N = N_0$ at $t = 0$, the integrated Eqn. (2-14) becomes (Lawler and Singer, 1993):

$$\ln\left(\frac{N}{N_0}\right) = -k_d C t \qquad (2\text{-}15)$$

The $C \cdot t$ concept applied in ozonation means that the log of inactivation is proportional to the numerical product of the residual ozone outlet concentration (C) and a characteristic contact time (t) (USEPA, 1999). The $C \cdot t$ rule promulgated by SWTR is widely adopted by waterworks as a guide to design and to operate ozonation systems, perhaps justified by its simplicity. However, as simplification is always accompanied by restriction. The inherent assumption of the Chick-Watson law is limited in applying the characteristic contact time for different types of reactors.

2.4.2 Factors influencing performance

The performance of an ozone contactor is influenced kinetically (reactions of ozone with the water matrix) and hydrodynamically (contactor hydrodynamics). The kinetic influences encompass all parameters which affect the ozone reaction kinetics, such as pH, temperature or raw water constituents (Glaze et al., 1987; Bablon et al., 1991a; Hoigné, 1998). The hydrodynamic influences are often quantified by means of hydraulic residence time or by evaluating the effective contact time, in order to assess whether sufficient time has been allowed for the reactions to complete (Bablon et al., 1991b; US EPA, 1999).

For conventional water treatment practice, the overall rate of ozonation process is controlled by the sum of the rates of the chemical reactions with individual types of solutes (Hoigné, 1998). Ozone-to-water mass transfer will only become rate-limiting if the ozone consumption is very fast (Hoigné, 1998).

The advantage of ozonation is largely attributed to the ability of ozone to inactivate micro-organisms and to oxidise the reduced inorganic compounds and the organic compounds with ozone-reactive functional groups. It is due to this selectivity of ozone that low doses often suffice to achieve the goals of disinfection and oxidation (Hoigné, 1998).

An ozonation process for water treatment must be effective at ozone concentrations of only a few $mg.L^{-1}$, at ambient temperature and within reaction times of a few minutes (Hoigné, 1998).

2.5 Fluid dynamics and CFD modelling

Fluid dynamics were generally divided into theoretical and experimental branches as the case with many other physical sciences. The advances in computer technology has revolutionised fluid dynamics such that systems of highly non-linear partial differential equations (PDEs) can be applied to *numerically* perform the experiments. In this sense, CFD is not pure theoretical analysis as there is still inadequacy in numerical assessment of the PDEs (convergence proofs, error truncations or numerical stability) and no rigorous physical models for all description of flow.

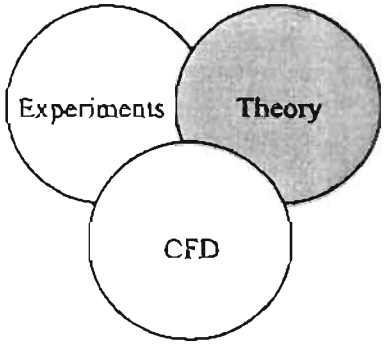

Figure 2-11: Fluid dynamics science

It must be noted here that it is not the focus of the thesis to conduct a full literature survey on the fluid dynamics modelling techniques. The modelling aspect of this investigation was limited by the financial resource and the available computational code at the time. The intention was not to find the best possible computational tool for use, but to interpret the simulated results in order to achieve the investigation objectives. The purpose of this section should therefore be to provide sufficient background for the discussion in the subsequent chapters.

2.5.1 History of computational fluid dynamics

The foundation of fluid mechanics relies on the equations derived by Navier (1827) and Poisson (1831), and de Saint Venant (1843) and Stokes (1845) independently more than a century ago. The equations are commonly referred to as the Navier-Stokes equations. Due to the complex, non-linear nature of the mathematical equations, no general analytical solutions has been obtained. The science of fluid dynamics started to branch in two directions towards the end of the 19th century (Kuipers and van Swaaij, 1998). One branch was the *theoretical hydrodynamics* which evolved from Euler's equations of motion for a frictionless, non-viscous fluid. The other branch was the highly empirical science of *hydraulics* which was driven by finding the solutions of practical problems.

The unification of the two branches was shown in Prandtl's *boundary layer* theory which demonstrated both experimentally and theoretically that viscous forces are important in boundary layer region and cannot be neglected. The initial development, mainly in aerodynamics, involved the approximate analytical solution or transformation and the relevant numerical integration. The CFD-based approach as an engineering tool started in the 1970s when the use of computers became feasible in solving the full set of conservation equations.

With the increasing computing power, the application of CFD is no longer limited in the aerodynamics study. CFD has found application in many ways, such as the designs of automobiles and aircraft, the designs or the improvement of reactors and even the flow study of environment. The simplest modelling is one which relates the inlets and the outlets of a process by some form of empirical or scaled-testing relationships. This is generally known as the *black box* approach which is applicable when little insight into the process is needed (De Clercq, 2003). The fundamental laws of physics and chemistry can be incorporated and solved to reveal more about the process performance. Depending on the complexity of physical problems, various modelling levels can be applied from the least computationally demanding

zero-dimension models, i.e.: assume an identical state at every point in space (De Clercq, 2003), to the physically-representative two- or three-dimensional models (Do-Quang et al., 2000). The dependence of the state variables on the spatial resolution can also be addressed by the latter, more complex models. The relatively inexpensive computing facility and its capability can probably justify the cost against the potential benefits.

CFD modelling has been applied in the investigation of stirred reactors (Koh and Xantidis, 1999), bubble columns (Ekambara and Joshi, 2003), tubular reactors (Hjertager et al., 2002), diffuser pumps (Shi and Tsukamoto, 2001), mixed anoxic wastewater treatment vessels (Brannock, 2003) as well as industrial ozonation towers (Cockx et al., 1999; Do-Quang et al., 2000a; Ta and Hague, 2004).

2.5.2 Governing equations

The mathematical description of any fluid flow is governed by the laws of conservation of mass, momentum and energy. For an incompressible fluid the energy equation is solved only when the physical problem involves heat transfer. The system of equations is thus reduced to one mass conservation Eqn. (2-16) and three momentum equations in the x-, y- and z-direction in Eqn. (2-17).

2.5.2.1 Mass conservation

In three-dimension, the conservation of mass or also known as the equation of continuity in Cartesian-tensor form is:

$$\underbrace{\frac{\partial \rho}{\partial t}}_{\text{Local derivative}} + \underbrace{\frac{\partial}{\partial x_i}(\rho u_i)}_{\text{Convective derivative}} = 0 \qquad (2\text{-}16)$$

where ρ is the fluid density, x_i is the length in dimension i, and u_i is the velocity in the i-th direction. The local derivative is physically the rate of change of the flow variable, which is ρ in this instance, at a fixed point. The convective derivative is physically the rate of change of the flow variable due to the movement of the fluid element.

2.5.2.2 Momentum conservation

The equation for the conservation of momentum is

$$\frac{\partial}{\partial t}(\rho u_i) + \frac{\partial}{\partial x_j}(\rho u_i u_j) = -\frac{\partial P}{\partial x_i} + \frac{\partial \tau_{ij}}{\partial x_j} + \rho g_i \qquad (2\text{-}17)$$

where τ_{ij} is the total stress tensor in the i-th direction acting on the j-th plane. ρg_i is the body force on the fluid element acting in the i-th direction and P is the static pressure. For an incompressible Newtonian fluid the viscous stress is proportional to the rates of deformation and volume dilation:

$$\tau_{ij} = \underbrace{\mu\left(\frac{\partial u_i}{\partial x_j} + \frac{\partial u_j}{\partial x_i}\right)}_{\text{Deformation}} \underbrace{- \frac{2}{3}\mu \frac{\partial u_i}{\partial x_i}\delta_{ij}}_{\text{Dilation}} \qquad (2\text{-}18)$$

where μ is the molecular viscosity and δ_{ij} is the Kronecker delta ($\delta_{ij} = 1$ for $i = j$; $\delta_{ij} = 0$ for $i \neq j$). The combination Eqns. (2-17) and (2-18) leads to the well-known Navier-Stokes equations.

The continuity equation in Eqn. (2-16) and three momentum balances in Eqn. (2-17) form a coupled system of nonlinear PDEs. To date, there is no general closed-form solution to these equations (Anderson, 1995).

2.5.3 Turbulence modelling

One of the unsolved problems in fluid dynamics is the prediction of turbulence. Turbulence occurs when velocity gradients are high, resulting in chaotic disturbances in the flow domain as a function of space and time (Chung, 2002). It is generated by contact of neighbouring layers of fluid moving at different velocities or by contact of a solid boundary such as walls. In turbulent flows, large eddies form continually, break down into smaller eddies and eventually disappear, and the turbulent kinetic energy is thereby dissipated in the process.

If the turbulence, large- or small-scale, is a viscous flow which locally obeys the Navier-Stokes equations, and that if a grid is fine enough to calculate the details of this turbulent flow directly from the Navier-Stokes equations with no additional modelling of turbulence effects, this class of CFD calculation is known as the Direct Numerical Simulation (DNS) of turbulent flows. The rigorous method by DNS requires a sufficiently fine grid to capture all scales of the energy range. It is therefore not applicable to industrial flow calculations due to exorbitant computational effort.

The governing Navier-Stokes equations can be, to some extent, averaged in space or time to remove the smaller scales. This gives rise to a less computationally expensive set of equations (refer to Appendix A). However the modified equations contain more unknowns than available equations. Such a problem is resolved by *turbulence modelling* or the Reynolds averaged Navier-Stokes (RANS) method to provide these unknowns in terms of the known quantities. Although turbulent flow is important in many spheres of engineering and has been a subject of extensive investigations for many decades (Bradshaw, 1978; Gatski, Sarkar and Speziale, 1992; Hanjalić, 1994a; Chung, 2002), no single turbulence model developed thus far is universally acclaimed to be superior. A list of various turbulence models is outlined in Appendix A.

The choice of a suitable turbulence model is dependent on the classes of flows, the level of accuracy required, the available computational means and the time available for the simulation.

2.5.4 Discretisation techniques

The term *discretisation* has specific meanings in setting up a mathematical model. Analytical solutions of partial differential equations involve closed-form expressions which are continuous throughout the domain. In essence, discretization is the process by which a closed-form mathematical expression is approximated by analogous expressions which prescribe values at a finite number of discrete points in the domain (Anderson, 1995).

The flow domain is replaced by a finite number of grid points. The grid points can be generated by dividing the domain of interest into control volumes or computational cells or elements which have a relatively small

size in comparison with the macroscopic volume of the domain (Kuipers and van Swaaij, 1998). This step is generally known as meshing. If the PDEs in the governing equations are replaced by approximate algebraic difference schemes which are expressed only in terms of the flow variables at the discrete grid points, the original PDEs can be replaced by a system of algebraic equations which can be solve for the flow variables at the grid points. In this sense, the PDEs are discretised and this method of discretization is also known as the method of finite differences.

The accuracy of the solution is dependent on the mesh type and its size. At present, most of the available meshing softwares have the capability to assist modellers in choosing the most suitable mesh. The details of meshing will not be dwelt on since it is not the main objective of the discussion.

The common forms of discretisation are summarised below from Chung (2002), Zwillinger (1997) and Anderson (1995). Since the subject is covered extensively in literature, only the essential aspects are highlighted for the purpose of the thesis.

Finite difference. The finite difference method is a technique to represent a system of PDEs by approximate algebraic difference equations. Most common finite-difference representations of derivatives are based on Taylor's series expansions.

Finite element. The finite element method gives solutions at discrete points or the so-called lattice points. Its disadvantage is the difficulty in applying the boundary conditions as it may be protruding. However it has a great advantage in accommodating complex geometry.

Finite volume. The finite volume method provides solutions across the discretised volumes. One of its advantages over the finite element method is its non-invasiveness in applying the boundary conditions because the values are located within the volume element. The finite volume method does not require a structured mesh (i.e.: where the grid points are allocated in the flow domain in a regular fashion) as it is often the case for the finite element method (Anderson, 1995).

2.5.5 Model formulation

In CFD modelling there is a sequence of steps required to translate the physical problem statement into a computationally achievable model. These steps are generalised and demonstrated in Figure 2-12:

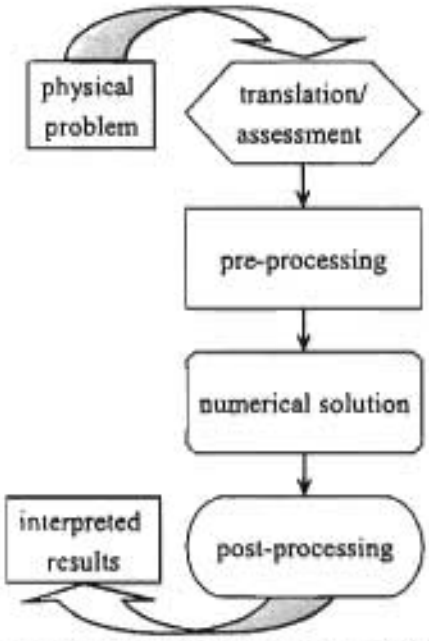

Figure 2-12: CFD modelling procedure (adapted from Fluent, 2003; Kuipers and van Swaaij, 1998; Anderson, 1995)

Assess the physical phenomena in order to formulate the target parameters and the basic assumptions. The first step is to analyse the flow problem into computable information and to identify with the applicable physical model, e.g.: compressible/incompressible flow; inviscid/viscous fluid; composition of fluid and its property etc (Fluent, 2003). Thereafter the target parameters are decided in order to meet the investigation goals. The parameters can include the physical quantities (such as velocity values) and the model-bound variable (such as the order of the numerical residual errors). These target parameters are important to CFD modelling since they direct the extent and the depth of model required for the flow analysis.

Pre-processing: generate grid and define boundary conditions. The second step is the so-called pre-processing of CFD modelling. It involves building a model for the flow geometry, applying a mesh for the volume discretisation and locating the boundaries of the flow model (Chung, 2002; Kuipers and van Swaaij, 1998). Various types of pre-processors have been developed and are available commercially. The in-depth discussion on grid generation is outside the scope of the investigation and can be found in numerous literature, e.g., Anderson (1995), Tucker (2001) or Chung (2002).

Solution strategy and tools. The next step is to enter the information into the flow model and to apply an appropriate solution strategy. A good space or time discretisation scheme is vital for obtaining a converging solution with less computational difficulty (Fluent, 2003). The solution methods are generally iterative and convergence is usually obtained by the use of relaxation techniques (Sharratt, 1990). Careful choice of relaxation parameters makes a major contribution towards both the rate of convergence and the production of a solution at all (Sharratt, 1990). Commercial CFD solvers usually include tools to observe the progress of the calculation.

Post-processing: results analyses. Post-processing is the final step in CFD analysis. This includes examination of the results and interpretation of the data and images. One needs to check whether the convergence criteria have been met and to post-process the data of interest further. Depend on the model complexity it may also be of interest to evaluate the dependence of solution accuracy on the grid refinement (Kuipers and van Swaaij, 1998; Sharratt, 1990).

2.5.6 Model validation and verification

Computational fluid dynamics is regarded a novel tool in the analyses and the designs of engineering processes. As with any form of modelling, the credibility of simulated results remains a major concern for the modellers. Despite the large knowledge base, the accuracy of the numerical solution is still uncertain (De Clercq, 2003). The processes of validation and verification are thus necessary in addressing the application of modelling techniques to physical problems. In some cases, the validation and verification of the CFD simulated results are difficult or may not be possible. However, it is important to realise that the difficulty in validation and verification effort should not be used as a reason for not using CFD (Sharratt, 1990).

The errors in the simulated solution are quantified in the step of verification. The simulation will reach a solution according to some pre-determined criteria set by the modellers. It is necessary to check whether the mesh provided to the modelled geometry is adequate. This is addressed by refining the mesh size and/or the time step (for unsteady state). Although the denser mesh reveals more flow details, the computing power required increases rapidly with the mesh density. The reduction in mesh size and/or time step are generally repeated until the computed solution shows no dependence on the sizes of mesh or time step. The mesh can then be considered sufficiently fine. Numerical errors can also arise from the approximation method applied in solving the governing equations. It is particularly notable when the high diffusion terms are present due to truncation error. This phenomenon is also known as the *numerical diffusion* (Sharratt, 1990).

The validation step involves the comparison of the simulated results with experimentally measured values. Errors and uncertainty of the conceptual and the computational models are identified and assessed during the validation process (De Clercq, 2003). The prediction of CFD can only be as good as the physical models applied and the boundary condition represented. Specific requirements have to impose on the quality of experimental data, such as the completeness in the data set and the error analyses in experimental measurements.

Therefore the uses of experimental, theoretical and computational sciences are required in developing, verifying and validating a CFD model.

2.6 Conclusions

Advanced oxidation processes, such as ozonation, may completely or partially oxidise organic compounds (e.g.: dyes or pesticides) which are difficult to degrade in conventional water treatment processes. The uniqueness in the ozone's resonance structure renders its selectivity and high reactivity in aqueous

reactions. As a result of partial oxidation, less recalcitrant compounds are formed and can be removed in subsequent processes. Under such conditions, ozonation is beneficial as pre-treatment steps to other processes.

To operate an ozonation effectively, it is important to achieve combined understanding of the contactor hydrodynamics and reaction kinetics. The use of CFD modelling has emerged as an engineering tool to provide insight into complex processes which would otherwise be intractable under a conventional *black box* approach, such as an ozonation. For example, CFD modelling has been used as an essential tool to design clarifiers in waterworks, and this support to water related projects has been sponsored by the WRC (Brouckaert and Buckley, 2002).

The present study will assist in the design stage of such plants incorporating the pre-ozonation system in future. Application of the CFD modelling enhances the understanding of the fluid dynamics in the system. Combining with appropriate ozonation kinetics, the work can be used to predict the effects due to equipment modifications, to provide better interpretation of experimental results and to improve the control of the system. Thereby ozone can be utilised efficiently to ensure the quality of the final water.

2.7 References

Air Liquide (2004) Gases: Gas Data – Ozone. Accessed on 30 November 2004 at URL http://www.airliquide.com/en/business/products/gases/gasdata/index.asp?GasID=137

Amirsardari Y., Yu Q. and Williams P. (1997) *Effects of ozonation and coagulation on turbidity and TOC removal by simulated direct filtration for potable water treatment.* Environmental Technology. 18 (11): 1143-1150.

Amy G.L., Chadik P.A., Sierka R.A. and Cooper W.J. (1986) *Ozonation of aquatic organic matter and humic substances: an analysis of surrogate parameters for predicting effects of trihalomethane formation potential.* Environmental Technology Letters 7 (2): 99-108.

Anderson J.D. Jr. (1995) *Computational fluid dynamics – the basics with applications.* International edition. McGraw-Hill Inc., New York, ISBN 0-07-113210-4.

Bablon G., Bellamy W.D., Bourbigot M.-M. et al. (1991a) *Chapter 2. Fundamental aspects.* In *Ozone in Water Treatment: Application and Engineering.* Langlais B., Reckhow D.A. and Brink D.R., eds., Lewis Publishers, Chelsea, Michigan. ISBN: 0-87371-474-1.

Bablon G., Bellamy W.D., Billen G., Bourbigot M.-M., Daniel F.B. Erb F., Gomella C., Gordon G. et al. (1991b) *Chapter 3. Practical application of ozone: principles and case studies.* In *Ozone in Water Treatment: Application and Engineering.* Langlais B., Reckhow D.A. and Brink D.R., eds., Lewis Publishers, Chelsea, Michigan. ISBN: 0-87371-474-1.

Bellamy W., Damez F., Langlais B., Montiel A., Rakness K.L., Reckhow D.A. and Robson C.M. (1991) *Chapter 4. Engineering aspects.* In *Ozone in Water Treatment: Application and Engineering.* Langlais B., Reckhow D.A. and Brink D.R., eds., Lewis Publishers, Chelsea, Michigan. ISBN: 0-87371-474-1.

Beltrán F.J. (1995) *Theoretical aspects of the kinetics of competitive ozone reactions in water*. Ozone: Science & Engineering **17** (2): 163-182.

Beltrán F.J., García-Araya J.F. and Álvarez P.M. (2001) *Domestic wastewater ozonation. A kinetic model approach*. Ozone-Science & Engineering **23** (3): 219-228.

Bin A.K. and Roustan M. (2000) *Mass Transfer in Ozone Reactors*. Proceedings of the International Specialised Symposium IOA 2000, Toulouse, France, 1-3 March: 99-131.

Boere J.A. (1992) *Combined use of ozone and granular activated carbon (GAC) in potable water-treatment – effects on GA quality reactivation*. Ozone-Science & Engineering. **14** (2): 123-137.

Bradshaw P. (1978) editor. Topics in applied physics volume 12: *Turbulence*. 2nd ed., Springer-Verlag. New York. ISBN: 0-387-08864-4.

Brady J.E. and Holum J.R. (1993) *Chemistry: The study of matter and its changes*. John Wiley and Sons, Inc., New York. ISBN: 0-471-59979-4.

Brannock M.W.D. (2003) *Computational fluid dynamics tool for the design of mixed anoxic wastewater treatment vessels*. PhD thesis, Department of Environmental Engineering, University of Queensland, Australia.

Brink D. R., Langlais B. and Reckhow D.A. (11991) *Chapter 1. Introduction*. In *Ozone in Water Treatment: Application and Engineering*. Langlais B., Reckhow D.A. and Brink D.R., eds., Lewis Publishers, Chelsea, Michigan. ISBN: 0-87371-474-1.

Brink D.R., Langlais B. and Reckhow D.A. (1991) *Chapter 1. Introduction*. In *Ozone in water treatment: application and engineering*. Langlais B., Reckhow D.A. and Brink D.R., eds. Lewis Publishers, Chelsea, Michigan. ISBN: 0-87371-474-1.

Brouckaert C.J. and Buckley C.A. (2002) *The application of computational fluid dynamics to water and wastewater treatment plant*. WRC report no: 648/1/02, ISBN: 1-86845-857-1. Pretoria.

Camel V. and Bermond A. (1998) *The use of ozone and associated oxidation processes in drinking water treatment*. Water Research **32** (11): 3208-3222.

Chandrakanth M.S. and Amy G.L. (1996) *Effects of ozone on the colloidal stability and aggregation of particles coated with natural organic matter*. Environmental Science and Technology **30** (2): 431-443.

Charpentier J.-C. (1981) *Mass-transfer rates in gas-liquid absorbers and reactors*. In *Advances in Chemical Engineering*, T.B. Drew, G.R. Cokelet, J.W. Hoopes and T. Vermeulen, eds., Academic Press, New York, ISBN 0-12-008511-9, **11**: 1-133.

Chung T.J. (2002) *Computational fluid dynamics*. Cambridge university press, Cambridge. ISBN: 0-521-59416-2.

Cockx A., Do-Quang Z., Lin A. and Roustan M. (1999) *Use of computational fluid dynamics for simulating hydrodynamics and mass transfer in industrial ozonation towers*. Chemical Engineering Science **54**: 5085-5090

Cronholm L.S. et al (1976) *Enteric virus survival in package plants and the upgrading of the small treatment plants using ozone*. Research report no. 98, Water resources research institute, University of Kentucky, Lexington, KY.

Danckwerts P.V. (1970) *Chapter 5. Absorption into agitated liquids*. In *Gas-liquid reactions*, McGraw-Hill, New York: 96-151.

De Clercq B. (2003) *Computational fluid dynamics of settling tanks: development of experiments and rheological, settling, and scraper submodels*. PhD thesis, School of Applied Biological Sciences, University of Gent, Belgium.

de Saint Venant B. (1843) *Note a joindre un mémoire sur la dynamique des fluids*. Comptes Rendus 17: 1240.

Do-Quang Z., Cockx A. and Liné A. (2000) *Recent advances in modelling tool development and application for ozone reactors design: The CFD approach*. Proceedings of the International Specialised Symposium IOA 2000, Toulouse, France. 1-3 March: 275-300.

Do-Quang Z., Roustan M. and Duguet J.-P. (2000a) *Mathematical modeling of theoretical Cryptosporidium inactivation in full-scale ozonation reactors*. Ozone: Science & Engineering 22: 99-111.

Driedger A.M., Rennecker J.L. and Mariñas B.J. (2000) *Sequential inactivation of Cryptosporidium parvum oocysts with ozone and free chlorine*. Water Research 34 (14): 3591-3597.

Ekambara K. and Joshi J.B. (2003) *CFD simulation of mixing and dispersion in bubble columns*. Transactions of the Institution of Chemical Engineers 81 part A: 981-1002, September.

Evans H., Bauer M., Goodman N., Hague J, Ta T. (2003) *The role of ozone in improving drinking water quality in London and Oxford*. Ozone: Science & Engineering 25 (5): 409-416.

Farvardin M.R. and Collins A.G. (1989) *Preozonation as an aid in the coagulation of humic substances – optimum preozonation dose*. Water Research 23 (3): 307-316.

Finch G.R. and Li H. (1999) Inactivation *of Cryptosporidium at 1°C using ozone or chlorine dioxide*. Ozone-Science & Engineering 21 (5): 477-486.

Fluent (2003) *Fluent 6.1 User Guide*, Lebanon, USA, Fluent Inc., 2003-01-25

Gatski T.B., Sarkar S. and Speziale C.G., ed. (1992) *Studies in turbulence*. Springer-Verlag Inc., New York. ISBN: 0-387-97613-2

Giese A.C. and Christensen E. (1954) *Effects of ozone on organisms*. Physiological Zoology 27 (2): 101-115.

Glaze W.H. (1987) *Drink-water treatment with ozone*. Environmental Science and Technology. 21 (3): 224-230.

Glaze W.H., Kang J.-W. and Chapin D.H. (1987) *The chemistry of water treatment & processes involving ozone, hydrogen peroxide and ultraviolet radiation*. Ozone: Science & Engineering 9 (4): 335-352.

Glaze W.H., Schep R., Chauncey W., Ruth E.C., Zarnoch J.J., Aieta E.M., Tate C.H. and McGuire M.J. (1990) *Evaluating oxidants for the removal of model taste and odour compounds from a municipal water supply*. Journal of the American Water Works Association 82 (5): 79-84.

Graham N., Preis S., Lambert S., Ma J. and Li G. (1994) *The impact of pre-treatment with ozone, chlorine dioxide and potassium permanganate on THM formation: laboratory case studies*. In *proceedings of the first International Research Symposium on Water Treatment By-Products*, Poitiers, France, 29-30 September, 1: 9.1-9.15

Graham N.J.D. (1999) *Removal of humic substances by oxidation/biofiltration processes* – a review. Water Science and Technology **40** (9): 141-148.

Greenwood N.N. and Earnshaw A. (1984a) *Section 14.1.4 Atomic and physical properties of oxygen*. In *Chemistry of the Elements*. Pergamon Press, Oxford, ISBN: 0-08-022057-6. 704-707.

Greenwood N.N. and Earnshaw A. (1984a) *Section 14.1.5 Other forms of oxygen: ozone*. In *Chemistry of the Elements*. Pergamon Press, Oxford, ISBN: 0-08-022057-6. 707-712.

Hanjalić K. (1994a) *Advanced turbulence closure models: a view of current status and future prospects*. Review. International Journal of Heat and Fluid Flow **15** (3): 178-203, June.

Hayes E.B. Matte T.D., Obrien T.R., McKinley T.W., Logsdon G.S., Rose J.B., Ungar B.L.P. Word D.M., Pinsky P.F., Cummings M.L., Wilson M.A., Long E.G., Hurwitz E.S. and Juranek D.D. (1989) *Large community outbreak of Cryptosporidiosis due to contamination of a filtered public water supply*. New England Journal of Medicine **320** (21): 1372-1376.

Heyouni A., Roustan M. and Do-Quang Z. (2002) *Hydrodynamics and mass transfer in gas-liquid flow through static mixers*. Chemical engineering science **57** (16): 3325-3333.

Ho L., Croué J.-P. and Newcombe G. (2004) *The effect of water quality and NOM character on the ozonation of MIB and geosmin*. Water Science and Technology **49** (9): 249-255.

Ho L., Newcombe G. and Croué J.-P. (2002) *Influence of the character of NOM on the ozonation of MIB and geosmin*. Water Research **36** (3):511-518.

Hoigné J. (1998) *Chemistry of aqueous ozone and transformation of pollutants by ozonation and advance oxidation processes*. In *The Handbook of Environmental Chemistry*, Vol. 5, Part C *Quality and Treatment of Drinking Water II*, Hrubec J., ed., Springer-Verlag, Berlin.

Hoigné J. and Bader H. (1983a) *Rate constants of reactions of ozone with organic and inorganic compounds in water – I. Non-dissociating organic compounds*. Water Research **17**: 173-183.

Hoigné J. and Bader H. (1983b) *Rate constants of reactions of ozone with organic and inorganic compounds in water – II. Dissociating organic compounds*. Water Research **17**: 185-194.

Hoigné J., Bader H., Wang W.R. and Staehelin J. (1985) *Rate constants of reactions of ozone with organic and inorganic compounds in water – III Inorganic compounds and radicals*. Water Research **19** (8): 993-1004.

Hjertager L.K., Hjertager B.H. and Solberg T. (2002) *CFD modelling of fast chemical reactions in turbulent liquid flows*. Computers and Chemical Engineering **26**: 507-515.

Jadashecart A., Ventresque C., Legube B. and Dore M. (1991) *Effect of ozonation on the chlorine demand of a treated surface-water and some macromoleculor compounds*. Ozone: Science & Engineering **13** (2): 147-160.

Kang J.-W., Park H.-S., Wang R-Y., Koga M., Kadokami K., Kim H.-Y, Lee E-T. and Oh S.-M. (1997) *Effect of ozonation for treatment of micropollutants present in drinking water source*. Water Science and Technology **36** (12): 299-307.

Kawamura F. (1932) *Journal of Chemical Society of Jopan, Pure Chemistry section*. **53**: 783-787.

Kilham LB (2002) *Measurement of dissolved ozone and the development of a new meter*. Access at URL at http://www.wcp.net/PDF/0102dissolved.pdf on 24 January 2003.

Kim Y., Lee Y., Gee C.S. and Choi E. (1997) *Treatment of taste and odor cousing substances in drinking water*. Water Science and Technology 35 (8): 29-36.

Kirk-Othmer (1967) Encyclopedia of Chemical Technology, 2nd ed., Volume 14, Wiley, New York, p 412.

Korich D.G., Mead J.R., Madore M.S., Sinclair N.A. and Sterling C.R. (1990) *Effects of ozone, chlorine dioxide, chlorine, and monochloramine on Cryptosporidium parvum oocyst Viability*. Applied and Environmental Microbiology **56** (5): 1423-1428.

Lawler D.F. and Singer P.C. (1993) *Analyzing disinfection kinetics and reactor design: a conceptiol approach versus the SWTR*. Journal of American Water Works Association **85** (11): 67-76.

Le Paulouë J. and Langlais B. (1999) *State-of-the-art of ozonation in France*. Ozone-Science & Engineering **21**: 153-162.

Lee SY, Ruutel P, Barratt PA, and Tsui YP (1999)*Impinging zone reactor and its mathemotical model for ozonation of waste water*. Ozone-Science & Engineering **21** (5): 501-522.

Legeron J.-P. (1982) *Chapter 27 Contact time of ozonization*. In *Ozonizaton manual for water and wostewater treatment*, Masschelein W.J. ed., John Wiley and Sons. Chichester. ISBN: 0-471-10198-2.

Li H., Finch G.R. Smith D.W and Belosevic M. (2001) *Sequential inactivation of Cryptosporidium parvum using ozone and chlorine*. Water Research **35** (18): 4339-4348.

Liechti P.-A. (2000) Control of ozonation systems - Ozone Demand under Variable Operating Conditions: commentaries. Proceedings of the International Specialised Symposium IOA 2000, Toulouse, France, 1-3 March.

Liley P.E., Thomson G.H., Friend D.G., Daubert T.E. and Buck E. (1997) *Section 2. Physical ond chemical data*. In *Perry's Chemicol engineers' handbook*, Perry R.H., Green D.W. and Maloney J.O. eds., 7th ed. McGraw-Hill. New York. ISBN: 0-07-115448-5. 2-125-2-128.

Lin S.H. (1993) *Ozonation kinetics of iron and monganese in aqueous solution*. Journal of Chemical technology and biotechnology **56**: 163-166.

Mackenzie W.R., Hoxie N.J., Proctor M.E., Gradus M.S., Blair K.A., Peterson D.E. Kazmierczak J.J., Addiss D.G., Fox K.R., Rose J.B. and Davis J.P. (1994) *A massive outbreak in Milwaukee of Cryptosporidium infection transmitted through the public water supply*. New England Journal of Medicine **331** (3): 161-167.

Mao H. and Smith D.W. (1995) *Influence of ozone application methods on efficacy of ozone decolorization of pulp mill effluents*. Ozone-Science & Engineering 17 (2): 205-236.

Martin N. and Galey C. (1994) *Static mixer for ozone oxidation and disinfection*. Ozone-Science & Engineering 16 (6): 455-473.

Mastronardi R.A., Fulton G.P., Farrar M. and Collins A.G. (1993) *Preozonation to improve and optimize diatomaceous-earth filtration*. Ozone-Science & Engineering 15 (2): 131-147.

McKnight K.F., Carlson M., Fortin P. and Ziesemer C. (1993) *Comparison of ozone efficiency for manganese oxidation between raw and settled water*. Ozone-Science & Engineering 15 (4): 331-341.

Mohammed A. and Smith D.W. (1992) *Effects of ozone on Kraft process pulp-mill effluent*. Ozone-Science & Engineering 14 (6): 461-485.

Munter R., Preis S., Kamenev S. and Sirde E. (1993) *Methodology of ozone introduction into water and wastewater treatment*. Ozone-Science & Engineering 15 (2): 149-165.

Navier M. (1827) *Mémoire sur les Lois du mouvement des fluides*. Mem. De l'Acad. De Sci. 6: 389.

Nebel C. (1981) *Ozone*. In Kirk-Othmer *Encyclopedia of Chemical Technology*, Grayson M. and Eckroth D., eds., 3rd edition. John Wiley & Sons, New York. ISBN 0-471-02069-9. 16, 683-713.

Nieminski E. and Evans D. (1993) *Pilot testing of trace metals removal with ozone at Snowbird Ski resort*. Ozone: Science & Engineering 17 (3): 297-309.

Ozonek J., Fijalkowski S. and Pollo I. (1997) *Exergy identification of energy utilization efficiency in an industrial process of ozone generation*. Ozone - Science & Engineering 19 (3): 201-226.

Paralkar A. and Edzwald J.K. (1996) *Effect of ozone on EOM and coagulation*. Journal of American Water Works Association 88 (4): 143-154.

Poisson S.D. (1831) *Mémoire sur les equations générales de l'equilibre et du mouvement des corps solides elastiques et des fluides*. J. de L'Ecole Polytechn 13: 139.

Pryor M.J., Nozaic D., Freese S.D., Rajagopaul R. (1999) *The use of granular activated carbon for the treatment of impounded surface water*. Water Science and Technology 39 (10-11): 197-200.

Rakness K.L., Hunter G.F., and DeMers L.D. (2000) *Drinking water ozone process control and optimization*. Proceedings of the International Specialised Symposium IOA 2000, Toulouse, France, 1-3 March.

Reckhow D.A., Edzwald J.K., and Tobiason J.E. (1993) *Ozone as an aid to coagulation and filtration*. AWWARF and AWWA, Denver, CO.

Reckhow D.A., Legube B. and Singer P.C. (1986b) *The ozonation of organic halide precursors: effect of bicarbonate*. Water Research 20 (8): 987-998.

Reckhow D.A., Singer P.C., and Trussell R.R. (1986a) *Ozone as a coagulant aid*. Seminar proceedings, Ozonation, Recent Advances and Research Needs, AWWA Annual Conference, Denver, CO.

Rencken G.E. (1994) *Ozonation at Wiggins water purification works, Durban, South Africa*. Ozone - Science & Engineering 16 (3): 247-260.

Rennecker J.L., Driedger A.M., Rubin S.A., and Mariñas B.J. (2000) *Synergy in sequential inactivation of Cryptosporidium parvum with ozone/free chlorine and ozone/monochloramine.* Water Research 34 (17): 4121-4130.

Rice R.G. (1997) *Applications of ozone for industrial wastewater treatment – a review.* Ozone-Science & Engineering 18 (6): 477-515.

Rice R.G. (1999) *Ozone in the United States of America - State-of-the-art.* Ozone-Science & Engineering 21 (2): 99-118.

Richardson A.J., Frankenberg R.A., Buck A.C., Selkon J.B., Colbourne J.S., Parsons J.W. and Mayonwhite R.T. (1991) *An outbreak of waterborne Cryptosporidiosis in Swindon and Oxfordshire.* Epidemiology and Infection 107 (3): 485-495.

Riesser, V.W., et al. (1976) *Possible mechanisms of poliovirus inactivation by ozone.* Forum on Ozone Disinfection, Fochtman E. G., Rice R.G., and Browning M.E.,eds., International Ozone Institute, Syracuse, NY.: 186-192.

Rischbieter E., Stein G. and Schumpe A. (2000) *Ozone solubilities in water and aqueous salt solutions.* Journal of Chemical and Engineering Data. 45 (2): 338-340.

Roache P.J. (1985) *Computational fluid dynamics.* Revised English edition, Hermosa publishers, Albuquerque, ISBN: 0-913478-05-9.

Roth J.A. and Sullivan D.E. (1981) *Solubility of ozone in water.* Industrial Engineering Chemistry Fundamentals 20 (2): 137-140.

Schwikkard G.W. (2001) *Advanced oxidation processes in water treatment.* PhD thesis, Department of Chemical Engineering, University of Natal, South Africa.

Sharratt P.N. (1990) *Computational fluid dynamics and its application in the process industries.* Transactions of the Institution of Chemical Engineers 68, Part A: 13-18, January.

Shi F. and Tsukamoto H. (2001) *Numericol study of pressure fluctuations caused by impeller-diffuser interaction in a diffuser pump stage.* Journal of Fluids Engineering 123: 466-474, September.

Skerrett H.E. and Holland C.V. (2000) *The occurrence of Cryptosporidium in environmental waters in the greater Dublin area.* Water Research 34 (15): 3755-3760.

Staehelin J. and Hoigné J. (1985) *Decomposition of ozone in water in the presence of organic solutes acting as promoters and inhibitors of radical chain reactions.* Environmental Science and Technology 19 (12): 1206-1213.

Staehelin J. and Hoigné J. (1982) *Decomposition of ozone in water: rate of initiation by hydroxide ions and hydrogen peroxide.* Environmental Science and Technology 16: 676-681.

Staehelin J., Bühler R.E. and Hoigné J. (1984) *Ozone decomposition in water studied by pulse radiolysis. 2. OH and HO_4 as chain intermediates.* Journal of Physical Chemistry 88: 5999-6004.

Stokes G.G. (1845) *On the theories of internal friction of fluids in motion.* Trans. Cambr. Phil. Soc. 8: 287.

Stumm W. (1958) *Journal of Boston, Society of Civil Engineers* 45: 68-79.

Ta C.T and Hague J. (2004) *A two-phase computational fluid dynamics model for ozone tank design and troubleshooting in water treatment.* Ozone-Science & Engineering 26: 403-411.

Tiefenbrunner F.H., Moll H.G., Grohmann A., Eichelsdörfer D., Seidel K. and Golderer G. (1990) *Ozone treatment of small-size swimming pools and whirlpools.* Ozone-Science & Engineering 12 (4): 393-400.

Tomiyasu H., Fukutomi H. and Gordon G. (1985) *Kinetics and mechanism of ozone decomposition in basic aqueous solution.* Inorganic Chemistry 24: 2962-2966.

Trapido M., Hirvonen A., Veressinina Y., Hentunen J and Munter R. (1997) *Ozonation, ozone/UV and UV/H_2O_2 degradation of chlorophenols.* Ozone: Science & Engineering 19 (1): 75-96.

Tucker P.G. (2001) *Computation of unsteady internal flows: Fundamental methods with case studies.* Kluwer academic publishers. Norwell, USA. ISBN: 0-7923-7371-5

US EPA (1999) *Disinfection Profiling and Benchmarking Guidonce Manual*, United States Environmental Protection Agency, Office of Water, EPA 815-R-99-013.

Vahala R., Ala-Peijari T., Rintala J. and Laukkanen R. (1998) *Evaluating ozone dose for AOC removal in two-step GAC filters* Water Science and Technology 37 (9): 113-120.

Wang G-S and Pai S-Y (2001) *Ozonation of dissolved organic matter in biologically treated wastewater effluents.* Ozone-Science & Engineering 23 (5): 351-358.

Westerhoff P., Song R., Amy G., and Minear R. (1997) *Application of ozone decomposition models.* Ozone-Science & Engineering 19 (1): 55-73.

Wilson D., Lewis J., Nogueria F., Faivre M. and Boison V. (1993) The use of ozoflotation for the removal of algae and pesticides from a stored lowland water. Ozone: Science & Engineering 15 (6): 481-496.

Zhu Q., Liu C. and Xu Z. (1989) *A study of contacting systems in water and wastewater disinfection by ozone. I. Mechanism of ozone transfer and inactivation related to the contacting method selection.* Ozone-Science & Engineering 11 (2): 169-188.

Zwillinger D. (1997) *Handbook of differential equations.* 3rd edition, Academic Press, Boston, Massachusetts, US. ISBN: 0-12-784396-5.

3

HYDRODYNAMIC MODEL OF THE OZONE CONTACTOR

"The first step to knowledge is to know that we are ignorant."

- Socrates (470-399 B.C.), Greek philosopher

The hydrodynamics within the Wiggins Waterworks' ozone contactor are expected to be complex and turbulent. A three-dimensional CFD model was constructed to simulate the physical phenomena with the aim of generating insight to the flow dynamics. Because of the physical constraints to measure detailed flow parameters within the full-scale contactor, the hydrodynamic model was validated through a global approach, known as the *residence time distribution* (RTD).

This chapter describes the CFD application to model the hydrodynamics of an ozone contactor and the validation of the predicted residence time distribution using experimental tracer data. The importance of understanding hydrodynamic behaviour is discussed in **Section 3.1** . The overall objective of the project is re-emphasised in **Section 3.2** with some additional goals towards the hydrodynamic modelling aspect of the ozone contactor. One of the major simplifications was the development of a one-phase (i.e., water only) hydrodynamic model to represent the two-phase system. The assumptions and the choice of modelling parameters are discussed in **Section 3.3** . The effect of the gas injection on the hydrodynamics was modelled by increasing the level of turbulence. **Section 3.4** describes the procedure of the experimental tracer tests which were carried out for the model validation. The predicted tracer responses corresponded well with the experimental results. Effects of various operational or modelling options on the overall hydrodynamics are compared in **Section 3.5** . General conclusions for this chapter are presented in **Section 3.6** .

3.1 Introduction

Fractions of fluid reside within a reactor for different length of times before exiting. It is typically characterised by the distribution of their residence times, the distribution of ages of fluid fractions leaving a mixing system. The use of RTD in the analysis of reactor performance appeared as early as 1935 in a pioneering paper by MacMullin and Weber; however, the concept was only used extensively after Danckwerts (1953) gave the structure to the subject by defining the distributions of interest (Fogler, 1997).

The common means of obtaining the RTD data is to perform tracer studies. The experimental residence time data can be obtained by performing a tracer test at a constant flow rate. The technique involves introducing a tracer at the inlet of the system and measuring its concentration at the outlet over the prescribed time intervals. Often modelling is applied in order to achieve better understanding of the physical hydrodynamic phenomena. In modelling, the residence time data deals with the transport of

conserved particles through a system, described in a time domain. The RTD curves are generated from the test results to reveal any mixing inefficiency, such as dead volumes or short-circuiting. For a complex system, detailed modelling must be combined with experimental verification.

3.1.1 Importance of residence time distribution in ozonation

An ozone contactor is employed to allow sufficient contact time between water and ozone for the aquatic reactions to occur. The efficiency of various target and inactivation reactions is dependent on this exposure time of the target pollutants to ozone. The hydrodynamic behaviour of a contactor thus plays a vital role in achieving the required goals of oxidation and disinfection, as the quality of treated water can be profoundly affected (Roustan et al., 2000). For the purpose of an effective control strategy and operation, it is important to understand the hydrodynamics and to have means to characterise them.

RTD is a well-known approach to characterise the mixing that occurs in a system. It is a *macro* measure of the flow response of a system. The spread of this residence time is used in the RTD analysis to detect non-ideality in flow. Thus the RTD data often provides enough information about the flow for analysis, design and troubleshooting. The hydrodynamics of an ozone contactor are a strong function of both the contactor configuration and the operating conditions of the system. The global influences can be reflected in the RTD of a contactor.

3.1.2 Mathematical properties of distribution function

Transient tracer tests are the most common choice for characterising the RTD of an ozone contactor (Roustan et al., 2000). In these tests, an amount of tracer is introduced either as a pulse or a step function at the inlet of the contactor, marking the fluid elements as they enter the contactor. The concentration of the tracer $C(t)$ is monitored with time at the outlet of the contactor. The recorded outlet concentration can be converted into a continuous function $E(t)$, such that

$$\begin{bmatrix}\text{fraction of tracer exiting}\\ \text{that has resided in the reactor}\\ \text{between t and t+}\Delta t\end{bmatrix} = \int_{t}^{t+\Delta t} E(t)\,dt \qquad \text{(Fogler, 1997)}$$

with restriction that it be non-negative:

$$E(t) \geq 0,\ t \geq 0 \tag{3-1}$$

The quantity $E(t)$ is known as the *residence time distribution density function*, analogous to the probability density function. The expression in Eqn. (3-1) indicates the probability of a fraction of fluid elements leaving the contactor between t and $t + \Delta t$. Seeing that the sum of the fractions of the tracer resides in the reactor between $t = 0$ and $t = \infty$ is 1, then the area under the $E(t)$ curve is unity.

$$\int_{0}^{\infty} E(t)\,dt = 1 \tag{3-2}$$

In practice, a normalised RTD density function, $E(\theta)$, is used instead of $E(t)$. The dimensionless time θ is defined as

$$\theta = \frac{t}{\bar{t}} \tag{3-3}$$

where $\bar{t}$ is the mean residence time and calculated using Eqn. (3-4):

$$\bar{t} = \frac{\int_0^\infty tC(t)\,dt}{\int_0^\infty C(t)\,dt} \tag{3-4}$$

The dimensionless RTD density function $E(\theta)$ can be seen as

$$E(\theta) \equiv \bar{t}E(t) \tag{3-5}$$

The area under the curve $E(\theta)$ is conserved to unity as Eqn. (3-2). This allows the comparison possible amongst the different settings of operating conditions and simulations.

3.1.3 Role of computational fluid dynamics

Flow modelling has long been recognised for its significance in the design and the optimisation of a process. Many empirical or semi-empirical strategies have been devised to solve complex problems involving non-ideal flow. A traditional approach to circumvent the difficulties encountered in complex flows is by means of the *RTD curve modelling*.

The RTD of real reactors lie between the two idealised flow patterns: plug flow reactor (PFR) and continuous-flow stirred tank reactor (CSTR). All segregated fluid element in PFR have the same residence time, whereas the ideal infinite mixing occurs in CSTR. Although they do not occur in reality, the concepts represent the extreme boundaries in which the non-ideal flow prevails. The normalised RTD density function for a PFR is

$$E(\theta) = \delta(\theta - 1) \tag{3-6}$$

where δ is the Dirac delta function.

For a CSTR, it is defined as Eqn. (3-7)

$$E(\theta) = e^{-\theta} \tag{3-7}$$

Nauman and Clark (1991) compiled a list of models used to represent the RTD of real reactors. Two models most commonly used are the tanks-in-series model and the axial dispersion reactor (ADR) model (Roustan, 2000).

The normalised RTD function for a cascade model of N tanks-in-series is

$$E(\theta) = N\frac{(N\theta)^{N-1}}{(N-1)}e^{-N\theta} \tag{3-8}$$

Eqn. (3-8) approaches the RTD density function of a PFR as N approaches infinity.

The ADR model is employed to represent the hydrodynamics of reactors in which dispersion can be assumed to be one-dimensional to occur mainly in the direction of the flow, i.e.: axial dispersion (Roustan, 2000). The normalised governing equation of an ADR is shown in Eqn. (3-9).

$$\frac{\partial E}{\partial \theta} = d\frac{\partial^2 E}{\partial z^2} - \frac{\partial E}{\partial z} \tag{3-9}$$

where z is the dimensionless distance in the axial direction, defined by $z = x/L$, in which x is downward distance in the axial direction and L is the reactor length; d is the dispersion number, defined by $d = D/uL$ in which D is the turbulent diffusivity or dispersion coefficient and u is fluid velocity.

The ADR model converges to a PFR with minimal or negligible dispersion ($d \rightarrow 0$) and to a CSTR if flow is highly mixed ($d \rightarrow \infty$). The level of dispersion in real reactors is somewhere between the two ideal reactors. The effect of dispersion decreases as the number of CSTRs, N, in cascade increases.

The above models all attempt to represent the RTD of the non-ideal flow in reactors by the macro-mixing patterns. In reality, there is a certain degree of mixing between the fluid elements passing through the reactor and the chemical reactions occur simultaneously. The information on the macro-mixing patterns may not be adequate to enable an accurate prediction of the extent of chemical reaction in a reactor with a non-ideal flow pattern (Kuipers and van Swaaij, 1998).

Levenspiel (1962) stated that '*...if we know precisely what is happening within the vessel, thus if we have a complete velocity distribution map for the fluid, then we are able to predict the behaviour of a vessel as a reactor. Though fine in principle, the attendant complexities make it impractical to use this approach....*' The position of this view has certainly changed due to the immense growth of computing power. The approach of obtaining the *complete velocity distribution map* can be achieved using CFD which combines the fluid dynamics theory and the numerical techniques, supported by fast computing facilities. The fundamental principles form the basis of the computed velocity distribution. The distribution function is then obtained directly from the velocity distribution, which replaces the abovementioned RTD curve modelling.

As discussed in **Section** 1.3 the use of a CFD model and experiments complement each other in gaining a holistic understanding. In practice, it may be difficult to obtain local flow measurements in large equipment. Nevertheless these experimental results and observation constitute the backbone for model verification. The use of simulated tracer tests after such validation provides an insight to the microscopic phenomena and enhances the understanding to the overall flow behaviour.

3.1.4 The $C \cdot t$ concept and the characteristic contact time

Under the Interim Enhanced Surface Water Treatment Rule (IESWTR), criteria for calculating the degree of inactivation of waterborne pathogens during disinfection of drinking water (Pontius, 1999; USEPA, 1999) are specified in terms of $C \cdot t$, which assumes that the log of inactivation is proportional to the numerical product of the residual ozone outlet concentration (C) and a characteristic contact time (t) (USEPA, 1999).

$$\log \frac{N}{N_0} \propto C \cdot t \tag{3-10}$$

3.3 Hydrodynamic model description

The current section describes the set up of a simplified, three-dimensional (3D) hydrodynamic model for the ozone contactor. This hydrodynamic model is referred to as the *base* model, as it forms the foundation from which the reaction model evolved.

It must be stressed that many details in the model were chosen arbitrarily or adopted the generally accepted values because it was not possible to resolve their influences experimentally. As mentioned earlier, the physical nature of the contactor under the investigation imposed difficulty in obtaining detailed experimental flow data within the contactor. Furthermore, these detailed experimental flow data may not be necessary if the contribution from the micro flow phenomena could be reflected in the macro flow characterisation such as the RTD.

3.3.1 Geometry and meshing

The contactor under investigation is one of the four in the pre-ozonation system at Wiggins Waterworks (Figure 3-1). Due to their configuration similarity, it was decided to concentrate on contactor No. 2 where some initial work had been done (Brouckaert et al., 2000).

Figure 3-1: Exterior view of the ozone contactors

The geometry of the base model was taken directly from a design drawing. At first the wire frame of the contactor was created using GAMBIT, a commercial grid generation pre-processor. The wire frame represents only the concrete surfaces that are in contact with water, with the exception of the upper surface which represents the free surface of water. It must be noted that the floor of the lowest level slopes to the right, towards the sludge drain. A drainage pipe is situated to the right of the inlet from the static mixer. The inlet has a circular cross-section as the static mixer is directly attached to the contactor. The outlet weir was represented as a rectangular slot, the height of which was set to the measured height of liquid flowing over the open broad-crested weir. These geometrical features led to considerable difficulties with the model.

In the form of Eqn. (3-10) the degree of inactivation is expressed in commonly used logarithmic terms.

The importance of the RTD is reflected in the requirements promulgated by the US Environmental Protection Agency (EPA) to ensure adequate disinfection in surface water treatment plants. The effective contact time for disinfection is taken to be T_{10} rather than the hydraulic retention time, where T_{10} is the time required for 10% of a pulse of a tracer introduced at the disinfectant dosing point to have reached the contactor outlet. Thus T_{10} is dependent on the RTD of a contactor and consequently affected by its geometry and operating conditions. For a given flow rate and contactor volume, T_{10} decreases as the degree of dispersion increases (i.e. the RTD becomes broader). Therefore, the efficiency of pathogen inactivation is assumed to decrease as the degree of dispersion increases. Under IESWTR, T_{10} can be determined directly from a tracer test, or calculated from the mean hydraulic residence time using baffling factors published with the guidelines (USEPA, 1999).

However the use of the $C \cdot t$ concept in analysing the treatment of resistant pathogens has been questioned (Lawler and Singer, 1993; Gyürék et al. 1997; Driedger et al. 2000). The use of the characteristic contact time may be a pragmatic parameter for characterising a conventional (chlorine-based) disinfection process; however, it is a misleading parameter to describe processes such as ozonation where the residual ozone varies more rapidly (Hoigné, 1998). T_{10} may be found applicable for certain configurations of reactors but not adequate for more complex flows. Hoigné (1998) also pointed out the simplicity of T_{10} is inadequate to address the formation of disinfection by-products. The $C \cdot t$ concept was found to be conservative by Lawler and Singer (1993). Although the mathematical simplicity perhaps justifies the more conservative approach, it may require a costly implementation unnecessarily for the operations of many waterworks.

3.2 Objectives

The main objective of this chapter is to gain a better understanding of the flow regimes in the contactor. Quantitatively this is expressed through the evaluation of the residence time distribution. The more specific goals oriented towards the main objective are as follows:

- To develop a three-dimensional CFD hydrodynamic model in Fluent;
- To assess the model simplification in order to account for the gas presence;
- To determine the RTD of the ozone contactor in terms of the operating condition ;
- To investigate the prospect of hydrodynamic improvements from the above results.

This study aims to demonstrate the application of a fundamental modelling approach to a full-scale ozone contactor. It is not about developing codes to solve the governing equations and therefore commercial software was used.

After the geometry had been entered, the fluid domain was then divided into elementary volumes, which are used by the finite element algorithms to integrate the equations of fluid motion. This process is known as meshing. In GAMBIT there are several meshing methods available, which are primarily differentiated from one another by the shape of the elementary volumes. Due to the complexity of the ozone contactor geometry, a tetrahedral meshing scheme was selected to provide greater flexibility for the details and to keep the number of nodes to the minimum.

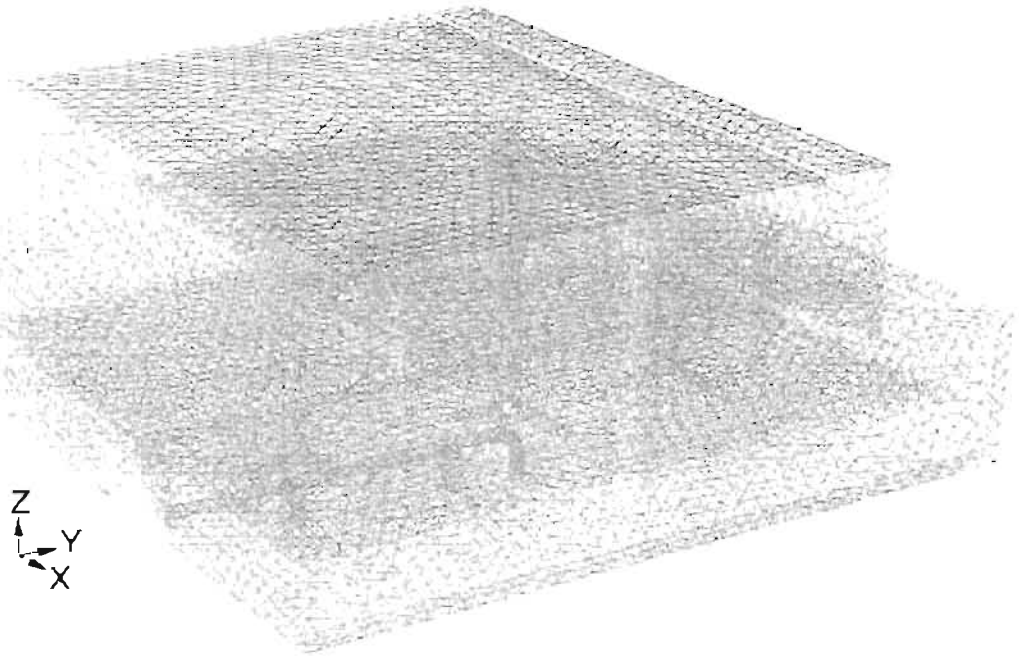

Figure 3-2: Tetrahedral mesh of the contactor

The grid was built using GAMBIT 1.3, shown in Figure 3-2. The contactor volume was divided into 103 105 tetrahedral volume elements with 23 273 nodes, giving an average volume of 8.2 L and an average length between nodes of about 200 mm.

3.3.2 Assumptions

Before reaching the inlet of the contactor, the water passes through a static mixer where the ozone-containing gas is injected as a side stream (see Section 1.2.2 for the system description). This gas consists of about 10 % ozone and 90 % oxygen. By the time the flow emerges from the static mixer to enter the contactor, almost all the ozone is dissolved. The oxygen, however, remains as gas bubbles. The ozone/oxygen side stream flow rate is about 1 % v/v of the main water flow rate.

Due to this comparably small gas flow, a complete full-scale two-phase modelling was considered unnecessary as the enormous computational effort may not bring additional benefits to further understanding of the contactor hydrodynamics. A decision was taken to proceed with water-phase modelling only. The presence of the bubbles was not taken into account explicitly. Instead it was assumed that its effect on the flow could be indirectly represented by an increase in the turbulent mixing in relation to the case with water only. Because of the difficulty of predicting the intensity of turbulence at the

inlet, a chosen parameter in the turbulence modelling was adjusted to give the best fit to the experimental data.

The simplification of reducing a two-phase physical problem to a one-phase model required the experimental verification to examine the extent of the effect of the gas on the hydrodynamics. Two experimental tracer tests were conducted under different operating conditions, namely *with* and *without* the injection of the ozone-containing gas. The difference in the operating conditions of the tests will be referred to as **with** and **without** *gas injection* throughout the thesis.

3.3.3 Physical models

FLUENT was the commercial CFD package used. There are a number of built-in physical models in FLUENT to deal with phenomena such as turbulence and species reactions. Since the objective was not to search for the most suitable physical model available, these built-in options were adequate for the use of this study. Details of the models employed are described in Appendix A for reference purpose since much of it is considered standard knowledge of CFD modelling.

3.3.3.1 Turbulence modelling

Turbulence is physically characterised by the fluctuating velocity field. As a consequence of these fluctuations, the rates of transport for quantities such as momentum or species concentration also change. For complex flows, these fluctuations occur over a wide range of length scales and frequencies, making it impractical to obtain a complete time-dependent solution. The instantaneous governing equation set is manipulated to remove these small-scale components of the flow by means of averaging. The information lost in the procedure of averaging is replaced by empirical parameters. Additional governing equations must be provided to match the same number of empirical unknowns. This process is known as the *turbulence modelling* or the *turbulence closure*.

FLUENT provides a number of established models for turbulence and boundary layer flow in the vicinity of walls. The *two-equation k-ε* model has gained its popularity in the application of practical engineering flow calculations. Variants of the *k-ε* model have been developed to address weaknesses that have been identified over many years of development.

The *standard k-ε* model is the simplest of the complete *two-equation* models. It is based on the assumption of local isotropy (Appendix A.2.1) which means the local production of kinetic energy, k, is in equilibrium with its dissipation rate, ε. This is generally valid for flow away from inlet and boundaries. However when strong anisotropy and non-equilibrium exists, for example in square ducts, the *standard k-ε* model is too crude to apply as it does not predict the secondary motion.

Nevertheless the *standard k-ε* model provides economy of computational time and reasonable accuracy for a wide range of turbulent flows. Its examples in industrial application can be found in stirred reactors (Koh and Xantidis, 1999), bubble columns (Ekambara and Joshi, 2003), tubular reactors (Hjertager et al., 2002), diffuser pumps (Shi and Tsukamoto, 2001), mixed anoxic wastewater treatment vessels (Brannock,

2003) as well as industrial ozonation towers (Cockx et al., 1999; Do-Quant et al., 2000; Ta and Hague, 2004).

A popular alternative and frequent comparison to the *standard k-ε* model is the *renormalisation group-theory* (RNG) *k-ε* model (Yakhot and Orszag, 1986). The purpose of RNG theory is to 'weed out' the small scales and to provide a coarse-grained description of system (Sukoriansky et al., 2003).

Hjertager et al. (2002) and Aubin et al. (2004) investigated the application of both *standard* and RNG models in turbulent liquid flows but found very little difference between the two. Analytis (2003) reported that the RNG model is only better along the axis of the injected gas from his containment test case measuring helium concentration in a rectangular box. Hjertager et al. (2002) concluded that almost no difference between the two turbulence models existed. Unfortunately no comments were made on the computational effort.

On the other hand, a number of applications have emerged with benefits using the RNG model. The RNG model has been reported to have a slight advantage over the standard *k-ε* model in certain classes of flows (Analytis, 2003; Hjertager et al., 2002; Oshinowo et al. 2000). For flows with a high mean shear rate or a massive separation, the eddy viscosity is over-predicted by the standard eddy viscosity formulation (Shih et al., 1995). In addition, the standard model dissipation rate equation does not always give the appropriate length scale for turbulence. Therefore, although the *standard k-ε* model is known to predict right results for flows in pipes, it is also known that it can over-predict the level of turbulence in complex geometries (Analytis, 2003). In such cases, Yakhot and Orszag (1986) showed that the RNG *k-ε* model gives superior predictions than the *standard k-ε* model. The RNG model increases the dissipation rate and hence decreases the level of turbulence, thereby resulting in a lower turbulence viscosity.

Tyack and Fenner (1999) applied the RNG model to a hydrodynamic separator where the standard *k-ε* model requires a far more refined mesh and is less capable to resolve the swirling flow. Lainé et al. (1999) applied the RNG turbulence model to a full-scale settling tank to assess the fluid temperature effect on the hydrodynamic characteristics. De Clercq (2003) applied the RNG model to his study of settling tanks. The literature found thus far has not seen the application of the RNG model on a full-scale ozone contactor. The systems of equations for both the standard and RNG models are detailed in Appendix A.2.1 and Appendix A.2.2 respectively.

For the base model, the RNG model was initially tried and the prediction of tracer agreed satisfactorily with the experimental results (Huang et al., 2002). A case using the *standard k-ε* model was carried out for comparison purpose. The effect of the different turbulence models on the predicted RTD of the ozone contactor is discussed in **Section 3.5.3** .

3.3.4 Boundary conditions and properties

The boundary conditions specify the flow variables on the boundaries of the physical model. Since the boundary conditions affect the resulting solution, it is critical to assign appropriate boundary conditions to the process being modelled. The various imposed boundary conditions are discussed in this section.

3.3.4.1 *Inlet boundary and turbulence quantities*

The water inlet was set as the *mass-flow-inlet* with uniform mass flow calculated from the prevailing flow rate during the experimental tracer tests (described in Section 3.4) and the inlet area. The inlet flow rates during the period were 107.3 and 108.6 ML.d^{-1} for the two experimental tracer tests carried out with and without ozone, i.e., with and without gas injection, respectively. These volumetric flow values were converted into mass flows and entered in the simulations.

For the chosen turbulence model, it is necessary to set values for k and ε at the inlet boundary. However it is difficult to estimate these values directly because they are not very intuitive. The alternative approach is to use other turbulence quantities which can be translated into k and ε. The combination of such quantities chosen for the hydrodynamic model was *turbulence intensity* and *turbulence length scale*.

The turbulence intensity, $\hat{I}$, is defined as the ratio of the root-mean-square of the velocity fluctuations, u' to the average flow velocity, $\bar{u}$, expressed as a percentage:

$$\hat{I} = \frac{\sqrt{(u')^2}}{\bar{u}} \tag{3-11}$$

For internal flows, the turbulence intensity at the inlet is dependent on the flow history upstream. A turbulence intensity of 1% or less is generally considered to be low in the level of turbulence and the values which are greater than 10% are considered high (Fluent, 2003). The combination of a turbulent upstream (from the static mixer) and the gas injection made it difficult and impractical to determine the explicit values of k and ε, or even $\hat{I}$. The turbulence intensity was then treated as an unknown parameter and, as a convenient means of estimation, adjusted to match the experimental tracer response as closely as possible.

As the flow exiting the static mixer is considered highly turbulent, it is expected to assume a high value of $\hat{I}$. As discussed in Section 3.3.2 , $\hat{I}$ was also employed to account for additional turbulence effect contributed by the presence of gas bubbles. Values of 10%, 20% and 50% were tested in the models and compared with the experimental results.

The length scale, l, is a physical quantity related to the size of the large eddies that contain the energy in turbulent flows (Fluent, 2003). For the present model the length scale represents a characteristic of the flow in the static mixer. The value of l was set to 0.1 m which corresponds the blade spacing of the static mixer, as eddies cannot be larger than the spacing. Although this may not be accurate, it should be noted that this is intended to provide an approximation of the inlet turbulent characteristic from the upstream flow history.

$$k = \frac{3}{2}\left(\bar{u}\hat{I}\right)^2 \tag{3-12}$$

$$\varepsilon = C_\mu^{3/4}\frac{k^{3/2}}{l} \tag{3-13}$$

where C_μ is an empirical constant, with a typical value of 0.9.

As with the uniform flow, constant profiles of the turbulence quantities across the inlet are typically adopted. The values of k and ε at the inlet boundary were computed using the Eqns. (3-12) and (3-13) from a fixed value of l_t and an adjustable value of $\hat{I}$.

3.3.4.2 Outlet

The outlet was set as an *Outlet Vent* type boundary. A frictional loss coefficient was assigned to the slot in order to simulate the head loss over the weir. This value was assigned somewhat arbitrarily high enough to ensure that the flow would be evenly distributed along the length of the weir.

3.3.4.3 Wall and roughness setting

The presence of walls affects the prediction of turbulent flows because the no-slip condition must be satisfied at the wall. This condition causes large gradients in the mean velocity field as normal and tangential fluctuations are reduced in close-to-wall flow and amplified in the outer part of the near-wall region.

The underlying assumption of the k-ε model is that the flow must be turbulent. This is not valid for the flow in the region near walls and extensive experimental investigation has categorised three distinct sub-layers in near-wall flows. Wall functions are the semi-empirical formulae developed to "bridge" the flow variables amongst these sub-layers. The standard wall functions are based on the proposal of Launder and Spalding (1974), and have been most widely used for industrial flows, which were chosen in the current model. The effect of wall roughness on the flow was represented by a roughness height of 0.00305 m (Tilton, 1997) and a default value of roughness constant of 0.5 to represent the concrete surfaces. The details of the system of equations describing wall functions are discussed in Appendix A.

3.3.4.4 Free surface

The free water surfaces were represented as rigid frictionless planes. More rigorous modelling of free surface flow would have led to a much more complex formulation, without significant benefits in terms of the objectives of the investigation. The free surface was considered to be a symmetry plane that the normal velocity component is zero.

3.3.4.5 Material properties

Since the problem statement has been simplified into a single-phase model, i.e., water only, the material properties used in the simulations were the density and viscosity of water. The properties were assumed constant at a temperature of 20°C, which corresponds to a density of 998.2 $kg.kL^{-1}$ and a viscosity of 1.003×10^{-3} $kg.m^{-1}.s^{-1}$.

Since the temperature of the water received by Wiggins Waterworks varies through seasons, the value of 20°C was taken a reasonable average for the purpose of the simulations.

3.3.5 Solution methods

The solution of the hydrodynamic model was achieved using a segregated, steady-state solver. The momentum and continuity balances were solved sequentially using this approach. Although very little numerical difficulty was experienced, the time taken to reach a converged solution was inevitably long. This could be contributed by the large size of the model and the use of less powerful computers at the time (parallel processors, 2×550 MHz).

Apart from the well-known physical models, FLUENT also incorporates widely recognised discretisation techniques for the calculation of flow variables. Table 3-1 is a summary of the discretisation schemes used in the hydrodynamic model.

Table 3-1: Summary of the discretisation scheme used in the model

Variable	Scheme
Pressure	Standard
Pressure-velocity coupling	SIMPLEC
Momentum	First order upwind
Turbulence kinetic energy	First order upwind
Turbulence dissipation rate	First order upwind

It must be reminded that a high degree of accuracy was not necessary for the purpose of this base model. Therefore the simplest forms of discretisation schemes were applied to most variables, in order to reduce the computation time.

The SIMPLEC algorithm was adopted for the pressure-velocity coupling. With SIMPLEC, the pressure-correction under-relaxation factor can be set at a higher value, which assists in reaching the convergence sooner if no other convergence problem is experienced.

3.3.6 Simulated tracer tests

Once the hydrodynamic solution was obtained, the tracer tests were simulated as a pulse test, modelled under unsteady-state to obtain the time-dependent flow information.

Since the velocity field has already been solved at this point, only the species transport equation would be solved here. The *tracer* was treated as a non-reacting species and thus the conservation equation of chemical species is simplified to the general form:

$$\frac{\partial}{\partial t}(\rho m_i) + \frac{\partial}{\partial x_j}(\rho u_j m_i) = -\frac{\partial}{\partial x_j} J_{i,j} \tag{3-14}$$

where m_i is the local mass fraction of each species i and $J_{i,j}$ is the diffusion flux of species i resulting from the concentration gradient in turbulent flow.

$$J_{i,j} = -\left(\rho D_{i,m} + \frac{\mu_t}{S_{ch}}\right)\frac{\partial m_i}{\partial x_j} \tag{3-15}$$

where S_{ch} is the turbulent Schmidt number, with a default setting of 0.7 in Fluent. The mass diffusion coefficient of the *tracer* in the mixture, $D_{i,m}$, was a required input in Fluent; however, it was not necessary to define a precise value since the interest of the modelling is *not* in the diffusion of the *tracer* within the total mixture (i.e.: water and the *tracer*). Therefore the mass diffusion coefficient of the *tracer* in the mixture was set to an arbitrary low value and thereby suppressing the first term in Eqn. (3-15). Usually, in a turbulent flow, the mass diffusion is dominated by the turbulent transport as determined by the turbulent Schmidt number. The turbulent Schmidt number measures the relative diffusion of momentum and mass due to turbulence and is on the order of unity in all turbulent flows (Fluent, 2003). Because the turbulent Schmidt number is an empirical constant that is relatively insensitive to the molecular fluid properties, it will not be necessary to alter the default value (0.7) for any species.

Since the mass fraction of the species must sum to unity, the N th mass fraction is determined as one minus the sum of the N-1 solved mass fractions. Thus the N th species should be selected as the species with the largest mass fraction overall in order to minimise numerical errors (Fluent, 2003).

The user-specified value at the inlet is the mass fraction of the tracer, which was arbitrarily set to 0.001 for a single time step of 1s, and changed to zero for the remainder of the time steps in the test. This approach was taken as there was a large uncertainty around the experimental tracer mixture (see Section 3.4) and the final comparison could be resolved by normalised RTD functions (see Section 3.5.3). These will be discussed in details in the respective sections.

Results of tracer concentration at the outlet were recorded in the centre and one on each side measured 2 m away from the edge, as in the experimental tests. The time discretisation was chosen to be sufficiently small at the beginning: 1 s interval for the first ten seconds, then 2 s interval to reach 30 s; then 5 s interval to reach 1200 s, and slowly increased to 10 s interval for the remainder of the simulated tests to 3300 s. This was approximately four times the estimated hydraulic residence time (12 to 13 min).

3.4 Experimental verification

Boyer et al. (2002) discussed various measurement techniques used in the gas-liquid reactors to obtain information for flow analysis. The use of a chemical tracer is classified as the global technique, yielding characteristics of the whole reactor or of a part of the reactor.

This section describes the experimental tracer tests which results were used to validate the base model. The simplification of one-phase (water) hydrodynamic model required two experimental tracer tests to be conducted under different operating conditions to examine the effect of the gas presence on the overall RTD. The tracer tests were carried out by the author and Mr C Brouckaert, assisted by trainees and staff at Wiggins Waterworks. The chemical analysis was undertaken by the Umgeni Water laboratory.

3.4.1 Choice of tracer

In a full-scale water treatment plant, the choice of tracers is limited due to the health aspect of the public consumption. In general an ideal tracer should include the following properties:

- Detectability at low concentration
- Adherence to the conservation law in the system investigated
- Low toxicity - especially in drinking water application

The types of tracers commonly used in industries are, for example, fluorescent dyes or various salts. Although fluorescent dyes are more readily available and low in cost, the dye may impose colour on the treated water, and large amount of dye would need to be dosed initially to supplement for the losses through self-decomposition and its reaction with ozone.

Lithium chloride (LiCl) was chosen for this study as it satisfied all of the criteria mentioned above. Its use has been found in various studies in the water and wastewater treatment process (Cockx et al., 1999; Seguret et al., 2000; De Clercq, 2003). The low detection threshold of Li^+ is an advantage to enable the dilute samples at the beginning and the tail of the tracer tests to be identified (Do-Quang et al., 2000; Cockx et al., 1999).

The choice of LiCl also resulted from previous experience at Umgeni Water on tracer studies of water and wastewater equipment. The analysis for Li^+ had already been set up and tested.

3.4.2 Experimental method

Two tracer tests were carried out on the ozone contactor under different operating conditions, i.e., with and without gas injection. In each test, LiCl was first dissolved in water to make the dosing concentrate. The concentrate was then dosed into the feed chamber for the contactor (shown as (a) in Figure 1-2).

A preliminary model was constructed to assist with planning of the physical tracer test, such as determining the tracer dose and sampling intervals (Brouckaert et al. 2000). Then the dosing solution was prepared for each test. It was unfortunate that the LiCl to be used in the tracer tests was damp due to leakage in the storage room. Because of the large quantity of LiCl required and the scheduled time for the tracer tests, it was decided to proceed using the damp LiCl salt and that the made-up LiCl concentrates should therefore be used in the calibration for the subsequent sample analyses. A sample of each dosing solution was analysed to be 34560 mg Li^+/L (with gas) and 39080 mg Li^+/L (without gas), yielding LiCl solutions of approximately 20% (m/m).

The duration of each test was 42 min, which was assumed sufficient to recover most of tracer as it was almost four times the mean residence time. The first sample was taken 4 min after dosing as this allowed the tracer to traverse from the feed chamber to the contactor. Since it was impossible to dose at the contactor inlet, this lag time was calculated to be approximately 16 s and subtracted in the numerical analysis. Thereafter samples were taken at 1 min intervals until the 10th min. One sample was taken at the 12th minute as the theoretical mean residence time was calculated to be 12.17 min. The subsequent samples were taken at 3 min intervals up to the 24th min and then at 6 min interval till the end of the tracer test.

Samples were taken at three points along the outlet weir. Figure 3-3 (a) shows one sampling point at the centre, and two other points were located 2 m from either side of the contactor walls (Figure 3-3 (b)).

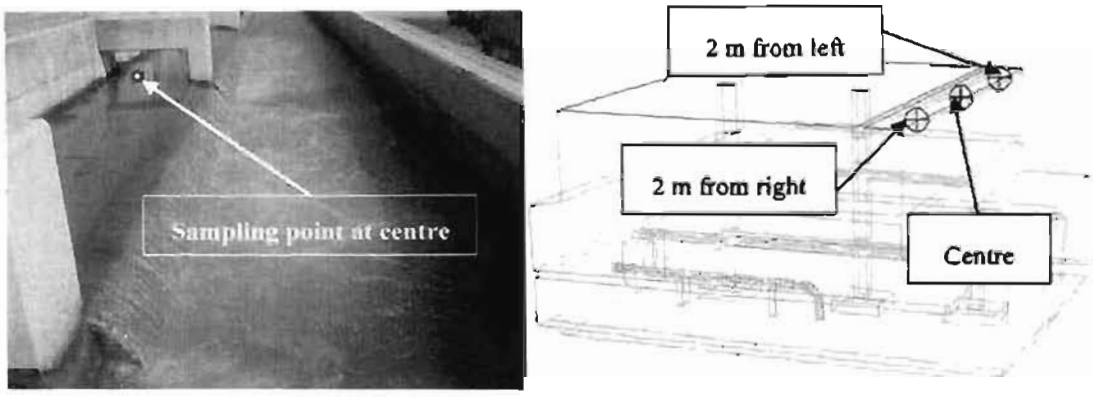

(a) Experimental (b) Simulated

Figure 3-3: Sampling points along the weir

Samples were taken simultaneously at all three points, and subsequently analysed using an atomic absorption (AA) spectrophotometer at the Umgeni Water laboratory. The water flow rate was maintained at a steady rate for the duration of both tracer tests. The water flow rate was recorded by the plant staff during the tests. The experimentally measured values are recorded in Appendix B.2.

3.5 Results and discussion

Both simulated and experimental results are first presented in their raw time-plots of the tracer response curves. The experimental mass balances required error analyses to assess the discrepancy. Various parameters were investigated for their effects on the RTD prediction. The results are discussed under separate sub-headings. The normalisation technique discussed in **Section 3.1.2** was employed to achieve a comparable basis amongst the different case scenarios.

3.5.1 Experimental results

The Li^+ concentrations measured at the three sample points were plotted against the corrected time to obtain the experimental response curves shown in Figure 3-4 and Figure 3-5. Since the weir forces the flow to be evenly distributed over its width, the measured values were averaged to estimate the concentration over the entire length of the weir, representing $C_{out}(t)$ for the calculation of tracer mass balance.

The hydraulic residence time and T_{10} were calculated for each test and plotted for comparison. While the flow remained relatively constant at about 107 $ML.d^{-1}$, T_{10} was less in the case with gas injection, suggesting that gas promotes mixing and forces portions of fluid to exit earlier than assumed.

The tracer response curves for the cases with and without gas injection showed a generally similar pattern, with some differences in detail. Without gas injection, the measured concentration appeared higher on the left side and the residence time residence distribution was narrower (Figure 3-5) than the case when gas was present (Figure 3-4). In both cases, the trends of the tracer response curves at the centre were similar to the

right. Although the difference in the response curves on the left was more striking in the absence of gas, the trends of the average responses were little changed.

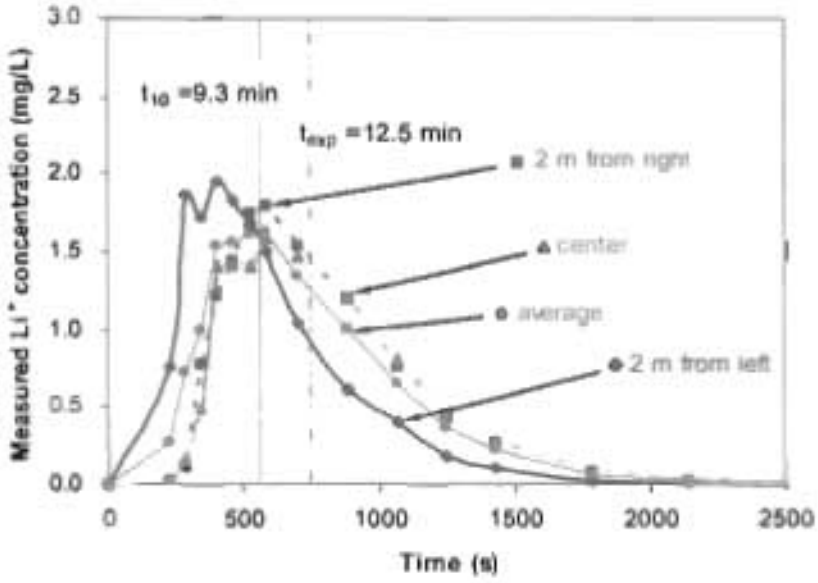

Figure 3-4: Experimental tracer response curves at various points along the outlet weir *With* gas injection

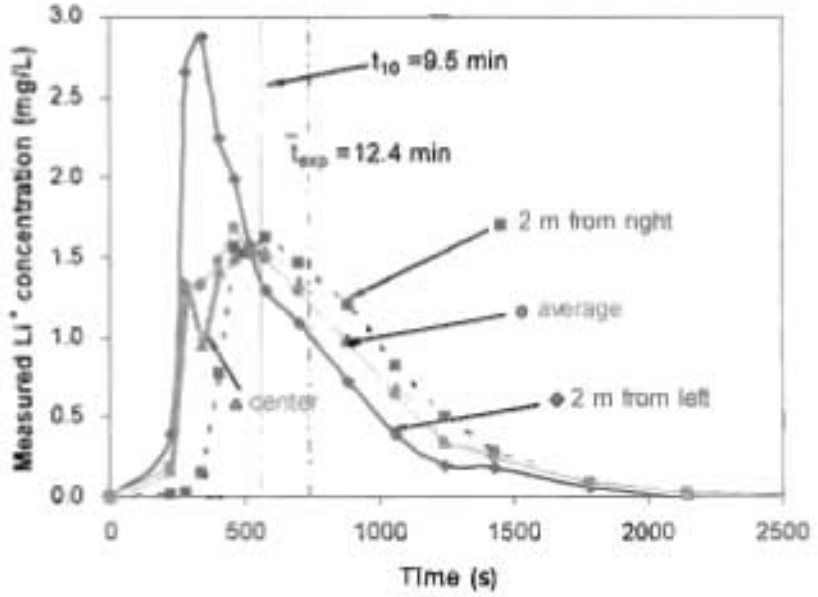

Figure 3-5: Experimental tracer response curves at various points along the outlet weir *Without* gas injection

The uneven distribution of tracer, with more going to the left side, was observed irrespective of gas injection. The effect was more pronounced when the gas was absent, as shown in Figure 3-5. This observation seems consistent with the notion that the gas bubbles increased the level of turbulent mixing in the contactor. It also shows that application of characteristic time T_{10} is inappropriate in a complex system

if the control point of the outlet concentration is inappropriately placed and the details of the hydrodynamics is not well-understood.

Tracer mass balances. A successful tracer test should obtain a 100% lithium recovery. Since the LiCl used to prepare the tracer concentrates was damp, the intention was for the laboratory to use the concentrate to prepare the calibration curve as the required tracer response results should be relative to what was injected. However, the intention was misunderstood and the laboratory performed an 'absolute' calibration with pure LiCl. This means that the uncertainties in the response measurements are compounded with the uncertainties the measurement of the concentrate. This was shown from the calculation of the tracer mass balances which indicated the Li^+ recovery of 129% and 119% for tests with and without gas injection respectively (see Appendix B.3). It seemed the only way to rectify this would have been to repeat the experiment.

Repeating the tracer experiment was prohibitive and included logistical difficulties. More importantly, it must be considered whether repeating the experiment could have significantly added to the understanding of the contactor in order to proceed to the next step of the investigation. From Figure 3-4 and Figure 3-5, it seemed that the gas injection affected the average tracer response curves very little, although the left-right asymmetry in the flow at the outlet was distinct in the absence of gas. A more accurate tracer response would not have deviated from this observation greatly. It was therefore attempted to reconcile the tracer recovery by some form of uncertainty analysis.

Mass of tracer entering the inlet. In each tracer test, the amount of tracer dosed (m_{in}) was calculated by multiplying the volume of the dosing solution (V_{dose}) and its measured Li^+ concentration (C_{dose}).

$$m_{in} = C_{\text{dose}} \times V_{\text{dose}} \tag{3-16}$$

The uncertainties which could contribute to an incorrectly calculated mass of tracer at the inlet were associated with: the analysis of Li^+ dosing concentrate, the mass of LiCl dosing solution weighed and the density of solution as a function of the mass percentage of LiCl in solution. As the dosing solution was highly concentrated, it must be diluted several times for the Li^+ value to fall below the detection upper limit. The errors carried down due to dilution were likely to be amplified. The measured Li^+ concentration thus bore the highest uncertainties of the calculation variables at the inlet. The Monte Carlo Method was applied to assess the extent of the uncertainties in dilution and the analysis technique on the measurement of Li^+ concentrate.

Mass of tracer exiting the outlet. The mass of tracer collected at the outlet (m_{out}) was computed by the following equation:

$$m_{out} = Q \int C_{out}(t)\, dt \tag{3-17}$$

where Q is the water flow rate and C_{out} is the average concentration of Li^+ at the outlet.

The accuracy of the flow rates measured was dependent on the flow meter. The sensitivity of the flow meter measuring the flow is reported to be 3% by the Wiggins Waterworks and this value was used as the

uncertainty associated with the flow. The integral $\int C_{out}(t)dt$ involved many uncertainties. The Li^+ concentration values of the samples were subjected to the uncertainties of the analysis technique and the use of an average value of the measurements to represent the Li^+ concentration for the entire weir. The uncertainty with the latter was estimated by comparing the simulated tracer concentration over the entire weir to the average value calculated from the three simulated sample points. The time involved in the tracer test was also subjected to errors in estimating the delay volume for the tracer to reach the inlet from the distribution tower. In order to assess the variance associated with the integral, the Monte Carlo Method was applied again to calculate the resulting variance from the contributing uncertainties.

Data reconciliation and Error analyses. Since all measurements contain some degrees of errors, it was necessary to account for the large discrepancies by means of an appropriate error analysis. All possible sources of uncertainties related to the calculation were considered and assessed for their effect on the mass balances.

The uncertainties or the errors included in the measurements were represented statistically in the form of variance. While the known variance associated to a variable was used in the analysis, a conservative value was estimated if the variance was not known. The more uncertain a variable was measured, the higher the value of variance was assumed.

The data reconciliation was performed with assumed variances on various terms in the mass balances in Eqns. (3-16) and (3-17) and thereafter the resulting deviation was examined between measured and reconciled values in relation to the assumed variances. Due to the complex nature of the analysis, the contribution of many sources of errors to an integral or a variable may be difficult to quantify into a single value. This was overcome by the Monte Carlo Method or known as the stochastic method which randomly generates a series of prediction at every measured value within the known or estimated variance. From these predictions, many values can be obtained for the integral or the variable. These values were normalised and the overall variance was calculated accordingly. The Monte Carlo simulation was used to only estimate the variance on the integrated outlet concentration.

The error analyses were performed using the Microsoft Excel Solver®. The variables discussed above were adjusted to minimise the objective function defined in Eqn. (3-18):

$$F_{obj} = \sum_{i=1} \frac{\left(Y_{i,m} - Y_{i,\,adj}\right)^2}{\sigma_i^2} \tag{3-18}$$

where $Y_{i,m}$ is the mean value of the ith variable, $Y_{i,\,adj}$ is its adjusted value and σ_i^2 is the known or calculated variance of the associated variable. In essence, the changes in the variables were minimised in Eqn. (3-18). This condition was subjected to the constraints that the net tracer mass must be zero, i.e.: Eqn. (3-16) = Eqn. (3-17), and the mean residence time must equal to the theoretical residence time (i.e.: $\bar{t} = V/Q$). The results are presented in Appendix B.4.

From the error analyses, the values of the dosing concentrates varied the most. It seemed that the concentrates were under-measured. This was deduced as the associated uncertainty was large and would have a significant impact on the calculation of the inlet tracer mass. On the other hand, the flow was shown to have approximately a 10% deviation from the set rate. This point differed from the information provided by Wiggins Waterworks. However, it will be revealed later that a 10% variation of flow has little effect on the hydrodynamic simulation.

The main outcome of the error analysis pointed to the most probably cause of the discrepancy is the lithium dose, because there was little deviation in the resulting mean residence time. This also indicates that even if repeating the tracer tests more accurately may bring more satisfaction with data reconciliation, it would most probably not contribute much more to our understanding of the reactor.

3.5.2 Simulated results

Experimentally the effect of gas injection on the overall RTD was slight. It was therefore decided to follow the single phase model approach, i.e., considering only water. Since the gas injection could not be represented directly in the single phase model, the effect was modelled by adjusting the turbulence intensity of the flow entering the contactor through the static mixer. The turbulence intensity $\hat{I}$ of the incoming flow is a required boundary condition for the turbulence model as explained in **Section 3.3.4.1** . As this value was not known explicitly with or without gas injection due to the effect of the static mixer blades, it seemed sensible to treat the turbulent intensity as an unknown parameter that could be adjusted to match the experimental tracer response as closely as possible.

The flow from the static mixer is expected to carry more turbulence into the system and the gas injection is also considered to contribute to further mixing, thus values of more than 10% were investigated. Results of using intensities of 10%, 20% and 50% are shown in Figure 3-6 (a) to (c). In all three cases, the tracer always appeared early on the left side. As $\hat{I}$ increases, the tracer response curve on the left becomes sharper and narrower, and the tracer concentration is also higher.

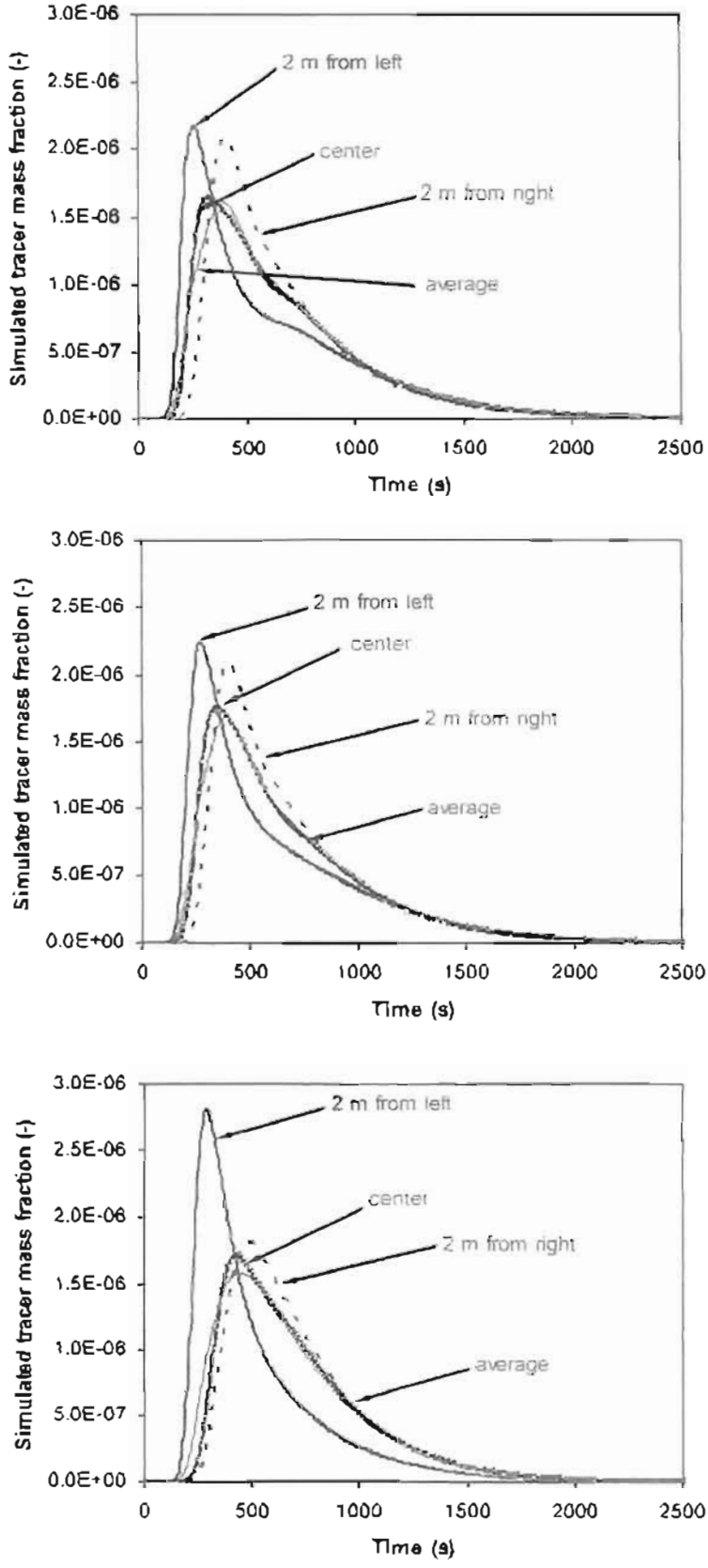

Figure 3-6: Simulated tracer responses varying the turbulence intensity values

From a qualitative comparison with the experimental results in Section 3.5.1 , the prediction of the turbulence intensity ratio at 50% was noted by its resemblance to the experimental response curves, though

in the contrary notion. It appeared that the gas injection is better represented by a *low* turbulence intensity value, differing to what was expected. However the difference between the simulated responses of the left hand side seems to *increase* with turbulence intensity.

Computational effort. At the time of carrying out these hydrodynamic models, the computational time was greatly constrained by the computing power available. Each scenario may take up to weeks to reach convergence due to the size of the model. However, there was little numerical instability experienced during the simulations, unlike that reported by Analytis (2003).

3.5.3 Comparison using normalised RTD functions

The mathematical properties of the RTD density function were discussed in **Section 3.1.2** . The density functions of the experimental and the simulated tracer responses were calculated using Eqn. (3-19), the fraction of tracer leaving the reactor which has resided in the reactor for times between t and $t + \Delta t$:

$$E(t) = \frac{C(t)}{\int_0^\infty C(t)} \tag{3-19}$$

The normalised time and RTD function calculated using Eqns. (3-3) and (3-5) were plotted in Figure 3-7. The model using a higher turbulence intensity value gave a much better fit to the *average* experimental results. Furthermore, there is very little difference noted between the experiments with and without gas injection. The gas presence in this global sense has no distinct effect on the *overall* RTD.

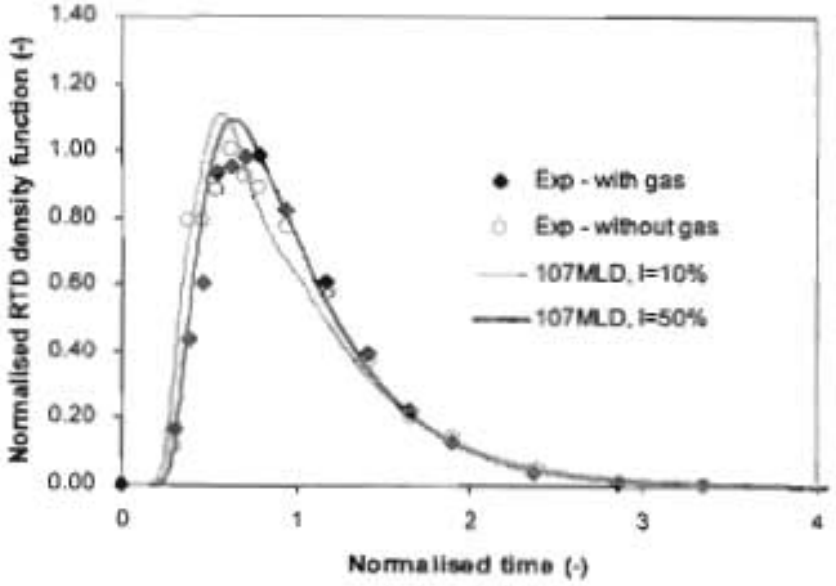

Figure 3-7: Comparison of predicted normalised RTD density function at different turbulence intensity with experimental data average over three points

From an operation point of view of an ozone contactor, it must be stressed that the main objective here is to match the *average* simulated tracer response as closely as possible to the experimental ones. Although the details of the predicted left-right distribution were contrary to the experimental observation, the *average* simulated tracer responses seemed to follow that the dispersion decreases as turbulence intensity increases.

Another important descriptive quantity of RTD is the spread of the distribution, commonly measured by the variance σ^2. The normalised variance, σ_θ^2 is defined as in Eqn. (3-20):

$$\sigma_\theta^2 = \int_0^\infty (\theta - 1)^2 E(\theta) d\theta \tag{3-20}$$

The dimensionless variance σ_θ^2 indicates the degree of dispersion, covering a theoretical range of zero to infinity. However, the range $0 \le \sigma_\theta^2 \le 1$ covers most practical situation as $\sigma_\theta^2 = 0$ for a PFR and $\sigma_\theta^2 = 1$ for a CSTR (Nauman and Clark, 1991).

Table 3-2: Summary of quantitative measure of the RTDs.

	Experimental		Simulated	
	with gas	without gas	I = 50%	I = 10%
σ_θ^2	0.2315	0.2586	0.2764	0.3671

The variance values were calculated for both experimental sets and all the simulated scenarios. Table 3-2 is an extract of these results confirming the notable resemblance of the simulated results. The hydrodynamic model conducted at a flow rate of 107 ML.d^{-1} and 50% turbulence intensity using the RNG k-ε model was considered satisfactory and it was decided to proceed with this model for the kinetic modelling in the next chapter.

3.5.4 Scenario study

Effect of flow rate variation. The set flow rate was originally 100 ML.d^{-1} but the observed flow was about 107 ML.d^{-1}. From the error analysis, it was also indicated that the flow rate may deviate about 10%.

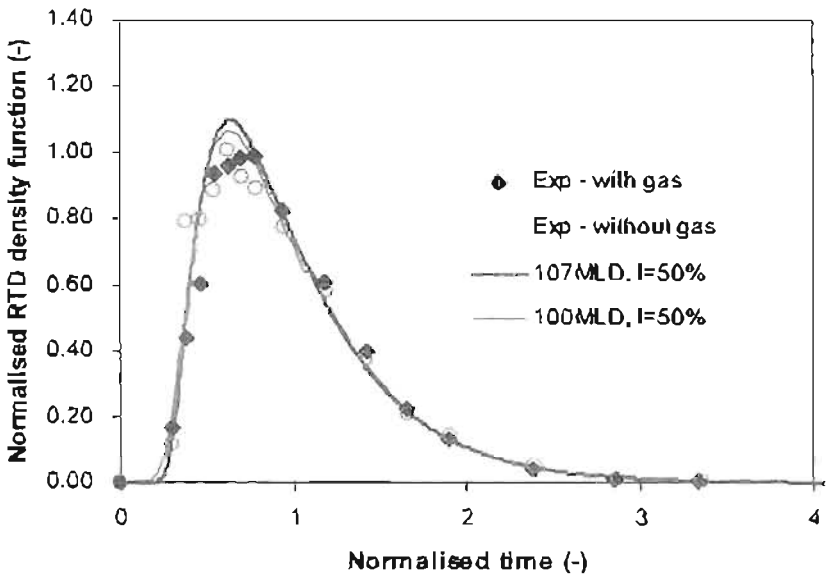

Figure 3-8: Comparison of predicted normalised RTD density function at different flow rates with experimental data

A simulation was carried out at 100 ML.d^{-1} for comparison purpose and the normalised results are plotted in Figure 3-8. As indicated in Figure 3-8, the variation of flow rates did not seem to have a distinct effect on the overall RTD.

Effect of turbulence models. No turbulence model is universally accepted to be superior to another. A comparison case was tested by applying the *standard* k-ε model. From the simulated results in Section 3.5.2 , an increase in turbulence resulted in a higher peak in RTD and a narrower spread of the tracer response. In Figure 3-9, the RTD prediction indicated that the *standard* k-ε model seems to over predict the level of turbulence in the contactor.

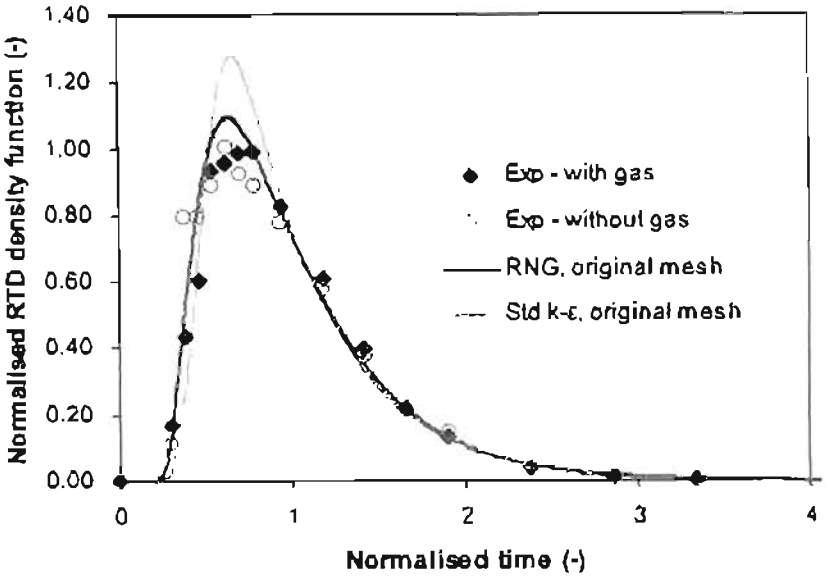

Figure 3-9: Comparison of predicted normalised RTD density function at different turbulence models with experimental data

This notion seems to be consistent with literature that the RNG k-ε model handles flows in complex geometries better as it increases the dissipation rate to resolve constrained flow over obstructions. Large extra strains exerted by such as the curved boundary layers, high swirling flows exhibit in the contactor could explain the better prediction of the RNG-based k-ε model over the standard k-ε model.

Effect of mesh. An appropriate mesh is essential to the accuracy of the resulting solution and the extent of computation time. It is important that the solution does not change significantly with the increase in grid density.

A refined mesh was later carried out in GAMBIT 2.1.2 to produce 185 405 tetrahedral elements with 40 489 nodes, an increase of almost 80% of the original meshed elements (refer to Section 3.3.1). Applying the *standard* k-ε model with 50% turbulence intensity at 107 ML.d^{-1} but only changing the mesh, the simulated results were shown in Figure 3-10. Contrary to expected, the predicted RTD by using the refined mesh did not improve from the prediction by the original, *coarser* mesh. Although the intention of this study is not about finding the optimum mesh, Figure 3-10 demonstrates that mesh refinement is not necessary in this case.

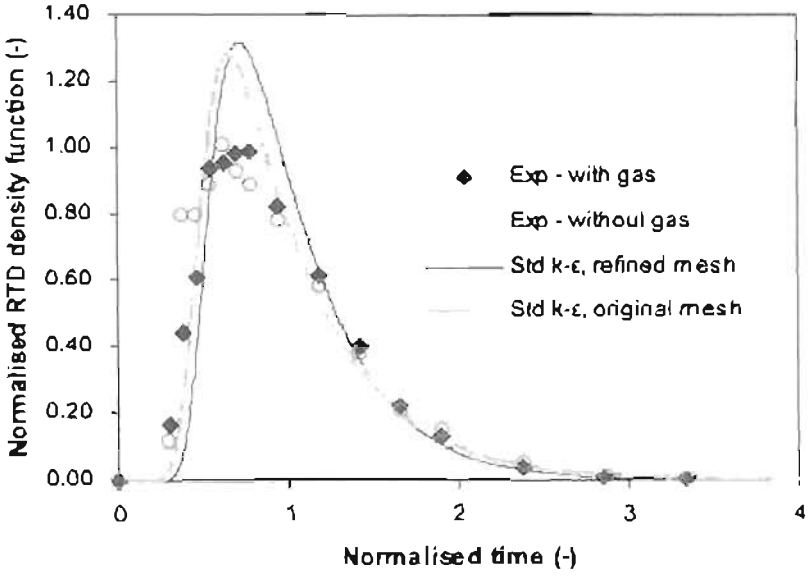

Figure 3-10: Comparison of predicted normalised RTD density function using different mesh with experimental data

3.5.5 Simulated contours

Based on the model using the RNG k-ε model with the turbulence intensity of 50%, various contour plots are drawn to provide a qualitative understanding of the internal hydrodynamics. In Figure 3-11, the contour plots of the tracer mass fraction in the bottom compartment (shown from the top) and in the whole contactor (shown from the side) demonstrate how the tracer traverses in the contactor with time.

From the top view of the bottom compartment, it can be observed that the flow impinges on the supporting pillar and a large circulation is formed on the left. A higher concentration of tracer is observed on the left of the bottom compartment compared to that on the right. From the side view of the contactor, it is noted that while the tracer front moves smoothly towards the exit, a fair amount of tracer seems to remain in the bottom compartment due to the dispersion.

Upon a closer inspection, it can be seen that the left-right distribution of flow which was observed in both experimental and simulated results is formed in the bottom compartment. The observation can probably be explained better by Figure 3-12, indicating the flow velocity in the bottom compartment. The flow impinges on the first pillar as it enters the contactor, hindered by the pipe on the right, and thereby forcing the flow towards left. Portion of fluid seems to spin off from the circulation on the left and advanced earlier than that on the right. The asymmetry in flow distribution is thus strongly influenced by the contactor geometry.

Figure 3-13 presents the contour plots of tracer concentration 5 min after the tracer injection. From a top view of the contactor Figure 3-13 (a) shows the tracer is retained on the *right* of the bottom compartment only. The uneven distribution of flow persists throughout the contactor. On the top compartment of the contactor, the tracer front can be noticed in Figure 3-13 (b), exiting the weir on the left earlier than on the right.

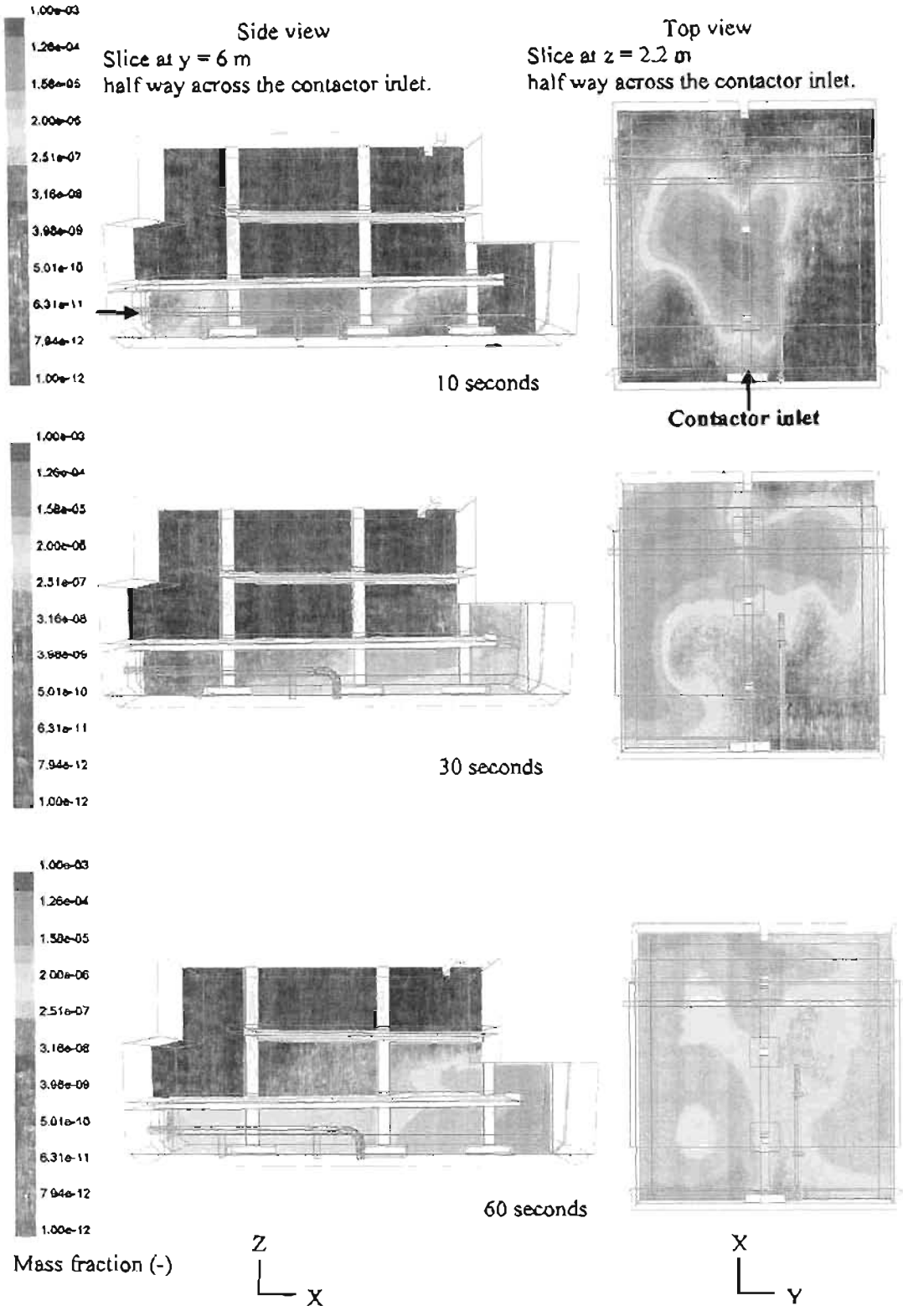

Figure 3-11: *Snap-shots* of the simulated tracer contours

It is worth mentioning that the modelling boundary is only limited to the ozone contactor. The static mixer upstream of the contactor was not modelled. The inlet to the contactor is indicated by a black arrow.

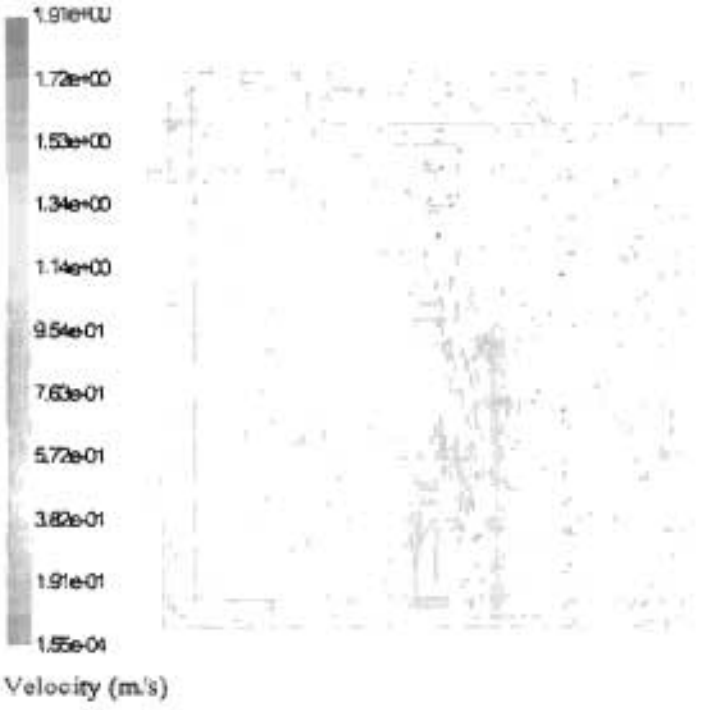

Figure 3-12: Velocity vectors in the bottom compartment 5 min after tracer injection

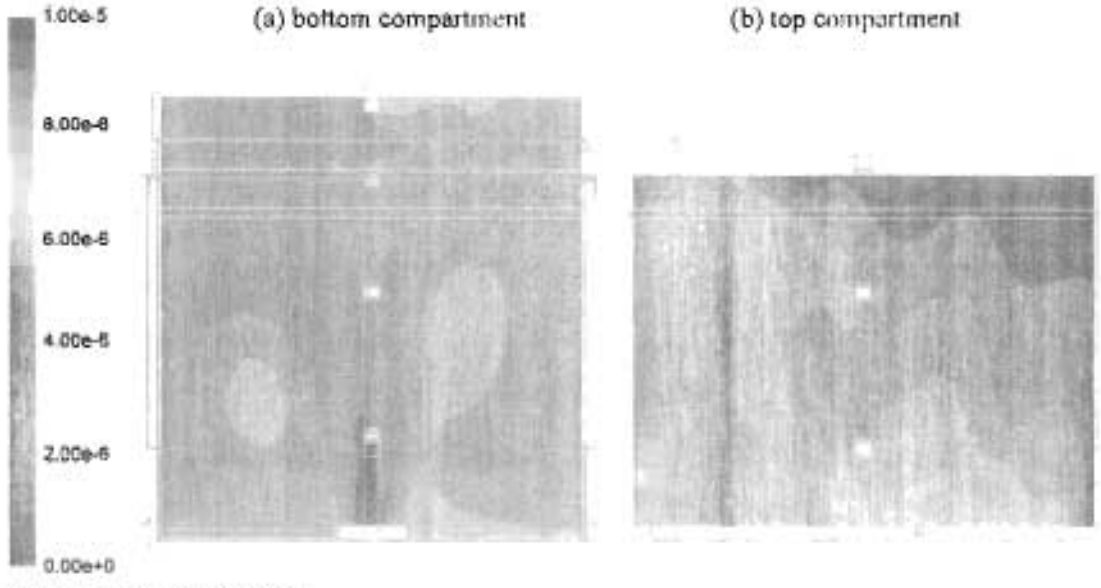

Figure 3-13: Contour plots of tracer in the top and bottom compartments 5 min after injection

3.6 Conclusions

One of the major simplifications in the study was using a one-phase, water-only, model to represent the two-phase system. Since the effect of gas injection on the average experimental RTD was slight, and the gas injection could not be represented directly in the single phase model, it was tried to represent the effect by adjusting the turbulent intensity of the flow entering the contactor through the static mixer.

The turbulent intensity of the incoming flow is a required boundary condition for the turbulence model. Even without gas injection, its value was not known due to the effect of the static mixer blades. Therefore it made sense to treat the turbulent intensity as an unknown parameter that could be adjusted to match the experimental tracer response as closely as possible.

The predicted overall RTD by the one-phase model agrees remarkably well with the experimental results. The variation of tracer response along the weir predicted by the model was confirmed by the experimental profiles, with tracer exiting earlier on the left than on the right. From the model, it was shown that the left-right flow distribution was initiated by the contactor geometry; however, the flow asymmetry predicted by the model responded in opposite ways to the experimental observation. Modifying the turbulence intensity ratio at the inlet to fit the experimental tracer data was initially an attempt to model the effect of gas injection. Although it is clearly a very rough approximation, the subsequent simulated results show that the effect from the upstream flow history is more substantial than the presence of the gas phase. Experimentally the effect of the gas injection neutralises the flow asymmetry. Therefore a decision had to be made as to which to accept to represent the goodness-of-fit to the measurements. For the function of the contactor, it was more important to match the overall RTD. The experimental tracer results also suggested that the gas injection has no distinct effect on the average tracer response cuves. The effect of the gas was manifested in the shift in the left-right distribution of flow in the contactor. Since this was considered of lesser importance to the reaction modelling, it was decided to continue with the single phase, water only model. It is also evident that, from the present study, CFD modelling provides a more robust approach than the $C \cdot t$ concept for dealing with systems with unconventional configurations.

It must be noted that in many instances, the effect of individual model parameters could not be differentiated experimentally. The type of model and the parameter values were chosen to represent as closely as possible to the experimental results. The flow details of the base model could not be validated by other experimental means. The model is therefore constrained to fit the predicted RTD to the experimental results. A full two-phase model, besides involving considerably greater computational difficulties, would also introduce many unknown factors and uncertainties concerning aspects such as bubble size, bubble coalescence etc. However, in terms of the main purpose for which the model is required, which is to predict the disinfection performance of the contactor, the very good agreement obtained between the approximate model and the overall experimental RTD, indicated that the model is adequate. It was decided to proceed with the one-phase, water-only model for the ozone reaction modelling.

3.7 References

Analytis G. Th. (2003) *Implementation of the renormalization group (RNG) k-ε turbulence model in GOTHIC/6.1b: solution methods and assessment.* Annals of Nuclear Energy 30: 349-387

Aubin J., Fletcher D.F. and Xuereb C. (2004) *Modeling turbulent flow in stirred tanks with CFD: the influence of the modelling approach, turbulence model and numerical scheme.* Experimental Thermal and Fluid Science 28: 431-445.

Boyer C., Duquenne A.-M. and Wild G. (2002) *Measuring techniques in gas-liquid and gas-liquid-solid reactor*. Chemical Engineering Science 57: 3185-3215.

Bradshaw P. (1978) *Introduction* in Topics in Applied Physics Volume 12: *Turbulence*, Bradshaw P., ed., 2nd ed., Springer-Verlag. New York. ISBN: 0-387-08864-4.

Brannock M.W.D. (2003) *Computational fluid dynamics tool for the design of mixed anoxic wastewater treatment vessels*. PhD thesis, Department of Environmental Engineering, University of Queensland, Australia.

Brouckaert C.J., Pryor M., Brouckaert B.M. and Buckley C.A. (2000) *A computational fluid dynamics study of an ozone contactor*. Proceedings of the 2000 WISA Biennial Conference and Exhibition, Sun City, South Africa, 28 May - 1 June.

Cockx A., Do-Quang Z., Lin A. and Roustan M. (1999) *Use of computational fluid dynamics for simulating hydrodynamics and mass transfer in industrial ozonation towers*. Chemical Engineering Science 54: 5085-5090

Danckwerts P.V. (1953) *Continuous flow systems – Distribution of residence times*. Chemical Engineering Science 2 (1): 1-13.

De Clercq B. (2003) *Computational fluid dynamics of settling tanks: development of experiments and rheological, settling, and scraper submodels*. PhD thesis, School of Applied Biological Sciences, University of Gent, Belgium.

Do-Quang Z., Cockx A. and Liné A. (2000) *Recent advances in modelling tool development and application for ozone reactors design: The CFD approach*. Proceedings of the International Specialised Symposium IOA 2000, Toulouse, France, 1-3 March: 275-300.

Ekambara K. and Joshi J.B. (2003) *CFD simulation of mixing and dispersion in bubble columns*. Transactions of the Institution of Chemical Engineers 81, Part A: 981-1002, September.

Fluent (2003) *Fluent 6.1 User Guide*, Lebanon, USA, Fluent Inc., 2003-01-25

Fogler H.S. (1997) *Elements of Chemical Reaction Engineering*. 2nd edition, Prentice-Hall of India Private Ltd., New Delhi, India. ISBN: -81-203-0745-3

Hjertager L.K., Hjertager B.H. and Solberg T. (2002) *CFD modelling of fast chemical reactions in turbulent liquid flows*. Computers and Chemical Engineering 26: 507-515.

Hoigné J. (1998) *Chemistry of aqueous ozone and transformation of pollutants by ozonation and advance oxidation processes*. In *The Handbook of Environmental Chemistry*, Vol. 5, Part C *Quality and Treatment of Drinking Water II*, Hrubec J., ed., Springer-Verlag, Berlin.

Huang T.H., Brouckaert C.J., Docrat M., Pryor M. and Buckley C.A. (2002) *A computational fluid dynamic and experimental study of an ozone contactor*. Water Science and Technology 46 (9): 87-93

Koh P.T.L. and Xantidis F. (1999) *CFD modelling in the scale-up of a stirred reactor for the production of resin beads*. Second International Conference on CFD in the Minerals and Process Industries, CSIRO, Melbourne, Australia, 6-8 December: 369-374. Accessed on 25 July 2002 at URL http://www.cfd.com.au/cfd_conf99/papers/064KOH.pdf

Kuipers J.A.M. and van Swaaij W.P.M. (1998) Computational fluid dynamics applied to chemical reaction engineering. Wei J. Anderson J.L., Bischoff K.B., Denn M.M. and Seinfeld J.H., eds, Advances in Chemical Engineering **24** : 227-328.

Lainé S., Phan L., Pellarin P. and Robert P. (1999) *Operating diagnostics on a flocculator-settling tank using Fluent CFD software*. Water Science and Technology **39** (4): 155-162.

Launder B.E. and Spalding D.B. (1974) *The Numerical Computation of Turbulent Flows*. Computer Methods in Applied Mechanics and Engineering **3**: 269-289.

Levenspiel O. (1962) *Chemical Reaction Engineering*, 2nd edition, New York: John Wiley and Sons, USA. ISBN: 0-471- 53019-0.

Levenspiel O. (1999) *Chemical Reaction Engineering*, 3rd edition, New York: John Wiley and Sons, USA. ISBN: 0-471-25424-X.

MacMullin R.B. and Weber M. Jr. (1935) Transactions of the American Institute of Chemical Engineers **31**: 409.

Nauman E.B. and Clark M.M. (1991) *Chapter 4. Residence Time Distribution*. In *Mixing in Coagulation and Flocculation*. Clark M.M., Amirtharajah A., and Trussell R.R., Denver, USA, American Water Works Association Research Foundation: 127-158.

Oshinowo L., Jaworski Z., Dyster K.N., Marshall E. and Nienow A.W. (2000) *Predicting the tangential velocity field in stirred tanks using the multiple reference frames (MRF) Model with validation by LDA measurements*. Proceeding of 10th European Conference Mixing, Delft: 281–288.

Pontius F.W. (1999) *Complying with the interim enhanced Surface Water Treatment Rule*. Journal of American Water Works Association **91** (4): 28-32; 187-188.

Roustan M., Kim J.H. and Marinăs B.J. (2000) *Hydrodynamics of ozone reactors*. International Specialised Symposium IOA2000: Fundamental and Engineering Concepts for Ozone Reactor Design, Toulouse, France.

Seguret F., Racault Y. and Sardin M. (2000) *Hydrodynamic behaviour of full-scale trickling filters*. Water Research **34** (5): 1551-1558.

Shi F. and Tsukamoto H. (2001) *Numerical study of pressure fluctuations caused by impeller-diffuser interaction in a diffuser pump stage*. Journal of Fluids Engineering **123**: 466-474, September.

Shih T.-H., Liou W.W., Shabbir A., Yang Z. and Zhu J. (1995) A new k-ε eddy viscosity model for high Reynolds number turbulent flows. Computers and Fluids **24** (3): 227-238.

Sukoriansky S., Galperin B. and Staroselsky I. (2003) *Cross-term and ε-expansion in RNG theory of turbulence*. Fluid Dynamics Research **33**: 319-331.

Ta C.T. and Hague J. (2004) *A two-phase computational fluid dynamics model for ozone tank design and troubleshooting in water treatment*. Ozone-Science & Engineering **26**: 403-411.

Tilton J.N. (1997) *Section 6 Fluid and particle dynamics*. In *Perry's Chemical Engineers' Handbook*. Perry R.H., Green D.W. ed., Maloney J.O. associate ed., 7th ed. New York: McGraw-Hill. ISBN: 0-07-049841-5.

Tyack J.N. and Fenner R.A. (1999) *Computational fluid dynamics modelling of velocity profiles within a hydrodynamic separator*. Water Science and Technology 39 (9): 169-176.

US EPA (1999) *Disinfection Profiling and Benchmarking Guidance Manual*. United States Environmental Protection Agency, Office of Water, EPA 815-R-99-013.

Versteeg H.K. and Malalasekera W. (1995) An Introduction to Computational Fluid Dynamics: the Finite Volume Method. Longman Scientific and Technical. Harlow, England.

Yakhot V. and Orszag S.A. (1986) *Renormalization group analysis of turbulence: I. Basic theory*. Journal of Scientific Computing 1 (1): 1-51.

4

OZONATION OF NATURAL WATERS

"Study the past if you would define the future"

- Confucius (551 BC - 479 BC), Chinese philosopher and reformer

The aqueous ozone reactions in natural waters are complex due to varying reactivity of the water matrix which consists of many organic and inorganic compounds. In literature, there have been very few general kinetic rate constants reported for natural waters. Many ozone kinetics investigations were carried out in synthetic waters which exclude the influence of the background bio-matrix. In natural waters, the major governing parameters of the reactions may vary greatly from one source water to another. For a water treatment plant receiving raw water from a fixed source, the analyses can also be influenced by factors such as the seasonal fluctuations, the different draw-off point or the upstream operating condition prior to ozonation.

This chapter discusses the methodology in characterising the effects of ozonation on the natural waters. Section 4.1 introduces the categorised routes of dissolved ozone depletion. The reactions between ozone and the constituents of the natural water matrix contribute the most in ozone decay. The raw water reaction kinetics are examined further in Section 4.2 where the generalised rate law is discussed. The possible surrogates in representing the matrix constituents are examined in Section 4.3 . The current approach of experimental characterisation is discussed in Section 4.4 . A generalised rate law which accounts for the water quality is proposed for the kinetics work in the current investigation. The concluding remarks of this discussion chapter are given in Section 4.5 .

4.1 Introduction

The use of ozone in water treatment is generally based on the concept that reactions occur between dissolved ozone and water-soluble substances. Due to the high reactivity of ozone and process limitation, the introduced gaseous ozone will not only react with the target compounds. The distribution of the gaseous ozone can be categorised into off-gas losses, consumption by ozone-consuming substances (OCS) and its self-decomposition (Bredtmann, 1982). For illustration, Figure 2-6 can be simplified to Figure 4-1.

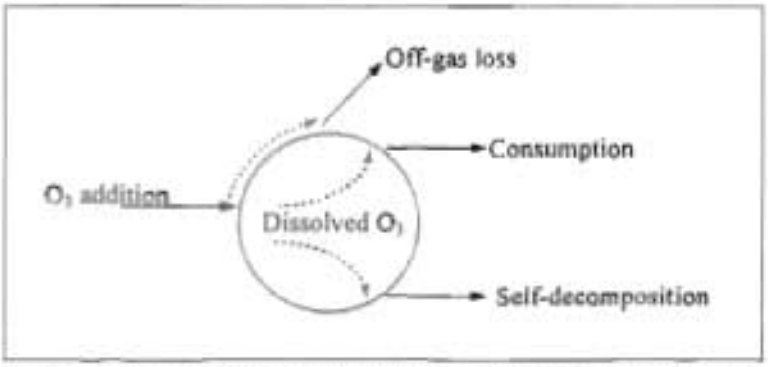

Figure 4-1: Ozone depletions in the treatment process (adapted from Huang et al., 2004b)

The off-gas loss is typically identified by performing a mass balance on ozone. The chemistry of ozone self-decomposition was discussed at length in Section 2.3.2.1 . In natural waters, the self-decomposition is very dependent on the pH or the concentrations of solutes which promote or initiate such reaction (Hoigné, 1998). The overall ozone consumption rate by OCS is however the key factor which differentiates one natural water from another.

The OCS is a collective term devised here to describe any inorganic or organic compounds which react with ozone. For conventional water treatment practice, the overall rate of ozonation processes is controlled by the sum of the rates of the chemical reactions with individual types of solutes (Hoigné, 1998). The reaction chemistry between ozone and individual compounds in synthetic waters was discussed in Sections 2.3.2.2 and 2.3.2.3 . Such information on individual molecular kinetic parameters assists in attaining an overall rate of the ozonation process.

4.2 Raw water reaction kinetics

In terms of treatability, a natural water is considered to have its own *characteristics* which are contributed by many factors discussed in the thesis thus far. The characteristics of water influence numerous aspects of water treatment, such as the point of disinfectant/oxidant application, performance of unit operations, process optimisation and potential operational benefits.

4.2.1 Fundamental theory

All primary reactions of ozone with dissolved compounds, M, can be formulated as bimolecular reactions (von Gunten, 2003; Hoigné, 1998; Hoigné and Bader, 1983a):

$$O_3 + M \xrightarrow{k_M} M_{ox} \tag{4-1}$$

such that the rate equation can be derived as in Eqn. (4-2):

$$-\frac{d[M]}{dt} = k_M [O_3][M] \tag{4-2}$$

Integrating both sides of Eqn. (4-2), the kinetic rate constant (k_M) is determined by plotting the log ratio of the dissolved compound concentration and the integrand involving the dissolved ozone concentration.

$$\ln\left(\frac{[M]}{[M]_0}\right) = -k_M \int [O_3]\, dt \tag{4-3}$$

Eqn. (4-3) forms the basis of the $C \cdot t$ concept. Compared to Eqn. (2-15) discussed in **Section 2.4.1** , it is evident that the left hand side of Eqn. (4-3) is commonly referred to as the log-kill ratio in evaluating the disinfection performance of an ozone contactor (US EPA, 1999; Bablon et al., 1991a).

$$\ln\left(\frac{N}{N_0}\right) = -k_d\ C\ t \tag{2-15}$$

The integrand involving the dissolved ozone concentration is simplified to an appropriately average concentration value, $\overline{[O_3]}$:

$$\ln\left(\frac{[M]}{[M]_0}\right) = -k_M\overline{[O_3]}\ t \tag{4-4}$$

The *average* ozone concentration in the $C \cdot t$ concept is taken to be the residual ozone concentration at the outlet (see **Section 2.4.1**). The underlying assumption of this approach is that such a residual ozone concentration must be kept throughout the contactor (i.e.: the outlet concentration is then considered an appropriately average value). However, the simplicity is often inferred with excessive conservatism which leads to overdosing.

4.2.2 Overall rate parameter

Eqn. (4-4) is applicable for the purpose of laboratory investigation where the specific solute/compound M is known and measurable for the initial value and at time t. However, in the process environment where the specific solute/compound M is not readily identifiable, it is more practical to observe the reaction rate from the viewpoint of dissolved ozone concentration instead of M.

Therefore the rate expression in Eqn. (4-2) can be re-written in terms of the disappearance rate of dissolved ozone as follows:

$$-\frac{d[O_3]}{dt} = k_{O_3}[O_3][M] \tag{4-5}$$

By replacing the specific solute/compound M with the OCS and referring to the overall kinetic parameter as k_r , a rate expression can be obtained for the overall reaction of ozone with OCS:

$$-\frac{d[O_3]}{dt} = k_r[O_3][OCS] \tag{4-6}$$

Integrating both sides of Eqn. (4-6) the overall rate constant (k_r) is calculated to be the slope of Eqn. (4-7):

$$\ln\left(\frac{[O_3]}{[O_3]_0}\right) = -k_r\int[OCS]\,dt \tag{4-7}$$

Eqn. (4-7) demonstrated the dependence of the ozone decay on the ozone dose ($[O_3]_0$) and a measure of the water quality ($[OCS]$). How to find the appropriate parameter(s) to represent the complex OCS is discussed in the next section.

4.3 Ozone-consuming substances and surrogates

The complexity and variety of the natural water constituents play a great role towards the seemingly unpredictable nature of water characteristics. Since it is not practical to analyse for every compound present in natural water, the studies of ozonation of natural waters always included many analytical data. Yet it is less often discussed which information should be considered as the key parameters (Hoigné, 1994). Hoigné (1994) proposed a list of data (see Table 4-1) as standards to be reported when disclosing the results of an ozonation experiment.

Although this list was well-intended to provide a common basis for comparison purpose with other ozonation studies, in practice this list is not always complete due to experimental constraints and time. Most investigators omit the parameters whose effects on the type of water tested are negligible.

Table 4-1: Minimal data set to report in ozonation study (Hoigné, 1994)

No.	Data name
1	effect of temperature
2	effect of pH
3	effect of alkalinity
4	dissolved organic material (DOM) as dissolved organic carbon (DOC)
5	UV absorbance at $\lambda = 255$ nm
6	nitrite, iron and manganese
7	chloride
8	bromide
9	ammonia
10	turbidity
11	chlorine residual
12	hydrogen peroxide
13	characterisation of the lifetime of dosed ozone
14	further parameters to be included

The exact nature of OCS in natural waters is variable and cannot be easily determined. Natural waters contain varying concentration of numerous organic and inorganic compounds (Bablon et al., 1991). Table 4-1 lists the ozone kinetic rate constants of selected organic and inorganic compounds, following Eqn. (4-5) as the rate expression. It is evident that the rate constants encompass a wide spectrum of values.

Table 4-2: Second-order kinetic rate constant of selected organic and inorganic compounds

Substance	Limit/Range	k_{O_3} $M^{-1}.s^{-1}$	Reference
INORGANIC			
NO_2^-	T = 22 °C	3.7×10^5	Hoigné et al. (1985)
SO_3^{2-}	T = 22 °C	$1.0\pm0.1\times10^9$	Hoigné et al. (1985)
Br^-	T = 20 °C	160±20	Hoigné et al. (1985)
Cl^-	T = 22 °C	$< 3\times10^{-3}$	Hoigné et al. (1985)
ClO_2 /$HClO_2$	T = 20 °C	$1.0\pm0.1\times10^3$	Hoigné et al. (1985)
Fe^{2+}	T = 22 °C	$> 5\times10^5$	Hoigné et al. (1985)
H_2S	T = 20 °C	$3\pm2\times10^4$	Hoigné et al. (1985)
HOCl	T = 20 °C	< 0.002	Hoigné and Bader (1983b)
HS^-	T = 20 °C	$1.1\pm0.4\times10^4$	Hoigné et al. (1985)
I^-	T = 25 °C	$\sim 2\times10^9$	Garland et al. (1981)
Mn^{2+}	pH = 5.5 to 7.0	3×10^3 to 2×10^4	Reckhow et al. (1991)
NH_3	T = 25 °C	20±1	Hoigné and Bader (1978)
ORGANIC			
benzene	pH = 1.7 to 3.0	2.0±0.4	Hoigné and Bader (1983a)
toluene	pH = 1.7	14±3	Hoigné and Bader (1983a)
phenols	-	10^5 to 10^9 †	Bablon et al. (1991b)
		10_5 to 10^9 ‡	
tetrachloroethylene	pH = 2.0	< 0.1	Hoigné and Bader (1983a)
ethanol	pH = 2.0	0.37±0.4	Hoigné and Bader (1983a)
acetic acid	pH = 2.5 to 5.0	$< 3\times10^{-5}$	Hoigné and Bader (1983b)
atrazine	pH = 3.4; T = 24 °C	$2.6\pm0.4\times10^9$	Haag and Yao (1992)
acetone	pH = 2	0.032±0.006	Hoigné and Bader (1983a)
glucose	pH = 2	0.045±0.05	Hoigné and Bader (1983a)

Notes:

† for dissociated or protonated form

‡ for non-dissociated form

While the rate constants for the reactions of most inorganic species are known, it is difficult to assess the ozone stability in natural waters due to the unknown effect of natural organic matter (NOM) (von Gunten, 2003). NOM is a term used to describe the complex matrix of organic material present in natural waters (Owen et al., 1995). In particular, surface and ground waters contain substantial organic matter that may be detrimental to the water quality (Camel and Bermond, 1998). Many investigators have examined the effects of NOM on the ozonation performance (Owen et al., 1995; Westerhoff et al., 1998; Park et al., 2000; Yavich and Masten, 2001). In other words, NOM has commonly been chosen to represent the amount of OCS. Although in principle, any of the compounds in Table 4-2 and many more in literature can be

considered as a representative compound for OCS, the choice of such compound will depend on the aim of ozonation and the available analytical methods/equipment.

In the water treatment process, the NOM present in natural waters is generally transformed into less recalcitrant compounds or removed through chemical oxidation. The influences of NOM include the biological re-growth in the distribution network, colour, taste and odour as well as the precursors to the DBP formation.

NOM can be divided into humic and non-humic fractions: the humic fraction is more hydrophobic in character and consists of humic and fulvic acids, whereas the non-humic fraction is less hydrophobic in character and comprises hydrophilic acids, proteins, amino acids and carbohydrates (Owen et al., 1995; Świetlik et al., 2004). The presence of humic substances is a potential concern as several functional groups (e.g.: R-OH, R-COOH or $R-NH_2$) have strong reactivities with halogens, complexation with metals and association with organic micro-pollutants (Westerhoff et al., 1998; Babion et al., 1991a; Yavich and Masten, 2001; Świetlik et al., 2004). This may, for example, lead to the formation of THMs upon the final chlorination.

The reduction or transformation of NOM has been evaluated using various surrogates including (but not limited to) the apparent molecular weight distributions, TOC, DOC, UV absorbance at 254 nm, THMFP or other DBP formation potentials (Pryor and Freese, 2000; Owen et al., 1995).

The humic fraction is generally less soluble and of higher apparent molecular weight than the non-humic fraction (Singer and Harrington, 1993) although the cut-off molecular weight differentiating the two fractions is not well-defined. The typical experimental approach is to fractionate NOM into a number of fractions according to their molecular weights and observe the shift in fractions due to ozonation.

The DOM is the portion of the total organic load in dissolved form. The dissolved and the total organic materials can be represented by measuring DOC and TOC respectively, where almost 90% of TOC is in dissolved form (Babion et al., 1991). The UV absorbance characteristics due to molecular size or functional groups also render itself as an indicator for the dissolved organic material. There are often linear correlations between DOC values of a water and the UV absorbances at 254 nm (Eaton et al., 1995; Hoigné, 1994) (Hoigné (1994) stated 255 nm; however, the value has been updated to 254 nm in Standard Methods.). The relative effect of ozonation on NOM can be observed from the trend of DOC, TOC or UV absorbance at 254 nm.

The measure of the DBPs or the DBP formation potential is another possible surrogate to assess the effect of ozonation on NOM. This method is targeted at specific functional groups of NOM especially where an ozone residual is present prior to chlorination or distribution network (Camel and Bermond, 1998).

The surrogate for NOM (and hence OCS) was chosen to be TOC and UV absorbance at 254 nm for the experimental work to come. The choice was based on the relative simplicity of the respective analytical methods. The equipment was readily available at Darvill Wastewater Works for measuring TOC and UV

absorbance as it forms part of the routine analyses at Umgeni Water (Pryor et al., 2002; Umgeni Water, 2003).

4.4 Experimental characterisations

High reactivity of ozone makes it an unstable oxidant in water. Its depletion rate is dependent on chemical composition of the water matrix, pH, ozone dosage and water temperature. The reaction rate can be complicated further in natural waters as the values of these influencing factors varies with season, weather conditions and waterworks management (Hoigné and Bader, 1994).

Experimental characterisation of natural waters have been studied by many (Hoigné and Bader, 1994; Owen et al., 1995; Westerhoff et al., 1997; Westerhoff et al., 1998; Park et al., 2000; Yavich and Masten, 2001); however, extrapolation or re-interpretation of the studied data is difficult since the water characteristics differs from one to another as well as the experimental constraints.

4.4.1 Pseudo first-order rate law

Staehelin and Hoigné (1985) proposed a pseudo-first order reaction rate expression as in Eqn. (4-8):

$$-\frac{d[O_3]}{dt} = k_c [O_3] \tag{4-8}$$

This leads to Eqn. (4-9) which relates the observed decay of dissolved ozone concentration with time:

$$\ln\left(\frac{[O_3]}{[O_3]_0}\right) = -k_c t \tag{4-9}$$

Many investigators adopted the approach of Eqn. (4-9) for simplicity because their primary interest was to achieve a required ozone residual. In the laboratory investigations, the dissolved ozone concentration is monitored with time (Hoigné and Bader, 1994). The overall rate constant k_c is then calculated as the slope of Eqn. (4-9).

From the pseudo first-order rate law, Hoigné and Bader (1994) also proposed two key parameters, the *instantaneous ozone consumption* (also known as *instantaneous demand*) and the *second half-life of dosed ozone*, as a generalised approach in describing the characteristics of a water. Part of ozone is reacted immediately within a few seconds of ozone addition to a natural water. This instantaneous ozone consumption is then succeeded by a slower depletion rate of ozone. This slower reaction is generally approximated with a pseudo first-order rate law as in Eqn. (4-8). Another operational parameter is to define the second half-life of ozone, which is the time taken for the residual ozone concentration to decrease from 50 to 25%.

The two parameters are independent of each other (Hoigné and Bader, 1994). Some raw waters were found to have substantial ozone consumption capacity even though the potential OCS concentrations are low (Park et al., 2000). This simplified pseudo first-order approach leaves uncertainties about the water quality which requires an extensive reporting list as discussed in Section 4.3 to justify.

Do-Quang et al. (2000) modelled the ozone consumption rate using Seine River water with a first-order constant of 1.67×10^{-3} s^{-1}. Cockx et al (1999) took a similar approach to model the ozone decay in a full-scale ozone contactor with a rate constant of 2.0×10^{-3} s^{-1}. Park et al. (2000) accounted for the presence of the NOM. A water with TOC equal to 0.7 $mg.L^{-1}$ and an ozone half-life as 462 s, the corresponding k_e was found to be 1.5×10^{-3} s^{-1} with respect to ozone; whereas another water containing TOC of 4.9 $mg.L^{-1}$ and exhibiting an ozone half-life of 18 s, the corresponding k_e was found to be 38.5×10^{-3} s^{-1}. Westerhoff et al. (1998) investigated the effect of NOM structure on its reactivity towards ozone. The first-order rate constant ranges from 3.9×10^{-3} s^{-1} for a groundwater to $> 16\times10^{-3}$ s^{-1} for a river water.

Extrapolating from the literature data is difficult as the rate constant varies across a wide spectrum. Although numerous experimental parameters were reported with the published rate constants, no universal correlation is currently available to relate the ozone consumption with the decomposition of OCS, or specifically NOM.

As discussed in **Section 2.3.2**, ozone reactions may proceed at the level of molecular ozone or through its decomposition product. The dissolved OCS may react with ozone or be oxidised by OH• formed from ozone decomposition. Therefore it must be noted that this differentiation is often not considered in the investigations of raw water reaction kinetics due to simplification. Hence the value of k_e also accounts for the radical reactions due to OH•. Since the overall rate law applies to only the decay of ozone, the simplification suffices so long as the mass transfer is not the rate-limiting step of the overall reactions.

4.4.2 Proposed second-order rate law

Based on the approach from Eqns. (4-2) and (4-3) in **Section 4.2.2**, Yavich and Masten (2001) investigated the effects of NOM by characterising the humic and non-humic substances in Huron River water. At 20°C and an initial humic substance concentration of 3.40 $mg.L^{-1}$, the rate constant can be as high as 7.06 $L.mg^{-1}.min^{-1}$.

At Wiggins Waterworks, the raw water quality can be affected adversely due to climate change. Ideally, the characterisation procedure must be repeated to account for the seasonal fluctuation. However, a lengthy characterisation procedure is too laborious to be incorporated into the plant operation. The current characterisation method can be modified by re-considering the rate law.

The integrated Eqn. (4-7) can account for the effects of the ozone dose and the raw water quality by a suitably chosen surrogate for the OCS.

$$\ln\left(\frac{[O_3]}{[O_3]_0}\right) = -k_e[\overline{OCS}]\,t \qquad (4\text{-}10)$$

The average surrogate concentration (shown as $[\overline{OCS}]$) adopted the similar approach as in Eqn. (4-4). The overall rate constant, k_e, accounting for the OCS can be evaluated in a similar manner.

Since the molar rate of ozone disappearance would be the same in both Eqns. (4-6) and (4-8), the rate constants in the resulting integrated solution by comparing Eqns. (4-9) and (4-10) can deduce the following:

$$k_e = k_r\overline{[OCS]} \qquad (4\text{-}11)$$

4.5 Conclusions

This chapter examines the current theory in characterising raw waters. A generalised rate law for raw water is accepted to be first-order to ozone and first-order to the target compound, which was based on the extensive database of the reaction rate constants between ozone and a specific compound.

The NOM is accountable for consuming most of the dosed ozone; however, it is difficult to analyse NOM due to its complexity. For the kinetic experiments discussed in this thesis, TOC and UV absorbance at 254 nm were selected as the surrogates for NOM (and hence OCS). The equipment was available and the two parameters also form part of the routine analyses.

A second-order rate law with an average OCS concentration (Eqn. (4-10)) was proposed to account for the effects of ozone dose and the raw water quality.

4.6 References

Bablon G., Bellamy W.D., Bourbigot M.-M. et al. (1991a) *Chapter 2. Fundamental aspects.* In *Ozone in Water Treatment: Application and Engineering*. Langlais B., Reckhow D.A. and Brink D.R., eds., Lewis Publishers, Chelsea, Michigan. ISBN: 0-87371-474-1.

Camel V. and Bermond A. (1998) *The use of ozone and associated oxidation processes in drinking water treatment.* Water Research **32** (11): 3208-3222.

Eaton, A.D., Clesceri, L.S. and Greenberg, A.E., eds. (1995) *Standard Methods for the Examination of Water and Wastewater*. 19th edition. American Public Health Association. Washington DC. ISBN 0-87553-223-3. 4/38-4/39.

Hoigné J. (1994). *Characterization of water quality criteria for ozonation processes: Part I: Minimal set of analytical data.* Ozone-Science & Engineering **16** (2): 113-120.

Hoigné J. (1998) *Chemistry of aqueous ozone and transformation of pollutants by ozonation and advance oxidation processes.* In *The Handbook of Environmental Chemistry*, Vol. 5, Part C *Quality and Treatment of Drinking Water II*, Hrubec J., ed., Springer-Verlag, Berlin.

Hoigné J. and Bader H. (1983a) *Rate constants of reactions of ozone with organic and inorganic compounds in water – I. Non-dissociating organic compounds.* Water Research 17: 173-183.

Hoigné J. and Bader H. (1994) *Characterisation of water quality criteria for ozonation processes. Part II: Lifetime of added ozone.* Ozone-Science & Engineering 16 (2): 121-134.

Huang T.H., Brouckaert C.J. and Buckley C.A. (2004b) *Integration of CFD modelling and kinetic study to improve the control strategy of an ozone contactor.* Proceedings of the 2004 WISA Biennial Conference and Exhibition, Cape Town, South Africa, 1 – 4 May.

Owen D.M., Amy G.L., Chowdhury Z.K., Paode R., McCoy M. and Viscosil K. (1995). *NOM characterisation and treatability.* Journal of American Water Works Association **87** (1): 46-63.

Park H.-S., Hwang T.-M., Kang J.-W., Choi H., and Oh H.-J. (2001) *Characterization of raw water for the ozone application measuring ozone consumption rate*. Water Research, 35 (11): 2607-2614.

Pryor M.J. and Freese S.D. (2000) *The treatment of eutrophic water using pre- and intermediate ozonation, peroxone and pica carbon*. WRC report No 694/1/00, ISBN: 1-86845-588-2. Pretoria.

Pryor M.J., Naidoo D, Bahrs P. and Freese S.D. (2002) *Ozone experiences at Umgeni Water*. Proceedings of the 2002 WISA Biennial Conference and Exhibition, Durban, South Africa.

Singer P.C. and Harrington G.W. (1993) Coagulation and DBP Precursors: Theoretical and practical considerations. Proceedings of the AWWA Conference on Water Quality Technology, Miami, Florida, 7-11 November.

Staehelin J. and Hoigné J. (1985) *Decomposition of ozone in water in the presence of organic solutes acting as promoters and inhibitors of radical chain reactions*. Environmental Science Technology 19 (12): 1206-1213.

Świetlik J., Dąbrowska A., Raczyk-Stanisławiak U. and Nawrocki J. (2004). *Reactivity of natural organic matter fractions with chlorine dioxide and ozone*. Water Research 38:547-558.

Umgeni Water (2003) *Annual Report: Technical and scientific statistics* 2001-2002.

US EPA (1999) *Disinfection Profiling and Benchmarking Guidance Manual*, United States Environmental Protection Agency, Office of Water, EPA 815-R-99-013.

Von Gunten U. (2003) *Ozonation of drinking water. Part I. Oxidation kinetics and product formation*. Water Research 37 (7): 1443-1467.

Westerhoff P., Aiken G., Amy G. and Debroux J. (1998) *Relationship between the structure of natural organic matter and its reactivity towards molecular ozone and hydroxyl radicals*. Water Research 33 (10): 2265-2276.

Westerhoff P., Song R., Amy G., and Minear R. (1997) *Application of ozone decomposition models*. Ozone-Science & Engineering 19 (1): 55-73.

Yavich A. A. and Masten S. J. (2001). *Modeling the kinetics of the reaction of ozone with natural organic matter in Huron River water*. Ozone-Science & Engineering 23 (2): 105-119.

5

KINETIC MODEL OF THE OZONE CONTACTOR

"It isn't that they can't see the solution. It is that they can't see the problem"

- *Scandal of Father Brown* (1935), G.K. Chesterton (1874 – 1936), English author and mystery novelist

In Chapter 3 a hydrodynamic model has been developed and verified, and then forms the foundation with which a kinetic model can be incorporated. In Chapter 4 a generalised rate law was identified in order to conduct the study in the current chapter. The capability of CFD modelling will be demonstrated further through the combination of the calculated flow field and the appropriate reaction kinetics to predict the concentration of the desired chemical species within the prescribed condition and reactor geometry.

In a full-scale plant, it is not always possible or economical to monitor the entire reactor with multiple sampling points. For all practical purposes, selecting one representative sampling point is more feasible but the selection of an appropriate position is not an obvious decision especially if one does not fully understand the reactor. The analysing of the contactor performance based on reaction kinetics which accounts for the target species and the ozone decay is a more accurate approach. A kinetic CFD model is thus a rigorous tool to provide insight to the whole reactor. The predicted results such as the concentration profiles are used to locating the best possible monitoring position. For the study in this chapter, the verification and validation of the CFD results was addressed by collecting ozone concentration data in the ozone contactor.

This chapter discusses the details of the kinetic modelling of Wiggins Waterworks' ozone contactor. **Section 5.1** presents the current operating strategy. **Section 5.2** outlines the specific objectives in relation to the overall goals. **Section 5.3** describes the kinetic model with a current review on the ozone contactor modelling. **Section 5.4** describes the experimental techniques and procedure of the full-scale plant testing. The results are discussed in **Section 5.5** while the sectional concluding remarks are given in **Section 5.6** .

5.1 Introduction

The on-line ozone sensors of the pre-ozonation system at Wiggins Waterworks are situated at the contactor outlet. For conventional ozone contactors, one of the operational objectives is to achieve the desired residual ozone concentration in water. The most obvious point to measure the ozone residual would be at the contactor outlet. For the contactors at Wiggins Waterworks, however, the objective is to utilise the introduced ozone efficiently such that all reactions are complete within the reactor and to prevent the

release of residual ozone to the atmosphere through the de-gassing over the open weir at the contactor outlet.

At present, the pre-ozonation system is operated using the ozone concentration sensed at the outlet. Although this location may be an obvious choice if a residual ozone concentration is required at the outlet, it is not appropriate for an outlet concentration of zero. While the feedback probably helps in identifying when over-dosage occurs, the information on the under-dosage and its extent cannot be captured.

The standard $C \cdot t$ approach would not have been appropriate, as the value of C that would be used in this approach is the residual ozone concentration at the contactor outlet. While this would be suitable for a mixed reactor, the Wiggins Waterworks' contactors are closer to plug-flow reactors, and are operated to have the residual outlet concentration as close to zero as possible. Consequently it was necessary to undertake more detailed reaction modelling in order to have an appropriate representation of the contactor's performance (Brouckaert et al., 2004).

5.2 Objectives

The main objective of this chapter is to gain insight to the ozone distribution within the contactor. This was achieved by incorporating the effects of the flow regimes with the ozone reaction rate constants found in literature. The specific goals are as follows:

- To develop an adequate kinetic model based on the hydrodynamically verified CFD model;
- To simulate the dissolved ozone concentration profiles using literature rate constant data and compare with the data from the ozone sensors on the full-scale plant;
- To suggest the best possible position for single-point monitoring.

5.3 Kinetic model description

The current section describes the inputs to the kinetic model based on the calculated flow results based on the hydrodynamic model from Chapter 3. The details of the geometry and the mesh have been described in **Section 3.3.1** . The assumptions of the kinetic model, the reactions represented, the implementation and the related boundary conditions are discussed from **Section 5.3.1** to **Section 5.3.4** .

5.3.1 Assumptions

The transfer efficiency of static mixers has been reported to be very high, approximately 85 to 98% (Bin and Roustan, 2000). It was based on this that static mixers were installed at Wiggins Waterworks to pre-mix ozone and water. Therefore a negligible off-gas loss was assumed for the present model. It was also assumed that the ozone mass transfer was completed in the static mixer. This assumption modifies Figure 4-1 to the distribution of dissolved ozone shown in Figure 5-1 .

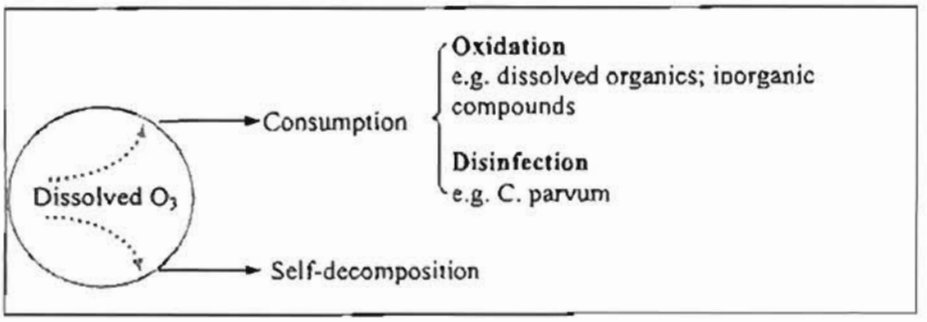

Figure 5-1: Distribution of dissolved ozone (adapted from Huang et al., 2004b)

The ozone-consuming substances (OCS) in raw water consist of oxidisable species such as dissolved organic compounds, or reduced inorganic species such as Fe (II) and Mn (II). The overall decrease in dissolved ozone concentration was modelled as:

$$-\frac{\partial[O_3]}{\partial t} = -k_s[O_3] - k_r[O_3][OCS] \qquad (5\text{-}1)$$

The first term on the right hand side of the equation describes the ozone self-decomposition reaction, the second the reaction with OCS. Values for the kinetic constants k_s and k_r were obtained from the literature.

Although pathogens form part of the OCS, they consume a very small mass of ozone due to their extremely low concentrations (Huang et al., 2004). The disinfection reaction was therefore modelled separately. A pathogenic organism typically resistant to water treatment chemicals was chosen as an indicator compound to assess the performance of the Wiggins Waterworks' ozone contactor.

The boundary conditions in the kinetic model were based on the operating values at the time when the experimental measurements were taken.

5.3.2 Simulated reactions

The details of ozone kinetics chemistry were discussed at length in **Section 2.3.2** from the viewpoint of the categorised compound groups. In natural waters where a significant number of different compounds are present, it becomes impractical to analyse for each individual compound present and to model for each reaction. From the viewpoint of process operation, it is more important to examine the reaction categories from the aspect of dissolved ozone using Eqn. (5-1). The rate constants for each reaction category implemented in the kinetic model are discussed in the following sub-sections.

5.3.2.1 Self-decomposition

The self-decomposition of ozone in water has been studied by several authors as a first-order reaction with respect to ozone (Park et al., 2000; Muroyama et al., 1999; Beltrán, 1995; Hoigné and Bader, 1994; Staehelin and Hoigné, 1985). It was also shown in **Section 2.3.3** that the self-decomposition of ozone cannot be ignored. The reaction rate was observed to increase with increasing pH and dissolved ozone concentration. The self-decomposition rate constant, k_s (s^{-1}), was examined by Beltrán (1995) at a wide range of pH values.

$$k_s = 4.8\times10^{-4}\ s^{-1} \qquad \text{At pH} = 7 \qquad (5\text{-}2)$$

Since the pH of the raw water received at the Wiggins Waterworks varies only slightly around an average of 7, the decomposition rate constant at pH 7 (refer to Eqn. (5-2)) determined by Beltrán (1995) was used for the present model. The applicable temperature is not known; however, the rate constant is particularly sensitive to pH. This was discussed in Section 2.3.2.1 that pH of water has a significant effect on the self-decomposition of ozone.

5.3.2.2 Consumption by ozone-consuming substances

Muroyama (1999) assumed the reaction between ozone and the OCS is first order with respect to ozone as well as to the OCS. The ozone consumption reaction rate constant, k_r, was referenced by Muroyama (1999) from experimental results. Muroyama reported 40 $kL.kg^{-1}.min^{-1}$ as an average reaction rate. Calculation details were included in the spreadsheet attached. This value was then inferred to be:

$$k_r = 21.33 \quad kL.kmol^{-1}.s^{-1} \tag{5-3}$$

The amount of OCS present in the water was estimated from the total organic carbon (TOC) content in water. High TOC generally indicates high level of NOM and hence OCS. The conversion from TOC to OCS is based on the assumption that all of the TOC is glucose. Glucose was a representative organic molecule which has the right atomic ratios (C:H:O) to approximate naturally occurring organic matter found in water. The amount of the carbohydrates present in river or groundwater is generally more abundant (100 to 500 mg $C.L^{-1}$) than other organic substances (Babion et al., 1991a). This representative molecule was introduced into the model to address the following:

- The Fluent reaction model formulation which needed a molecular species to be specified;
- The kinetic constant value from literature was converted into molar units as required by Fluent by assuming 1:1 stoichiometry;
- The measurement of TOC is a routine analysis at Umgeni Water. The amount of OCS mass fraction present in the water was re-calculated from the TOC measurements as though the NOM were glucose.

A typical value of TOC in the Wiggins Waterworks' raw water is 3.3 $mg.L^{-1}$, which yields 8.26 $mg.L^{-1}$ OCS.

5.3.2.3 Disinfection

The probability of primo-infection by ingestion of a potentially pathogenic organism, possibly through the drinking water route is quite well established (Masschelein, 2000). The primo-infection probabilities of some selected organisms which are potentially infectious are listed in Table 5-1.

Because the existence of these organisms at extremely low concentrations can pose serious health risks, it is reasonable to model a pathogenic organism as a performance indicator of the ozonation. For the purpose of the study, *Cryptosporidium parvum* oocyst is the chosen performance indicator.

Table 5-1: Infection probability of potential pathogens (Masschelein, 2000)

Potential infectious organism	Primo-infection probability
Salmonella typhi	0.0004
Giardia (lamblia)	0.02
Cryptosporidium parvum (estimate)	0.02 (preliminary)
Shingella	0.007

Cryptosporidium parvum oocyst (*C. parvum*) is found to be extremely resistant to most commonly used disinfectants (Korich et al., 1990). *C. parvum* can survive at low temperature for a long period of time (Driedger et al., 2000). Ozone remains an effective disinfectant for *C. parvum*, even at low temperatures where the efficacy of ozone is decreased to 1/3 of the value produced at room temperature (Finch et al., 1999; Li et al., 2001). In comparison with Giardia, it has been reported that *C. parvum* is 30 times more resistant to ozone, and 14 times more resistant to chlorine (Korich et al., 1990). The waterborne disease cryptosporidiosis has been recognized as a cause of diarrhoea-type illness. Traditional chlorination was shown to be not effective against *C. parvum* (Li et al., 2001).

The reaction kinetics between *C. parvum* and ozone is based on the classical Chick-Watson inactivation model presented in Eqns. (2-14) and (2-15), for n = 1:

$$\frac{dN}{dt} = r_d = -k_d C^n N \tag{2-14}$$

$$\ln\left(\frac{N}{N_0}\right) = -k_d C t \tag{2-15}$$

where N/N_0 is the survival ratio of the micro-organism, C is the residual ozone concentration, t is the contact time, and k_d is the inactivation rate constant.

The value of k_d appears to be influenced by the quality of water, such as pH and temperature (Joret et al. 1997, Gyürék et al. 1999; Rennecker et al. 2000, Driedger et al. 2000, Li et al. 2001). This is reflected by the wide range of k_d reported in the literature. The disinfection rate constant, k_d , is calculated from the experimental results reported by Li et al. (2001) using an average residual ozone concentration 0.85 mg.L^{-1} and a contact time of 4 min, with the observed kill of 1.5 log-units. From Eqn. (2-15),

$$\begin{aligned} k_d &= 0.441 \ \text{L.mg}^{-1}.\text{min}^{-1} \\ &= 352.9 \ \text{kL.kmol}^{-1}.\text{s}^{-1} \end{aligned} \tag{5-4}$$

5.3.3 Reaction model

The mass balance equation for chemical species in FLUENT takes the following general form (Fluent, 2003):

$$\frac{\partial}{\partial t}(\rho Y_i) + \frac{\partial}{\partial x_j}(\rho \bar{u} Y_i) = -\frac{\partial}{\partial x_j}\bar{J}_i + R_i + S_i \tag{5-5}$$

where Y_i is the local mass fraction of each species, R_i is the net rate of production by chemical reaction; S_i is the rate of creation by addition from the dispersed phase plus any user-defined sources (Fluent, 2003).

Since the mass fraction of the species must add up to unity, the *N*th mass fraction is determined as one minus the sum of the *N*-1 solved mass fractions. For this reason, the *N*th species should be the one which has the largest overall mass fraction in order to minimise numerical error.

The source term in Eqn. (5-5) represents the reaction rates. The laminar finite-rate model in FLUENT was chosen for the purpose of the kinetic modelling study. Since the flow field has been solved in the hydrodynamic model in **Chapter** 3, the laminar finite-rate model reduces computational effort by avoiding the re-calculation of the hydrodynamics-related variables. The net production rate is defined by Eqn. (5-6), neglecting the turbulent fluctuations (Fluent, 2003):

$$R_i = M_{w,i} \sum_{r=1}^{N_R} \bar{R}_{i,r} \tag{5-6}$$

where $M_{w,i}$ is the molecular weight of species i and $\bar{R}_{i,r}$ is the Arrhenius molar rate of creation/destruction of species i in reaction r.

For the r_{th} reaction which is non-reversible, the general form is given in Eqn. (5-7):

$$\sum_{i=1}^{N} \nu'_{i,r} M_i \xrightarrow{k_{f,r}} \sum_{i=1}^{N} \nu''_{i,r} M_i \tag{5-7}$$

where N is the number of chemical species in the system; $\nu'_{i,r}$ is the stoichiometric coefficient for *reactant* i in reaction r; $\nu''_{i,r}$ is the stoichiometric coefficient for *product* i in reaction r; M_i stands for the species i; $k_{f,r}$ is the forward rate constant for reaction r (Fluent, 2003).

5.3.4 Boundary condition

The reaction modelling in FLUENT requires the reactant concentrations to be specified as mass fractions at the inlet. A typical ozone dose of 2.5 $mg.L^{-1}$ ozone is translated into a mass fraction of 2.5×10^{-6}. The OCS concentration is represented using glucose as a representative compound as discussed in Section 5.3.2.2. For an average TOC concentration of 3.3 $mg.L^{-1}$, the corresponding mass fraction is calculated to be 8.26×10^{-6}. In the case of pathogens, the mass fraction is not known or relevant. The parameter of interest is the survival ratio, N/N_0, representing the probability that a viable organism will survive the process. To represent this in the model, the inlet mass fraction was set to an arbitrary value of 10^{-6}, and survival ratios were calculated by ratioing simulated mass fractions to this value. The value 10^{-6} was simply chosen to be sufficiently low that its effect on the ozone consumption would be negligible.

5.4 Experimental verification

A programme of measurements was undertaken to obtain ozone concentration data for verification and calibration of the model. This section also describes the means to monitor the ozone concentration on the full-scale contactor.

5.4.1 Monitoring strategy

The experimental verification was divided into two monitoring stages at the Wiggins Waterworks' ozone contactor. The first stage was a general-monitoring which was carried out under normal plant operation. Its objective was to gather the ozone concentration data and observe the general trends. Under normal plant operation, there may be more than one contactor on-line. Therefore the second stage of controlled-monitoring was conducted when only the contactor of interest was in operation. The latter stage was necessary for model validation. Water flow rate and the ozone dosage set-point, and hence the injected gas flow, were maintained at steady values during the controlled-monitoring (second stage).

The value of the residual ozone concentration in water depends on sampling method and equipment. For example, if the sampling line is too long, ozone continues to react along the sampling line and therefore the concentration detected will not reflect the true value.

The general-monitoring was carried out by the author, assisted by trainees from Wiggins Waterworks. The controlled-monitoring was carried out by the author and Mr C Brouckaert, with the assistance of Wiggins Waterworks' operation staff.

5.4.2 Ozone analysers on full-scale contactor

Wiggins Waterworks uses commercial ozone analysers, the Residual Ozone System by Orbisphere laboratories, Switzerland, to detect the dissolved ozone concentration on the full-scale ozone contactors. An Orbisphere residual ozone system consists of two components: an indicating instrument and an ozone sensor made of titanium (Orbisphere, 1997). An electrical potential is applied to the two noble metal electrodes. The electrical potential is reduced by the amount of ozone measured, and ozone permeates through the membrane due to the difference in partial pressure. The resulting proportional current is translated into measured ozone concentration in parts per million (ppm). The measurement range is reported to be between 0 and 10 ppm dissolved ozone. The accuracy of results is about ±1% to ±5% depending on the calibration methods used (Orbisphere, 1997).

5.4.3 Sampling system

For the contactor under investigation, six Orbisphere residual ozone systems were installed to sample from different locations within the contactor; however, lack of maintenance and the skills for servicing contributed to inconsistent measurements. In addition, sampling water from the internal points proved to be difficult. The original set up could not transfer water from the sampling location to the measuring sensor fast enough to avoid significant loss of ozone from the continuing ozone reaction or decomposition. The set up also encountered operational problems such as sampling tubes being blocked by algae. The six sensors were taken off the main plant and some preliminary tests were performed using all six sensors on a pilot-scale ozonation column. Only three were found to give reasonable readings when compared against laboratory test results. The three systems were then re-installed on contactor No. 2 in an arrangement shown in Figure 5-2.

Sampling integrated with ozone analysers. The indicators are enclosed in stainless steel cases (indicated in Figure 5-2 (a)). The attached sensors are embedded in a flow cell collecting the water sample which was pumped from various internal locations in the contactor.

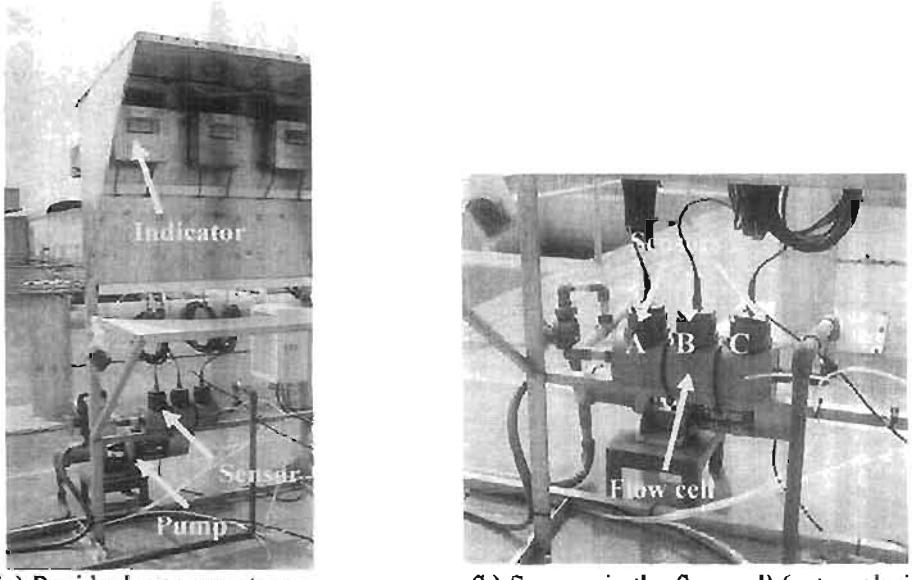

(a) Residual ozone systems (b) Sensors in the flow cell (external view)

Figure 5-2: Sampling system

The sensors (labelled A, B and C in Figure 5-2 (b)) are situated halfway in the flow cell which is 110 mm in diameter and 300 mm in length. The sensors are immersed in water to ensure that the gas flow does not influence the measurement, and to improve the stability of sampling operation.

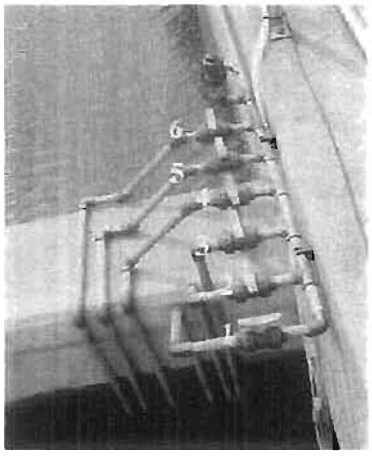

Figure 5-3: Sampling lines (Huang et al., 2003)

Each sampling point has an individual line leading to a manifold connected to the sensors (see the numbered pipes in Figure 5-3), such that water can be drawn to the flow cell from each sampling point. Changing the sampling position is accomplished by opening the valve for the point to be measured. Therefore only one point can be measured at a time. With all three sensors placed in a common water cell, it means that the measurement is performed in triplicate.

Sampling points. Water is pumped from six internal sampling positions throughout the three horizontal compartments (Figure 5-4).

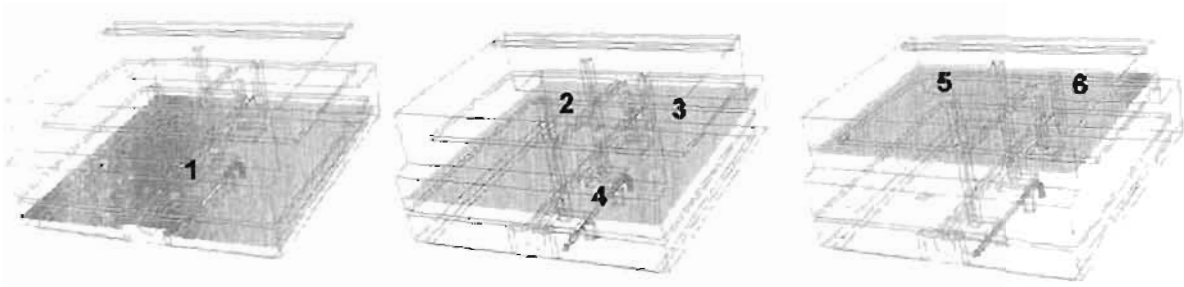

(a) bottom compartment (b) middle compartment (c) top compartment

Figure 5-4: Sampling positions in the ozone contactor (Huang et al., 2003)

The incoming flow first passes Point 1 in the bottom compartment (Figure 5-4 (a)); then Points 2 and 3 on either half of the contactor as flow enters the middle compartment; then Point 4 on the right half of the contactor as flow approaches the end of the middle compartment (Figure 5-4 (b)). Finally flow passes Points 5 and 6 which are again located on either half of the contactor (Figure 5-4 (c)). The positions of these points were chosen based on previous modelling work. The sampling flow rate was approximately 20 $L.min^{-1}$ (1.2 $kL.h^{-1}$) with little variation from different sampling points of varying heights. This flow rate was assumed to be fast enough so that the ozone reacted during the time of transfer to the water cell is negligible.

5.4.4 Testing procedure

The measurements using the ozone analysers were taken from the indicating instruments. Sensor readings were taken for all six internal sample points. After changing to the desired sampling point, 10 to 15 min of waiting time were allowed for signal stabilisation. This waiting time was also necessary to ensure that all water from the previous sampling point was purged from the sampling system. A general *scan* of all six sample point would take just over an hour.

For every measurement done at an internal point, the outlet concentration was also taken using the sensor located at the mid-point along the outlet weir.

The general-monitoring was carried out during February and March 2002 and the controlled-monitoring was conducted over 21 and 22 March 2002. Two flow settings of 120 and 100 $ML.d^{-1}$ were tested for controlled-monitoring, each with two ozone dose settings of 3.5 and 2.5 $mg.L^{-1}$. A scan of all six sample points was carried out at each respective setting. The change in dosage was treated as a step test, each continued 40 min long which is approximately three times the average residence time of the contactor.

It is important to note the advantage of the present arrangement of using three sensors for single-point measurement, as compared to the previous approach of allocating one sensor per point. Although the present set-up was more time consuming in operation (i.e.: measuring all six points would take > 1 h as opposed to taking six readings at the same time), it reduces the risk of relying on single residual ozone sensor reading, and it was easy to detect the faulty sensor if malfunction occurs. Sampling blockage was not encountered due to the higher flow rate. The piping arrangement of the internal sample collection is assumed to have negligible effect on the overall contactor hydrodynamics.

5.5 Results and discussion

The experimental results are first presented to examine the result trend and the sampling techniques. Comparisons were made between the simulated results and the experimental data under various operating conditions.

5.5.1 General-monitoring results

The general-monitoring was carried out over a period of three weeks under normal plant operation. The main objectives of the general-monitoring were to address any instrumentation problem, familiarise with procedure, decide on the number of variables to monitor. Information on the ozone concentration, flow rate, ozone dosage and the number of contactor operation were recorded. There was no parameter to monitor the water quality as this would either require immediate analyses or special sample storage in order to eliminate the influence of bio-growth in samples. Since the incoming water quality was checked by the Wiggins Waterworks on a weekly basis, water quality monitoring did not form part of the rigorous experimental data collection.

5.5.2 Controlled-monitoring results

The controlled-monitoring tests were carried out at a prescribed flow rate and ozone dose, when only the contactor of interest was in operation. The analyser readings were taken for all six points and compared to the outlet. Two sets of results are plotted in Figure 5-5 and Figure 5-6. The analyser readings were in ppm, while the ozone doses were referred in mg/L in the waterworks. These two units for the current section are used inter-changeably.

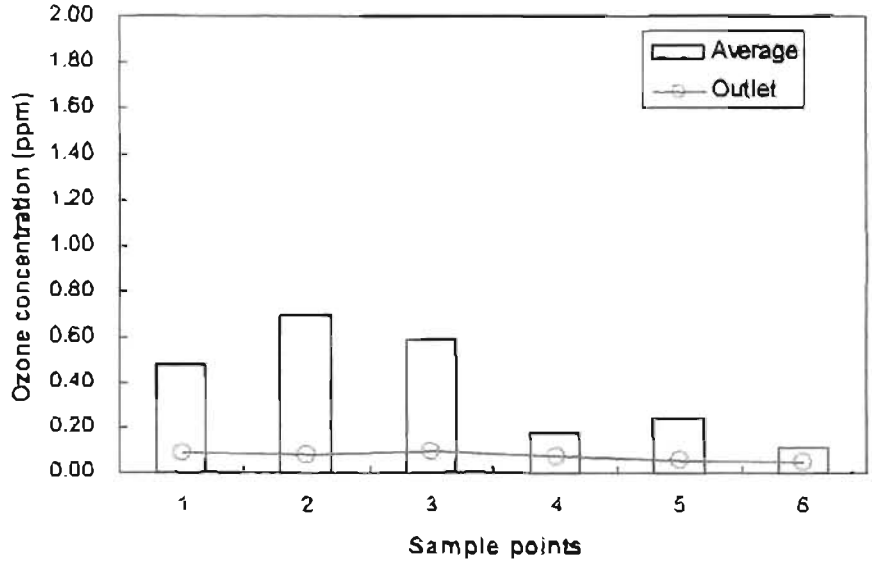

Figure 5-5: Dissolved ozone concentration profile, in comparison with the outlet measurement. Flow rate = 106 ML.d^{-1}; ozone dose = 2.5 mg.L^{-1}

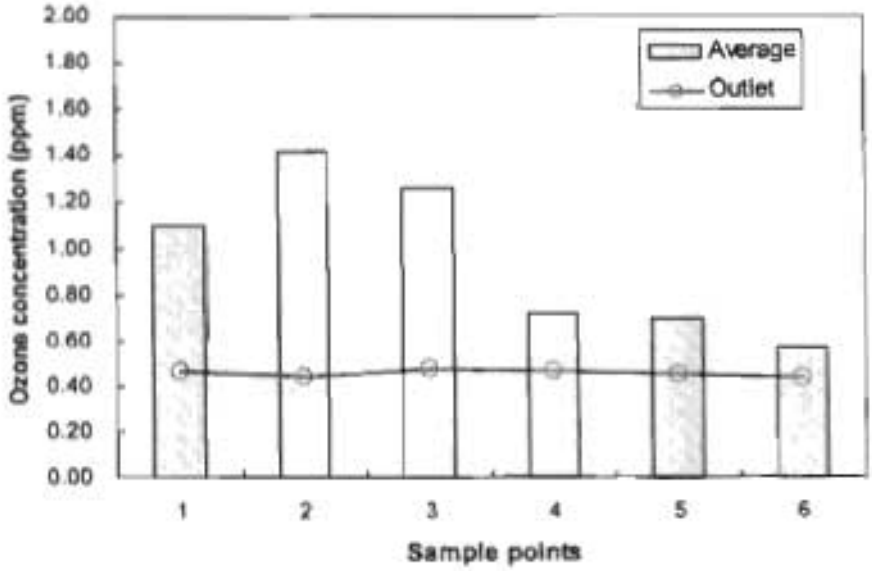

Figure 5-6: Dissolved ozone concentration profile, in comparison with the outlet measurement. Flow rate = 106 ML.d^{-1}; ozone dose = 3.5 mg.L^{-1}

From a previous study (Brouckaert et al., 2000) the dispersion in the bottom compartment was found to be increased by the asymmetry of the contactor. Part of the flow was diverted towards the left side of the contactor, and therefore the sampling positions on the left side were expected to yield higher values than those on the right side as shown in Figure 5-5 and Figure 5-6 (point 2 is higher than 3, point 5 is higher than 6). This indicates that the hydrodynamics of the contactor may deviate from what has been observed in the previous chapter when flow is much less than 100 ML.d^{-1}.

It is surprising to see that the values at Points 2 and 3 are higher than Point 1 which is the sampling position closest to the inlet and was expected to register the highest concentration. It is likely that the sampling point happened to be positioned in an area more susceptible to the localised flow/reaction phenomena. It is also possible that ozone may still be dissolving in the bottom compartment. Nevertheless, the reasonable control point should be where the reactions are almost complete, and not where ozone reactions commence. Therefore it would not significantly affect the selection of the positioning of the residual ozone sensor, which was the main goal of the current investigation.

The analyser at the outlet is currently used for the operation of contactor; however, it is considered that this position may not be the best and effective position to monitor the dissolved ozone concentration. Figure 5-5 and Figure 5-6 showed that the concentration at the outlet is much lower than those registered at the internal sample points. A more desired position to monitor the ozone residual would be somewhere within the contactor where the ozone reactions are near completion. In addition, the ozone concentration is in a range where the analysers have adequate sensitivity. At low doses such as shown in Figure 5-5, an outlet concentration of 0.1 ppm could not reveal whether adequate ozone has been added or more ozone was required.

From Figure 5-5 and Figure 5-6, most of the dissolved ozone seems to have been consumed by the time flow emerges from the middle compartment. Therefore Point 4 was proposed to be the new position for monitoring and to carry out the step-tests. In a dose step-up test from 2.5 to 3.5 mg.L^{-1} (shown in Figure

5-7), Point 4 is able to respond to the changes in water or operating condition more quickly than the outlet point and that the reading is higher than minimum measurement threshold of 0.1 ppm.

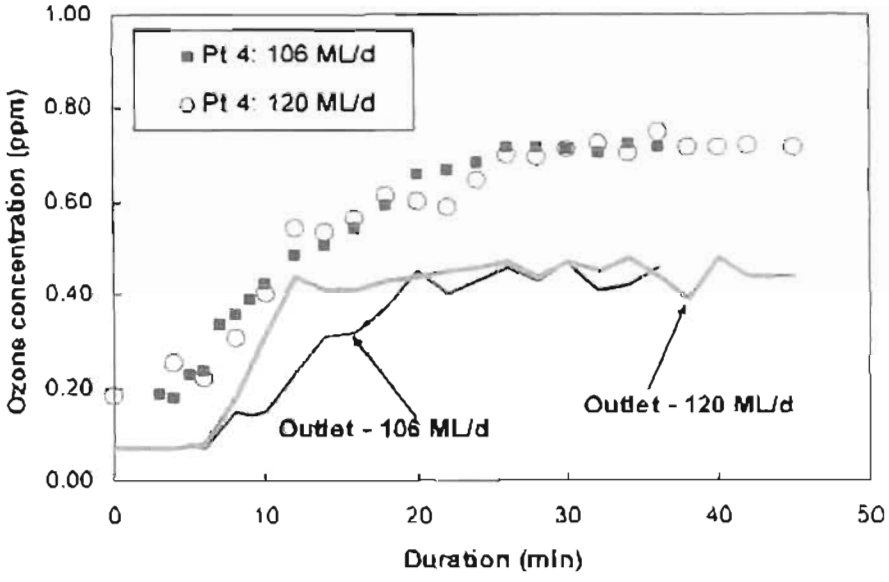

Figure 5-7: Comparison between the current position (outlet) and the proposed point (Point 4). Step-up in dose from 2.5 to 3.5 mg.L^{-1}

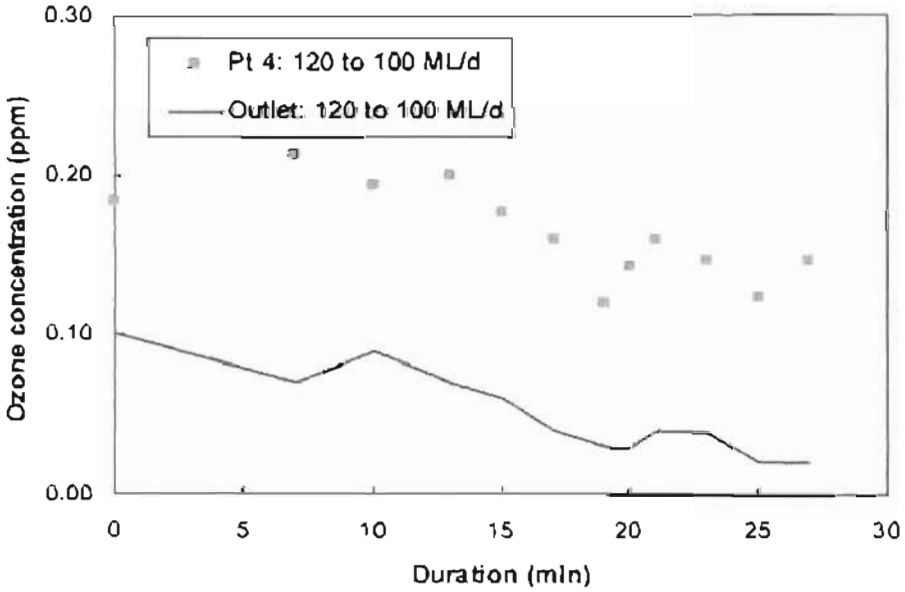

Figure 5-8: Comparison between the current position (outlet – in green line) and the proposed point (Point 4 – in orange dots). Step-down in flow rate from 120 to 100 ML.d^{-1}; ozone dose = 2.5 mg.L^{-1}

In a flow step-down test (shown in Figure 5-8), Point 4 gave more a pronounced response that the outlet point. Although the expected change in measured ozone residual due to the flow step-down is small, the measurement at Point 4 is still well above the analyser threshold of 0.1 ppm.

5.5.3 Simulated profiles

Two OCS loading scenarios were compared to examine the effect of water quality (in terms of OCS) on the ozone residual. The mass fractions of modelled compounds at the inlet for the base case are summarised in

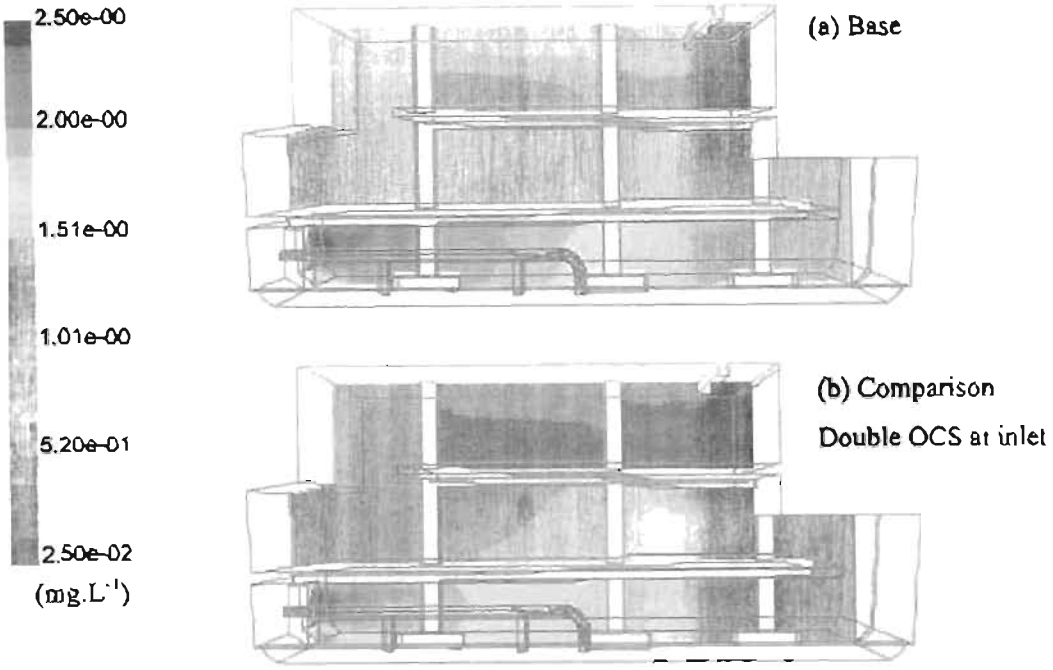

Table 5-2. The comparison is made with a higher OCS inlet mass fraction which is twice the input value for the base case.

Table 5-2: Input value for kinetic modelling of ozone reactions. Base case

Compound	Inlet mass fraction
O_3	2.5×10^{-6}
OCS	8.26×10^{-6}
C. parvum	1.0×10^{-8}

The simulated ozone residual profiles are presented in Figure 5-9. The simulated disinfection performance indicator discussed in **Section 5.3.2.3** , *C. parvum*, is presented in the form of survival ratio shown in Eqn. (2-15). The disinfection performance indicator profiles are presented in Figure 5-10.

The colour maps in Figure 5-9 and Figure 5-10 were in log-scale in order to cover the large range of values and demonstrate the change in concentration of survival ratio effectively. Therefore the minimum values in both figures are not zero but some values which are considered small enough.

Figure 5-9: Simulated ozone concentration. Base case vs. Comparative case. Flow rate = 106 ML.d^{-1}; ozone dose = 2.5 mg.L^{-1}

At the higher inlet OCS level, the distribution of ozone concentrations throughout the reactor is significantly altered (Figure 5-9 (b)). This significantly increases the *C. parvum* survival ratios (Figure 5-10). The disinfection performance of the contactor on the prescribed operating condition is illustrated in Figure 5-10 (a), indicating the survival ratio of *C. parvum* is less than 1%; however, with a higher OCS level, the survival increases to 10% (Figure 5-10 (b)). It suggests that an increase in OCS loading would require an increase in the ozone dosage. Hence the current operating strategy needs to be modified to optimise the ozone utilisation.

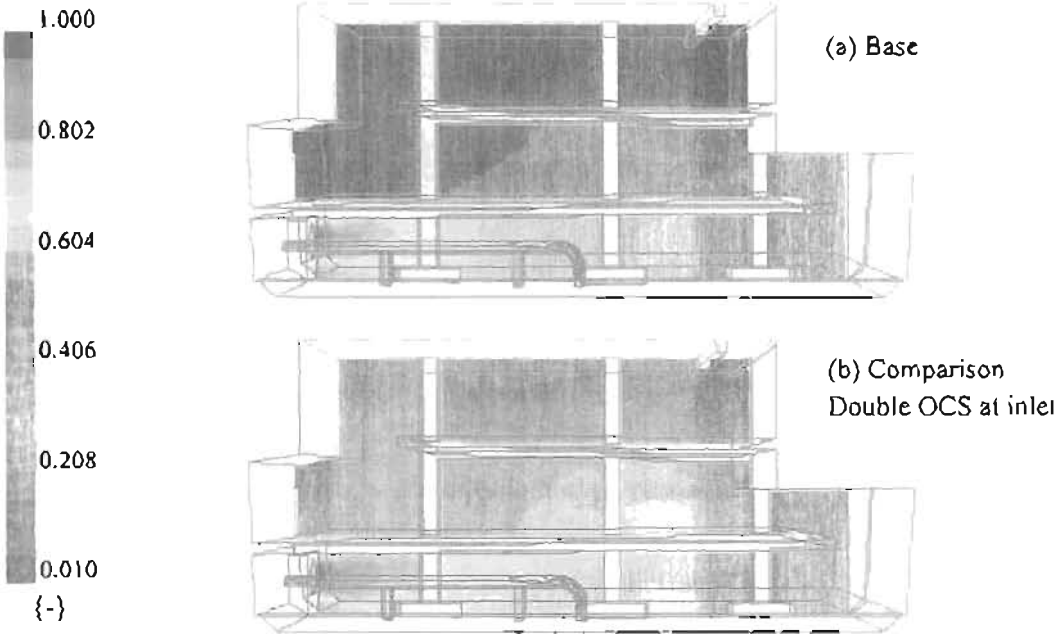

Figure 5-10: Simulate survival ratio of *C. parvum*. Base case vs. Comparative case. Flow rate = 106 ML.d^{-1}; ozone dose = 2.5 mg.L^{-1}

5.5.4 Results comparison

The analyser measurements were also compared with the dissolved ozone concentration predicted by the current kinetic model (Figure 5-11). Although the results shared similar trends, the predicted ozone residuals were much higher than the measured data. This indicates that the literature rate constant of ozone reaction with OCS, which bears the largest uncertainty, may not be adequate to represent the ozonation system at the Wiggins Waterworks.

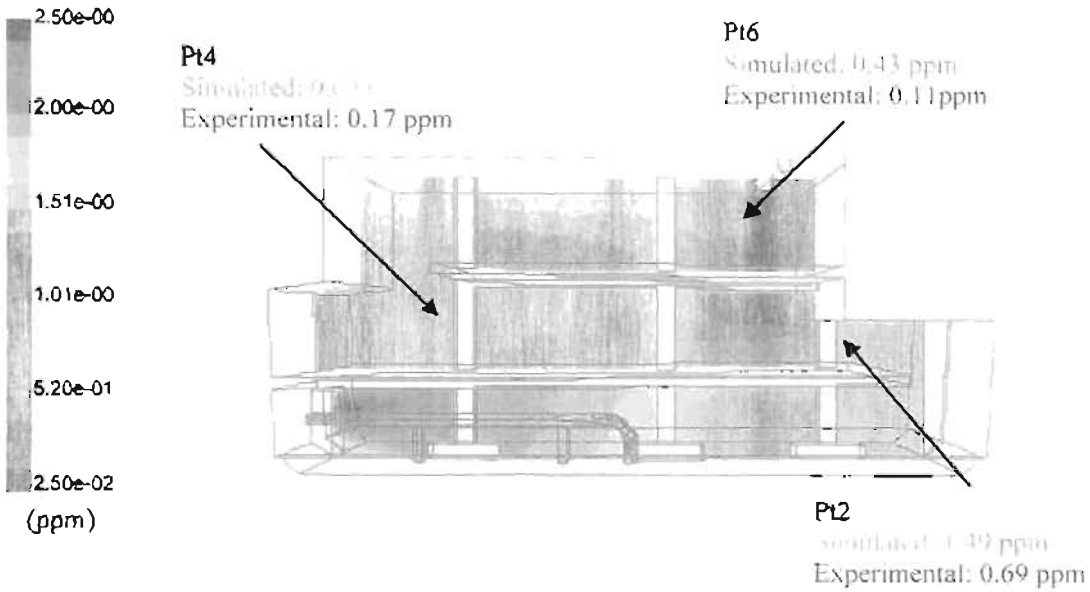

Figure 5-11: Comparison between the simulated and experimental ozone residual. Flow rate = 106 ML.d^{-1}; ozone dose = 2.5 mg.L^{-1}

Apart from measurements taken at steady state, a number of step-tests were carried out to assess the effect of variation in flow rate and ozone dose. Due to the lengthy time required to conduct a scan of all six sample points, measurements were only taken at Point 4 as it was considered to be the most suitable point for monitoring. As can be seen from Figure 5-12, the simulation using the literature value of k, does not predict the measured response well.

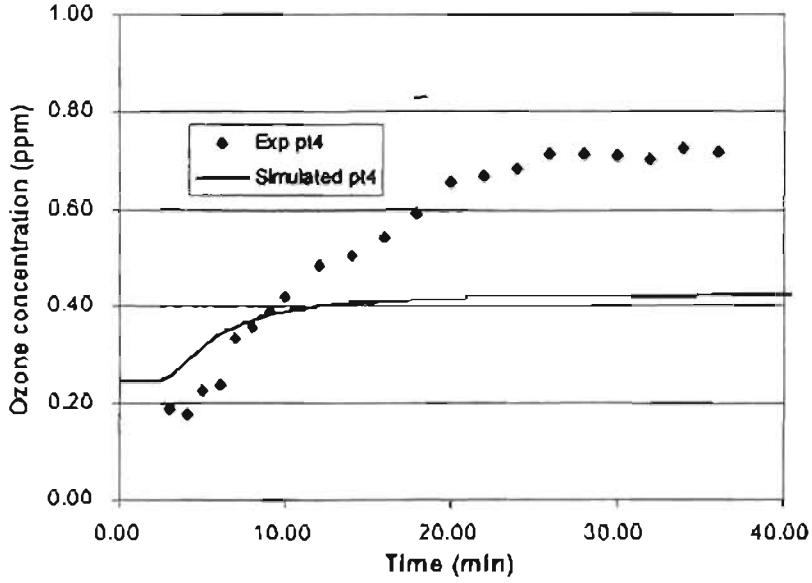

Figure 5-12: Comparison of measured and simulated ozone concentrations at Point 4. Flow rate = 106 ML.d^{-1}; ozone dose stepped from 2.5 to 3.5 mg.L^{-1}.

The comparison of ozone concentrations between the experimental value and the simulated time response at Point 4 in Figure 5-12 suggested that the literature value of k, was too high. As a result, the simulated ozone concentration was depleted faster than the experimentally observed trend.

A number of simulations were tested by adjusting the rate constant for the OCS reaction. The predicted results were compared against the measured experimental data as well as those of the base model.

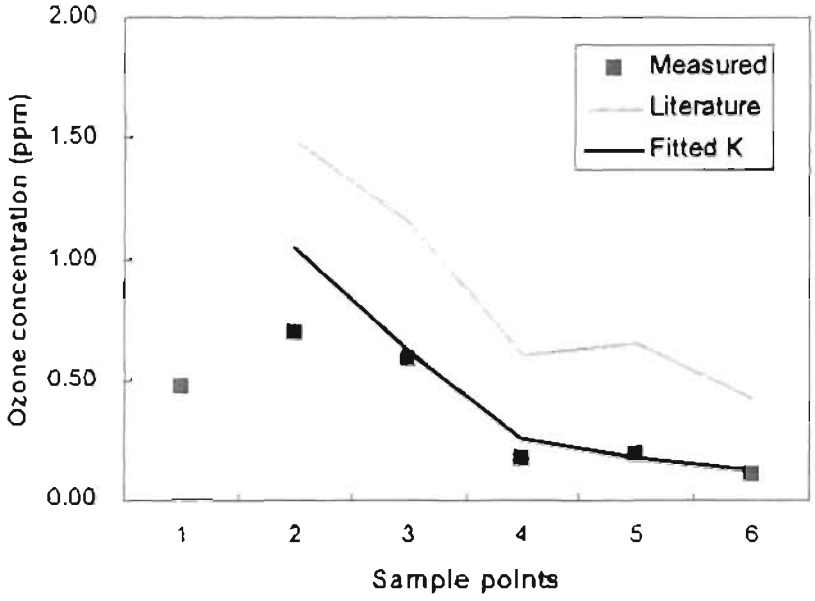

Figure 5-13: Comparison of the measure ozone residual and the simulated results using literature and fitted values. Flow rate = 106 ML.d^{-1}; ozone dose = 2.5 mg.L^{-1}

The predicted results by increasing the rate constant from 12 to 56 kL.kmol^{-1}.s^{-1} produced results fitting better to the experimentally observed values (Figure 5-13). The same phenomenon was observed at a higher flow rate of 120 ML.d^{-1} (Figure 5-14) where k_r is also raised to 56 kL.kmol^{-1}.s^{-1}.

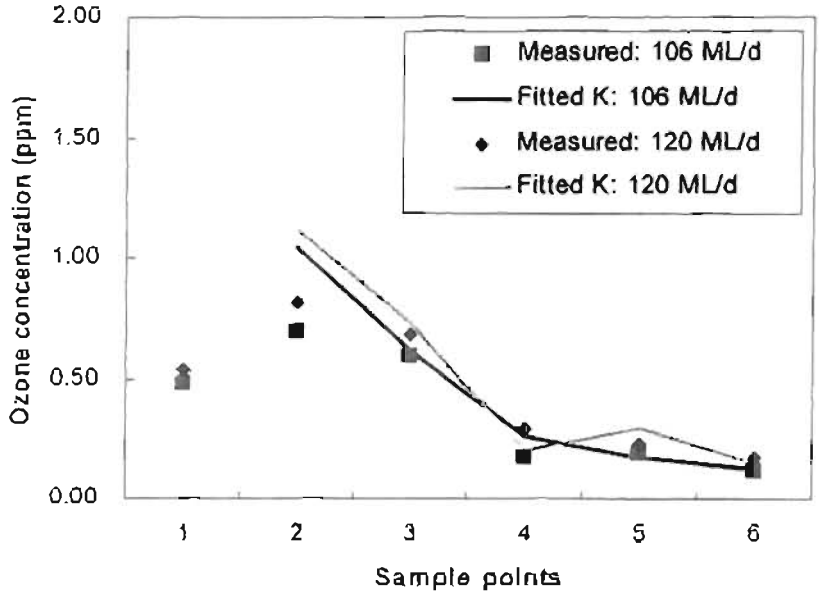

Figure 5-14: Comparison of the measure ozone residual and the simulated results using adjusted rate constant. Ozone dose = 2.5 mg.L^{-1}; k_r = 56 kL.kmol^{-1}.s^{-1}

The comparison in Figure 5-13 leads to contradictory findings to that of Figure 5-12. Apart from the known operating variables such as the ozone doses and flow rates, parameters such as TOC or any variables related to the water quality were not determined specifically at the time of the experimental tests. Although the kinetic model predicted similar profiles of ozone concentration, the contradiction in results

suggests that further experimental work was necessary to characterise the ozone reactions for the local water source.

5.5.5 Ozone mass balance

A simplified ozone balance test was carried out on the full-scale contactor. The dose rate was taken as the amount of ozone entering the system. In order to measure the exit ozone concentration, a sample was drawn before the gas reaches the thermal destructor unit (TDU). The ozone concentration in the gas was measured using an auto analyser. The flow rates, pressure and temperature of the gas were recorded. The measurements have proven to be difficult, as the overhead gas flowing to the TDU was greatly influenced by the air drawn from the vacuum breaker at the top of the contactor.

It was assumed that the ozone loss from the gas phase equalled the mass dissolved in water, i.e.: all other losses were assumed to be negligible. The result showed that the transfer efficiency was 97%. A summary of the mass balance is tabulated in Table 5-3. The detailed calculation is included in Appendix C.

Table 5-3: Summary of ozone mass balance on the full-scale contactor

	Unit	Value
Ozone in	($g.h^{-1}$)	14 583
Ozone out	($g.h^{-1}$)	376
Transferred	($g.h^{-1}$)	14 207
Efficiency	(%)	97.4

In terms of the modelling work thus far, the mass transfer efficiency of ozone to water using a static mixer was assumed to be complete. Though simplified, this ozone mass balance indicated that the assumption was reasonable.

5.6 Conclusion

Although most literature points towards a first-order reaction with respect to ozone, very little information is available for a generalised reaction order with respect to OCS. This is largely due to uncertainty in the natural water matrix.

The model with the adjusted rate constant gave a good prediction of ozone residual profiles for both steady-state cases of 106 $ML.d^{-1}$ and 120 $ML.d^{-1}$ (Figure 5-14); whereas the predicted results using literature the rate constant correlated poorer to the experimental data (Figure 5-13). In addition, the time response of the step tests suggested a lower rate constant while the simulated ozone concentration at steady state suggested the opposite. All of this suggests that the hydrodynamics aspect of the model is sufficiently accurate; however, the details of the reaction model require improvement.

Although the kinetic rate constants were obtained from literature, the findings thus far have supported that Point 4 is a better position for monitoring than the current outlet point. It can also be deduced that most of the dissolved ozone was consumed by the end of the middle compartment.

A simple ozone balance was performed and the mass transfer efficiency of the static mixer was calculated to be over 97%, assuming all ozone that disappeared from the gas phase entered into solution. This additional test was necessary to check the assumption used by the model that the ozone transfer is complete with negligible losses.

5.7 References

Bablon G., Bellamy W.D., Billen G., Bourbigot M.-M., Daniel F.B. Erb F., Gomella C., Gordon G. et al. (1991b) *Chapter 3. Practical application of ozone: principles and case studies.* In *Ozone in Water Treatment: Application and Engineering*. Langlais B., Reckhow D.A. and Brink D.R., eds., Lewis Publishers, Chelsea, Michigan. ISBN: 0-87371-474-1.

Bablon G., Bellamy W.D., Bourbigot M.-M. et al. (1991a) *Chapter 2. Fundamental aspects.* In *Ozone in Water Treatment: Application and Engineering*. Langlais B., Reckhow D.A. and Brink D.R., eds., Lewis Publishers, Chelsea, Michigan. ISBN: 0-87371-474-1.

Beltrán F.J. (1995) *Theoretical aspects of the kinetics of competitive ozone reactions in water.* Ozone-Science & Engineering, **17** (2): 163-181.

Bredtmann M (1982) *Significance of the ozone to water contacting system.* In *Ozonation Manual for Water and Wastewater Treatment.* Masschelein. W.J. New York, John Wiley and Sons: 129-132.

Brouckaert C.J., Pryor M., Brouckaert B.M. and Buckley C.A. (2000) *A computational fluid dynamics study of an ozone contactor.* Proceedings of the 2000 WISA Biennial Conference and Exhibition, Sun City, South Africa.

Clesceri L.S., Greenberg A.E. and Eaton A.D. eds. (1998) *Standard Methods for the Examination of Water and Wastewater*, 20th edition, American Public Health Association, Washington DC.

Cockx A., Do-Quang Z., Lin A. and Roustan M. (1999) *Use of computational fluid dynamics for simulating hydrodynamics and mass transfer in industrial ozonation towers.* Chemical Engineering Science **54**: 5085-5090.

Do-Quang Z., Cockx A. and Liné A. (2000) *Recent advances in modelling tool development and application for ozone reactors design: The CFD approach.* Proceedings of the International Specialised Symposium IOA 2000, Toulouse, France, 1-3 March: 275-300.

Driedger A.M., Rennecker J.L., and Mariñas B.J. (2000) *Sequential inactivation of Cryptosporidium parvum oocysts with ozone and free chlorine.* Water Research **34** (14): 3591-3597.

Driedger AM, Rennecker JL, and Mariñas BJ (2000) *Sequential inactivation of Cryptosporidium parvum oocysts with ozone and free chlorine.* Water Research **34** (14): 3591-3597.

Finch G.R. and Li H. (1999) *Inactivation of cryptosporidium at 1°C using ozone or chlorine dioxide,* Ozone-Science & Engineering **21** (5): 477-486.

Garland J.A. and Curtis H. (1981) *Emission of iodine from the sea surface in the presence of ozone.* Journal of Geophysics Research **86**: 3183-3186.

Gyürék L.L., Li H, Belosevic M. and Finch GR (1999) *Ozone inactivation kinetics of Cryptosporidium in phosphate buffer.* Journal of Environmental Engineering **125** (10): 913-924.

Haag, W.R. and Yao, C.C.D. (1992) *Rate constants for reaction of hydroxyl radicals with several drinking water contaminants*. Environmental Science and Technology **26** (5): 1005-1013.

Hoigné J. and Bader H. (1978) *Ozonation of water: kinetics of the oxidation of ammonia by ozone and hydroxyl radicals*. Environmental Science and Technology **12**: 79-84.

Hoigné J. and Bader H. (1983a) *Rate constants of reactions of ozone with organic and inorganic compounds in water – I. Non-dissociating organic compounds*. Water Research **17**: 173-183.

Hoigné J. and Bader H. (1983b) *Rate constants of reactions of ozone with organic and inorganic compounds in water – II. Dissociating organic compounds*. Water Research **17**: 185-194.

Hoigné J. and Bader H. (1994) *Characterisation of water quality criteria for ozonation processes. Part II: Lifetime of added ozone*. Ozone-Science & Engineering **16** (2): 121-134.

Hoigné J., Bader H., Wang W.R. and Staehelin J. (1985) *Rate constants of reactions of ozone with organic and inorganic compounds in water – III Inorganic compounds and radicals*. Water Research **19** (8): 993-1004.

Huang T.H., Brouckaert C.J. and Buckley C.A. (2003) *A computational modelling and experimental study of an ozone contactor*, Proceedings of the South African Chemical Engineering Congress, Sun City, 3-5 September 2003.

Huang T.H., Brouckaert C.J. and Buckley C.A. (2004b) *Integration of CFD modelling and kinetic study to improve the control strategy of an ozone contactor*. Proceedings of the 2004 WISA Biennial Conference and Exhibition, Cape Town, South Africa, 1 – 4 May.

Huang T.H., Brouckaert C.J., Pryor M. and Buckley C.A. (2004a) *Application of computational fluid dynamic modelling to an ozone contactor*, Water SA **30** (1): 51-56.

Joret J-C, Mennecart V, Robert C, Compagnon B, and Cervantes P (1997) *Inactivation of indigenous bacteria in water by ozone and chlorine*. Water Science and Technology **35** (11-12): 81-86.

Kilham LB (2002) *Measurement of dissolved ozone and the development of a new meter*. Access on 24 January 2003 at URL http://www.wcp.net/PDF/0102dissolved.pdf

Korich D.G., Mead J.R., Madore M.S., Sinclair N.A. and Sterling C.R. (1990) *Effects of ozone, chlorine dioxide, chlorine, and monochloramine on Cryptosporidium parvum oocyst Viability*. Applied and Environmental Microbiology **56** (5): 1423-1428.

Li H., Finch G.R. Smith D.W and Belosevic M. (2001) *Sequential inactivation of Cryptosporidium parvum using ozone and chlorine*. Water Research **35** (18): 4339-4348.

Masschelein W.J. (2000) *Considerations on the Chick-Watson law applied to the ozonation of drinking water*. Ozone-Science & Engineering **22**: 227-239.

Muroyama K, Norieda T, Morioka A, and Tsuji T (1999) *Hydrodynamics and computer simulation of an ozone oxidation reactor for treating drinking water*. Chemical Engineering Science, **54**: 5285-5292.

Orbisphere (1997) *Residual ozone system (R.O.S.) – Operator's manual. Model 26506 indicating instrument/Model 31331.15 sensor*. Orbisphere Laboratories. Switzerland.

Park H.-S., Hwang T.-M., Kang J.-W., Choi H., and Oh H.-J. (2001) *Characterization of raw water for the ozone application measuring ozone consumption rate*. Water Research, **35** (11): 2607-2614.

Rakness K.L., Hunter G.F., and DeMers L.D. (2000) *Drinking water ozone process control and optimization*. Proceedings of the International Specialised Symposium IOA 2000, Toulouse, France, 1-3 March: 231-254.

Reckhow D.A., Knocke W.R., Kearney M.J., Parks C.A. (1991) *Oxidation of iron and manganese by ozone*. Ozone-Science & Engineering **13** (6): 675-695.

Rennecker JL, Driedger AM, Rubin SA, and Mariñas BJ (2000) *Synergy in sequential inactivation of Cryptosporidium parvum with ozone/free chlorine and ozone/monochloramine*. Water Research **34** (17): 4121-4130.

Staehelin J. and Hoigné J. (1985) *Decomposition of ozone in water in the presence of organic solutes acting as promoters and inhibitors of radical chain reactions*. Environmental Science Technology **19** (12): 1206-1213.

Von Gunten U. (2003) *Ozonation of drinking water: Part I. Oxidation kinetics and product formation*. Water Research **37** (7): 1443-1467.

Westerhoff P., Aiken G., Amy G. and Debroux J. (1998) *Relationship between the structure of natural organic matter and its reactivity towards molecular ozone and hydroxyl radicals*. Water Research **33** (10): 2265-2276.

Yavich A.A. and Masten S.J. (2001) *Modelling the kinetics of the reaction of ozone with natural organic matter in Huron River water*. Ozone-Science & Engineering **23** (2): 105-119.

6

WIGGINS WATERWORKS' OZONE KINETICS EXPERIMENTS

"Kinetics is nature's way of preventing everything from happening all at once."
- S.E. LeBlanc (Fogler, 1997)

"Everything should be made as simple as possible, but not one bit simpler."
- Albert Einstein, US (German-born) physicist, (1879-1955)

A simplified but operation-orientated procedure is necessary to assist in regular monitoring of raw water at Wiggins Waterworks. A lumped-parameter kinetics study has been developed in the current chapter to provide sufficient information relating ozone depletion to raw water quality, without the lengthy and costly analyses of a detailed kinetics study.

This chapter discusses the laboratory experiments and the chemical analyses involved. The results of this work are required for updating the kinetic model.

Section 6.1 introduces the concept of water characterisation and its applicability as a regular monitoring analysis for plant operation. **Section 6.2** specifies the distinct goals required to achieve the overall objectives. **Section 6.3** discusses the assumptions involved. **Section 6.4** describes the experimental procedure designed to cater for the needs of the current study, the associated assumptions and the analytical methods used. The results are discussed in **Section 6.5** and the sectional concluding remarks are given in **Section 6.6 .**

6.1 Introduction

It is not practical to analyse for each individual chemical compound present in NOM, surrogate characterisation methods were sought to characterise NOM (Owen et al., 1995).

The method should be chosen on the basis that the reproducibility and the stability of the results are relatively high. For the analysis of ozone in solution, there are two analytical methods currently used: indigo spectrophotometric method, and iodide titrimetric method. The latter method is however limited by the range of dissolved ozone concentration that the method is sensitive to.

Due to the complexity of the ozone reactions in water, the ozone depletion rate can be strongly affected by the water quality as suggested by most literature (Finch et al., 1999; Park et al., 2001; Westerhoff et al., 1997). The experiments were conducted under strict conditions in order to minimize external interferences; however, their applications on the full-scale plant study have not yet been demonstrated.

Furthermore, since the quality of water varies in a range throughout a day; it is not practical to apply such strict conditions for day-to-day operation for a full-scale plant. The laboratory operation of water characterisation must be as simple as possible and can be performed easily in all utilities which apply ozone (Hoigné and Bade, 1994).

6.2 Objectives

The main objective of the investigation in this chapter is to experimentally determine a kinetic rate constant for the generalised ozone-OCS reaction using raw water received by Wiggins Waterworks. The investigation was carried out using a laboratory ozonation column. The specific goals for the experimental work include the following:

- To experimentally characterise raw water received by Wiggins Waterworks;
- To find a suitable surrogate to quantify OCS present in raw water;
- To develop a laboratory ozonation procedure for plant operation purpose.

6.3 Assumptions

The experiments were conducted using Inanda Dam water at the Wiggins Waterworks. Raw water had an average alkalinity of 50 $mg.L^{-1}$ as $CaCO_3$, and did not vary significantly during the period of testing. For this reason the effect of alkalinity was not investigated in this study.

It is generally acknowledged by Umgeni Water that instantaneous ozone demand is very little for the water received and therefore can be neglected. The term instantaneous ozone demand will be explained in the next section.

6.4 Equipment and methods

The kinetic experiments were conducted in the laboratory at the Darvill Wastewater Works of Umgeni Water in Pietermaritzburg, using the existing ozonation column. Raw water was collected with a 25 L drum at the raw water line leading to the PEF at Wiggins Waterworks. Due to the capacity of the column and the prevention of possible deterioration of the water sample upon standing, the collected water was generally tested within a day.

The experimental work was carried out over a period of three months. The preliminary runs were conducted to qualitatively examine the effects of numerous operating parameters; whereas the main runs were performed with additional chemical analyses to examine the raw water quality.

The main experimental procedure consists of two parts: the ozonation of raw water followed by the chemical analyses. The equipment required and the procedures undertaken are described in this section.

6.4.1 Laboratory ozonation

A schematic diagram of the laboratory ozonation setup is shown in Figure 6-1.

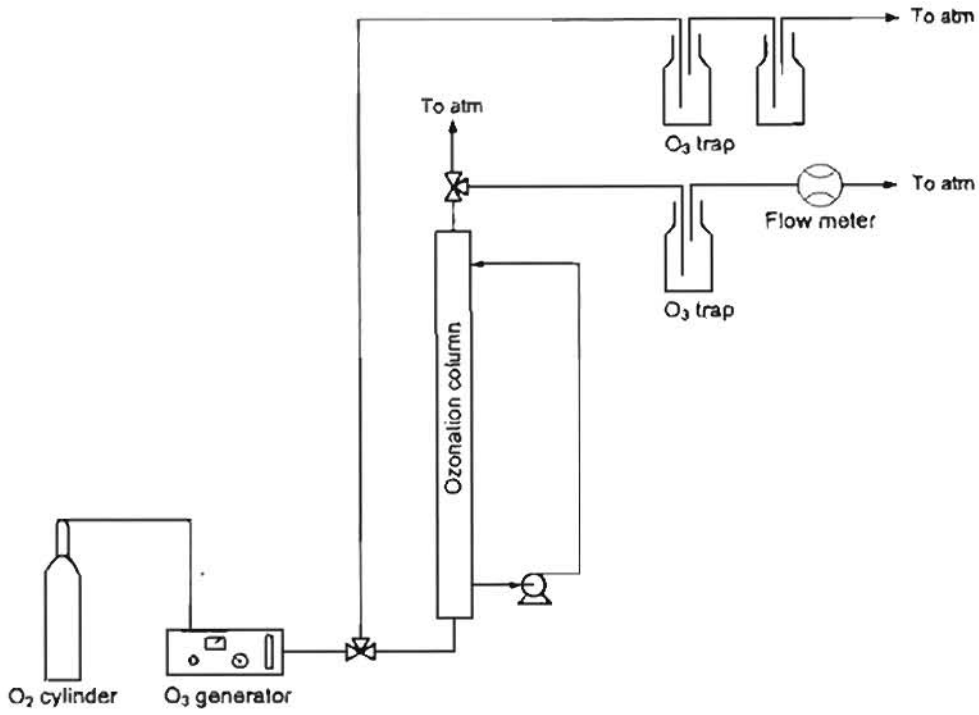

Figure 6-1: Schematic diagram of the laboratory ozonation process

Ozone was generated from oxygen (<10 mg.L^{-1} moisture) using a laboratory ozone generator (Sorbios model GSG 001.2) at a pressure of 0.5 bar and a oxygen flow rate of 15 L.h^{-1} to produce approximately 1 g ozone per hour. The ozone was introduced to the glass column (1.4 m high with an internal diameter of 60 mm and a capacity of 4.5 L) at the base through a sintered glass diffuser. To ensure sufficient mixing, a peristaltic pump was used to circulate the water-gas mixture in a counter-flow direction from the base (above the diffuser) to the top of the column. The spent gas left the column at the top and was directed to an ozone trap filled with potassium iodide solution before passing through a flow meter (Alexander Wright Model no. 3 DM3 B). When ozone was not in use, it was passed through two sets of ozone traps before being released to the atmosphere.

During the experimental procedure, the working area was kept well-ventilated to avoid the possible ozone leakage accumulating near the apparatus. The room was also conditioned to minimise the effect of the surrounding temperature on the ozonation.

The preliminary runs were conducted to investigate the effect of numerous operating parameters. The main runs were conducted with additional chemical analyses.

6.4.1.1 Dose calibration procedure

The experimental work was carried out in two parts and stated in the thesis: first the ozone dose calibration (since the sensitivity of ozone generation has been mentioned), then the second part for the actual experiments. The calibration was done using the iodometric method because the expected dissolved ozone concentration is high. The actual kinetic experiments were performed with the indigo method, although the iodometric method was used as an aid for the experiments which have high initial ozone concentration.

On the basis of introducing 1 L of ozone-containing gas at the prescribed settings (Pressure = 0.5 bar; Flow = 15 L.h^{-1}, Voltage = 180 V), the ozonation column was filled with KI solution. The time taken to introduce 1 L of gas was recorded along with the iodometric measurement on the dissolved ozone concentration in the column. This step was repeated until the variation did not exceed more than 5%. The calculation then proceeded to determine the amount of ozone-containing gas required to achieve the desired ozone dose.

Figure 6-2 shows the initial setup of the ozonation column in (a) and as the dose calibration was nearly completed in (b).

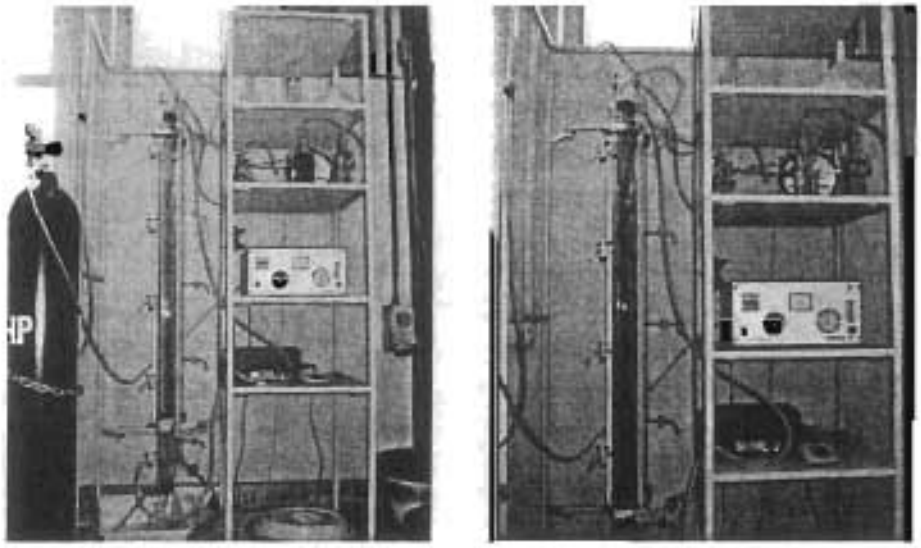

(a) initial setup (b) near completion

Figure 6-2: Dose calibration using ozonation column

The colour of the KI solution was observed to turn from colourless to dark yellow, indicating the reaction with ozone.

6.4.1.2 Sample ozonation

After calibration, the column was thoroughly rinsed with tap water and then with the sample water to prepared for sample ozonation. A 4.5 L raw water sample was placed in the column. While the sample was re-circulated, the required ozone-containing gas was passed through the column. Approximately 30 s was allowed for further mixing time irrespective of ozone doses. This step also ensured all gas exiting the column was passed through the ozone trap containing KI solution. The ozone that remained in the overhead gas was captured in the trap in order to perform a mass balance.

The dissolved ozone concentration was determined by the indigo colorimetric method. The first sample was taken after the 30 s mixing period and thereafter at increasing time intervals for another six samples up to around 20 to 25 min after the ozone addition. The amount of ozone in the KI trap was determined by the iodometric method.

For each sample ozonation, the time taken to dose, the flow meter reading, the pH of sample water were measured and recorded. For each sample taken, the ozone concentration (by indigo method), the UV absorbance at 254 nm and TOC were measured and recorded. The details of the chemical analyses are discussed in the next section.

6.4.2 Determination of ozone concentration

Ozone concentration can be determined either by titrimetric or colorimetric method. Both methods were employed in the experimental procedure.

6.4.2.1 Iodometric titration

The iodometric titration method was used in the dose calibration of the ozonation column and the off-gas captured in the ozone traps. The principle involves ozone liberating free iodine from potassium iodide (KI) solution under slightly acidic conditions. The liberated iodine is titrated using sodium thiosulphate ($Na_2S_2O_3$) using starch as an indicator. The titration must be carried out at pH 3 or 4 since the reaction is not stoichiometric at neutral pH as a result of partial oxidation of the thiosulphate to sulphate (Clesceri et al., 1998).

The procedure used is described in 4500-Cl B of Standard Methods for the Examination of Water and Wastewater (Clesceri et al., 1998) by replacing chlorine with ozone. A measured volume of ozonated sample with KI was mixed in a conical flask with 5 mL glacious acetic acid and titrated with 0.01N $Na_2S_2O_3$ until the yellow colour of the liberated iodine faded. 1 mL of starch indicator was then added and titrated further until the blue colour completely disappeared. This method is applicable when the oxidant (in this case, ozone) is around and above 1 $mg.L^{-1}$.

Since strong oxidising agents such as manganese or chlorine may interfere with results, a blank solution is always prepared to determine the presence of such compounds.

6.4.2.2 Indigo method

The indigo colorimetric method was used to determine the dissolved ozone concentration in the ozonated water samples. In an acidic solution, ozone rapidly decolourises indigo (Clesceri et al., 1998). The indigo compound contains only one double bond (C=C) which can be expected to react with ozone with a very high reaction rate constant (Bader and Hoigné, 1981). At low pH the amino groups are protonated and therefore unreactive. Therefore it is assumed that one mole of indigo reacts with one mole of ozone. The decrease in absorbance is linear with increasing concentration (Clesceri et al., 1998). Figure 6-3 shows the discolouration of indigo solution as ozone concentration in the samples increases from right to left. The flask on the extreme left is the blank solution. This method is selective (Clesceri et al., 1998) and the decolourised products scarcely consume further ozone (Hoigné and Bader, 1994).

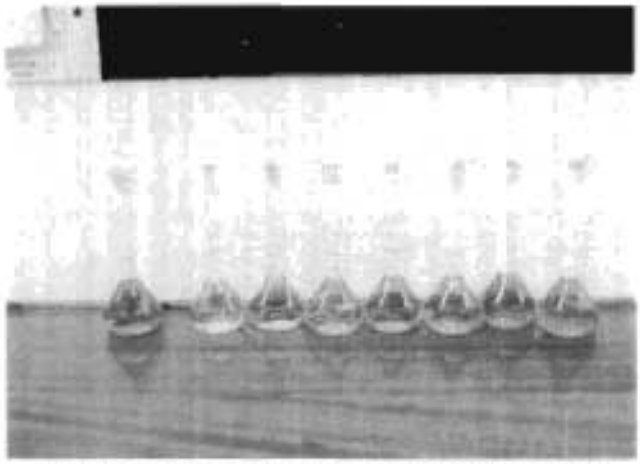

Figure 6-3: Decay of indigo colour due to ozone

The procedure used is described in Section 4500-O_3 B. in Standard Methods (Clesceri et al., 1998). 5 mL indigo reagent was placed in a 50 mL volumetric flask which was then filled with the ozonated sample to the mark. Care must be taken to choose an appropriate volume of sample such that complete decolourisation does not occur. One blank was prepared using distilled water and the raw water sample each. A corrected blank on the ozonated samples was prepared by adding a few grains of $Na_2S_2O_3$ to remove all the ozone. The absorbances were measured at 600 nm on a Pharmacia LKB Ultraspec UI spectrophotometer using a 10 mm quartz cell.

Best reproducibility was achieved when the glassware used for handling of aqueous ozone was conditioned by repetitive use for the same procedures. The stability of the colour intensity is a crucial requirement in a time-critical experiment such as the determination of the ozone concentration. Shechter (1973) has reported the effect of the colour change for the spectrophotometric method can be kept to minimum if the analysis is carried out in a short time period.

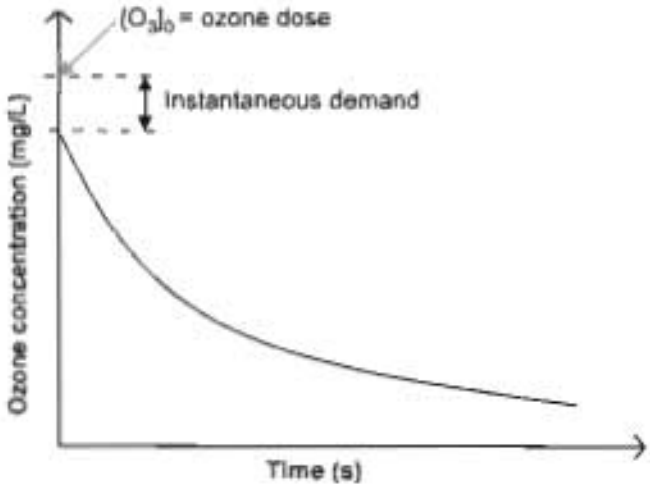

Figure 6-4: Differentiation between ozone dose and instantaneous demand.

It must be noted that the term *ozone dose* is different from the instantaneous demand (see Figure 6-4). In the experiments, ozone dose means the amount of ozone transferred into solution. The difference between the dose and the immediate ozone concentration is known as the instantaneous demand.

6.4.3 Measurements

The following chemical analyses were performed only for the main ozonation runs.

6.4.3.1 254 nm and TOC

The UV absorbance was measured using a Pharmacia LKB Ultraspec III spectrophotometer. The water samples (blank or ozonated water) was first filtered through 0.45 μm membrane filters and then placed in a 10 mm quartz cell. The UV light source was provided by a deuterium lamp. This procedure is described in Section 5910 B of Standard Methods (Clesceri et al., 1998).

The TOC concentrations were analysed using the persulphate-ultraviolet oxidation method. The procedure is described in Section 5310 C of Standard Methods (Clesceri et al., 1998). The analyses were performed in duplicate.

6.4.3.2 pH and temperature

pH of the sample was measured using a MeterLab PHM 201 portable pH meter. The temperature was measured using a laboratory thermometer. Both the pH and the temperature of the samples were recorded.

6.5 Results and discussion

The kinetic experiments were largely limited to the available experimental setup. While the Standard Methods (Clesceri et al., 1998) proposes to make up an ozone stock and to use the stock for dosing, it was found extremely difficult to obtain such a stock solution and furthermore, the ozone stock concentration needed to be standardised at every dose point.

The proposed method is a semi-batch for the initial period of dosing ozone, thereafter it is a closed system, where the external loop provided the additional mixing effects. The disadvantage of this method is that the first measurement can only be taken after the 'dose' is completed.

An ozone mass balance was checked for each test. While the overhead ozone was capture by KI traps, the remainder was assumed to have dissolved in the water. Seeing that it is a closed system after the ozone dose, this assumption was considered good enough to continue with the investigation.

The effect of the water matrix was examined qualitatively in the preliminary runs. This was achieved by performing laboratory ozonation on samples of the raw water and the ultra-pure Milli-Q water (Millex, Millipore). Every sample was injected with ozone-containing gas at different ozone doses. The decrease in dissolved ozone concentration was monitored over time. For the ultrapure water, the self-decomposition of ozone should be solely accountable for the decay in the ozonated sample. Figure 6-5 shows results of decay using iodometric method at high and low ozone doses (4.5 and 2.25 $mg.L^{-1}$) respectively.

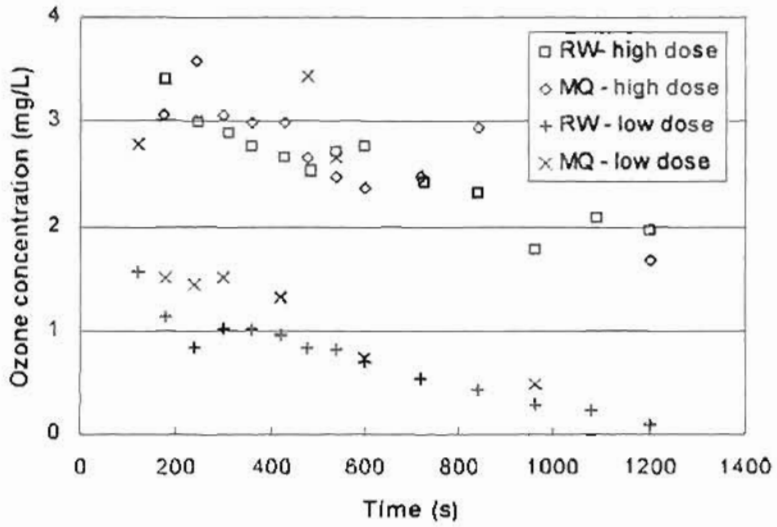

Figure 6-5: Ozone decay in ozone-saturated raw and ultra-pure waters.
RW – raw water; MQ – ultra-pure water

The general trend of decay in raw water seemed less erratic than in ultra-pure water. The residual ozone was registered lower in raw water, indicating that there were further reactions between ozone and the bio-matrix of water.

The tests described above also saw the discrepancies between the two methods of determining the ozone concentrations. The comparison is plotted in Figure 6-6.

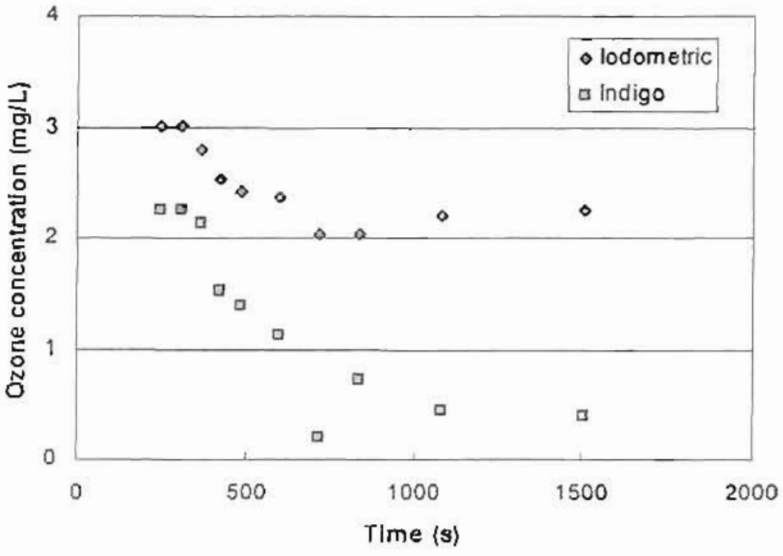

Figure 6-6: Measure of residual ozone using different methods.

The deviation of the measurements at higher ozone concentrations was due to the incorrect sample size which caused the complete discolouration of indicator in the indigo method. However, the difference in the measurements between the iodometric and indigo methods were notably significant at lower concentrations. This confirmed the measurement threshold (approx. 1 $mg.L^{-1}$) of the iodometric method at

low ozone concentrations and the more sensitive indigo method was to be applied in the expected working range.

The main runs were carried out on the raw water collected at the Wiggins Waterworks only. From the water samples gathered, one was more turbid than the rest. This demonstrated the variance in quality of the water received at the Wiggins Waterworks. The observed ozone decay in the turbid and clear water samples at various ozone doses are plotted in Figure 6-7 and Figure 6-8 respectively.

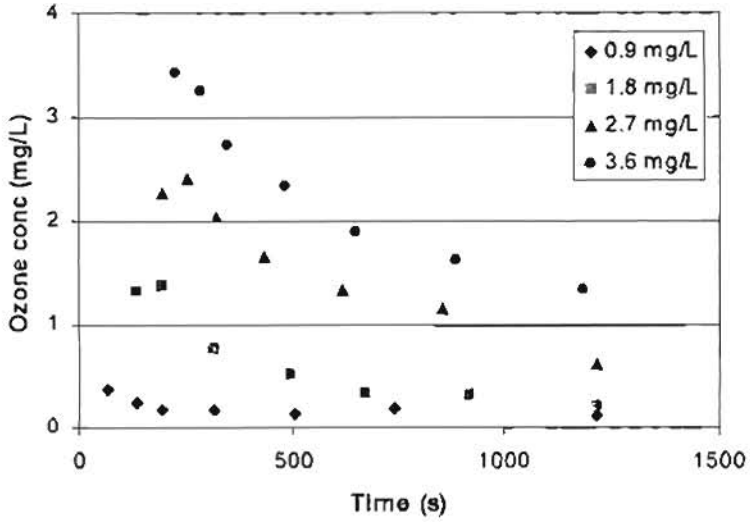

Figure 6-7: Decay of ozone in the turbid water sample at various ozone doses.

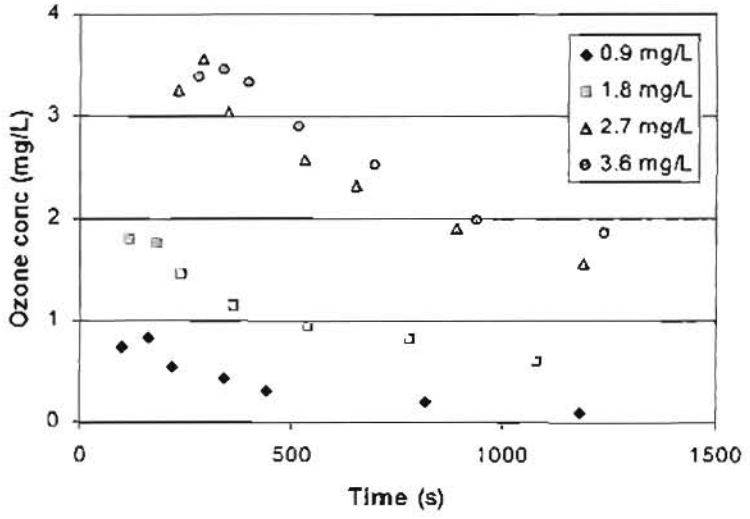

Figure 6-8: Decay of ozone in the clear water sample at various ozone doses.

The ozone-dosing method in a laboratory ozonation may consider using gaseous ozone or an ozone-containing stock solution. The advantage of dosing gas is that the raw water samples are not diluted by the addition of an ozone stock (Hoigné and Bader, 1994); however, the apparatus poses inherent restrictions on parameters such as the mass transfer efficiency or the formation of a concentration gradient.

It should be noted that the present apparatus has a limited working range of ozone doses. This was reflected at high ozone doses where the subsequent measurements were occasionally higher than the initial

values (see Figure 6-7 and Figure 6-8). It seemed that ozone was still dissolving after the initial samples. This could be due to inappropriate timing of the initial sampling as it was taken immediately after dosing.

The mass balances performed on all the experimental runs also indicated that mass transfer efficiency seemed to decrease as the dose increases. A sample calculation is shown in Table 6-1. High doses of batch type ozonation require longer time to inject the gas. It could be argued that the associated uncertainties such as the inconsistency in ozone production or the poor mixing within the ozonation column were amplified. The lowest dose achievable with the present apparatus was 0.9 $mg.L^{-1}$.

Table 6-1: Efficiency of ozone doses

Water sample	Run name	Aim	Ozone applied	Actual dose	Efficiency
		($mg.L^{-1}$)	($mg.L^{-1}$)	($mg.L^{-1}$)	(%)
Turbid	Run 0526-0.9	0.9	0.96	0.96	100
Turbid	Run 0527-1.8	1.8	1.79	1.60	89
Turbid	Run 0526-2.7	2.7	2.88	2.30	80
Turbid	Run 0527-3.6	3.6	3.35	2.29	69
Clear	Run 0531-0.9	0.9	1.20	1.13	94
Clear	Run 0601-1.8	1.8	1.50	1.31	88
Clear	Run 0531-2.7	2.7	3.48	2.38	68
Clear	Run 0531-3.6	3.6	4.40	2.83	64

When the raw water samples exhibit low instantaneous demand (such as the raw water received by Wiggins Waterworks), the effect of mass transfer efficiency became significant in a laboratory setup. While it was aimed to dose at a multiple of the minimum achievable dose, the addition of gas and the efficiency of gas dissolution required the actual doses to be re-calculated at the end of the runs. The efficiency of the current setup to transfer gaseous ozone to water was best at lower ozone doses (< 2 $mg.L^{-1}$).

In both ozonation of turbid and clear waters, the initial concentrations obtained from ozone mass balances were registered lower than the subsequent samples. This highlighted the possibility of continuing dissolution of ozone or that the concentration gradient was present in the column.

The results from the main runs were first evaluated using the pseudo first-order rate reaction discussed in Section 4.4.1 . The associated rate law and the expression used to calculate the rate constant were as follows:

$$-\frac{d[O_3]}{dt} = k_c [O_3] \tag{4-8}$$

$$\ln\left(\frac{[O_3]}{[O_3]_0}\right) = -k_c t \tag{4-9}$$

The effects of ozone dose on the pseudo first-order rate constants are shown in Figure 6-9. The clear water sample seemed to exhibit an inverse relationship between the dose and k_c. As the dose increases, the rate constant decreases. This could be attributed to reactions which were accelerated when the ozone dose was high, and thereby resulting in a slower subsequent decay.

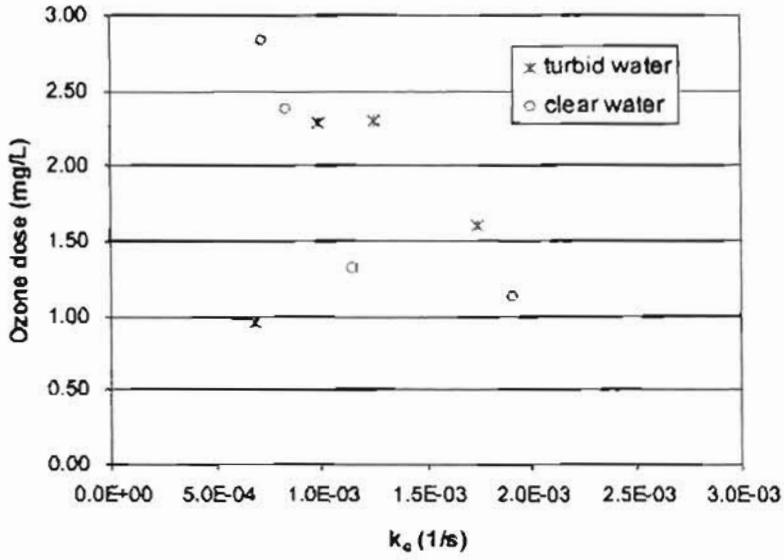

Figure 6-9: Effect of ozone dose on the pseudo first-order rate constants.

The more turbid water seemed to exhibit a lesser apparent trend towards the ozone doses, as the run with the lowest dose (0.9 mg.L^{-1}) did not correlate well with Eqn. (4-9). Unfortunately this could not be tested again as no similar water sample was available.

The simplicity of Eqn. (4-9) overlooks the importance of the bulk organic matter (as measured by TOC) in determining the ozone decay. The proposed second-order rate law (Eqn. (4-10)) accounts for the effects of water matrix by measurements of TOC.

$$\ln\left(\frac{[O_3]}{[O_3]_0}\right) = -k_r[\overline{OCS}]\,t \qquad \textbf{(4-10)}$$

The results of the second-order rate constants with the corresponding ozone dose and equivalent OCS concentration are presented in Table 6-2 and Table 6-3 for turbid and clear water samples respectively.

Table 6-2: Rate data for the turbid water

Run name	Ozone dose	OCS equiv	k_o	k_r
	(mg.L^{-1})	(kmol glucose.kL^{-1})	(s^{-1})	(kL.kmol^{-1}.s^{-1})
Run 0526-0.9	0.96	8.19×10^{-5}	6.83×10^{-4}	8.35
Run 0527-1.8	1.60	7.13×10^{-5}	1.74×10^{-3}	24.47
Run 0526-2.7	2.30	8.15×10^{-5}	1.26×10^{-3}	15.44
Run 0527-3.6	2.29	6.96×10^{-5}	9.86×10^{-4}	14.18

Table 6-3: Rate data for the clear water

Runs	Ozone dose	OCS equiv	k_c	k_r
	($mg.L^{-1}$)	($kmol\ glucose.kL^{-1}$)	(s^{-1})	($kL.kmol^{-1}.s^{-1}$)
Run 0531-0.9	1.13	8.29×10^{-5}	1.91×10^{-3}	23.08
Run 0601-1.8	1.31	8.32×10^{-5}	1.15×10^{-3}	13.84
Run 0531-2.7	2.38	7.87×10^{-5}	8.41×10^{-4}	10.69
Run 0531-3.6	2.83	7.78×10^{-5}	7.28×10^{-4}	9.36

The effects of the ozone doses were well recognised for natural waters (Hoigné and Bader, 1994; Bablon et al., 1991b). This is different from the kinetics in solutions where the ozone consumption is controlled by a dominant solute (Hoigné and Bader, 1994). The second-order rate constants ranged from 8 to 25 $kL.s.kmol^{-1}$ for the conditions tested. This re-affirms the need to perform the raw water characterisation, instead of relying on a single rate constant value.

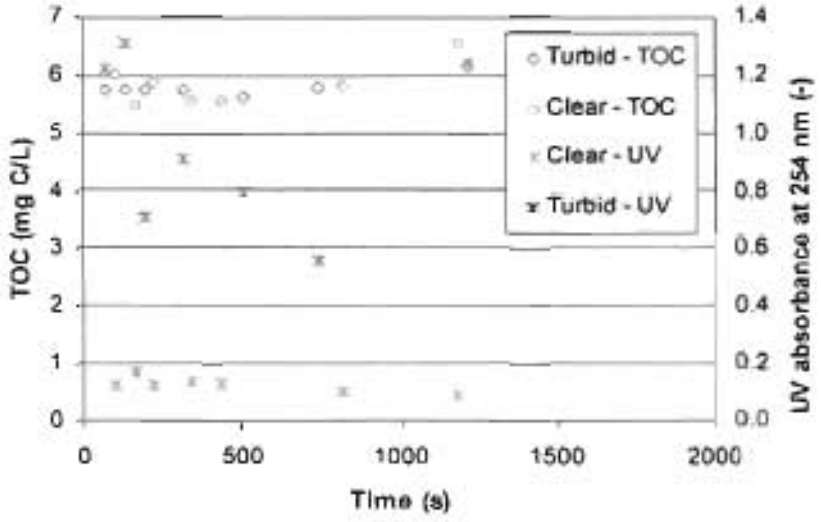

Figure 6-10: Observed change in TOC and UV absorbance with time. Ozone dose = 0.9 $mg.L^{-1}$.

An example of the change in TOC and UV absorbance with time is plotted in Figure 6-10 at an ozone dose of 0.9 $mg.L^{-1}$. The general trend indicates a decrease in UV absorbance and very little effects in the TOC. This was found in accordance with the study by Pryor and Freese (2000), particularly for fairly low TOC concentrations (3 to 6 $mg.L^{-1}$).

Ozonation of a raw water sample usually leads to a decrease in the humic fractions and an increase in the non-humic fraction (Yavich and Masten, 2001). Ozonation also increases the degradability of larger compounds through oxidation, resulting in smaller compounds. Although the shift between the fractions and the enhanced bio-degradability of OCS cannot be interpreted directly from the TOC measurement, the reduction in UV absorbance shows the effect of ozone on the NOM, particularly when the quality of received water is poor.

6.6 Conclusions

An experimental characterisation method was developed to characterise the raw water received at the Wiggins Waterworks. In order to achieve the optimal performance of ozonation, raw water should be monitored at regular intervals. The water must be characterised by a laboratory method which is as simple as possible and which can be operated easily in the utilities applying ozone (Hoigné and Bader, 1994). The laboratory characterisation described in this chapter was intended to encompass these considerations.

TOC was chosen to be an indicator of the OCS. Although the effect of ozone on TOC was slight at very low concentrations, the reduction in UV absorbance was observed. The TOC values can be re-calculated as an equivalent OCS concentration. This point is also applied for calculating the boundary conditions of the kinetic model in the previous chapter. For modelling and operational purposes, the time-average TOC can be replaced by the TOC at the contactor inlet.

6.7 References

Bablon G., Bellamy W.D., Billen G., Bourbigot M.-M., Daniel F.B. Erb F., Gomella C., Gordon G. et al. (1991b) *Chapter 3. Practical application of ozone: principles and case studies.* In *Ozone in Water Treatment: Application and Engineering*. Langlais B., Reckhow D.A. and Brink D.R., eds., Lewis Publishers, Chelsea, Michigan. ISBN: 0-87371-474-1.

Bader H. and Hoigné J. (1981). *Determination of ozone in water by the indigo method.* Water Research **15**: 449-456.

Clesceri L.S., Greenberg A.E. and Eaton A.D. eds. (1998) *Standard Methods for the Examination of Water and Wastewater*, 20th edition, American Public Health Association, Washington DC.

Driedger A.M., Rennecker J.L., and Mariñas B.J. (2000). *Sequential inactivation of Cryptosporidium parvum oocysts with ozone and free chlorine.* Water Research **34** (14): 3591-3597.

Finch G.R. and Li H. (1999). *Inactivation of Cryptosporidium at 1°C using ozone or chlorine dioxide,* Ozone-Science & Engineering **21** (5): 477-486.

Hoigné J. (1994). *Characterization of water quality criteria for ozonation processes: Part I: Minimal set of analytical data.* Ozone-Science & Engineering **16** (2): 113-120.

Hoigné J. and Bader H. (1994) *Characterization of water quality criteria for ozonation processes. Part II: Lifetime of added ozone.* Ozone-Science & Engineering **16** (2): 121-134.

Korich DG, Mead JR, Madore MS, Sinclair NA, and Sterling CR (1990). *Effects of ozone, chlorine dioxide, chlorine, and monochloramine on Cryptosporidium parvum oocyst viability.* Applied and Environmental Microbiology **56** (5): 1423-1428.

Li H., Finch G.R. Smith D.W and Belosevic M. (2001). *Sequential inactivation of Cryptosporidium parvum using ozone and chlorine.* Water Research **35** (18): 4339-4348.

Owen D.M., Amy G.L., Chowdhury Z.K., Paode R., McCoy M. and Viscosil K. (1995). *NOM characterisation and treatability.* Journal of American Water Works Association **87** (1): 46-63.

Park H.-S., Hwang T.-M., Kang J.-W., Choi H., and Oh H.-J. (2001). *Characterization of raw water for the ozone application measuring ozone consumption rate.* Water Research **35** (11): 2607-2614.

Pryor M.J. and Freese S.D. (2000) *The treatment of eutrophic water using pre- and intermediate ozonation, peroxone and pica carbon.* WRC report No 694/1/00, ISBN: 1-86845-588-2. Pretoria.

Shechter H. (1973) *Spectrophotometric method for determination of ozone in aqueous solutions.* Water Research. 7: 729-739.

Westerhoff P., Aiken G., Amy G. and Debroux J. (1998). *Relationships between the structure of natural organic matter and its reactivity towards molecular ozone and hydroxyl radicals.* Water Research 33 (10): 2265-2276.

Westerhoff P., Song R., Amy G., and Minear R. (1997). *Application of ozone decomposition models.* Ozone-Science & Engineering 19 (1): 55-73.

Yavich A. A. and Masten S. J. (2001). *Modeling the kinetics of the reaction of ozone with natural organic matter in Huron River water.* Ozone-Science & Engineering 23 (2): 105-119.

7

CONCLUSIONS

"Success is a journey, not a destination."
- Ben Sweetland (Fogler, 1997)

"The next best thing to knowing something is knowing where to find it."
- Samuel Johnson (1709-1784), English author, critic, and lexicographer

Water is a valuable resource in South Africa. The importance of supplying safe drinking water has been emphasised due to the outburst of cholera in recent years. The demand of potable water is increasing with the growth of population. One of the provisions in meeting this rising demand is to optimise the capacity and the performance of potable water treatment plants. The use of ozone in water treatment has become popular primarily due to the increasing difficulty in contaminant reduction and to the more stringent policy on water quality.

The physical aspects of any fluid flow are governed by the conservation principles of mass, momentum and energy. Computational fluid dynamics (CFD) modelling, in essence, translates these fundamental laws of fluid mechanics from integrals or partial derivatives to discretised algebraic forms which are solved to obtain numerical values of the flow field at discrete points in space/time.

Its application to industries has been a powerful tool in design or research to gain better understandings of fluid phenomena, without the expense of plant interruption or re-construction of the physical model. In the case of multi-component and reacting flow, appropriate reaction schemes are incorporated in order to predict the effect of the operating parameters on the individual species. This knowledge is used to improve designs or control strategy for enhanced performance.

This study investigated the potential application of CFD modelling in analysing the operation of the ozone contactor at Wiggins Waterworks, by combining the effects of hydrodynamics and ozone reaction kinetics. In terms of the original objectives, the following conclusions can be drawn:

Objective 1: to determine the actual residence time distribution as a function of flow conditions through the contactor. This objective required a suitable hydrodynamic model for the ozone contactor. The experimental tracer tests were performed to verify the model. A three-dimensional, water-phase only, CFD model was constructed to simulate the hydrodynamics of the full-scale ozone contactor. The presence of the gas bubbles and the effect of gas injection were modelled by increasing the turbulence in the hydrodynamic model. The prediction using 50% turbulence intensity ratio agrees remarkably well with

the experimental data. The use of turbulence to represent the effects of gas is clearly an approximation and cannot be expected to provide an accurate flow pattern in detail; however, the effect of gas on the overall residence time distribution was surprisingly small in the experimental data. Although the model predicted the left/right flow distribution opposite to the observed trend, the overall residence time distribution is of greater importance in terms of the operation of an ozone contactor. From the close resemblance between the model prediction and the experimental results, the hydrodynamic model was deemed appropriate.

Objective 2: to establish a qualitative understanding of the dissolved ozone concentration profile throughout the ozone contactor. The second objective required the development of a kinetic model to build onto the verified hydrodynamic model. As a partial validation of the model, residual ozone concentrations were measured from the six internal sampling points through a series of monitoring tests. Depletion of ozone in water is due to its self-decomposition and its reactions with OCS. The rate constants were taken from literature and the predicted dissolved ozone concentration values were compared with those obtained on the contactor at steady state operation and during step tests. Most of the ozone reactions appeared to complete at the end of second compartment of the contactor. Both the monitoring tests and the simulated results suggest that the monitor point should be moved from the contactor to Point 4 which is situated at the end of second compartment. *C. parvum* was chosen to be the indicator compound for the disinfection performance of the contactor. By doubling the OCS concentration at the inlet, the survival ratio of C. parvum was shown by the model to increase from 1 % to 10 %. This demonstrated the influence of water quality on the contactor performance, if no appropriate action was taken to adjust accordingly.

Objective 3: to determine the ozone reaction kinetic constants for the actual raw water. An accurate prediction of the ozone concentration profile requires the application of the correct ozone kinetics involved. The outcome of the kinetic model and the wide range of rate constants found in literature for individual compounds necessitated the ozone kinetics experiments to be carried out in order to determine the rate constants applicable for the local water source. In raw waters, the depletion of ozone is influenced by the presence of NOM. The observed ozone decay was found in good agreement using the pseudo first-order rate law. By measuring the total organic carbon (TOC) as a surrogate for NOM, the experimentally determined rate constants can be calculated using second-order rate law to account for the effects of the ozone dose and the water quality. The re-calculated second-order rate constants ranged between 8 and 25 $kL.kmol^{-1}.s^{-1}$ (or $M^{-1}.s^{-1}$) in the kinetic experiments performed in this thesis for the raw water received at Wiggins Waterworks.

Objective 4: to select the best possible position for single-point monitoring of residual ozone concentration in order to achieve the most efficient use of the ozone. Although the rate constants on the ozone-OCS reaction inferred from the results at steady state and during step tests were contradictory, the combined hydrodynamic/kinetic model has served its purpose by identifying a suitable point (Point 4) for single-monitoring of residual ozone concentration on the full-scale contactor.

7.1 General comments

Computational experience and effort. The study of the ozone contactor at Wiggins Waterworks was commenced with a simplified hydrodynamic model to predict the RTD, and progressed to a more complex, physical modelling of reaction kinetics. The full-scale ozone contactor was reproduced to a virtual model. It should be noted that, as with any modelling, a virtual model represents a close resemblance to the reality at its best and is never the physical process itself. In this study of ozonation, the computational effort was considerable to simulate a full-scale process. A number of assumptions or simplifications made for the model were to avoid unnecessary computational effort. These assumptions or simplifications must be well understood before the model is used for future study.

Water characterisation method. During the course of the investigation, it became clear that a suitable method was required for the characterisation of raw water. It was evident from the experience of many researchers that long-term monitoring is necessary for optimal performance of an ozone contactor. Therefore the characterisation method should be as simple as possible and easily incorporated into a routine analysis. However, the focus of the kinetics experimental work in **Chapter 6** was to identify such a method and not on the precision of the method. A rigorous statistical analysis was therefore not considered necessary. The statistical checks will require a more controlled approach when performing the experiments. For example, controlled raw water samples were not available during the method identification.

7.2 Recommendations and future work

This study has focused on the investigation of the ozone contactor at Wiggins Waterworks using a combined hydrodynamic/kinetic CFD model. The fundamental understanding of the system can be used as a foundation for more application-focused investigations. The following work is recommended to be performed to continue with the investigation of ozonation in water treatment.

- The repetition of the analysis work and modelling was unfortunately not possible at the time of the completion of the thesis, as the software was no longer available for the study. Even if the software is available and the experimentally determined constants are implemented in the model, this means that the on-site monitoring work needs to be conducted at the same time for the comparison to be meaningful. For a full validation of the kinetic model, the on-site monitoring work should be repeated in conjunction with the characterisation experiments.
- The characterisation method of raw water must undergo a detailed method development if the method is to be included into Umgeni Water's routine analysis. The precision and accuracy of the method identified in this thesis must be assessed.
- A long-term monitoring strategy is recommended to quantify the drift in raw water quality due to seasonal fluctuations. The combined hydrodynamic/kinetic model should be applied to explored various operating scenarios in order to achieve the required performance.

- The monitoring point should be moved from the current position at the outlet to the proposed position at Point 4 which is at the end of the second compartment. A long-term monitoring strategy should be set up to evaluate the effects of drifting water quality due to seasonal fluctuations.

APPENDICES

"This is not the end.
It is not even the beginning of the end.
But it is the end of the beginning."
- Winston Churchill (1874-1965)

A

TURBULENCE THEORY FUNDAMENTALS

It is beyond the scope of the thesis to present the rigorous derivation of the governing differential equations. The mathematical background can be referred to in many fluid dynamic textbooks, e.g.: Holland and Bragg (1995); Anderson (1995); Chung (2002). Hence this appendix serves to provide details that are most relevant to the discussion in the main body, while other available methods are attended to with only short reviews.

It should be reminded that the equations discussed here consider the incompressible turbulent flow. Effects of heat transfer are not included as it is neglected in the CFD model of the ozone contactor.

A.1 Turbulence models

Turbulence is characterised by random fluctuations. Therefore, instead of the deterministic method, statistical methods have been applied extensively in the past investigations. Generally one is interested not in the complete details of the behaviour of the three velocity components and the pressure, but in the mean rates of transfer of mass or momentum (Bradshaw, 1978). The simplest form of statistical average of a flow variable $f(x,t)$ is the sum of the time-average $\bar{f}$ and the time-varying fluctuating component f':

$$f(x,t) = \bar{f}(x,t) + f'(x,t) \tag{A-1}$$

$$\bar{f}(x,t) = \frac{1}{\Delta t}\int_{t}^{t+\Delta t} f(x,t)dt \tag{A-2}$$

Hence the continuity equation in Eqn. (2-16) can be re-written in the time-average flow as follows:

$$\frac{\partial \rho}{\partial t} + \frac{\partial}{\partial x_i}\left(\rho \bar{u}_i\right) = 0 \tag{A-3}$$

Substituting Eqn.(A-3) into the momentum equation in Eqn. (2-17) gives the *Reynolds-average Navier-Stokes equation* below:

$$\frac{\partial}{\partial t}\left(\rho \bar{u}_i\right) + \frac{\partial}{\partial x_j}\left(\rho \bar{u}_i \bar{u}_j\right) = -\frac{\partial \bar{P}}{\partial x_i} + \underbrace{\frac{\partial}{\partial x_j}\left[\mu\left(\frac{\partial \bar{u}_i}{\partial x_j} + \frac{\partial \bar{u}_j}{\partial x_i} - \frac{2}{3}\frac{\partial \bar{u}_l}{\partial x_l}\delta_{ij}\right)\right]}_{\text{Laminar}} + \underbrace{\frac{\partial}{\partial x_j}\left(-\rho\overline{u_i' u_j'}\right)}_{\text{Turbulent}} + \rho g_i \tag{A-4}$$

In common practice, the bar on the mean variables is dropped for convenience. The Reynolds stress tensors $-\rho\overline{u_i'u_j'}$ are the additional unknowns which need extra equations to bring closure to Eqn. (A-4).

Reynolds and Cebeci (1978), Hanjalić (1994a) and Chung (2002) have given comprehensive reviews on the turbulence models currently available. In general the models are characterised into zero-, one-; two-equation models; Reynolds stress models (RSM) and large-eddy simulations (LES). These models are summarised into Table A- 1 below:

Table A- 1: Classes of turbulent flow partial differential equation models

Category	Closure method	No. of transport eqns.	Additional turb. variables; calculation methods
zero-eqn. models	eddy viscosity	0	none; stress tensor is related to constant μ_t
one-eqn. models	eddy viscosity	1	k; μ_t is related k in order to calculate stress tensor
two-eqn. models	eddy viscosity	2	k,ε; both are related to μ_t
RSM	Reynolds stress transport eqn.	4: only two contain new variables	k,ε; both are used to calculate stress tensor components
LES	Reynolds stress transport eqn.	6	employ PDEs to calculate stress tensor components

where k is the turbulent kinetic energy and ε is its dissipation rate energy. Large-eddy simulation is time-dependent and perhaps the only way to deal *accurately* with difficult flows as it calculates the larger eddies and models the smaller ones. It is however computationally intensive and limited for industrial purpose. The RSM is resembled to the simplification of LES, where it allows $\overline{u_i'u_j'}$ to be calculated by correlations of tensors to k and ε. However the use of RSM is not as well-recognised and industrially validated as the first three eddy viscosity models.

The eddy viscosity concept, hypothesised by Boussinesq in 1877, assumes that the Reynolds stresses are proportional to the mean-velocity gradients and may be expressed as:

$$-\rho\overline{u_i'u_j'} = \mu_t\left(\frac{\partial u_i}{\partial x_j}+\frac{\partial u_j}{\partial x_i}\right)-\frac{2}{3}\left(\rho k+\mu_t\frac{\partial u_i}{\partial x_i}\right)\delta_{ij} \qquad \text{(A-5)}$$

where μ_t is the turbulent or eddy viscosity. The advantage is the relatively low computational cost associated with the computation of μ_t.

The *standard* k-ε and the renormalisation-group (RNG) based k-ε model applied in the thesis fall under the two-equation (k-ε) models using Boussinesq hypothesis. Discussion from this point onwards focuses on these two models. Further details of the other turbulence models should be referred in books such as Gatski et al., (1992); Landahl and Mollo-Christensen (1986); and Chung (2002).

A.1.1 Standard k-ε model

The *standard* k-ε model is probably the most widely established, especially for its industrial application (Hanjalić, 1994a; Versteeg and Malalasekera, 1995). It consists of two equations describing the turbulent kinetic energy k and its dissipation rate ε (Fluent, 2003).

$$\frac{\partial}{\partial t}\rho k + \frac{\partial}{\partial x_i}\left(\rho k u_i\right) = \frac{\partial}{\partial x_j}\left[\left(\mu + \frac{\mu_t}{\sigma_k}\right)\frac{\partial k}{\partial x_j}\right] + G_k + G_b - \rho\varepsilon \tag{A-6}$$

$$\frac{\partial}{\partial t}\left(\rho\varepsilon\right) + \frac{\partial}{\partial x_i}\left(\rho\varepsilon u_i\right) = \frac{\partial}{\partial x_j}\left[\left(\mu + \frac{\mu_t}{\sigma_\varepsilon}\right)\frac{\partial \varepsilon}{\partial x_j}\right] + C_{1\varepsilon}\frac{\varepsilon}{k}\left(G_k + C_{3\varepsilon}G_b\right) - C_{2\varepsilon}\rho\frac{\varepsilon^2}{k} \tag{A-7}$$

where G_k represents the generation of turbulence kinetic energy due to the mean velocity gradients, calculated using Eqn. (A-8); G_b is the generation of turbulence kinetic energy due to buoyancy, calculated using Eqn. (A-9); $C_{1\varepsilon}$, $C_{2\varepsilon}$, $C_{3\varepsilon}$, are constants based on empirical calibration; and σ_k, σ_ε are the turbulent Prandtl numbers for k and ε respectively.

$$G_k = -\rho\overline{u_i' u_j'}\frac{\partial u_j}{\partial x_i} \tag{A-8}$$

$$G_b = \beta g_i \frac{\mu_t}{\mathrm{Pr}_t}\frac{\partial T}{\partial x_i} \tag{A-9}$$

where β is the coefficient of thermal expansion. The term G_k can be related to the Boussinesq hypothesis in the form of Eqn. (A-10).

$$G_k = \mu_t S^2 \qquad \text{and} \qquad S = \sqrt{2S_{ij}S_{ij}} \tag{A-10}$$

where S is the mean strain tensor. S_{ij} is defined as:

$$S_{ij} = \frac{1}{2}\left(\frac{\partial u_i}{\partial x_j} + \frac{\partial u_j}{\partial x_i}\right) \tag{A-11}$$

The turbulent viscosity μ_t in Eqn. (A-7) is defined by Eqn. (A-12)

$$\mu_t = \rho C_\mu \frac{k^2}{\varepsilon} \tag{A-12}$$

where C_μ is a constant. All constants used in the *standard* k-ε model are listed in Table A- 2.

Because energy is assumed to transfer from larger eddies to smaller ones and eventually dissipates, in the time-average *standard* k-ε model this 'cascade' process of moving from large-scale motion to small on tends not to transmit directional preferences (Bradshaw, 1978). The eddy viscosity is thus assumed isotropic, i.e.: invariance to direction (Landahl and Mollo-Christensen, 1986) and is the same for all Reynolds stresses. However, this is not true when normal and shear stresses are comparable to inertia and pressure gradient terms. The statistical independence does not hold because motions fluctuate in space and time.

The system being investigated here exhibits strong turbulent flows. Since effort has been made to simplify the two-phase problem into the one-phase model, the effect of the buoyancy term G_b is relatively small when compared to G_k.

A.1.2 RNG *k*-ε model

A popular alternative to the *standard* *k*-ε model is the renormalisation-group (RNG) based *k*-ε model proposed by Yakhot and Orszag (1986). The transport equations are shown below:

$$\frac{\partial}{\partial t}(\rho k)+\frac{\partial}{\partial x_i}(\rho k u_i)=\frac{\partial}{\partial x_j}\left(\alpha_k \mu_{eff}\frac{\partial k}{\partial x_j}\right)+G_k+G_b-\rho\varepsilon \tag{A-13}$$

$$\frac{\partial}{\partial t}(\rho \varepsilon)+\frac{\partial}{\partial x_i}(\rho \varepsilon u_i)=\frac{\partial}{\partial x_j}\left(\alpha_k \mu_{eff}\frac{\partial \varepsilon}{\partial x_j}\right)+C_{1\varepsilon}\frac{\varepsilon}{k}(G_k+C_{3\varepsilon}G_b)-C_{2\varepsilon}\rho\frac{\varepsilon^2}{k}-R_\varepsilon \tag{A-14}$$

where G_k and G_b are defined the same as the *standard* *k*-ε model by Eqn. (A-8) and Eqn. (A-9). The quantities α_k and α_ε are the inverse effective Prandtl numbers for k and ε respectively. A differential equation is assigned to calculate the effective viscosity μ_{eff} to account more accurately for low-Reynolds-number flow. The inverse effective Prandtl numbers α_k and α_ε are calculated through analytical formulae derived from RNG theory. Computing equations of these Prandtl numbers can be referred to Fluent (1998).

The main difference between the RNG and standard k-ε models is within the additional term in the ε, such that R_ε is calculated by

$$R_\varepsilon=\frac{C_\mu \rho \eta^3(1-\eta/\eta_0)}{1+\beta\eta^3}\frac{\varepsilon^2}{k} \tag{A-15}$$

where $\eta \equiv Sk/\varepsilon$, $\eta_0 = 4.38$ and $\beta = 0.012$. The effect of this term can be seen by replacing the last two terms in Eqn. (A-14) by $-C_{2\varepsilon}^{*}\rho\frac{\varepsilon^2}{k}$ and further defined by Eqn. (A-16) below.

$$C_{2\varepsilon}^{*}\equiv C_{2\varepsilon}+\frac{C_\mu \rho \eta^3(1-\eta/\eta_0)}{1+\beta\eta^3} \tag{A-16}$$

From Eqn. (A-16), in regions of weakly to moderately strained flows ($\eta<\eta_0$), R_ε makes a positive contribution to ε-equation Eqn. (A-14) and $C_{2\varepsilon}^{*}\approx 2.0$ which is comparable to $C_{2\varepsilon}$ in the *standard* *k*-ε model. Consequently the RNG model gives results analogous to that of the *standard* *k*-ε model. However, in regions of large strain rate ($\eta>\eta_0$) R_ε makes a negative contribution such that $C_{2\varepsilon}^{*}$ is less than $C_{2\varepsilon}$, thereby enhancing the dissipation term and reducing k. It is attributed to this faster dissipation that the RNG-based *k*-ε model responds more promptly to strained flow than *standard* *k*-ε model.

Table A- 2: Model constants

k-ε model variance	$C_{1\varepsilon}$	$C_{2\varepsilon}$	C_μ	σ_k	C_ε
Standard	1.44	1.92	0.09	1.0	1.3
RNG	1.42	1.68	0.089		

A.2 Wall function

The inherent assumption of k-ε models is that the flow is fully turbulent. In the near-wall region, the flow variables have large gradients, requiring excessive mesh as walls are a source of turbulence. In order to represent the near-wall flow reasonably well without the excessive mesh refinement, the so-called wall function is needed to make the turbulent model suitable for wall-bounded flows.

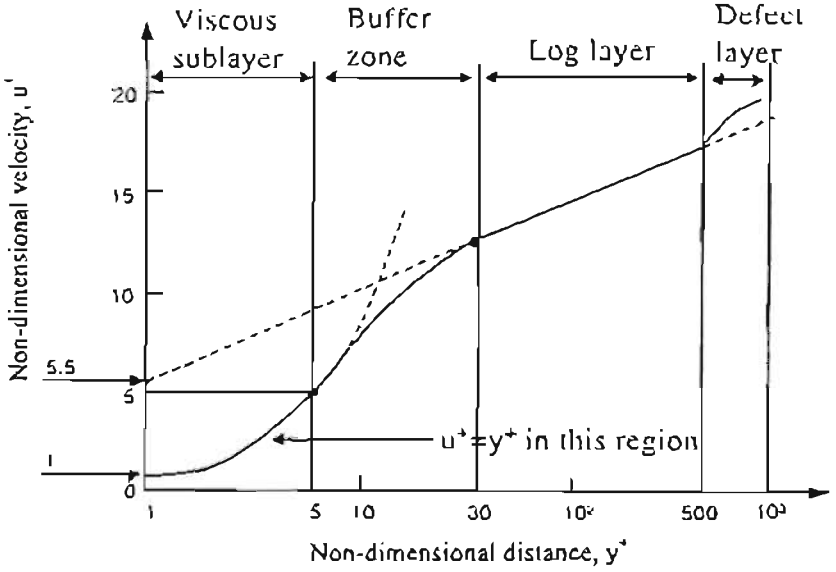

Figure A-1: Turbulent boundary layer velocity profile (Chung, 2002)

Many studies have shown that the near-wall flow can be divided into three layers (Chung, 2002) as in Figure A-1 typically in the non-dimensional form of velocity, u^+, and distance, y^+.

$$u^+ = \frac{u}{u_\tau} \tag{A-17}$$

$$y^+ = \frac{\rho u_\tau y}{\mu} \tag{A-18}$$

where y is the distance perpendicular to the wall and u_τ is known as the friction velocity ($= \tau_w/\rho$ and τ_w is the surface shear stress).

The innermost layer, known as the viscous sublayer, is almost laminar and the molecular viscosity has a major role in momentum and mass transfer. Turbulence dominates the outer layer, known as the fully-turbulent layer. The effect of the molecular viscosity and turbulence are both significant in the interim region between the viscous sublayer and the fully-turbulent layer.

Wall functions are semi-empirical formulae to 'bridge' this region between walls and the core of turbulent flow. Application of these functions alleviates the need to modify the turbulence model for the presence of the wall and effectively reduces the computational time as a coarser mesh can be used in this near-wall region. It must be cautioned that wall functions should only be used in high-Reynolds-number flow.

The standard wall functions proposed by Launder and Spalding (1974) are chosen for the CFD model of the ozone contactor under this investigation based on their wide application to industrial flows. The law-of-the-wall for the mean velocity is given as:

$$u^* = \frac{1}{\kappa}\ln\left(Ey^*\right) \tag{A-19}$$

where E is the empirical roughness constant (= 9.81 for smooth walls) and κ is the von Kármán constant (= 0.42). This logarithmic law Eqn. (A-19) is known to be valid for y^* larger than 30. In the case where cell nodes fall within this value, the laminar law can be applied as Eqn. (A-20).

$$u^* = y^* \tag{A-20}$$

The k equation is solved for the entire flow domain applying a zero normal gradient for k. The wall functions assume the local equilibrium hypothesis, such that the production of kinetic energy G_k and its dissipation rate ε are equal in the wall-adjacent volume. Therefore G_k can be calculated by Eqn. (A-21),

$$G_k = \tau_w \frac{\partial u}{\partial y} \tag{A-21}$$

and the shear stress by Eqn. (A-22).

$$\tau_w = \frac{\rho C_\mu^{1/4} k^{1/2} u}{u^*} \tag{A-22}$$

The dissipation ε at the wall-adjacent cells is computed by Eqn. (A-23)

$$\varepsilon = \frac{C_\mu^{3/4} k^{3/2}}{\kappa y} \tag{A-23}$$

It should be reminded that, strictly speaking, this semi-empirical function is only valid for smooth walls. Some modifications are required to include the effect for the roughness of the walls.

A.2.1 Setting the Roughness Parameters

The law-of-the-wall modified for roughness takes the form of Eqn. (A-24)

$$u^*\left(\frac{C_\mu^{1/4} k^{1/2}}{u_\tau}\right) = \frac{1}{\kappa}\ln\left[Ey^*\left(\frac{C_\mu^{1/4} k^{1/2}}{u_\tau}\right)\right] - \Delta B \tag{A-24}$$

where ΔB (takes the form of $1/\kappa \ln f_r$ where f_r is the roughness function) is an additive constant in the log-law to account for the shift of intercept due to the roughness effect.

ΔB is dependent on the type and size of the roughness. Although no general roughness function is valid for all types of roughness, ΔB was found to be well-correlated with the non-dimensional height K_s^+.

$$K_s^+ = \rho K_s C_\mu^{1/4} k^{1/2} / \mu \tag{A-25}$$

where K_s is the physical roughness height.

Fluent (2003) reported that three distinct regimes can be identified depending on the K_s^+ value. Formulae proposed by Cebeci and Bradshaw based on Nikuradse's data (Fluent, 1998) are implemented to compute ΔB for each regime, and are summarised in Table A-3.

Table A-3: Roughness functions

Regime	Value of Ks+	Formulae to calculate ΔB
smooth	$K_s^+ \leq 2.25$	0
transitional	$2.25 < Ks^+ \leq 90$	$\frac{1}{\kappa}\ln\left[\frac{K_s^+ - 2.25}{87.75} + C_s K_s^+\right] \times \sin\left(0.4258\left(\ln K_s^+ - 0.811\right)\right)$
rough	$K_s^+ > 90$	$\frac{1}{\kappa}\ln\left(1 + C_s K_s^+\right)$

Therefore two roughness parameters must be specified so that the roughness modelling takes effect: the roughness height K_s and the roughness constant C_s. Again there is no universal rule in choosing the values of K_s and C_s. $C_s = 0.5$ was chosen so that using k-ε model will reproduced results analogous to those data for pipes roughened with tightly-packed, uniform sand-grain roughness.

A.3 References

Anderson J.D. Jr. (1995) *Computational fluid dynamics – the basics with applications*. International edition. McGraw-Hill Inc., New York, ISBN 0-07-113210-4.

Bradshaw P (1978) *Introduction* in Topics in applied physics volume 12: *Turbulence*, ed. Bradshaw P., 2nd ed., Springer-Verlag. New York. ISBN: 0-387-08864-4.

Cebeci T. and Bradshaw P. (1977) Momentum transfer in boundary layers. Hemisphere publishing corporation, New York.

Chung T.J. (2002) *Computational fluid dynamics*. Cambridge university press, Cambridge. ISBN: 0-521-59416-2

Fluent (1998) *Fluent 5 User Guide*, Lebanon, USA, Fluent Inc.

Gatski T.b., Sarkar S. and Speziale C.G., editors(1992) *Studies in turbulence*. Springer-Verlag Inc., New York. ISBN: 0-387-97613-2

Hanjalić K. (1994a) *Advanced turbulence closure models: a view of current status and future prospects*. Review. International Journal of Heat and Fluid Flow, 15 (3): 178-203, June.

Holland F.A. and Bragg R. (1995). *Fluid flow for chemical engineers*. 2nd ed., London: Arnold, ISBN: 0-340-61058-1

Landahl, M. and Mollo-Christensen E. (1986) *Turbulence and random processes in fluid mechanics*. Cambridge university press, Cambridge. ISBN: 0-521-26306-9

Launder B.E. and Spalding D.B. (1974) *The Numerical Computation of Turbulent Flows*. Computer Methods in Applied Mechanics and Engineering, 3:269-289

Reynolds W.C. and Cebeci T. (1978) *Calculation of turbulent flows* in Topics in applied physics volume 12: *Turbulence*, ed. Bradshaw P., 2nd ed., Springer-Verlag. New York. ISBN: 0-387-08864-4.

Reynolds W.C. and Cebeci T. (1978) *Calculation of turbulent flows* in Topics in applied physics volume 12: *Turbulence*, ed. Bradshaw P., 2nd ed., Springer-Verlag. New York. ISBN: 0-387-08864-4.

Yakhot V. and Orszag S.A. (1986) *Renormalization group analysis of turbulence: I. Basic theory.* Journal of scientific computing 1 (1):1-51.

B

RTD EXPERIMENTAL AND SIMULATED DATA

Experimental data of the RTD study and a sample of the analysed results discussed in **Chapter 3** are presented in this Appendix. Due to the limit of the thesis length, the complete set of simulated data is not tabulated here but included in the spreadsheet (*STrawdata.xls*) in the accompanying CD. There are four worksheets labelled according to their respective model and flow settings.

All the calculations of the RTD density function discussed in Chapter 3 can be found in *Tracer tests.xls*.

B.1 Experimental tracer concentration measurements

The atomic absorption data of the Li^+ measurement is captured below. The three sample points were at 2m from the right (labelled 1), 2m from the left (2) and at the centre position of the weir (3).

Table B- 1: Concentration of Li^+ at the three sample points along the weir: Tracer test with gas injection (a)

Time	Li^+ concentration (mg/L)			
(min)	a1	a2	a3	Average
0	0	0	0	0
4	0.02	0.76	0.04	0.27
5	0.12	1.87	0.17	0.72
6	0.77	1.72	0.49	0.99
7	1.22	1.96	1.42	1.53
8	1.44	1.83	1.43	1.57
9	1.75	1.68	1.41	1.61
10	1.79	1.5	1.58	1.62
12	1.54	1.04	1.48	1.35
15	1.20	0.61	1.20	1.00
18	0.76	0.40	0.81	0.66
21	0.46	0.18	0.46	0.37
24	0.27	0.11	0.27	0.22
30	0.08	0.03	0.08	0.06
36	0.03	0.01	0.03	0.02
42	0.01	0	0.01	0.01

Table B-2: Concentration of Li^+ at the three sample points along the weir: Tracer test without gas injection (b)

Time	Li+ concentration (mg/L)			
(min)	b1	b2	b3	Average
0	0	0	0	0
4	0.01	0.39	0.17	0.19
5	0.02	2.66	1.30	1.33
6	0.15	2.88	0.96	1.33
7	0.77	2.25	1.42	1.48
8	1.56	1.99	1.50	1.68
9	1.52	1.57	1.55	1.55
10	1.62	1.30	1.54	1.49
12	1.46	1.09	1.34	1.30
15	1.21	0.72	0.98	0.97
18	0.82	0.39	0.69	0.63
21	0.50	0.20	0.34	0.35
24	0.28	0.19	0.27	0.25
30	0.09	0.06	0.10	0.08
36	0.03	0.01	0.03	0.02
42	0.01	0.01	0.01	0.01

B.2 Plant operation records on the ozone contactor no. 2

Table B-3: Flow data for the tracer test carried out with gas injection

2001-06-07	Raw water flow	Oxygen flow into ozonator	Oxygen/ozone flow into contact tank	Ozone dose
Time	ML/d	Nm^3/h	Nm^3/h	mg/L
12h40	108	39	35	1.5
12h45	107	39	36	1.5
12h50	107	39	34	1.5
12h55	108	39	31	1.5
13h00	107	39	34	1.5
13h05	108	39	34	1.5
13h10	107	39	34	1.5
13h15	107	39	34	1.5
13h20	107	39	34	1.5

Table B-4: Flow data for the tracer test carried out without gas injection

2001-06-07	Raw water flow	Oxygen flow into ozonator	Oxygen/ozone flow into contact tank	Ozone dose
Time	ML/d	Nm^3/h	Nm^3/h	mg/L
14h15	109	0	0	0
14h20	108	0	0	0
14h25	108	0	0	0
14h30	109	0	0	0
14h35	109	0	0	0
14h40	109	0	0	0
14h45	108	0	0	0
14h50	109	0	0	0
14h55	108	0	0	0
15h00	109	0	0	0

B.3 Mass balances

The calculation of mass balances can be found in the worksheet labelled *tracerMB* in the spreadsheet file, *Tracer tests.xls*. The results of Li^+ mass balances are presented in Table B-5.

Table B-5: Li^+ mass balance of the experimental tracer tests

Variable	Unit	a. With ozone	b. Without ozone
Inlet			
measured Li^+ in dosing solution	mg Li^+/L	34560	39080
mass of dosing solution	kg	34.92	34.42
density	kg/L	1.02	1.02
mass of tracer at inlet	kg Li^+	1.183	1.319
Outlet			
integrated C	kg.s/kL	1.229	1.255
flow rate	ML/d	107.333	108.6
converted to kL/s	kL/	1.2427	1.257
mass of tracer at outlet	kg Li^+	1.5277	1.57778
discrepancy		29.06%	19.63%

B.4 Error analysis – Monte Carlo Method

B.4.1 Matlab code calculation

The calculation code is in the Matlab file, *tracerMB.m*.

```
%-----------------------------------------------------------------------
%EXPERIMENTAL TRACER TESTS
%Statistical analysis of LiCl mass balance
%Study of the ozone contactor at Wiggins Waterworks
%Tzu Hua Huang
%-----------------------------------------------------------------------
% Objective:
% to evaluate the effect of uncertainties on the calculation of the time integral of outlet Li+ conc (in kg.s/m^3)
%
clear all;
% Two tracer tests: With gas (a) & Without gas (b)
% Three sample points in each test: Right (1), Left (2) & Centre (3)
%
% The small letters (a or b) denote the experimentally measured values or the calculation using these values;
% the capital letters (A or B) denote the calculated data with uncertainties or the calculation using these data.
%
% generate normalised random numbers
n=1000;
random_no = randn(1,n);

%-----------------------------------------------------------------------
% a. TRACER TEST WITH GAS
%-----------------------------------------------------------------------
%
% a.1 Calculate mass of tracer (in kg.s/m^3)with uncertainties
%
% experimental measurements
% measured Li+ concentration of the three sample points at the outlet  in mg/L
a1 = [0; 0.02; 0.12; 0.77; 1.22; 1.44; 1.75; 1.79; 1.54; 1.2; 0.76; 0.46; 0.27; 0.08; 0.03; 0.01];
a2 = [0; 0.76; 1.87; 1.72; 1.96; 1.83; 1.68; 1.5; 1.04; 0.61; 0.4; 0.18; 0.11; 0.03; 0.01; 0];
a3 = [0; 0.04; 0.17; 0.49; 1.42; 1.43; 1.41; 1.58; 1.48; 1.2; 0.81; 0.46; 0.27; 0.08; 0.03; 0.01];
% measured time at which samples were taken in sec
t_a = [0; 240; 300; 360; 420; 480; 540; 600; 720; 900; 1080; 1260; 1440; 1800; 2160; 2520];
% recorded flow rates during the test in ML/day
Qs_aMLD = [108; 107; 107; 108; 107; 108; 107; 107; 107];
% convert the flow rates to m^3/s
Qs_a = Qs_aMLD*1000000/1000/24/3600;
%
% estimated time of delay in the distribution tower and the static mixer
% estimated volume in m^3
V_delay = 20;
%
% relative uncertainties associated with each variable
% flow: reported sensitivity of flow meter
s_a_flow = 0.03;
% averaging method: estimated effect on onverall RTD by averaging three sample values
s_a_avgmethod = 0.005771621;
% analytical method: relative std. deviation of each measurement
s_a1_analytical = [0; 0.155; 0.0148; 0.0127; 0.015; 0.0178; 0.0177; 0.0177; 0.0074; 0.0191; 0.0154; 0.0142; 0.0171; 0.0163; 0.0108; 0.0035];
s_a2_analytical = [0; 0.0111; 0.0131; 0.0013; 0.011; 0.0158; 0.0089; 0.0122; 0.012; 0.0283; 0.01; 0.0131; 0.0295; 0.0235; 0.0136; 0.0335];
```

```
s_a3_analytical = [0; 0.0069; 0.0217; 0.0039; 0.0035; 0.0183; 0.0097; 0.0226; 0.0148; 0.0046; 0.0175;
0.0112; 0.031; 0.0094; 0.0078; 0.0415];
% timing: estimated time variance
s_a_time = 0.01;
% delay estimate
s_a_delay = 0.1;
%
for i=1:n
    % generate values of measured data under random disturbance
    A1(:,i) = a1+s_a1_analytical*random_no(:,i).*a1;
    A2(:,i) = a2+s_a2_analytical*random_no(:,i).*a2;
    A3(:,i) = a3+s_a3_analytical*random_no(:,i).*a3;
    t_A(:,i) = t_a+s_a_time*random_no(:,i).*t_a;
    Qs_A(:,i) = Qs_a+s_a_flow*random_no(:,i).*Qs_a;
    % calculate the average of the samples at each time interval
    Li_a(:,i) = (A1(:,i)+A2(:,i)+A3(:,i))/3;
    % generate values under random disturbance
    Li_A(:,i) = Li_a(:,i)+s_a_avgmethod*random_no(:,i).*Li_a(:,i);

    % mean flow
    Qs_Am(:,i) = mean(Qs_A(:,i));
    % correct for the time delayed in the ditribution and the static mixer
    V_Adelay(:,i) = V_delay+s_a_delay*random_no(:,i)*V_delay;
    t_A_delay(:,i) = V_Adelay(:,i)/Qs_Am(:,i);
    t_A_corr(:,i) = t_A(:,i)-t_A_delay(:,i);
    % the start of the tracer test is at time = 0s
    t_A_corr(1,i) = 0;

    % calculate the total mass of tracer at the outlet in kg/(m^3.s)
    C_A(:,i) = 1/1000*Li_A(:,i);
    IntC_A(:,i) = trapz(t_A_corr(:,i),C_A(:,i));

    % calculate the second moment for mean residence time
    for j=2:16
        % the start of the tracer test is at time = 0s
        tC_A(1,i) = 0;
        c1a(j,i) = C_A(j,i)-C_A(j-1,i);
        t1a(j,i) = t_A_corr(j,i)-t_A_corr(j-1,i);
        t3a(j,i) = t_A_corr(j,i).^3-t_A_corr(j-1,i).^3;
        ct1a(j,i) = C_A(j,i).*t_A_corr(j-1,i);
        ct2a(j,i) = C_A(j-1,i).*t_A_corr(j,i);
        t2a(j,i) = t_A_corr(j,i).^2-t_A_corr(j-1,i).^2;
        tC_A(j,:) = c1a(j,:)./t1a(j,:).*t3a(j,:)/3-(ct1a(j,:)-ct2a(j,:))./t1a(j,:).*t2a(j,:)/2;
    end
    IntC_A(:,i) = sum(tC_A(:,i));
    MRT_A = IntC_A./IntC_A;
end
%-------------------------------
IntCavg_A = mean(IntC_A)
IntCnorm_A = IntC_A/IntCavg_A;
x1 = (IntCnorm_A-1).^2;
x2 = x1.^0.5;
eps_AIntC = mean(x2)

IntCavg_A = mean(IntC_A)
IntCnorm_A = IntC_A/IntCavg_A;
v1 = (IntCnorm_A-1).^2;
v2 = v1.^0.5;
eps_AIntC = mean(v2)
```

```
MRTavg_A = mean(MRT_A)
MRTnorm_A = MRT_A/MRTavg_A;
w1 = (MRTnorm_A-1).^2;
w2 = w1.^0.5;
eps_AMRT = mean(w2)

Q_Aavg = mean(mean(Qs_A));
Q_A_MLD = Q_Aavg*3600*24/1000
%-----------------------------------------------------------------------
%
% a.2 Calculate the concentration of the tracer at the inlet with uncertainties
%
% experimental measurements
% measured Li+ concentration of the three sample points in mg/L
a_conc = 34560;
%
% relative uncertainties associated with each variable
% analytical method: estimated sensitivity of the analytical method
s_a_conc = 0.0075;
% analytical method: assumed error relating the dilution of concentrated sample
s_a_dil = 0.05;
n_a = 3;
%
for i=1:n
    A_c(:,i) = a_conc+n_a*s_a_dil*random_no(:,i)*a_conc;
    A_conc(:,i) = A_c(:,i)+s_a_conc*random_no(:,i).*A_c(:,i);
end
%-------------------------------------
A_concavg = mean(A_conc)
A_concNorm = A_conc/A_concavg;
y1 = (A_concNorm-1).^2;
y2 = y1.^0.5;
eps_Aconc = mean(y2)

%=======================================================================
% b. TRACER TEST WITHOUT GAS
%=======================================================================
%
% b.1 Calculate mass of tracer (in kg.s/m^3)with uncertainties
%
% experimental measurements
% measured Li+ concentration of the three sample points at the outlet  in mg/L
b1 = [0; 0.01; 0.02; 0.15; 0.77; 1.56; 1.52; 1.62; 1.46; 1.21; 0.82; 0.5; 0.28; 0.09; 0.03; 0.01];
b2 = [0; 0.39; 2.66; 2.88; 2.25; 1.99; 1.57; 1.3; 1.09; 0.72; 0.39; 0.2; 0.19; 0.06; 0.01; 0.01];
b3 = [0; 0.17; 1.3; 0.96; 1.42; 1.5; 1.55; 1.54; 1.34; 0.98; 0.69; 0.34; 0.27; 0.1; 0.03; 0.01];
% measured time at which samples were taken in sec
t_b = [0; 240; 300; 360; 420; 480; 540; 600; 720; 900; 1080; 1260; 1440; 1800; 2160; 2520];
% recorded flow rates during the test in ML/day
Qs_bMLD = [109; 108; 108; 109; 109; 109; 108; 109; 108; 109];
% convert the flow rates to m^3/s
Qs_b = Qs_bMLD*1000000/1000/24/3600;
%
% estimated time of delay in the distribution tower and the static mixer
% estimated volume in m^3
V_delay = 20;
%
% relative uncertainties associated with each variable
% flow: reported sensitivity of flow meter
s_b_flow = 0.03;
% averaging method: estimated effect on onverall RTD by averaging three sample values
```

```
s_b_avgmethod = 0.005771621;
% analytical method: relative std. deviation of each measurement
s_b1_analytical = [0; 0.0411; 0.0066; 0.0128; 0.0167; 0.003; 0.026; 0.0138; 0.0046; 0.0134; 0.0106;
0.0213; 0.0073; 0.0167; 0.0297; 0.015];
s_b2_analytical = [0; 0.0111; 0.0131; 0.0013; 0.011; 0.0158; 0.0089; 0.0122; 0.012; 0.0283; 0.01; 0.0131;
0.0295; 0.0235; 0.0136; 0.0335];
s_b3_analytical = [0; 0.0204; 0.0135; 0.0118; 0.0069; 0.0091; 0.0168; 0.006; 0.006; 0.0131; 0.0167;
0.0181; 0.0138; 0.0119; 0.011; 0.0156];
% timing: estimated time variance
s_b_time = 0.01;
% delay estimate
s_b_delay = 0.1;
%
for i=1:n
    % generate values of measured data under random disturbance
    B1(:,i) = b1+s_b1_analytical*random_no(:,i).*b1;
    B2(:,i) = b2+s_b2_analytical*random_no(:,i).*b2;
    B3(:,i) = b3+s_b3_analytical*random_no(:,i).*b3;
    t_B(:,i) = t_b+s_b_time*random_no(:,i).*t_b;
    Qs_B(:,i) = Qs_b+s_b_flow*random_no(:,i).*Qs_b;
    % calculate the average of the samples at each time interval
    Li_b(:,i) = (B1(:,i)+B2(:,i)+B3(:,i))/3;
    % mean flow
    Qs_Bm(:,i) = mean(Qs_B(:,i));
    % correct for the time delayed in the dirtribution and the static mixer
    V_Bdelay(:,i) = V_delay+s_b_delay*random_no(:,i)*V_delay;
    t_B_delay(:,i) = V_Bdelay(:,i)/Qs_Bm(:,i);
    t_B_corr(:,i) = t_B(:,i)-t_B_delay(:,i);
    % the start of the tracer test is at time = 0s
    t_B_corr(1,i) = 0;

    % generate values of calculated under random disturbance
    Li_B(:,i) = Li_b(:,i)+s_b_avgmethod*random_no(:,i).*Li_b(:,i);

    % calculate the total mass of tracer at the outlet in kg/(m^3.s)
    C_B(:,i)= 1/1000*Li_B(:,i);
    InC_B(:,i) = trapz(t_B_corr(:,i),C_B(:,i));

        % calculate the second moment for mean residence time
    for j=2:16
        % the start of the tracer test is at time = 0s
        tC_B(1,i) = 0;
        c1b(j,i) = C_B(j,i)-C_B(j-1,i);
        t1b(j,i) = t_B_corr(j,i)-t_B_corr(j-1,i);
        t3b(j,i) = t_B_corr(j,i).^3-t_B_corr(j-1,i).^3;
        ct1b(j,i) = C_B(j,i).*t_B_corr(j-1,i);
        ct2b(j,i) = C_B(j-1,i).*t_B_corr(j,i);
        t2b(j,i) = t_B_corr(j,i).^2-t_B_corr(j-1,i).^2;
        tC_B(j,:) = c1b(j,:)./t1b(j,:).*t3b(j,:)/3-(ct1b(j,:)-ct2b(j,:))./t1b(j,:).*t2b(j,:)/2;
    end
    IntC_B(:,i) = sum(tC_B(:,i));
    MRT_B = IntC_B./InC_B;
end;
%-----------------------------------
InCavg_B = mean(InC_B)
InCnorm_B = InC_B/InCavg_B;
x3 = (InCnorm_B-1).^2;
x4 = x3.^0.5;
eps_BInC = mean(x4)
```

```
IntCavg_B = mean(IntC_B)
IntCnorm_B = IntC_B/IntCavg_B;
v3 = (IntCnorm_B-1).^2;
v4 = v3.^0.5;
eps_BIntC = mean(v4)

MRTavg_B = mean(MRT_B)
MRTnorm_B = MRT_B/MRTavg_B;
w3 = (MRTnorm_B-1).^2;
w4 = w3.^0.5;
eps_BMRT = mean(w4)

Q_Bavg = mean(mean(Qs_B));
Q_B_MLD   Q_Bavg*3600*24/1000

%
% b.2Calculate the concentration of the tracer at the inlet with uncertainties
%
% experimental measurements
% measured Li+ concentration of the three sample points in mg/L
b_conc = 39080;
%
% relative uncertainties associated with each variable
% analytical method: estimated sensitivity of the analytical method
s_b_conc = 0.005;
% analytical method: assumed error relating the dilution of concentrated sample
s_b_dil = 0.05;
% no. of dilutions
n_b = 3;
%
for i=1:n
   B_c(:,i) = b_conc+n_b*s_b_dil*random_no(:,i)*b_conc;
   B_conc(:,i) = B_c(:,i)+s_b_conc*random_no(:,i).*B_c(:,i);
end
B_concavg = mean(B_conc)
B_concNorm = B_conc/B_concavg;
y3 = (B_concNorm-1).^2;
y4 = y3.^0.5;
eps_Bconc = mean(y4)
```

B.4.2 Error analysis results

The details of the calculation can be found in the worksheet labelled *tracerMB* in the spreadsheet file, *Tracer tests.xls*. Summaries of the error analysis results are tabulated in Table B-6 and Table B-7.

Table B-6: Monte Carlo analysis of the mass balance – a. With Ozone

Sources of uncertainties	Unit	Std errors, ε	Mean	Adjusted	Variance	Calc var
volume of contactor		1.00%	845.2	847.01	71.436	3.271
Inlet						
analysis of the concentrate		0.75%	-	-	-	-
dilution of conc sample		5.00%	-	-	-	-
acc effect on measurements	mg Li^+/L	12.64%	34549	38912	19070633	19041560
scale for weighing dosing soln	kg	0.03%	34.92	34.92	0.0001	4.1E-08
density of dosing soln	kg/L	5.00%	1.02	1.02	0.002601	0
mass of tracer at inlet	kg Li^+	-	1.183	1.33219421	-	-
Outlet						
analysis of test samples		from raw data		-	-	-
mean taken as average of 3pts		0.58%		-	-	-
sampling time error		1.00%		-	-	-
delay volume		10.00%		-	-	-
acc effect on integral C over t	kg.s/kL	2.25%	1.228	1.192	0.000763	0.001301
acc effect on integral tC over t	kg.s^2/kL	2.97%	920.76	903.108	747.835	311.608
flow rate	ML/d	3.00%	107.19	96.5779	10.342	112.743
mass of tracer at outlet	kg Li^+	-	1.523	1.3327	-	-
Losses						
losses of tracer	kg Li^+	0.01%				
Constraints		Value to adhere	Value from mean	Value from adj		
net mass balance	kg Li^+	0	-0.341	-1.29E-13		
mean residence time	s	757.76		757.76		

Table B-7: Monte Carlo analysis of the mass balance – b. Without Ozone

Sources of uncertainties	Unit	Std errors, ε	Mean	Adjusted	Variance	Calc var
volume of contactor		1.00%	845.2	848.054	71.436	8.1438
Inlet						
analysis of the concentrate		0.50%	-	-	-	-
dilution of conc sample		5.00%	-	-	-	-
acc effect on measurements	mg Li^+/L	12.44%	39072	43600	23625012	20504917
scale for weighing dosing soln	kg	0.03%	34.92	34.92	0.000103	2.937E-09
density of dosing soln	kg/L	5.00%	1.02	1.02	0.002601	0
mass of tracer at inlet	kg Li^+	-	1.338	1.493	-	-
Outlet						
analysis of test samples		from raw data		-	-	-
mean taken as average of 3pts		0.58%		-	-	-
sampling time error		1.00%		-	-	-
delay volume		10.00%		-	-	-
acc effect on integral C over t	kg.s/kL	2.12%	1.2539	1.259	0.000707	2.76E-05
acc effect on integral tC over t	$kg.s^2/kL$	3.21%	934.61	900.78	900.06	1144
flow rate	ML/d	3.00%	108.46	102.423	10.587	36.441
mass of tracer at outlet	kg Li^+	-	1.574	1.493	-	-
Losses						
losses of tracer	kg Li^+	0.01%				
Constraints		Value to adhere	Value from mean	Value from adj		
net mass balance	kg Li^+	0	-0.236	9.15E-11		
mean residence time	s	715.38		715.38		

C

MONITORING EXPERIMENTAL AND SIMULATED DATA

Experimental data of the monitoring study and a sample of the analysed results discussed in **Chapter 5** are presented in this Appendix. Due to the limit of the thesis length, the complete set of simulated data is not tabulated here but included in the spreadsheet (*Monitor.xls*) in the accompanying CD.

The comparison with the simulated results is presented in this appendix. For the full calculation the spreadsheet (*Monitor vs FNT.xls*) should be referred to.

C.1 Steady state data

Table C- 1: Raw data of the controlled monitoring. Flow = 100 ML.d^{-1}; dose = 3.5 mg.L^{-1}.

Date	Test no.	Flow rate (ML.d^{-1})		Doses (mg.L^{-1})	
2002-03-21	1	100		3.5	
		Ozone analyser measurements			
Time	Point no.	A	B	C	Outlet
		(ppm)	(ppm)	(ppm)	(ppm)
13:00	1	0.58	0.42	0.58	0.08
13:15	2	0.90	0.61	1.03	0.07
13:30	3	0.81	0.55	0.86	0.04
13:50	4	0.29	0.18	0.29	0.05
14:05	5	0.22	0.13	0.21	0.00
14:15	6	0.16	0.09	0.11	0.06

Table C- 2: Raw data of the controlled monitoring. Flow = 120 ML.d^{-1}; dose = 2.5 mg.L^{-1}.

Date	Test no.	Flow rate (ML.d^{-1})		Doses (mg.L^{-1})	
2002-03-21	2	120		2.5	
		Ozone analyser measurements			
Time	Point no.	A	B	C	Outlet
		(ppm)	(ppm)	(ppm)	(ppm)
9:17	1	0.56	0.41	0.63	0.10
9:31	2	0.82	0.58	1.04	0.11
9:50	3	0.74	0.52	0.78	0.12
10:08	4	0.33	0.21	0.34	0.10
10:27	5	0.27	0.16	0.26	0.14

Date	Test no.	Flow rate ($ML.d^{-1}$)		Doses ($mg.L^{-1}$)	
2002-03-21	2	120		2.5	
		Ozone analyser measurements			
Time	Point no.	A	B	C	Outlet
		(ppm)	(ppm)	(ppm)	(ppm)
10:41	6	0.21	0.13	0.18	0.13

Table C- 3: Raw data of the controlled monitoring. Flow = 120 $ML.d^{-1}$; dose = 3.5 $mg.L^{-1}$.

Date	Test no.	Flow rate ($ML.d^{-1}$)		Doses ($mg.L^{-1}$)	
2002-03-21	3	120		3.5	
		Ozone analyser measurements			
Time	Point no.	A	B	C	Outlet
		(ppm)	(ppm)	(ppm)	(ppm)
12:50	1	1.12	0.79	1.36	0.51
13:01	2	1.35	0.94	1.73	0.52
13:14	3	1.27	0.89	1.56	0.44
12:28	4	0.74	0.52	0.88	0.44
13:30	5	0.69	0.48	0.71	0.44
13:40	6	0.65	0.45	0.64	0.42

Table C- 4: Raw data of the controlled monitoring. Flow = 106 $ML.d^{-1}$; dose = 2.5 $mg.L^{-1}$.

Date	Test no.	Flow rate ($ML.d^{-1}$)		Doses ($mg.L^{-1}$)	
2002-03-22	4	106		2.5	
		Ozone analyser measurements			
Time	Point no.	A	B	C	Outlet
		(ppm)	(ppm)	(ppm)	(ppm)
9:27	1	0.48	0.36	0.59	0.09
9:42	2	0.75	0.55	0.78	0.08
9:54	3	0.64	0.48	0.65	0.10
9:15	4	0.22	0.15	0.15	0.07
10:08	5	0.29	0.20	0.22	0.06
10:45	6	0.13	0.08	0.12	0.05

Table C- 5: Raw data of the controlled monitoring. Flow = 106 $ML.d^{-1}$; dose = 3.5 $mg.L^{-1}$.

Date	Test no.	Flow rate ($ML.d^{-1}$)		Doses ($mg.L^{-1}$)	
2002-03-22	5	106		3.5	
		Ozone analyser measurements			
Time	Point no.	A	B	C	Outlet

		(ppm)	(ppm)	(ppm)	(ppm)
11:59	1	1.11	0.85	1.33	0.46
12:10	2	1.49	1.05	1.71	0.44
12:21	3	1.29	0.97	1.52	0.47
11:47	4	0.73	0.57	0.85	0.46
12:35	5	0.75	0.57	0.77	0.45
12:45	6	0.61	0.46	0.63	0.43

C.2 Step test data

Table C- 6: Raw data of the step test monitored at Point 4. Step-up in dose at 120 ML.d^{-1}.

Date	Test no.	Flow rate (ML.d^{-1})		Doses (mg.L^{-1})	
2002-03-21	1	120		2.5 to 3.5	
		Ozone analyser measurements			
Time	Duration.	A	B	C	Outlet
	(min)	(ppm)	(ppm)	(ppm)	(ppm)
11:38	0	0.22	0.16	0.17	0.07
11:42	4	0.21	0.15	0.40	0.07
11:44	6	0.22	0.16	0.28	0.08
11:46	8	0.24	0.17	0.51	0.18
11:48	10	0.29	0.21	0.70	0.32
11:50	12	0.39	0.28	0.96	0.44
11:52	14	0.48	0.35	0.77	0.41
11:54	16	0.54	0.40	0.74	0.41
11:56	18	0.57	0.42	0.84	0.43
11:58	20	0.60	0.44	0.76	0.44
12:00	22	0.62	0.45	0.69	0.45
12:02	24	0.62	0.46	0.85	0.46
12:04	26	0.65	0.48	0.97	0.47
12:06	28	0.71	0.51	0.86	0.44
12:08	30	0.72	0.52	0.89	0.47
12:10	32	0.74	0.53	0.90	0.45
12:12	34	0.74	0.53	0.84	0.48
12:14	36	0.75	0.54	0.95	0.44
12:16	38	0.77	0.55	0.82	0.39
12:18	40	0.75	0.54	0.86	0.48
12:20	42	0.73	0.53	0.90	0.44
12:23	45	0.74	0.53	0.87	0.44

Table C- 7: Raw data of the step test monitored at Point 4. Step-down in dose at 120 ML.d^{-1}.

Date	Test no.	Flow rate (ML.d^{-1})		Doses (mg.L^{-1})	
2002-03-21	2	120		3.5 to 2.5	
		Ozone analyser measurements			
Time	Duration.	A	B	C	Outlet
	(min)	(ppm)	(ppm)	(ppm)	(ppm)
13:55	0	0.70	0.50	0.68	0.41
13:58	3	0.70	0.49	0.93	0.43
13:59	4	0.71	0.50	0.71	0.45
14:01	6	0.70	0.49	0.67	0.39
14:03	8	0.67	0.46	0.49	0.32
14:05	10	0.62	0.43	0.39	0.24
14:06	11	0.59	0.40	0.38	0.21
14:07	12	0.55	0.38	0.36	0.18
14:08	13	0.52	0.36	0.28	0.17
14:09	14	0.49	0.34	0.27	0.15
14:10	15	0.46	0.31	0.26	0.14
14:11	16	0.44	0.30	0.26	0.11
14:12	17	0.41	0.28	0.22	0.10
14:13	18	0.39	0.26	0.25	0.09
14:15	20	0.35	0.23	0.19	0.10
14:16	21	0.33	0.22	0.22	0.10
14:17	22	0.31	0.21	0.25	0.11
14:18	23	0.29	0.20	0.31	0.09
14:19	24	0.29	0.20	0.30	0.12
14:21	26	0.27	0.19	0.24	0.07
14:23	28	0.26	0.18	0.20	0.10
14:25	30	0.24	0.17	0.20	0.09
14:27	32	0.22	0.16	0.16	0.06
14:29	34	0.21	0.15	0.23	0.08
14:31	36	0.21	0.15	0.19	0.09

Table C- 8: Raw data of the step test monitored at Point 4. Step-down in flow at dose of 2.5 mg.L^{-1}.

Date	Test no.	Flow rate (ML.d^{-1})		Doses (mg.L^{-1})	
2002-03-22	3	120 to 100		2.5	
		Ozone analyser measurements			
Time	Duration.	A	B	C	Outlet
	(min)	(ppm)	(ppm)	(ppm)	(ppm)

Date	Test no.	Flow rate ($ML.d^{-1}$)		Doses ($mg.L^{-1}$)	
2002-03-22	3	120 to 100		2.5	
		Ozone analyser measurements			
Time	Duration.	A	B	C	Outlet
	(min)	(ppm)	(ppm)	(ppm)	(ppm)
14:55	0	0.21	0.14	0.20	0.10
15:02	7	0.21	0.14	0.29	0.07
15:05	10	0.22	0.19	0.17	0.09
15:08	13	0.21	0.14	0.25	0.07
15:10	15	0.20	0.13	0.20	0.06
15:12	17	0.20	0.13	0.15	0.04
15:14	19	0.19	0.12	0.05	0.03
15:15	20	0.17	0.11	0.15	0.03
15:16	21	0.17	0.11	0.20	0.04
15:18	23	0.17	0.11	0.16	0.04
15:20	25	0.16	0.10	0.11	0.02
15:22	27	0.16	0.10	0.18	0.02

Table C- 9: Raw data of the step test monitored at Point 4. Step-up in dose at 106 $ML.d^{-1}$.

Date	Test no.	Flow rate ($ML.d^{-1}$)		Doses ($mg.L^{-1}$)	
2002-03-22	4	106		2.5 to 3.5	
		Ozone analyser measurements			
Time	Duration.	A	B	C	Outlet
	(min)	(ppm)	(ppm)	(ppm)	(ppm)
11:10					
11:13	3	0.20	0.14	0.22	0.07
11:14	4	0.20	0.15	0.18	0.07
11:15	5	0.20	0.14	0.34	0.08
11:16	6	0.21	0.15	0.35	0.07
11:17	7	0.22	0.16	0.62	0.11
11:18	8	0.25	0.19	0.63	0.15
11:19	9	0.29	0.21	0.67	0.14
11:20	10	0.32	0.24	0.70	0.15
11:22	12	0.41	0.32	0.72	0.23
11:24	14	0.48	0.37	0.66	0.31
11:26	16	0.51	0.40	0.72	0.32
11:28	18	0.55	0.43	0.79	0.37
11:30	20	0.60	0.46	0.91	0.45
11:32	22	0.67	0.50	0.83	0.40

Date	Test no.	Flow rate ($ML.d^{-1}$)	Doses ($mg.L^{-1}$)
2002-03-22	4	106	2.5 to 3.5

Time	Duration.	Ozone analyser measurements			
		A	B	C	Outlet
	(min)	(ppm)	(ppm)	(ppm)	(ppm)
11:34	24	0.72	0.52	0.81	0.43
11:36	26	0.75	0.54	0.85	0.46
11:38	28	0.75	0.56	0.83	0.43
11:40	30	0.74	0.56	0.83	0.47
11:42	32	0.74	0.57	0.80	0.41
11:44	34	0.74	0.57	0.86	0.42
11:46	36	0.73	0.57	0.85	0.46

C.3 Ozone mass balance

Table C- 10: Raw data of calculation of ozone mass balance. Dose setting = 3.5 $mg.L^{-1}$.

Gas flow ($L.s^{-1}$)*	Gas flow ($Nm^3.h^{-1}$)	P (kPa)	T (°C)	Gas flow ($mol.h^{-1}$)***	Pre-TDU O_3 (ppm)**	O_3 to TDU ($mol.h^{-1}$)	O_3 to TDU ($g.h^{-1}$)
524	1886.4	101.9	32.9	75545	71	5.34	256
527	1897.2	101.9	32.1	76177	102	7.79	374
527	1897.2	101.8	30.7	76452	106	8.11	389
525	1890.0	101.8	30.1	76313	107	8.13	390
527	1897.2	101.9	29.5	76831	109	8.36	401
524	1886.4	101.8	29.0	76445	109	8.32	400
525	1890.0	101.8	28.8	76642	109	8.35	401
525	1890.0	101.9	28.5	76793	108	8.28	397

*Flow meter is calibrated in 1997, at P=1 atm, and T =25 °C

**Unit in ppm or % - gas pressure, relative to calibration pressure in ppm

*** N = pF/(RT)

D

RAW WATER CHARACTERISATION DATA

The characterisation experimental data used in **Chapter 6** are presented in this Appendix. Due to the limit of the thesis length, only the main runs of the experimental data are listed in this Appendix. The rest of the data are not tabulated here but included in the spreadsheet (*Kinetics exp.xls*) in the accompanying CD.

Table D-1: Characterisation of raw water – turbid water sample.

Run 0526-0.9		INDIGO			
	sample size	absorbance	O3 conc	TOC	254nm
	(mL)	(-)	($mg.L^{-1}$)	($mgC.L^{-1}$)	(-)
MQ water		0.344	-	0.520	0.000
RW blank	20	0.347	-	6.040	0.049
RW corr blnk	20	-	-	6.160	0.778
Initial condition	20	0.347	0.959	6.160	0.778
time	sample size	absorbance	O3 conc	TOC	254nm
(sec)	(mL)	(-)	($mg.L^{-1}$)	($mgC.L^{-1}$)	(-)
0	20	0.347	0.959	6.160	0.778
70	20	0.315	0.381	5.770	1.227
136	20	0.326	0.250	5.770	1.314
195	20	0.332	0.179	5.760	0.705
315	20	0.332	0.179	5.760	0.908
506	20	0.335	0.143	5.620	0.791
740	20	0.330	0.202	5.810	0.556
1215	20	0.337	0.119	6.170	1.244

Run 0526-2.7		INDIGO			
	sample size	absorbance	O3 conc	TOC	254nm
	(mL)	(-)	($mg.L^{-1}$)	($mgC.L^{-1}$)	(-)
MQ water		0.344	-	0.520	0.000
RW blank	20	0.339	-	5.630	0.049
RW corr blnk	20	-	-	5.730	0.842
Initial condition	20	0.339	2.296	5.730	0.842
time	sample size	absorbance	O3 conc	TOC	254nm
(sec)	(mL)	(-)	($mg.L^{-1}$)	($mgC.L^{-1}$)	(-)
0	20	0.339	2.296	5.730	0.842
195	20	0.149	2.262	5.860	0.592
255	20	0.137	2.405	5.640	0.339
320	20	0.168	2.036	5.560	0.535
435	20	0.200	1.655	5.730	0.245
620	20	0.227	1.333	5.760	0.854
855	20	0.242	1.155	5.990	0.589
1215	20	0.286	0.631	5.920	1.023

Run 0527-1.8		INDIGO			
	sample size	absorbance	O3 conc	TOC	254nm
	(mL)	(-)	($mg.L^{-1}$)	($mgC.L^{-1}$)	(-)
MQ water		0.357	-		0.000
RW blank	20	0.329	-	5.240	0.029
RW corr blnk	20	-	-	5.200	0.677
Initial condition	20	0.329	1.599	5.200	0.677
time	sample size	absorbance	O3 conc	TOC	254nm
(sec)	(mL)	(-)	($mg.L^{-1}$)	($mgC.L^{-1}$)	(-)
0	20	0.329	1.599	5.200	0.677
135	20	0.218	1.321	5.400	0.552
196	20	0.213	1.381	5.430	0.228
317	20	0.264	0.774	5.180	0.879
495	20	0.286	0.512	4.830	1.128
675	20	0.300	0.345	5.380	0.640
915	20	0.302	0.321	4.890	0.882
1215	20	0.311	0.214	5.400	0.543

Run 0527-3.6		INDIGO			
	sample size	absorbance	O3 conc	TOC	254nm
	(mL)	(-)	($mg.L^{-1}$)	($mgC.L^{-1}$)	(-)
MQ water		0.357	-		0.000
RW blank	20	0.337	-	4.980	0.036
RW corr blnk	20	-	-	4.820	0.899
Initial condition	20	0.337	2.295	4.820	0.036
time	sample size	absorbance	O3 conc	TOC	254nm
(sec)	(mL)	(-)	($mg.L^{-1}$)	($mgC.L^{-1}$)	(-)
0	20	0.337	2.295	4.820	0.899
225	20	0.049	3.429	5.020	0.815
285	20	0.064	3.250	4.610	0.844
346	20	0.107	2.738	4.930	0.839
483	20	0.141	2.333	4.750	0.832
649	20	0.178	1.893	5.170	0.892
885	20	0.201	1.619	4.960	0.846
1185	20	0.224	1.345	5.160	0.717

Table D-2: Characterisation of raw water – clear water sample.

Run 0531-0.9		INDIGO			
	sample size	absorbance	O3 conc	TOC	254nm
	(mL)	(-)	($mg.L^{-1}$)	($mgC.L^{-1}$)	(-)
MQ water		0.345	-		0.000
RW blank	20	0.347	-	5.730	0.030
RW corr blnk	20	-	-	5.580	0.596
Initial condition	20	0.347	1.131	5.580	0.596
time	sample size	absorbance	O3 conc	TOC	254nm
(sec)	(mL)	(-)	($mg.L^{-1}$)	($mgC.L^{-1}$)	(-)
0	20	0.347	1.131	5.580	0.596
100	20	0.285	0.738	6.030	0.601
163	20	0.277	0.833	5.480	0.823
220	20	0.301	0.548	5.900	0.611
340	20	0.310	0.440	5.570	0.677
440	20	0.321	0.310	5.560	0.633
820	20	0.330	0.202	5.840	0.497
1180	20	0.339	0.095	6.580	0.437

Run 0531-3.6		INDIGO			
	sample size	absorbance	O3 conc	TOC	254nm
	(mL)	(-)	($mg.L^{-1}$)	($mgC.L^{-1}$)	(-)
MQ water		0.345	-		0.000
RW blank	20	0.348	-	5.490	0.055
RW corr blnk	20	-	-	5.940	0.626
Initial condition	20	0.348	2.828	5.940	0.626
time	sample size	absorbance	O3 conc	TOC	254nm
(sec)	(mL)	(-)	($mg.L^{-1}$)	($mgC.L^{-1}$)	(-)
0	20	0.348	2.828	5.940	0.626
280	20	0.064	3.381	5.660	1.007
340	20	0.057	3.464	5.380	0.801
400	20	0.069	3.321	5.680	0.924
520	20	0.105	2.893	5.590	0.688
700	20	0.137	2.512	5.420	0.770
940	20	0.183	1.964	5.790	0.922
1240	20	0.193	1.845	5.470	0.779

Run 0531-2.7		INDIGO			
	sample size	absorbance	O3 conc	TOC	254nm
	(mL)	(-)	($mg.L^{-1}$)	($mgC.L^{-1}$)	(-)
MQ water		0.345	-		
RW blank	20	0.349	-	5.460	0.057
RW corr blnk	20	-	-	5.870	0.555
Initial condition	20	0.349	2.381	5.870	0.555
time	sample size	absorbance	O3 conc	TOC	254nm
(sec)	(mL)	(-)	($mg.L^{-1}$)	($mgC.L^{-1}$)	(-)
0.1	20	0.349	2.381	5.870	0.555
230	20	0.076	3.250	5.670	0.703
290	20	0.050	3.560	5.760	0.806
350	20	0.094	3.036	5.690	0.316
530	20	0.133	2.571	5.830	0.573
655	20	0.154	2.321	5.450	0.743
890	20	0.189	1.905	5.830	0.777
1190	20	0.218	1.560	5.500	0.412

Run 0601-1.8		INDIGO			
	sample size	absorbance	O3 conc	TOC	254nm
	(mL)	(-)	($mg.L^{-1}$)	($mgC.L^{-1}$)	(-)
MQ water		0.355	-		0.000
RW blank	20	0.347	-	6.130	0.026
RW corr blnk	20	-	-	5.210	0.882
Initial condition	20	0.347	1.313	5.210	0.882
time	sample size	absorbance	O3 conc	TOC	254nm
(sec)	(mL)	(-)	($mg.L^{-1}$)	($mgC.L^{-1}$)	(-)
0	20	0.347	1.313	5.210	0.882
120	20	0.196	1.798	6.090	1.061
183	20	0.199	1.762	5.800	0.777
243	20	0.226	1.440	6.370	0.783
365	20	0.251	1.143	6.010	1.084
540	20	0.268	0.940	6.380	0.976
782	20	0.279	0.810	5.850	0.688
1080	20	0.297	0.595	5.860	1.094

E

CFD MODELS OF THE OZONE CONTACTOR

Due to the large size of the contactor model and the vast number of cases studied, only the combined hydrodnamic/kinetic model is included in the accompanying CD. The mesh file is also attached. Various simulated data files are labelled and placed in the corresponding directories. For more details of the cases, please refer to *README.txt*.